Plasma membrane profiling of multiple myeloma and the identification of novel monoclonal antibody targets

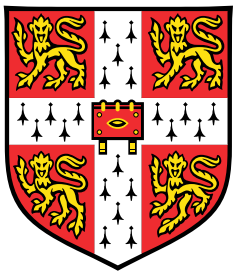

Georgina Suzanne Ferrier Anderson

Department of Haematology
University of Cambridge

This dissertation is submitted for the degree of
Doctor of Philosophy

Lucy Cavendish College

November 2018

Declaration

This dissertation is the result of my own work and includes nothing which is the outcome of work done in collaboration except as declared in the Preface and specified in the text.

It is not substantially the same as any that I have submitted, or, is being concurrently submitted for a degree or diploma or other qualification at the University of Cambridge or any other University or similar institution except as declared in the Preface and specified in the text. I further state that no substantial part of my dissertation has already been submitted, or, is being concurrently submitted for any such degree, diploma or other qualification at the University of Cambridge or any other University or similar institution except as declared in the Preface and specified in the text.

It does not exceed the prescribed word limit for the relevant Degree Committee.

Georgina Suzanne Ferrier Anderson
November 2018

Acknowledgements

First and foremost I would like to thank my PhD supervisor Mike Chapman for all his help and advice over the last four years, for keeping me pointed in the right direction and for sharing his enthusiasm for R! I'd also like to thank my second supervisor Paul Lehner for his input and ideas that have helped shape this thesis.

I would also like to thank all the past and present members of both the Chapman and Pina lab; Pepe, Sylvanie, Anna A, Anna T, Teresa, Filipa and Alice. Mostly for being there to support me when the PhD got tough, but also for encouraging me and making the lab work all that more enjoyable. In particular, Anna A for all her advice, particularly with the protein production and purification; Sylvanie for all her help with processing the many, many patient samples and for listening to all my ideas and helping me put them into place; and last but not least, Pepe for all his hard work in helping me write this thesis, as well as for all his help over the last few months to finish off numerous experiments. Furthermore, a huge thank you to James for all his help with the mass-spectrometry and for answering all of my questions (and there were many) about the PMP workflow.

Also a big thank you to all the current and past members of Lucy Cavendish College Boat Club. Thank you for encouraging me to share my enthusiasm for rowing as Lower Boats Captain, for reminding me that everyone goes through the same worries and fears during their PhD and that, yes, there is a light at the end. To my friends from home, thank you for your support and patience with me over the last few years. To my partner Dan, you have been so supportive, reminding me that I can do it, and have done your best to keep me sane. Thank you for making sure I have been fed these last few months! To my family, especially my parents, thank you for trying to understand and always being so curious and excited about my work. I'm sorry I can't answer every medical or biological question you have. Finally, for Emily. You may have teased me more times than I would have liked about being so keen on science, but you were also so supportive during my PhD and were fantastic in reminding me about how amazing all of this has been. Thank you.

Abstract

Plasma membrane proteins are ideal therapeutic targets, being both easily accessible and involved in mediating numerous cellular processes. However, the development of therapeutic agents targeting these proteins has been hindered by the difficulties associated with their identification and characterisation. Transcriptomic approaches are unreliable and previous proteomic efforts have failed to sufficiently enrich for plasma membrane (PM) proteins or were not quantitative. Plasma membrane profiling (PMP) is a novel proteomic technique that overcomes previous limitations and enables the identification and quantification of hundreds to thousands of PM proteins across multiple samples. We have adopted this technique to characterise the whole cell surface proteome in myeloma and to identify a novel antibody-drug conjugate (ADC) target.

Eight primary samples and ten human myeloma cell lines were profiled by mass spectrometry using PMP. A total of 2,077 proteins were identified with high confidence across all samples of which at least 1,319 were PM proteins. This represents a substantial improvement over other reported datasets, both in terms of total PM proteins identified and in the number of primary samples quantitated. This dataset was validated by repeat profiling and by comparing the relative PMP expression values against flow cytometry expression for six different antigens. To identify a novel antibody-drug conjugate target, proteins were ranked according to a combination of a) presence of a targetable extracellular domain b) high and ubiquitous on-tumour expression and c) low off-tumour expression. High-ranking candidates were screened for internalisation by flow cytometry and microscopy.

One target, SEMA4A, which was rapidly internalised and exhibited restricted healthy tissue expression, was taken forward to test for *in vitro* killing activity. An anti-SEMA4A ADC induced cell death exclusively in high SEMA4A-expressing cell lines *in vitro* and demonstrated potent activity in an *in vivo* xenograft model of myeloma. We also observed that the knock-down of SEMA4A using RNA-interference causes a competitive disadvantage, suggesting that target-downregulation would not be a viable mechanism of tumour escape.

Table of contents

List of figures

List of tables

Nomenclature

Roman Symbols

2-DE 2-dimension electrophoresis

ACN Acetonitrile

ADC Antibody drug conjugate

ADCC Antibody-dependent cell-mediated cytotoxicity

ADCP Antibody dependent cellular phagocytosis

Akt Protein kinase B

APRIL A proliferation inducing ligand

ASC Antibody-secreting cell

ASCT Autologous stem cell transplantation

BAFF B-cell activating factor

BCL-2 B-cell lymphoma 2

BCMA B-cell maturation antigen

BH Benjamini-Hochberg

BMA Bone marrow aspirate

BMSC Bone marrow stromal cell

Breg Regulatory B cell

C1q Complement component 1q

CAM-DR Cell adhesion mediated drug resistance

CAR Chimeric antigen receptor

CCL C-C motif chemokine ligand

CCND1 Cyclin D1

CCND2 Cyclin D2

CCR C-C motif chemokine receptor

CD Cluster of differentiation

CDC Complement mediated cytotoxicity

CID Collision-induced dissociatation

CSR Class switch recombination

CTLA-4 Cytotoxic T-lymphocyte–associated antigen 4

CXCL C-X-C motif chemokine ligand

CXCR C-X-C motif chemokine receptor

DC Dendritic cell

Dox Doxycycline

EFS Event-free survival

EMD Extramedullary disease

ER Endoplasmic reticulum

FA Formic acid

FBS Fetal bovine serum

FCM Flow cytometry

FDC Follicular dendritic cell

FGFR3 Fibroblast growth factor receptor 3

FRT Flippase recognition target

GC Germinal centre

GEP Gene expression profiling

GOCC Gene Ontology Cellular Compartment

GOCC Gene Ontology Cellular Compartment

HMCL Human myeloma cell line

ICAT Isotope-coded affinity tag

IDO Indoleamine 2,3-dioxygenase

Ig Immunoglobulin

IgH Immunoglobulin heavy chain

IHC Immunohistochemistry

IL Interleukin

IMAC Immobilised metal affinity chromatography

IMiD Immunomodulatory drug

IMWG International Myeloma Working Group

JAK Janus kinase

LAMP1 Lysosomal-associated membrane protein 1

LC Liquid chromatography

Mϕ Macrophage

mAb Monoclonal antibody

MAPK Mitogen-activated protein kinase

MCL-1 Myeloid cell leukaemia sequence 1 protein

MDE Myeloma defining event

MFI Median fluourescence intensity

MGUS Monoclonal gammopathy of undetermined significance

MICA MHC Class I chain-related protein A

MM Multiple myeloma

MMSET Multiple myeloma SET domain

MS Mass spectrometry

MZ Marginal zone

NK Natural killer

OB Osteoblast

OC Osteoclast

OS Overall survival

PC Plasma cell

PCL Plasma cell leukaemia

PCR Polymerase chain reacion

PD-1 Programmed cell death protein 1

PD-L1 Programmed death-ligand 1

PFS Progression-free survival

PI Proteasome inhibitor

PI3K Phosphoinositide-3-kinase

PMP Plasma Membrane Profiling

qRT-PCR quantitative real time-PCR

RNAi RNA-mediated interference

RRMM Relapsed/refractory multiple myeloma

RT Room temperature

RTP RNA-to-protein

SCID Severe Combined Immunodeficiency

SDS-PAGE Sodium dodecyl sulfate-polyacrylamide gel electrophoresis

SHM Somatic hypermutation

SILAC Stable isotope labelling by amino acids in cell culture

SLAMF7 Signalling lymphocytic activation molecule F7

SMM Smouldering multiple myeloma

STAT Signal transducers and activators of transcription

T_{FH} Follicular helper T cells

TACI Transmembrane activator and CAML interactor

TAM Tumour associated macrophage

TD T-dependent antigen

TFA Trifluoroacetic acid

TGF-β1 Transforming growth factor beta 1

TI T-independent antigen

TMT Tandem mass tag

Treg Regulatory T cell

VCAM1 Vascular cell adhesion protein 1

VLA-4 Very late antigen-4

Chapter 1

Introduction

1.1 Overview of Myeloma

Multiple Myeloma (MM) is a haematological malignancy characterised by the clonal expansion of plasma cells within the bone marrow. It is the second most common blood cancer, accounting for around 13% [1], and is considered to be a disease strongly associated with age, with 43% of new cases between 2009 and 2011 occurring in people aged 75 or over [2]. Despite recent therapeutic advancements, myeloma is still typically considered 'treatable' rather than 'curable' and it is expected that the majority of patients will relapse, with a 10 year survival rate of just 33% [2].

1.2 Pathophysiology

Preceding myeloma is a premalignant stage known as monoclonal gammopathy of undetermined significance (MGUS) [3]. This is an asymptomatic disorder characterised by the presence of an abnormal immunoglobulin in an individual's serum or urine that originates from the proliferation of a single plasma cell clone. These patients, however, do not exhibit myeloma or other lymphoproliferative disorder symptoms [4]. Although nearly all MM cases are precceded by MGUS [3], not every MGUS will transform into myeloma. The rate of progression is considered to be on average 0.5-1% per year [5], although this is difficult to conclusively determine as MGUS is asymptomatic and therefore usually identified incidentally. Furthermore, some risk factors may be associated with an enhanced rate of progression [6]. Between MGUS and MM is an intermediate, more advanced stage known as smouldering multiple myeloma (SMM). This is still considered an asymptomatic stage but exhibits an increased rate of progression of around 10% [7]. Although there is limited

evidence to suggest that early therapeutic intervention at this stage may convey a survival benefit, MGUS and SMM are typically untreated and instead patients are monitored for disease progression [8].

Active myeloma is diagnosed by the presence of >10% clonal bone marrow plasma cells; biopsy-proven bony or extramedullary plasmacytoma; and any one or more of the classic CRAB features and myeloma defining events (MDEs). CRAB features define the presence of end-organ damage that includes hyper**C**alcaemia, **R**enal failure, **A**naemia and lytic **B**one lesions. Renal dysfunction is commonly the result of the accumulation and precipitation of light and heavy chains within the kidney, forming urinary casts that obstruct the renal tubules. Renal failure may also be attributed to immunoglobulin light chain amyloidosis and light chain deposition disease, as well as the direct toxicity of light chains on the renal tubules and glomeruli [9]. Renal insufficiency may in turn contribute to the elevated serum calcium levels. Tumour-mediated bone destruction also contributes to the observed hypercalaemia [10]. Approximately 80 to 90% of myeloma patients suffer from osteolytic lesions that may result in bone fractures, pain, spinal cord compression as well as reduced mobility [11]. The observed anaemia may be attributed to several factors, including the crowding of the bone marrow and functional impairment of the megakaryocyte-erythroid progenitors [12]. MDEs include >60% clonal bone marrow plasma cells, a serum involved/uninvolved free light chain ratio of >100 or >1 focal lesion as detected by MRI [13].

Typically, patients will initially respond well to the first line of treatment following diagnosis and enter a period of remission. Inevitably patients relapse, and although they may still respond to additional lines of therapy, these periods of remission shorten and individuals may become refractory to all currently available treatments, known as relapsed/refractory multiple myeloma (RRMM) [14]. A subset of patients may subsequently develop extramedullary disease (in which the malignant plasma cells escape the bone marrow [15]) or plasma cell leukaemia (PCL) (a rare and aggressive gammopathy defined by the presence of >20% of plasma cells in the peripheral blood) [16][17].

1.3 Molecular classification

Multiple myeloma is a highly heterogenous disease both at the genetic level, involving numerous translocations (both primary and secondary), chromosomal abnormalities, mutations and epigenetic modifications, but also at the clonal level. These genetic events can be broadly grouped into primary and secondary events. Primary genetic events are observed in MGUS

and are present in all clones within the tumour. These primary events are believed to play a role in establishment of the disease but not in driving malignant progression. Secondary genetic events, on the other hand, are considered to be the drivers of myeloma. Unlike primary events which are present in the premalignant stage of MM, secondary events may occur at any stage of the disease but typically occur more frequently in SMM and MM or are associated with more advanced end-stage disease. Multiple secondary genetic events may also occur within the same patient and can overlap within subclones [18]. The presence of particular genetic events can heavily influence a patient's prognosis, with some abnormalities associated with rapid disease progression or a poor response to commonly used therapeutics (table 1.1), although these are not the sole predictors of disease outcome and other criteria, including age and co-morbidities, are also taken into account.

High risk	Intermediate risk	Low risk
del(17p)	t(4;14)	Trisomies
t(14;16)	del(13)	t(11;14)
t(14;20)	Hypodiploidy	t(6;14)
Median OS 2-3 years	Median OS 4-5 years	Median OS 8-10 years

Table 1.1 The mSMART risk stratification system for active MM. OS=Overall survival. Adapted from [19]

Clonally, the myeloma tumour is also heterogenous. Recent studies have shown the presence of multiple independent, yet related, subclones within a tumour that carry different mutations. It was initially considered that myeloma tumours typically contain at least 5 such subpopulations, however, recent evidence suggests that is most likely an under-estimation [20][21]. Interestingly, it has recently been shown that this heterogenous subclonal structure is present at all stages of disease, including MGUS [21]. As myeloma progresses, the genetic complexity of the disease correspondingly increases, with an increase in the number of non-synonymous mutations [21] . Contrary to the traditional dogma of a linear evolution, events typically appear to accumulate in a branching evolutionary pattern known as the Darwinian model (figure 1.1). The multiple steps involved in myeloma tumorigenesis result in a changing pattern of subclones and increasing complexity as the disease progresses [22]. External selection pressures, such as treatment, also contribute to these changing patterns of dominant subclones with previously minor drug-resistant subclones increasing in prominence at relapse [23][24][25][26]. It is therefore of great importance to take into account this clonal heterogeneity when identifying novel therapeutics to prevent the selection of a highly resistant subclone.

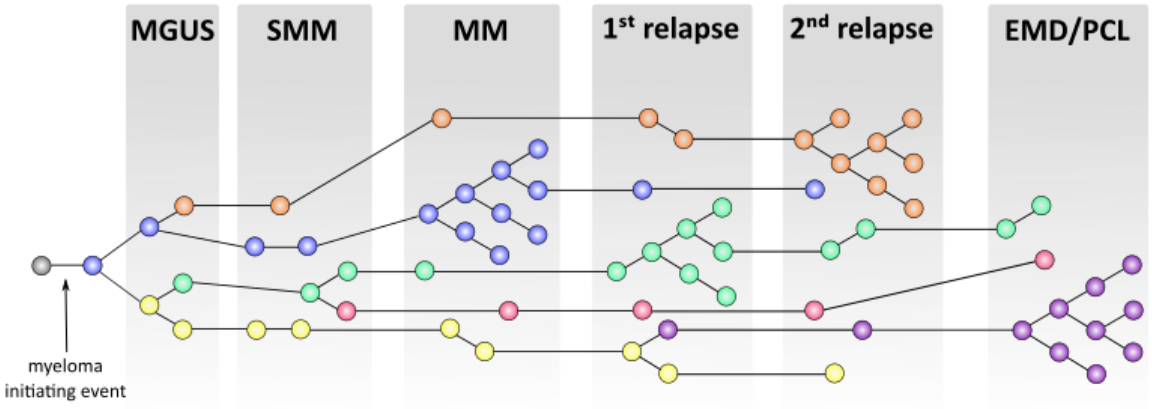

Fig. 1.1 *A branching evolution of myeloma.* Myeloma consists of a highly heterogenous subclonal structure. Over the course of the disease the predominant clone changes as minor subclones emerge or acquire further mutations that allow them to survive treatment. Different subclones are represented by individual colours. MGUS=monoclonal gammopathy of undetermined significance, SMM=smouldering multiple myeloma, MM=multiple myeloma, EMD=extramedullary disease, PCL=plasma cell leukaemia. Adapted from [23][27].

Primary cytogenetic events are broadly classed into two groups: hyperdiploid or non-hyperdiploid. Those with a hyperdiploid karyotype (approximately 40% of MM cases [13]) exhibit numerous trisomies of odd-numbered chromosomes (typically 3, 5, 7, 9, 11, 15, 19 and 21) with a low prevalence of immunoglobulin heavy chain (IgH) translocations (14q32) [28]. Hyperdiploid myeloma is associated with a better prognosis, and some trisomies may in fact overcome the poor prognosis conferred by other cytogenetic abnormalities [29]. Non-hyperdiploid myeloma includes hypodiploid, pseudodiploid and near-tetraploid; and is associated with a high prevalence of IgH or immunoglobulin light chain translocations (κ, 2p12 or λ, 22q11) and a less favourable outcome [28]. The five most recurrent translocations are: t(11;14), t(4;14), t(14;16), t(14;20) and t(6;14).

1.3.1 Primary translocations

One of the most common translocations is the t(11;14)(q13;32) (15% of MM cases [28]), resulting in the aberrant over-expression of Cyclin D1 (CCND1) [30]. Cyclin D1 belongs to the cyclin protein family and is a critical for progression through the G1 phase of the cell cycle. As such, amplification of CCND1 is associated with a release from the normal control of cell cycle and subsequently, enhanced cellular proliferation [31]. Aside from cell cycle dysregulation, amplification of CCND1 may also contribute to drug resistance in MM [32].

Qiang *et al* observed an increased expression of multidrug resistant protein 1 (MDR1), a cell membrane protein involved in the efflux of toxins (including therapeutics), in cyclin D1-positive patients [33]. Although this translocation is considered to be a 'standard-risk' cytogenetic, several studies have noted an increased prevalence in PCL [17]. Cyclin D3 is also targeted by an IgH translocation (t(6;14)), although this is a much rarer event [28].

Interestingly, dysregulation of cell cycle progression appears to be a common event in myeloma regardless of translocation status and cyclin D has been reported as dysregulated in up to two-thirds of myeloma and highly expressed in many of the remaining samples [34][30]. This includes the two cyclin D translocation subgroups but also the c-Maf subgroup which is associated with cyclin D2 (CCND2) dysregulation [35]. Further CCND1 biallelic dysregulation that appeared independent of a subgroup was observed in 40% of tumours. [34].

Another recurrent translocation (15% of cases [28]) is the t(4;14) translocation which promotes the amplification of fibroblast growth factor receptor 3 (FGFR3) and multiple myeloma SET domain (MMSET) [36]. Unlike the other translocations identified in MM, two genes with oncogenic potential are dysregulated. However, it appears that MMSET is the primary target and is overexpressed in all t(4;14) tumours, whilst FGFR3 is only expressed in approximately 70% of cases [36].

MMSET is a member of the nuclear receptor binding SET domain (NSD) family and possesses lysine methyltransferase activity. Amplification of MMSET is primarily associated with an increase in H3K36 dimethylation (associated with active transcription) and a corresponding decrease in H3K27 trimethylation (a repressive mark) [37]. These alterations result in the dysregulation of numerous signalling pathways including those regulating cell cycle, apoptosis and adhesion [37][38]. MMSET overexpression is also associated with an enhanced DNA damage repair. Shah *et al* observed that a loss of MMSET in a t(4;14) human myeloma cell line (HMCL) (KMS11) reduced the efficiency of both non-homologous end joining (NHEJ) and homologous recombination (HR), two pathways involved in the repair of double strand breaks, with a corresponding enhanced sensitivity to the alkylating agent melphalan [39]. Pei *et al* similarly reported a link between MMSET and DSB repair [40]. This is in concordance with the poor prognosis that was initially associated with the t(4;14) subgroup prior to the introduction of novel agents when alkylating agents were the mainstay of myeloma therapy. These patients, despite an initial response to melphalan, experienced shorter periods of remission and quicker disease progression [41].

Although FGFR3 may not be the direct target of the t(4;14) translocation, it may still play a key role in oncogenic transformation. FGFR3 belongs to the FGFR family of tyrosine kinase receptors that are involved in the activation of multiple pathways implicated in tumorigenesis including the Mitogen-activated protein kinase (MAPK), phosphoinositide 3-kinase/protein kinase B (PI3K/Akt) and Janus kinase/signal transducers and activators of transcription (JAK/STAT) signalling pathways [42]. Because of the role that FGFR3 has in these critical pathways, it is clear how genetic alterations of the receptor may have oncogenic potential and the activation or over-expression of FGFR3 has been observed to promote proliferation and cell survival as well as drug resistance [43][44][45]. Activating mutations, although rare, have also been reported for FGFR3 and are acquired during tumour progression [44][46].

The two remaining common translocations (t(14;16) and t(14;20)) dysregulate the transcription factors c-Maf and MafB respectively and are commonly grouped together as the MAF subgroup. Aberrant Maf signalling dysregulates a number of genes, including CCND2, C-C motif chemokine receptor type 1 (CCR1), NUAK Family Kinase 1 (NUAK1) and integrin subunit beta 7 (ITGB7), increasing the rate of cell cycle progression and adhesion of myeloma cells to the stroma [35][41]. This subgroup is relatively rare (5-7% [28]), but is considered a 'high-risk' genetic event (table 1.1) and unlike the t(4;14) subgroup, the introduction of bortezomib has had minimal impact on the prognosis of these patients [41]. This may be in part explained by the observed stabilisation of c-Maf and MafB by bortezomib, with t(14;20) cells exhibiting a reduced sensitivity to both bortezomib and carfilzomib [41][33]. Similar to cyclin D, c-Maf is also frequently dysregulated in cells independent of a t(14;16) translocation, with high c-Maf expression reported in up to 50% of patients and HMCLs [35]

1.3.2 Secondary mutations

As previously mentioned, secondary genetic events are considered to drive the disease and are typically associated with later disease. These genetic events may include additional translocations (secondary translocations), chromosomal deletions/amplifications and mutations in key signalling pathways.

Chromosome 13 abnormalities, either monosomy or deletion of the long arm (del(13q)), are a common occurrence in MM and have been reported to occur in up to half of MM tumours. These events are one of the earliest secondary events occurring in myeloma progression, occurring as early as MGUS (albeit rarely) [47] and are indicative of an adverse

prognosis for both progression-free survival (PFS) and overall survival (OS) [13]. The exact target of the chromosome 13 deletion is currently unknown and there are several proposed targets. One such target is the retinoblastoma protein (RB1), a tumour suppressor protein involved in cell cycle regulation. The RB1 gene locus is at 13q14, a commonly deleted region [48].

Chromosome 1 is also frequently dysregulated in MM, with either deletions of the short arm (del(1p)) or amplifications of the long arm (dup(1q)). The prevalence of chromosome 1 aberrations highly depends on the disease stage and 1q gains are typically infrequent in MGUS (0 to 29%). The incidence of chromosome 1 aberrations increases with disease advancement, with a reported prevalence of 45 and 44% in SMM and newly diagnosed MM respectively and up to 72% in RRMM [49][50]. This high frequency and association with later disease suggests it plays a key role in driving disease progression. Subsequently, dup(1q) is associated with a poor event-free survival (EFS) and OS [50]. Similar to chromosome 13, the exact targets of these deletions/amplifications are unknown, although 1p has been reported to contain several putative tumour suppressor genes [51]. For dup(1q), two minimally amplified regions have been identified: 1q21-23 and 1q31-q42 [52] and several potentially oncogenic targets have been identified. This includes mucin 1 (MUC-1, 1q22) which activates MYC to dysregulate target genes including CCND2 [53], PDZ domain containing 1 (PDZK1, 1q21.1) involved in chemotherapeutic resistance [54], cyclin-dependent kinases regulatory subunit 1 (CKS1B, 1q21.1) involved in cell cycle progression [52], myeloid cell leukaemia sequence 1 protein (MCL-1, 1q21.2) that may be essential for HMCL survival and is associated with relapse and shorter OS [55], as well as B cell lymphoma 9 (BCL9, 1q21.2), and FC receptor like 4 (FCRL4, 1q23.1) [52].

A third common chromosomal abnormality is del(17p), which is considered to target the well known tumour suppressor p53 (17p13.1). p53 is also found mutated in myeloma, although this is a rare event [56] and is typically associated with del(17p) [57]. DNA damage stabilises p53, inducing cell cycle arrest, senescence, and if not resolved, apoptosis [58]. These mutations/deletions are likely to be key mediators in disease progression, occurring rarely in MGUS and newly diagnosed MM (13%) but up to almost half of patients with advanced-stage disease [49][59][60].

The Ras GTPase family members, KRAS and NRAS, are also targeted by activating mutations in myeloma ($\approx$30% of patients [61]). These GTPases mediate a number of signalling pathways, regulating many cellular processes including cell cycle progression, growth,

migration, apoptosis and senescence [62]. Although NRAS mutations appear to be more frequent, 17-18% and 6-7% for N- and K- Ras respectively in newly diagnosed MM, only KRAS mutations are associated with a poorer prognosis and shorter OS [63].

The nuclear factor kappa B (NFkappaB) family of transcription factors are also implicated in myeloma tumorigenesis. Genetic events targeting this signalling pathway have been reported in 9-17% of patients, supporting myeloma survival, proliferation and drug-resistance [64]. Other genetic events in myeloma include activating mutations in the PI3K/Akt signalling pathway [65] and chromosomal rearrangements of the transcription factor MYC [66].

1.4 The Plasma Cell

1.4.1 Immunoglobulins

Myeloma is a cancer of the plasma cell (PC), which are terminally-differentiated B cells that secrete high titres of a specific immunoglobulin (Ig). These secreted glycoproteins are one of the major components of humoral immunity, specifically recognising and binding to antigens to target pathogens for destruction. Immunoglobulins are comprised of two identical heavy chains and two identical light chains (κ or λ). Each heavy chain consists of one variable domain and three to four constant domains, depending on the class of antibody. Meanwhile, light chains are comprised of just one of each. The light chain variable region is encoded by two gene segments: variable (V_L) and joining (J_L). A third gene segment (diversity (D_H)) encodes the heavy chain variable region, alongside V_H and J_H. The antigen binding domain of the antibody is known as the Fab region (antibody-binding fragment) whilst the Fc (fragment, crystallisable) domain is the primary recognition site for effector functions and other antibodies (figure 1.2) [67].

Diversity within the antibody repertoire is achieved by three processes that occur during B cell and plasma cell development. The first process is the combinatorial rearrangement of the V, D and J gene segments to create a functional variable domain. Encoded within the germline are multiple copies of each of the three gene segments. The selection of just one segment for each type (V, D or J) and the different combinations of these provide initial diversity [69] . Further diversification is provided by the introduction of point mutations to the variable region by somatic hypermutation (SHM). Finally, antibodies may undergo class switch recombination (CSR), in which the constant regions of the heavy chain are switched,

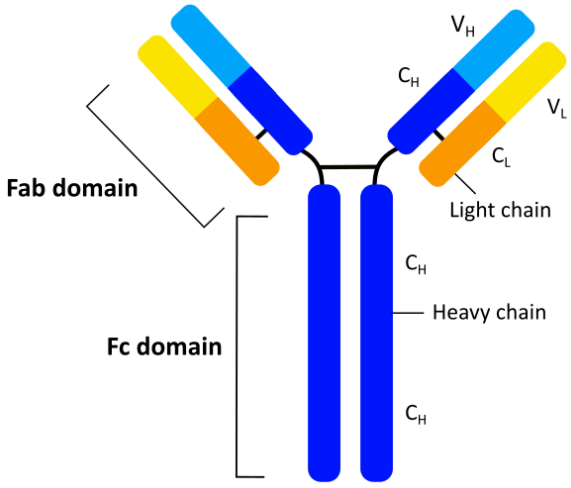

Fig. 1.2 *Structure of immunoglobulin.* Immunoglobulins are comprised of two heavy and two light chains that contain variable (V_L or V_H) and constant (C_L or C_H) domains. Target antigen is bound by the Fab domain and effector functions mediated by the FC domain. Adapted from [68]

changing the isotype of the antibody from IgM to another class [70]. There are five major isotypes of Ig in humans: IgA, IgD, IgE, IgG and IgM. IgA and IgG are further divided into two (IgA1 and IgA2) and four (IgG1, IgG2, IgG3, IgG4) subclasses respectively. These Igs may be either surface bound or secreted [67].

Secreted Igs recognise and bind foreign antigens on the surface of pathogens, coating the microbe or virus in a process termed opsonisation. These opsonised pathogens can then be recognised and destroyed by the immune system by either activation of the complement system (Complement-mediated cytotoxicity (CDC)) or immune effector cells. Binding of the complement component 1q (C1q) to the Fc domain of the bound antibody triggers the activation of the complement cascade, resulting in the formation of the membrane attack complex (MAC) on the target cell. This disrupts the cell surface membrane and triggers cell death by osmotic lysis [71]. Alternatively, the Fc domain of the antibody may be recognised by one of the many Fc receptors expressed on immune effector cells, triggering antibody-dependent cellular phagocytosis (ADCP) by phagocytic cells which engulf the target cell, or triggering antibody-dependent cell-mediated cytotoxicity (ADCC) [71]. ADCC is primarily mediated by natural killer (NK) cells, but may also be mediated by monocytes, macrophages, neutrophils, eosinophils and a subset of T cells. Receptor binding triggers cell death by one of the three mechanisms: 1) release of granules containing perforin which forms large pores in the target cell membrane and enables the diffusion of the cytotoxic granzyme into the

cytoplasm, 2) upregulation of Fas ligand on the effector cell to induce apoptosis in the target cell or 3) the release of reactive oxygen species (ROS) [72][73].

1.4.2 Plasma cell development

Antibody-secreting cells (ASCs) are derived from the mutipotent, bone-marrow residing haematopoietic stem cells (HSCs). HSCs differentiate through several rounds of progenitor cells before emerging as a progenitor B (pro-B) cell that is committed to the B lineage. Maturation of the pro-B cell continues in the bone marrow initially before cells migrate to the spleen. As these cells differentiate into mature B cells, they undergo V(D)J recombination to produce monomeric IgM. This is expressed on the cell surface in association with two polypeptide chains (Cluster of differentiation (CD)79a and CD79b) to form a functional B cell receptor (BCR). During this process auto-reactive B cells, cells expressing BCRs with an affinity for self-antigens, or cells without a functional BCR are removed [74]. As B cells mature, they also begin expressing IgD at the cell surface, in a process mediated by alternative RNA splicing [75]. The majority of these naïve IgM+IgD+ mature B cells are recirculating B cells known as follicular B cells. This subset of B cells localise to the blood and the B cell follicles of secondary lymphoid organs. B cells may also reside within the marginal zone (MZ) of the spleen and are therefore termed marginal zone B cells [74]. A third population, B-1 cells, represent a very small but unique subclass of B cells that contribute to the innate immune system. B-1 cells are responsible for the constitutive, spontaneous secretion of resting Ig (natural Ig) that occurs in the absence of infection [76].

B cell activation occurs in response to the BCR recognition of their cognate antigen. Antigens are broadly grouped into two types, those that require T cell assistance for full B cell activation (T-dependent (TD)) and those that don't (T-independent (TI)). Follicular B cells appear to be more specialised for responding to TD antigens whilst MZ B cells are specialised towards TI antigens, although these roles aren't strictly enforced and both subsets may respond to either antigen [77][78]. Activation of both subsets takes place in the lymph nodes and spleen. These secondary lymphoid organs are comprised of several distinct regions that are selectively enriched for particular immune cell subsets [79].

Follicular B cells and follicular dendritic cells (FDCs) reside within areas known as follicles. Adjacent to these follicles are T-cell rich zones (the paracortex or periarteriolar lymphoid sheath in the lymph node or spleen respectively). Also surrounding the follicles are macrophages. The spleen also contains an additional structure, the marginal zone, which contains both MZ B cells and macrophages [79]. This zone separates the follicle-containing

white pulp from the red pulp of the spleen.

The temporal and spatial control of B and T lymphocytes within these regions is tightly regulated by chemokines. Circulating naïve follicular B cells are recruited to the C-X-C motif chemokine ligand 13 (CXCL13)-expressing follicle by high CXC Chemokine Receptor 5 (CXCR5) expression [80][81], where they may encounter their cognate antigen. Activation of B cells following BCR recognition of the antigen results in the upregulation of C-C motif chemokine receptor type 7 (CCR7) expression, promoting the migration of the activated B cells to the border of the B and T cell zones along a C-C motif chemokine ligand 19 (CCL19) and CCL21 gradient. Concurrently, naïve CD4+ T cells are primed by dendritic cells (DCs) in the T cell zone and differentiate into follicular helper T cells (T_{FH}). T_{FH} cells upregulate CXCR5, downregulate CCR7 and P-selectin glycoprotein ligand 1 (PSGL1) and migrate towards the B cell follicle border [82]. At the border, activated B cells present the antigen on their cell surface, which is recognised by the T_{FH} cells and triggers T_{FH} CD40L expression, providing a co-stimulatory signal necessary for B cell survival [83].

Activated B cells may then either migrate to extrafollicular sites and differentiate into PCs or return to the follicle with the T_{FH} cells and undergo an intense period of proliferation to form germinal centres. The plasma cells generated via the extrafollicular route are short-lived and secrete typically low-affinity antibody, providing an early and rapid response to infection [79]. Similarly to follicular B cells, MZ B cells may participate in either the extra-follicular or GC response [84]. In the GC, B cells undergo affinity maturation, a process in which the activated GC B cells undergo multiple rounds of proliferation and SHM to enhance antibody affinity and avidity. This process is regulated by both the T_{FH} cells and FDCs, promoting the survival of high-affinity B cells as well as CSR [83][82]. Eventually, B cells enter one of two fates: memory B cell or plasma cell. Memory B cells contribute to immunological memory; repeat exposure to their cognate antigen triggers reactivation and the rapid differentiation into plasma cells [85]. Emerging PCs leave the follicles of the secondary lymphoid organs and migrate to specialised plasma cell niches, predominantly the bone marrow. Bone marrow homing is primarily regulated by the upregulation of CXCR4. CXCR4 expression promotes the migration of these cells towards the CXCL12-high bone marrow [86]. Within the bone marrow, plasma cells may remain short-lived or fully mature into quiescent and sessile long-lived plasma cells, providing Ig-mediated immunity for several decades [87][88]. Outside of the bone marrow, PCs also reside in other sites including the gut and tonsils [89][90] or may also be recruited to sites of inflammation, associated with an upregulation of CXCR3 [91].

The mechanism regulating the decision to become a short-lived or long-lived plasma cell is unclear. One proposed theory is the competition model, proposing that the total number of PC niches is finite and that short-lived PCs entering the bone marrow must compete with older, resident long-lived PCs to survive [92]. This model has been supported by the finding that antigen-specific PCs in the bone marrow were replaced following subsequent repeat immunisations with different antigens [93]. It is unlikely, however, that this model fully explains the decision to become a long-lived plasma cell. Even *in vitro*, where survival factors are not limited, only a fraction of the population become long-lived PCs [94]. Cell-intrinsic factors may also be involved, such as a failure to cope with the metabolic stress caused by secreting high Ig titres or a failure to express key survival receptors [95].

1.5 The bone marrow niche

Regardless of its role in determining the longevity of plasma cells, it is axiomatic that the bone marrow niche plays a vital role in PC survival. This is evidenced by the rapid apoptosis of plasma cells following their removal from the bone marrow [96][97]. The bone marrow niche is a complex microenvironment and consists of both a cellular and non-cellular compartment. During oncogenic transformation, myeloma cells alter this microenvironment to further promote malignant cell survival, proliferation, metastasis and resistance to therapeutics.

1.5.1 Non-cellular compartment

Interleukin-6

Interleukin-6 (IL-6) is one of the quintessential plasma cell growth factors. Initially identified in 1983 as human B-cell differentiation factor (BCDF) from T cell-conditioned media, IL-6 was shown to promote the terminal differentiation of B cells into ASCs [98]. The use of an IL-6 targeted antibody subsequently demonstrated that the cytokine was also a potent growth factor for myeloma cells and is secreted in both a paracrine and autocrine manner [99][100]. Additionally, IL-6 acts as an anti-apoptotic factor [101], protecting MM cells against both spontaneous and dexamethasone-induced apoptosis [102]. Although the addition of IL-6 can support PC survival *in vitro* in the absence of stromal cells or growth factors, it does not appear to be essential *in vivo* as IL-6 deficient mice do not appear to exhibit any impairments in long-term immunity [97].

Vascular endothelial growth factor

Vascular endothelial growth factor (VEGF) expression is dysregulated in a number of malignancies, supporting the growing tumour by mediating the formation of new blood vessels to provide additional oxygen and nutrients [103]. Equally in myeloma, angiogenesis is dysregulated, with elevated VEGF production compared to normal donors [104] and a corresponding increase in the bone marrow microvessel density that is associated with a poor prognosis [105]. Both bone marrow stromal cells (BMSCs) and PCs secrete VEGF, which supports normal and malignant PCs in an indirect manner by enhancing BMSC IL-6 production [104][106]. VEGF also directly targets the myeloma cells, promoting proliferation, growth, migration and survival through the upregulation of anti-apoptotic factors, including MCL-1 [107]. Aside from VEGF, BMSCs also secrete other pro-angiogenic factors such as basic fibroblast growth factor (bFGF), hepatocyte growth factor (HGF), osteopontin (OPN) and metalloproteinase-1 (MMP-1) [103].

Transforming growth factor beta 1

Transforming growth factor beta 1 (TGF-β1), an anti-inflammatory cytokine secreted by both BMSCs and PCs, is also upregulated in myeloma. Although it does not directly stimulate myeloma cell growth or survival, it promotes the transcription and secretion of IL-6 and VEGF from BMSCs [108][104]. As an anti-inflamamtory cytokine, TGF-β1 also contributes to the immunosuppressive microenvironment of MM, preventing the expression of pro-inflammatory cytokines, suppressing immune effector functions and promoting the expansion and suppressive function of CD4+CD25+ regulatory T cells (Tregs) [109][110]. Additionally, TGF-β1 contributes to disease progression and exacerbates bone disease through the suppression of osteoblast differentiation [111].

B-cell activating factor/A proliferation-inducing ligand

Other key growth factors that make up the non-cellular compartment of the bone marrow niche include B-cell activating factor (BAFF) and A proliferation-inducing ligand (APRIL). BAFF and APRIL are both members of the tumour necrosis factor (TNF) superfamily and share significant homology. Although both growth factors bind B-cell maturation antigen (BCMA) and Transmembrane Activator and CAML Interactor (TACI), only BAFF binds BAFF receptor (BAFF-R) [112].

The role of these ligands in supporting the survival of long-term BMPCs was demonstrated by O'Connor *et al*. Blockade of both APRIL and BAFF *in vivo* using TACI-Ig (the extracellular domain of TACI fused to the Fc portion of human IgG1) caused a decay in the long—lived ASC population [113]. Of the three receptors, the pro-survival functions of APRIL/BAFF appear to be predominantly mediated by BCMA. Unlike TACI and BAFF-R, which are heterogeneously expressed across MM patient samples, BCMA is both highly and consistently expressed on myeloma cells [112]. Furthermore, although BCMA -/- mice exhibit normal early humoral immunity, with no significant defects in peripheral B cell frequencies or GC formation, they exhibit a substantial reduction in the number of long-lived ASCs [113]. Interestingly, the antagonism of both APRIL and BAFF *in vivo* is required to replicate this BM PC impairment, suggesting a certain level of redundancy [114]. Considering their role in supporting long-lived PCs, it is unsurprising that the serum levels of both growth factors are elevated in myeloma compared to normal donors [112].

Both BAFF and APRIL are secreted by a multitude of cell types, primarily cells of the myeloid lineage [115][116]. APRIL and BAFF promote cell cycle progression [117][118], and protect MM cells from lenalidomide and dexamethasone induced cell death through the upregulation of anti-apoptotic proteins such as B-cell lymphoma 2 (BCL-2) and MCL-1 [112][118]. Similarly to TGF-β, APRIL contributes to an immunosuppressive environment, inducing Programmed death-ligand 1 (PD-L1) expression on MM cells and supporting Treg survival and function [119][120].

1.5.2 Interactions between myeloma cells and the bone marrow cellular compartment

Bone marrow stromal cells

As already mentioned, the CXCR4/CXCL12 axis is involved in the homing of PCs from the secondary lymphoid organs to the bone marrow. One of the primary sources of CXCL12 are the bone marrow stromal cells, which reside in close contact with the plasma cells [121]. BMSCs are considered one of the most vital constituents of the bone marrow niche and the addition of stromal cells to *in vitro* plasma cell cultures prevents the rapid decline in viability, maintaining a subpopulation of these cells for several weeks [96]. These CXCL12-expressing cells also highly express vascular cell adhesion molecule 1 (VCAM1), an Ig-like adhesion molecule that binds to the integrin very late antigen-4 (VLA-4) [121]. VLA-4 is highly expressed on PCs [122] and the interactions between these two cell surface proteins

mediates the adhesion of PCs to BMSCs [123]. Aside from PC homing, BMSCs are also a rich source of cytokines and growth factors which promote both normal and malignant PC survival, including IL-6, VEGF and TGF-β [100][108][106]. The co-culture of BMSCs and plasma cells promotes the expression of these growth factors [96][106], but also, in the context of myeloma, conveys therapeutic resistance (cell adhesion mediated drug resistance (CAM-DR)). Several groups have demonstrated that the co-culture of BMSCs and HMCLs significantly reduces the cytotoxic effects of several commonly used therapeutic agents. This resistance is mediated in predominantly a contact-dependent manner, although soluble factors also appear to play a role [124][125][126]. The use of RNA-mediated interference (RNAi) or blocking antibodies has revealed that loss of integrins, such as VLA-4, reverses this resistance. Interestingly, drug resistance was not conferred by stromal cell-conditioned media alone, suggesting that this resistance is mediated by a dynamic interaction between the two cell types [124].

In addition to the BMSCs, other cell types within the bone marrow niche contribute to plasma cell survival, including eosinophils, monocytes/macrophages, dendritic cells and Tregs. These immune cells are frequently dysregulated in myeloma, both numerically and functionally, promoting a pro-tumour immunosuppresive environment.

Eosinophils

Eosinophils are known producers of crucial plasma cell growth factors such as IL-6, APRIL and TNFα [127][128] and are found in close proximity to plasma cells [129][130]. The number of eosinophils in direct contact with plasma cells substantially increases with disease progression, from approximately 20% in normal donors and MGUS, to 60-70% in MM [129], suggesting that these cells are a key component of the bone marrow niche. In concordance with this, eosinophils have been shown to support plasma cells *ex vivo* in a contact-independent manner [127][129]. Although clear components of the plasma cell niche, the essentiality of these cells has been challenging to determine.

An initial report by Chu *et al* suggested that eosinophils were a crucial component of the bone marrow niche [127]. Using ΔdblGATA-1.BALC/c mice, which exhibit a complete deficiency in eosinophils [131], Chu *et al* reported significantly lower bone marrow plasma cell frequencies, both at steady state and following antigen challenge. Bone marrow PCs were initially restored following the adoptive transfer of eosinophils from an immunocompetent mouse. In immunocompetent mice, eosinophil ablation using anti-Siglec-F (a cell surface

protein found predominantly on eosinophils) antibodies resulted in the rapid and substantial loss of established bone marrow plasma cells, suggesting that eosinophils were vital in maintaining bone marrow plasma cells. Wong *et al* [132] also reported that the growth of MOPC315.BM, an aggressive murine myeloma cell line, was delayed in both ΔdblGATA-1.BALB/c mice and in wild-type (WT) BALB/c mice following eosinophil depletion using an anti-IL-5 antibody. Wong *et al* also noted that only the bone marrow niche was affected, with no observable differences in MOPC315.BM frequencies in peripheral tissues between WT and ΔdblGATA-1 mice. A third group also reported a reduction in bone marrow PC frequencies following IL-5-antibody-mediated eosinophil depletion, that corresponded with a decrease in total IL-6 and APRIL mRNA [133].

Meanwhile, several other groups have tried and failed to demonstrate the essentiality of eosinophils in maintaining bone marrow PCs. Cravedi *et al* [134] reported no discernible differences in the frequencies of bone marrow PCs in ΔdblGATA1.BALB/c mice compared with WT mice at steady state, although there was a slight difference following alloantigen stimulation that coincided with an increase in splenic PCs. In sharp contrast, on the C57BL/6 (B6) background, they observed a reduced frequency of both bone marrow and splenic plasma cells in naïve ΔdblGATA1.B6 mice but any differences were lost following immunisation. Two other groups have also reported no discernible differences in bone marrow PC frequencies in either the ΔdblGATA1 mice or in immunocompetent mice following Siglec-F antibody mediated depletion[135][136]. Interestingly, Haberland *et al* initially reported a significant increase in the numbers of PCs within the bone marrow and spleen in the in ΔdblGATA-1 mice compared to WT controls. However, this was completely abrogated following backcrossing of these mice to the WT mice, suggesting that the discrepancies in these studies may have been caused by a difference in the microbiota as a result of the different facilities used to source the mice [136].

It therefore appears unlikely that eosinophils are absolutely vital for plasma cell survival in the bone marrow niche. There are many cellular sources of IL-6 and APRIL within the bone marrow, and it is possible there is a certain level of redundancy/flexibility. In line with this, ΔdblGATA-1 mice have been reported to also exhibit numerical and functional aberrations in basophils [137]. Basophils also express the IL-5 receptor [138] whilst a subset of monocytes have been reported to express Siglec-F [139] and so the reported loss in bone marrow plasma cells may have been a result of the disruption of several cellular components. Although not essential, eosinophils may still contribute to malignant plasma cell survival and promote an immunosuppressive environment through the production of anti-inflammatory cytokines

such as IL-4, IL-10, IL-13 and TGF-β [128]. Eosinophils also contribute to immunological tolerance by upregulating CD80 expression. CD80 binds cytotoxic T-lymphocyte–associated antigen 4 (CTLA-4) and PD-L1, two checkpoint molecules that provide inhibitory signals to immune effector cells [140]. In addition to immune evasion, eosinophils contribute to bone destruction through the secretion of IL-3 and monocyte chemoattractant protein-1 (MCP-1) [129].

Macrophages

Macrophages (Mϕ) have long been known to promote the survival and progression of a number of solid and haematological malignancies. These tumour-associated macrophages (TAM) closely resemble M2-macrophages (alternatively activated),which are involved in regulating the immune response, secreting high levels of anti-inflammatory cytokines [141]. These macrophages are therefore pro-tumorigenic, promoting immune evasion and are concordantly elevated in those patients with active MM (27%) compared to non-active myeloma, MGUS and control patients (9.2, 7.4 and 1.5% respectively) [142].

Mϕ infiltration is driven by a number of chemoattractants in the bone marrow, including MCP-1, also known as CCL2), CXCL12, macrophage inflammatory protein 1-alpha (MIP-1α, or CCL3), MIP-1β, CCL14 and CXCL10, that are upregulated in MM[143][141][144]. These chemoattractants stimulate macrophage proliferation, and in conjunction with other factors such as IL-10, promote the polarisation towards a TAM phenotype [141]. As well as promoting the infiltration and polarisation of Mϕs, myeloma cells also upregulate cell surface expression of CD47 [145]. CD47 is an integrin-associated receptor and acts as an immune checkpoint, binding signal regulatory protein alpha (SIRPα) on macrophages to inhibit phagocytosis of the tumour cell [145]. In a similar fashion, CD47 prevents cell killing by CD8+ T cells and attenuates the cross-priming abilities of dendritic cells, encouraging immunological tolerance [146].

In the bone marrow these polarised macrophages secrete high levels of IL-6 [147], IL-10 [141] and VEGF [145], promoting plasma cell survival, immune-suppression and neovasculogenesis respectively. TAMs also stimulate BMSCs, promoting an increased production of IL-6, CXCL10 and Regulated on Activation, Normal T cell Expressed and Secreted (RANTES, CCL5) [148]. It has been reported that patients with elevated levels of CXCL10 exhibit reduced CXCR3 expression on both peripheral blood and bone marrow natural killer cells. Disruption of the CXCR3 axis is associated with an impaired recruitment of NK cells

into the tumour and CXCL10 expression may therefore be another mechanism promoting immune evasion in myeloma [149]. Mϕ also protect myeloma cells from both spontaneous and drug-induced apoptosis in a contact-dependent manner [150].

Megakaryocytes

Megakaryocytes are also producers of IL-6 and APRIL and, similar to eosinophils and stromal cells, are in close contact with plasma cells within the bone marrow, constituting part of the niche [151][132]. Megakaryocyte-deficient mice (c-Mpl-/-) exhibit significantly reduced numbers of plasma cells within the bone marrow compared to WT mice, although interestingly, there were no differences in the frequencies of splenic plasma cells. Following immunisation, there were initially fewer numbers of antigen-specific bone marrow PCs in the c-Mpl-/- mice compared to controls. At a later timepoint, however, the frequencies of antigen-specific PCs between the two groups was comparable [151]. As previously mentioned, it may be that there is a level of redundancy within the bone marrow. In concordance with this, Wong *et al* [132] observed that megakaryocytes supported myeloma growth and survival only under suboptimal conditions.

Dendritic cells

Dendritic cells are crucial in mediating the anti-tumour response of the immune system. Tumour cells by themselves are poor antigen presenting cells and generally require assistance for the efficient stimulation of immune effector cells, such as cytotoxic CD8+ T cells. Dendritic cells, conversely, efficiently process and present captured tumour antigens on both MHC-class II and on MHC-class I (cross-presentation) to stimulate helper (CD4+) and cytotoxic T cells [152]. Because of their crucial role in priming the immune system, these cells are frequently targeted by the tumour. These dysregulated cells promote both the survival and immune-evasion of plasma cells and concordantly are identified in close proximity to these cells *in vivo* and at increased frequencies in the bone marrow of patients [153].

These dendritic cells predominantly protect malignant PCs from CD8+ T cell-mediated lysis. This protection appears to be mediated in a contact dependent manner, and *in vitro* is abrogated following the addition of a CD28-blocking antibody [154]. Plasma cell CD28 expression is upregulated in myeloma and the incidence of CD28+ cells increases with

disease progression, from 19% at MGUS to 93% at extramedullary disease. Serial studies in individual patients confirmed the emergence of CD28+ myeloma cells with tumoural expansion and therapeutic failure [155]. The binding of malignant plasma cells to DCs via CD28 stimulates dendritic cell IL-6 production as well as indoleamine 2,3 dioxygenase (IDO) [156]. IDO is a key anti-inflammatory factor and induces both T cell anergy, inhibiting cell activation and promoting apoptosis, and promotes the differentiation of naïve CD4+ T cells to the immunoregulatory Tregs [156][157] Additionally, DCs fail to upregulate the co-stimulatory molecule CD80 following activation, potentially as a result of the high levels of TGF-β and IL-10 within the myeloma bone marrow [158]. In addition to protecting MM cells from immune-mediated destruction, CD28-mediated interactions with DCs promote plasma cell survival and proliferation as well as a reduced sensitivity to drug-induced apoptosis [153].

T cells

Cytotoxic T lymphocytes are one of the predominant immune effectors capable of specifically recognising tumour-associated antigens to induce target cell lysis, either through the release of cytotoxic granules or through Fas-mediated apoptosis. Full T cell activation requires two independent signals. The first is the recognition of the MHC-bound antigen, shortly followed by the binding of T cell CD28 receptor to either CD80 or CD86 ligands. CD28 also binds to inhibitory ligands, known as checkpoint molecules, that regulate the immune homeostasis by dampening effector cell activation [159]. As with other immune effectors, these cells are dysregulated in cancer and cytotoxic T cell anergy is a frequent observation in MM patients. These cells exhibit a low proliferative response to stimuli and a reduced cytotoxic response as a result of impaired degranulation and cytokine secretion [160]. These anergic T cells upregulate the inhibitory checkpoint molecules, including PD-L1, CTLA-4, CD244 and CD160 and concurrently downregulate CD28 [160]. This is in part mediated by the upregulation of IDO within the tumour and impaired DC priming, but also through the upregulation of CD86 and PD-1 on MM plasma cells [161][162].

Regulatory T cell populations are also skewed in myeloma. These CD25+FOXP3+ T cells are crucial in maintaining homeostasis and self tolerance through the suppression of immune responses. This suppression is mediated through the production of IL-10 and TGF-β, limiting the expansion and functions of effector cells, inhibiting pro-inflammatory cytokine production and polarising DCs towards a tolerogenic phenotype [163]. The frequency of these cells in the bone marrow increases with disease stage and infiltration correlates with a lower OS [164]. Tregs may also directly promote myeloma cell survival and have been

shown to contribute to normal BM PC homeostasis. The loss of these cells following systemic infection correlated with a depletion in the frequencies of long lived plasma cells, that was rescued following administration of an IL-2-anti-IL-2 antibody complex that restored Treg frequencies [165]. The high levels of anti-inflammatory cytokines within the bone marrow promote Treg differentiation and enhance their recruitment into and activity in the tumour [163][120]. This includes the already mentioned IDO, IL-10 and TGF-β but also includes APRIL. Compared with CD25- conventional T cells, Tregs express significantly higher levels of the APRIL receptor, TACI. The APRIL/TACI axis inhibits caspase 3/7 and capase 8-mediated apoptosis, enhances Treg IL-10 and TGF-β secretion and potentiates Treg mediated suppresion of conventional T cells [120].

Other T lymphocyte subsets elevated in myeloma include Th22 and Th17 cells. The differentiation of Th17 cells from naïve CD4+ T cells is promoted in myeloma by the high tumour levels of TGF-β and IL-6. These cells are the predominant producers of IL-17 which exerts immuno-regulatory effects, triggering BMSC RANKL upregulation to stimulate osteoclastogenesis and thereby promoting bone re-absorption, and enhances myeloma cell proliferation and adhesion to BMSCs [166][167]. Th22 cells are also derived from CD4+ T helper cells, primarily involved in the secretion of IL-22. The frequency of these cells increases with disease progression and IL-22 has been shown to enhance myeloma cell growth and prevent drug-induced apoptosis [168].

Natural Killer cells

Natural killer cells are one of the most important regulators of cell-mediated cytotoxicity, involved in the killing of both cancerous and infected cells. NK cells, similarly to CD8+ T cells, exert their cytotoxic effects on target cells through the release of perforin/granzyme and the direct ligation of Fas-receptors. However, in contrast to T cells, NK cells are not regulated by antigen specificity. Instead they are capable of selectively targeting malignant cells without prior priming, regulated by a careful balance of inhibitory and activating receptors. Reactivity against 'self' is prevented by the inhibitory receptors which bind MHC Class I molecules and prevent NK cells from targeting normal, healthy cells [169]. 'Loss of self', the downregulation of MHC-Class I through cellular stress such as viral infection or malignancy, removes this inhibition and triggers cell lysis.

As myeloma progresses, NK cells generally exhibit a reduction in cytotoxic potential [170] as a result of the immunosuppressive environment within the tumour. The anti-

inflammatory cytokines already mentioned, including TGF-β and IL-10, trigger the downregulation of activating receptors on the NK cell surface, such as Natural Cytotoxicity Triggering Receptor 3 (NCR3), Natural killer group 2 member D (NKG2D), CD224, DNAX Accessory Molecule-1 (DNAM1) and CD335 [171][172]. Conversely, inhibitory receptors, such as PD-1, are upregulated [173]. These cytokines also suppress the secretion and activity of pro-inflammatory cytokines, such as IL-12 and IL-18, that activate NK cells [174], and IL-6 has been implicated in downregulating NK cell expression of perforin and granzyme B [175]. Myeloma cells are also capable of adapting their surface molecule expression to evade immune detection. Typically tumours are considered to downregulate MHC Class I molecules in order to prevent Cytotoxic T cell mediated killing, concurrently rendering these more susceptible to NK cell attack. Conversely, myeloma cells upregulate MHC Class I expression with disease progression that correlates with an increased resistance to NK cell-mediated cytotoxicity [176], suggesting that escape from NK cells is important in the pathogenesis of myeloma. Other mechanisms of immune escape involve the upregulation of inhibitory ligands, such as PD-1 ligand (PD-L1) [162], and the increased shedding of MHC Class I chain-related protein A (MICA) [177].

Regulatory B cells

A small subset of B cells, termed regulatory B cells (Bregs), also contribute to the immunosuppresive tumour microenvironment. The frequencies of these IL-10 secreting CD19+CD24^{hi}CD38^{hi} cells are significantly higher in newly diagnosed MM compared to patients on maintenance therapy [178] and have been implicated in attenuating NK cell ADCC against myeloma cells using elotuzumab [179].

Osteoclasts

One of the common features of disease in myeloma are bone lesions, with more than 80% of MM patients developing osteolytic bone disease [11]. Under normal physiologic states bone marrow remodelling is controlled by three cell types: osteoblasts, osteocytes and osteoclasts. Osteoclasts (OC) are involved in mediating bone resporption, whilst osteoblasts (OB) are involved in bone production [180]. In MM the OC-OB balance is disrupted and osteoclastogenesis is promoted whilst osteoblastogenesis is inhibited. As already mentioned, the VLA-4:VCAM-1 interaction between the stroma and myeloma cells promotes the secretion of several cytokines and growth factors. This includes the pro-osteoclastogenic cytokine

RANKL and IL-6. Simultaneously, these cells promote the downregulation of osteoprotegerin (OPG), an inhibitor of OC activation and differentiation. Other pro-osteoclastogenic cytokines and chemokines upregulated in MM include IL-1, IL-3, TNF-α, CCL3 and MIP-1α [181][182]. Malignant plasma cells also upregulate Dickkopf-1 (DKK1) that further blocks osteoblast differentiation [183], and CD47 expression. CD47 has already been described as preventing immune-recognition of the tumour, but may also contribute to the observed osteolytic disease. CD47-mediated contact promoted the differentiation of immature dendritic cells into multinucleated giant cells that bore functional and phenotypical similarity to OC. Blockade of CD47 inhibited osteoclastogenesis and reduced bone marrow resorption [184].

1.6 The treatment of myeloma

The last two decades have seen a dramatic improvement in the estimated OS for myeloma patients. This can almost certainly be attributed to the introduction of autologous stem cell transplantation (ASCT) and novel agents such as the proteasome inhibitors (PIs) and immunomodulatory drugs (IMiDs). These have become the mainstay of treatment for myeloma, typically used as multi-drug regimes in combination with chemotherapeutics and/or corticosteroids, although the specific combination depends on disease stage, health and fitness, prior lines of therapy and country legislation.

1.6.1 Autologous stem cell transplantation

For eligible patients (<65-75 years of age and generally low-risk), high dose myeloablative therapy followed by a stem cell transplant (HDT-ASCT) to repopulate the bone marrow is typically the first line of therapy. Initial reports demonstrated that HDT-ASCT dramatically improved both event-free and overall survival (OS) compared to conventional chemotherapeutics and as a result has been the mainstay of therapy for over 20 years [185].

1.6.2 Proteasome inhibitors

The ubiquitin-proteasome system plays an essential role in cellular protein homeostasis. Short-lived regulatory proteins such as those involved in cell cycle, DNA repair and apoptosis, as well as damaged and misfolded proteins, are targeted for degradation by ubiquitination. Polyubiquitinylated proteins are then detected and cleaved by the proteasome, a multicatalytic enzyme complex [186]. Proteasome inhibitors disrupt this system and prevent the

degradation of proteins, which accumulate within the cell and trigger endoplasmic reticulum (ER) stress. The cells response to this proteotoxic stress is the unfolded protein response (UPR) in an attempt to re-establish ER homeostasis. Failure of the UPR triggers cell cycle arrest and apoptosis [187]. Cancer cells, and especially plasma cells which secrete high titres of Ig, have an elevated proteasome activity and are considerably more sensitive to proteasome inhibition than other cell types [188].

Bortezomib (Velcade) reversibly inhibits the chymotrypsin-like activity of the proteasome [187] and was the first in class PI, receiving FDA accelerated approval in 2003 as a result of the dramatic survival benefits observed. In a phase III clinical trial comparing bortezomib and dexamethasone, survival at a median follow up of 22 months showed a 6-month survival benefit. This benefit was so considerable, that the high-dose dexamethasone arm was halted and all patients were offered bortezomib instead [189]. Although bortezomib has considered to be one of the predominant therapeutics behind the dramatic improvements in myeloma OS in the last two decades and despite initial encouraging results in individuals, resistance does occur and patients eventually relapse. This resistance is mediated through several mechanisms, including the upregulation of the proteasome subunits and mutations in the bortezomib binding domain [190]. This has led to the advent of second generation PIs, such as carfilzomib, ixazomib and oprozomib and encouragingly, thus far there appears to be no cross-resistance between bortezomib and carfilzomib [191]. However, because the of the ubiquitous expression of the proteasome, there is the likelihood of numerous off-tumour effects. As a result, recent research has focussed on upstream targets, such as NEDD8. NEDD8 is a ubiquitin like protein, regulating the activity of the cullin RING (really interesting new gene) ubiquitin E3 ligase family. However, thus far, these avenues have been fairly disappointing, and the leading therapeutic, MLN4924 (pevonedistat), has shown limited efficacy in RRMM patients in a phase I trial, achieving stable disease (SD) as a best result [192].

1.6.3 Immunomodulators

Despite its notoriety, thalidomide has emerged as an efficacious treatment for myeloma and has become one of the mainstays of therapy. Thalidomide was initially trialled in cancer more than 50 years ago in 1965 due to its anti-angiogenic properties [193]. Despite demonstrating anti-myeloma activity, thalidomide did not receive any further interest until the late 90's when Singhal *et al* trialled the immunomodulator (IMiD) in five patients with end-stage myeloma as a 'compassionate-use protocol'. One patient with more than 95% plasma cell infiltration in the bone marrow, who had been unresponsive to multiple salvage therapies,

showed a dramatic improvement with nearly a complete remission within three months [194]. As a result thalidomide was introduced for the treatment of myeloma in combination with dexamethasone in 2006. A close derivative, lenalidomide, was also approved in the same year for RRMM and in 2015 for newly diagnosed patients. The exact mechanism of these agents was largely unknown for several years and they were broadly classified as IMiDs for their immunomodulatory actions, enhancing the activation and cytolytic activity of NK cells [195] and inhibiting Tregs [196]. These anti-angiogenic agents potentiate the effect of dexamethasone and PIs and have also been shown to induce apoptosis and G1 arrest in myeloma cells, as well as downregulating IL-6 and TNFα production [197].

More recently, the primary target of thalidomide and its derivatives has been reported as cereblon (CRBN) [198]. CRBN is a component of the cullin-4 RING E3 ubiquitin ligase, part of the ubiquitin-proteasome pathway. Thalidomide/lenalidomide prevent the ubiquitination and degradation of CRBN, stabilising this ubiquitin ligase complex and promoting the ubiquitination and degradation of target proteins, including IKAROS Family Zinc Finger 1 and 3 (IKZF1 and IKZF3) [198]. These two proteins are implicated in a number of cellular processes, particularly in B and T cells, including IKZF3 in the repression of IL-2 expression [199]. Similarly to PIs, patients eventually become resistant to IMiDs, although there appears to be no cross-resistance between these two agents or a third IMiD (pomalidomide) [200]. Having recently identified the predominant target of IMiD activity, novel immunomodulators are arising that specifically target CRBN. This includes CC-122 (avadomide), CC-220 and CC-90009, all of which are in early-stage clinical trials for haematological malignancies. Thus far, CC-122 has shown early promise as a single-agent, with an overall response rate (ORR) of 18% in heavily pre-treated RRMM [201].

1.6.4 Chemotherapeutics

The alkylating agent, melphalan, has been used as a front-line therapy in combination with steroids for myeloma for over 50 years [202]. Melphalan induces multiple DNA cross-links, disrupting DNA replication and transcription and promoting cell death by apoptosis [203]. Despite its efficacy, melphalan is associated with severe side effects including bone marrow suppression and the long-term risk of leukaemia/myelodysplastic syndrome [204]. Cyclophosphamide is another routinely used alkylating agent that has demonstrated equivalent efficacy to melphalan, but a much more favourable toxicity profile [205]. Despite initial efficacy, patients inevitable acquire resistance to the agents through the upregulation

of drug-efflux pumps and the overexpression of DNA repair proteins [206].

To combat resistance, more alkylators are being introduced for the treatment of myeloma, including bendamustine which was recently licenced in Europe for MM. This is an old alkylating agent that exerts its anti-cancer effect in a unique mechanism compared to other alkylators [207]. Bendamustine has been shown to be both efficacious and well tolerated in both RRMM and newly diagnosed MM in combination with bortezomib and prednisolone or with thalidomide and dexamethasone [208][209]. Importantly, this chemotherapeutic has demonstrated efficacy in disease that is refractory to other alkylating agents [207]. Other agents include tinostamustine, a fusion molecule of bendamustine and the histone deacetylase inhibitor vorinostat [210]; evofosfamide, a hypoxia-activated prodrug of the DNA alkylator bromo-isophosphoramide mustard [211]; and melflufen, a melphalan pro-drug [212].

1.6.5 Corticosteroids

Alongside melphalan, corticosteroids such as dexamethasone have long been used in the treatment of myeloma. These synthetic steroid hormones induce cell cycle arrest and apoptosis following binding to and activation of the glucocorticoid receptors [213]. In conjunction with their cytotoxic effects, corticosteroids can also be used to decrease the severity of chemotherapeutic side effects, acting as antiemetics and relieving high fever, weakness and fatigue [214]. However, resistance does occur as cells both downregulate the number of receptors and express alternative isoforms [215].

1.7 Novel therapeutic agents

Despite the recent improvements in myeloma OS, the disease is still considered incurable and the majority of patients are expected to eventually relapse and become refractory to all available lines of therapy. These patients have an incredibly poor outlook. In a study undertaken by the International Myeloma Working Group (IMWG) to assess the outcome of these patients, they reported that individuals who had become refractory to bortezomib and at least one IMiD had a median event-free survival and overall survival of just five and nine months respectively [216]. This study highlights the need for therapeutics with new

mechanisms of action to treat these refractory populations.

1.7.1 Small molecule inhibitors

Numerous small molecule inhibitors have been trialled in myeloma in an attempt to increase specificity of treatment and to reduce the side-effects commonly associated with traditional chemotherapeutics. This includes histone deacetylase (HDAC) inhibitors, such as panobinostat, the first and only HDAC inhibitor to receive FDA approval for the treatment of RRMM. These inhibitors inhibit the formation of aggresomes (aggregation of misfolded proteins), triggering the UPR, and increase the acetylation of proteins involved in numerous oncogenic pathways [217]. Other small molecule inhibitors currently under investigation include afuresertib, an inhibitor of the serine/threonine protein kinase Akt; ABT-199 (Venclexta), a BCL-2 inhibitor; the BTK inhibitor ibrutinib; CDK inhibitor dinaciclib; kinesin spindle protein inhibitor filanesib; as well as various other PI3K, MDM2 and kinase inhibitors [218].

1.7.2 Immumnotherapy

Recently, there has been a surge of interest in immunotherapy for the treatment of myeloma. This covers a broad spectrum of approaches to stimulate or enhance the immune system to attack the tumour and includes the adoptive transfer of T cells, monoclonal antibodies and oncolytic viruses. Haematological malignancies are considered to be particularly amenable to immunotherapy for several reasons. Firstly, as part of the haematopoietic system, these cells are in constant contact with immune cells and are localised to where adoptively transferred T cells will naturally home to. Additionally, these cells are routinely subject to immune regulation and are therefore immunostimulatory by nature. In contrast to solid tumours, these malignancies are much easier to penetrate, and sampling is relatively easier for assessing therapeutic efficacy. Finally, the cell surface of many haematopoietic cells has been extensively characterised and there are several well-established antigens to target [219].

CAR T cells

Chimeric antigen receptor (CAR) T cells are genetically engineered T cells. These cells have been modified to express a tumour antigen-specific receptor that is comprised of a single-chain variable fragment (similar to an immunoglobulin) linked to an intracellular T

cell signalling domain. This redirects patient derived T cells against the tumour [220]. These have shown promising success in a number of haematological malignancies, including acute lymphoblastic leukaemia (ALL), chronic lymphocytic leukaemia (CLL), diffuse large B-cell lymphoma (DLBCL) and Non-Hodgkin lymphoma (NHL) [220]; and are being investigated in myeloma, with more than 35 active registered CAR T cell clinical trials [221]. The most advanced CAR T cell therapy for myeloma is bb2121, targeting BCMA. bb2121 has shown early promising activity, with an ORR of 89% in heavily pre-treated patients. These patients had received a median of 7 prior lines of therapy including a proteasome inhibitor and an IMiD, involving 29% who were refractory to bortezomib, lenalidomide, carfilzomib, pomalidomide and daratumumab, demonstrating that these novel CAR T cells can be used to circumvent current mechanisms of resistance [222].

Oncolytic viruses

Oncolytic viruses are another promising, novel approach for the treatment of myeloma. These modified viruses specifically infect, replicate in and kill tumour cells. The release of tumour antigens following target cell death triggers a second response against the tumour, stimulating the immune system to target the remaining, antigen-expressing tumour cells. Several clinical trials are currently ongoing, including a phase I/II trial using the Edmonston strain of measles virus engineered to express the human sodium iodine symporter (MV-NIS). This virus enters the cells through CD46, a cell surface protein upregulated in MM [223] and concentrates radioactive iodine within the myeloma cells [224].

Monoclonal antibodies

Amongst the novel immunomodulatory agents, one of the most promising and advanced areas of development has been in monoclonal antibodies (mAb), with two recent FDA approvals for their use in myeloma. The use of monoclonal antibodies for the treatment of cancer is not novel and it has now been more than 20 years since the FDA approval of the first therapeutic antibody for cancer, rituximab (Rituxan) [225]. Since then, antibody therapy has revolutionised the treatment for both solid and haematological malignancies, with more than 20 antibodies currently FDA approved [226]. These antibodies have become increasingly popular as therapeutics for a number of reasons. Firstly, unlike small molecules, they are highly specific for their target and as a consequence tend to exhibit much fewer side effects. As a result of this specificity, side effects also tend to be much more predictable, and in

combination with recombinant manufacturing technology, these antibodies tend to have a much shorter development time compared to traditional small molecule drugs. Furthermore, these antibodies are less likely to exhibit drug-drug interactions with other agents and because of their distinct mechanisms of action, can be used in multi-drug combinations. These molecules also tend to have long half-lives and can be administered on a less frequent dosing schedule (typically weekly to start and then fortnightly or even every three weeks) than conventional chemotherapeutics [226][227][228].

These therapeutic antibodies mediate tumour cell elimination through a variety of mechanisms. As already mentioned (section 1.4.1), these antibodies can target a tumour cell for immune-mediated killing via ADCC, ADCP or CDC. Alternatively, these antibodies can directly ligate tumour cell surface receptors, triggering apoptosis or inhibiting essential growth factor signalling cascades or can target immune cell surface receptors, enhancing their activation or reversing immune-suppression. In addition, antibodies may also be directly conjugated to cytotoxins as antibody drug conjugates (ADCs) [226].

Daratumumab
Daratumumab is a first in class, fully human IgG1 monoclonal antibody targeting CD38, a type II membrane glycoprotein. CD38 is a nucleotide-metabolising ectoenzyme and receptor, involved in mediating migration, bone marrow stromal cell adhesion and signal transduction; and is expressed on nearly all other lymphoid and myeloid cells, as well as non-haematopoietic tissue [229]. The high expression of CD38 on myeloma cells, as well as its receptor function, made CD38 an attractive target for a therapeutic monoclonal antibody for myeloma.

Daratumumab was initially identified from a panel of 42 CD38-targeted human mAbs as the only antibody that induced ADCC and CDC in myeloma cell lines, subsequently demonstrating anti-tumour activity in an *in vivo* xenograft model [230]. Daratumumab has since been shown to also mediate myeloma cell death through ADCP [231]. Daratumumab demonstrated encouraging results in early clinical trials and was well-tolerated with single-agent efficacy in heavily pre-treated RRMM with an ORR of 31% in a combined analysis of the phase I/II GEN501 and phase II SIRIUS study [232]. The addition of lenalidomide/bortezomib and dexamethasone further enhances daratumumab activity and this multi-drug combination significantly prolonged progression-free survival (PFS) from just 7.1 months for bortezomib and dexamethasone alone to 16.7 months (POLLUX trial, median) [233]. The triplet combination of lenalidomide-dexamethasone and daratumumab

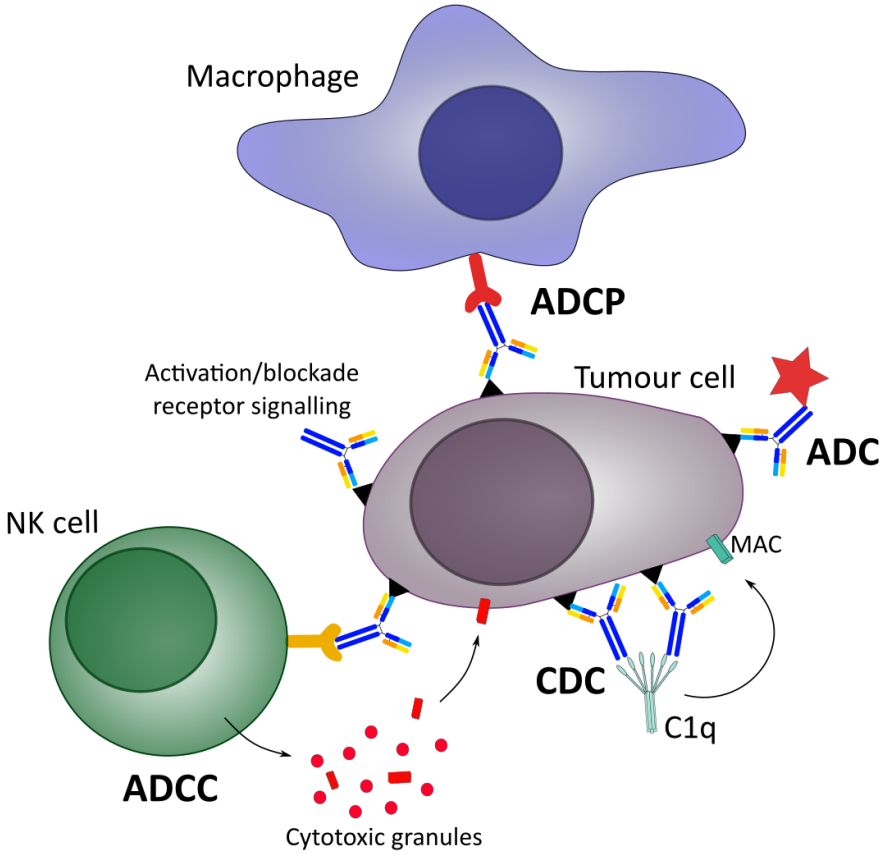

Fig. 1.3 *Mechanism of action for therapeutic monoclonal antibodies.* Therapeutic antibodies can be utilised in cancer in several ways. Antibodies can be targeted directly against the tumour cell to induce apoptosis, prevent receptor-ligand interactions or deliver toxins directly to the tumour. Alternatively, mAbs can be used to enhance immune responses against the tumour cell. ADCC=Antibody dependent cell-mediated cytotoxicity. CDC=Complement dependent cytotoxicity. ADCP=Antibody dependent cellular phagocytosis. MAC=Membrane attack complex.

was approved both by the FDA in 2016 and early this year as a monotherapy by The National Institute for Health and Care Excellence (NICE), although only as a fourth-line agent for RRMM patients in England and Wales [234].

Aside from mediating direct myeloma cell cytotoxicity through ADCC/CDC, daratumumab also targets the immunoregulatory compartment within the tumour microenvironment [178]. As aforementioned, CD38 is highly expressed on numerous leukocytes, including NK cells, monocytes, B cells and T cells. Both Bregs and Tregs are sensitive to daratumumab. Following treatment, there is a significant reduction in the frequencies of both of these populations, reversing immune suppression and allowing the expansion and activity of the pro-inflammatory, anti-tumour immune cell populations. Furthermore, CD38 has been implicated in the formation of osteoclasts and treatment with daratumumab has been observed to reduce both the number and activity of these immunosuppresive cells, which may further contribute to promoting an anti-tumour immune response [235].

The promise of CD38 has led to the advent of other CD38 targeting antibodies: such as isatuximab. This monoclonal antibody binds a distinct epitope, directly inducing apoptosis and inhibiting enzyme activity, as well as triggering cell death through ADCC, CDC, and ADCP [236]. Following on from a promising phase II trial, ORR of 50% as a single agent [237], isatuximab is currently recruiting for phase III trials (IKEMA (NCT03275285) and IMROZ (NCT03319667)).

Elotuzumab

Elotuzumab is another first in class, humanised IgG1 antibody that targets Signalling lymphocytic activation molecule F7 (SLAMF7, also known as CS1 and CD319), a type I membrane protein. SLAMF7 was initially identified by an extensive bioinformatic analysis of genes upregulated in plasma cells compared to normal B cells [238], although it has been subsequently shown to be expressed on numerous leukocyte subsets including NK cells, NK-like T cells, CD8+ T cells, monocytes and dendritic cells [239]. Similar to daratumumab, elotuzumab mediates myeloma cell killing through ADCC and CDC [238]. However, despite demonstrating a favourable safety profile, elotuzumab does not demonstrate any single agent activity, with no objective responses achieved in a phase I trial [240]. A follow up phase I/II trial demonstrated that, despite this, elotuzumab acted synergistically with lenalidomide and dexamethasone and a phase III trial reported a modest improvement in PFS and OS (4.1 months for both) with an equivalent safety profile at a three year follow up compared to lenalidomide-dexamethasone alone in RRMM [241]. Elotuzumab also indirectly medi-

ates anti-tumour activity by targeting the SLAMF7-expressing NK cells. Antibody binding provides a co-stimulatory priming signal, enhancing the activity of these anti-tumour cells [239]. Currently elotuzumab is FDA approved, and although it is approved for use in Europe, elotuzumab has not received NICE approval for use in the UK by the NHS [242].

Checkpoint inhibitors

As already eluded to in section 1.5, the immune system is constantly regulated by a carefully controlled balance of positive and negative signals to maintain immunological homeostasis. Tumours take advantage of these inhibitory signals to promote immunological tolerance, upregulating negative co-stimulatory molecules such as PD-L1. These checkpoint molecules are key inhibitors of immune activation, and therapeutic blockade may have the potential to reverse the immunosuppressive tumour microenvironment and enhance the anti-tumorigenic immune response. However, thus far checkpoint inhibitors have proven disappointing in early clinical trials with limited efficacy as a single agent although they may act in synergy with immunomodulators such as lenalidomide [243][244].

Antibody drug conjugates (ADCs)

Although naked antibodies that trigger immune-mediated killing have shown encouraging results, these are heavily reliant on a fully functioning immune system. In myeloma, and many other cancers, the immune system is frequently dysregulated and myeloma NK cells have been shown to be much less effective than their normal counterparts at mediating ADCC by elotuzumab, partly explaining its poor single agent efficacy [245]. As a result, these antibodies are commonly used in combination with chemotherapeutics to achieve anti-tumour efficacy, and as a result, systemic toxicities are still a concern [246]. In contrast to naked antibodies, ADCs do not rely on a fully functioning immune system and instead combine the specificity and stability of antibody therapeutics with the cytotoxicity of chemotherapeutics or radioisotopes. These antibodies recognise specific tumour antigens and, following tumour cell binding, are internalised. Once in the cytoplasm, the linker between the antibody and toxin is cleaved by various methods, releasing the cytotoxic payload and inducing cell death [247]. Although ADCs offer several advantages over naked antibodies, their challenging development has hindered the availability of these antibodies in the clinic. One of the predominant difficulties faced by these first-generation ADCs included the highly heterogenous conjugation methods resulting in variable drug:antibody ratios (DAR) [248], with one report observing a DAR as variable as 0 to 6 in one batch. This DAR is highly critical, too low and the drug is not potent enough, meanwhile, too high and the ADC may aggregate [249].

Furthermore, the linkers of these early ADCs were highly unstable, deconjugating in the plasma and releasing the payload before reaching the tumour [249]. The introduction of site-specific conjugation techniques and improved linkers in the third- and fourth-generation ADCs have overcome these hurdles, and the full potential of ADCs is now being realised with more than 100 ADC clinical trials currently active [221], several of which are for myeloma.

The most advanced and promising ADCs currently under trial in myeloma are lorvotuzumab mertansine, indatuximab ravtansine and GSK2857916. Lorvotuzumab mertansine is a CD56 (NCAM-1) targeted antibody conjugated to the maytansinoid mertansine (DM1), that was both well-tolerated and achieved an ORR of 18% as a single agent and 58% with lenalidomide-dexamethasone in a phase I trial in RRMM [250][251]. Indatuximab ravtansine is an anti-CD138 antibody conjugated to DM4 that shown encouraging activity, achieving an ORR of 78% in combination with an immunomodulator and dexamethasone [252][253]. One of the most promising ADCs thus far is GSK2857916, targeting BCMA. As a single agent, GSK2857916 demonstrated an ORR of 60% in a phase II study and was recently granted FDA breakthrough therapy designation for RRMM [254]. Other ADCs currently in or have recently completed early phase trials includes the anti-CD74 hLL1-DOX (NCT01101594), another BCMA-directed ADC MEDI2228 (NCT03489525), the anti-CD48 SGN-CD48A (NCT03379584), a CD46-ADC FOR46 (NCT03379584) and SGN-CD352A (NCT02954796) against CD352 (SLAMF6) [221], but the results from these trials have not yet been released.

These ADCs have demonstrated proof-of-concept clinical success in myeloma, with encouraging safety profiles. However, several of these agents have failed to demonstrate significant single-agent activity. Furthermore, resistance to some naked antibodies, such as daratumumab, is beginning to emerge [255] and as such there is still an urgent requirement for the discovery and characterisation of novel antibody targets.

1.8 Plasma membrane profiling

1.8.1 The plasma membrane as a drug target

Membrane proteins play an essential role in nearly all cellular processes, involved in the transduction of growth, proliferation and survival signals; movement of substances across the membrane; adhesion; migration; and regulation of the immune system. As such these proteins are of significant interest as therapeutic targets. This is evidenced by the fact that

although they only compromise 20-30% of the human proteome, they make up more than half of all current drug targets [256].

In addition, these molecules are much more accessible for therapeutic modulation compared to intracellular targets, particularly in the case of monoclonal antibodies. These therapeutic agents are too large to pass through the cell membrane and the majority of them rely on their effector functions to mediate cell killing, requiring extracellular accessibility to recruit immune effector cells. As a result, nearly all antibody therapies target extracellular antigens [257]. Although the cell surface proteome represents a highly attractive therapeutic target, analysis of these proteins has been considerably difficult.

One common technique is to use gene expression profiling (GEP), relying on mRNA abundance as a surrogate for protein expression, and has been used with some degree of success [238]. However, gene expression is regulated by numerous factors, both pre and post-transcriptionally and as a consequence, the overlap between gene and protein expression is low [258]. Interestingly this may depend on the function of the gene. For instance, a few studies have reported that some genes, such as structural genes, have a very high correlation whilst those genes involved in signal transduction and the regulation and development of biological processes tend to have a very poor correlation between mRNA and protein abundance [259][260]. Recently, Dytfeld *et al* attempted to identify differentially-regulated proteins indicative of a very good partial response or greater to bortezomib and observed that nearly all of the 166 proteins identified by GEP were different to those identified as differentially regulated by mass spectrometry [261]. Overall, RNA can be considered a poor approach for the identification and characterisation of novel plasma membrane protein targets.

Proteomics on the other hand, allows the direct comparison of not only protein expression between groups but also provides information on protein-protein interactions and post-translational modifications. As already discussed, several proteins have already been identified as potential targets for myeloma. The majority of these, including CD38, CD46, CD48 and CD352 [262][223][263][264], were identified by flow cytometry, either relying on published literature that suggested a role in other neoplasms or PC differentiation or by arbitrarily testing panels of newly described antibodies. Not only is this approach highly restricted by the availability of reliable antibodies and/or prior knowledge but is also highly limited by the number of proteins that can be analysed at once.

1.8.2 Plasma membrane proteomics

Mass spectrometry (MS) is a powerful analytical technique capable of quantifying thousands of proteins in a single run. Peptides are initially ionised and then separated according to their mass-to-charge ratio *(m/z)*. The resultant protein mass 'fingerprints' are then used to identify each protein and the relative abundance of each ion used for quantification [265]. This technique has provided invaluable insight into the myeloma cell proteome but has traditionally been limited in its detection of membrane proteins due to their relatively low abundance. As already mentioned, these proteins make up less than a third of the whole cell proteome and are easily obscured by the vast array of highly expressed intracellular proteins, resulting in their significant under-representation in whole cell proteome studies [266]. Pre-fractionation enrichment is therefore vital to reduce the complexity of the sample and to enable the identification of these low-abundance proteins. A number of methodologies have been utilised, such as 2-DE (2-dimension electrophoresis) separation, isolation by physiochemical properties or enrichment by affinity-based approaches.

2-dimension electrophoresis

2-DE has been the traditional approach for the analysis and separation of proteins in complex samples. The first step in 2-DE is the separation of proteins by their isoelectric point, the pH at which the molecule has neutral charge, across an immobilised pH gradient. Proteins are then resolved according to their molecular weight as in polyacrylamide gel electrophoresis (PAGE). Gels can then be stained using silver, coomassie or fluorescent dyes to compare the relative protein expression between of samples between gels. Unknown proteins are then excised, digested and identified by peptide mass fingerprinting of tandem MS [267]. Although 2-DE has been the staple of quantitative protein analysis for the last few decades, this technique often struggles with reproducibility and is limited in its detection of membrane proteins. These proteins are typically hydrophobic as a result of their transmembrane domain and as a result require strong detergents to solubilise them, which may slow or skew protein migration [268]. These highly hydrophobic proteins also tend to precipitate at their pI, preventing them from entering the acrylamide gel [268]. Furthermore, membrane proteins are also frequently quite large proteins, and may fall outside of the 2-DE range (10 to 150kDa) [269].

Density gradient centrifugation

An alternative, crude approach is density gradient centrifugation, using sucrose to separate membrane fractions from other subcellular structures. However, because plasma membranes exhibit similar physiochemical properties to other intracellular membranes, there is often a high level of contamination from other subcellular membranes such as mitochondria, golgi and rough ER and the overall enrichment is often low (less than 30%) [270]. Although the reported enrichment has improved with the addition of a two-phase aqueous polymer partition, the overall number of plasma membrane proteins identified has been low, ranging from 105 to 580 proteins [270][271][272].

High pH and proteinase K

The high pH and proteinase K method offers a substantial improvement over this crude technique. Agitation at a high pH favours the formation of membrane 'sheets' and protease accessible peptides are then cleaved from the membrane using proteinase K (a serine protease with a broad cleavage specificity) and separated by centrifugation. Using this technique, Blackler *et al* reported a 72% enrichment for integral membrane proteins, although the total number of plasma membrane proteins identified was still low [273]. It is also possible that, using this technique, many proteins that don't have a cleavage site or are inaccessible are excluded from analysis.

Colloidal silica-beads

Colloidal silica-beads have also been used to varying success. A thin layer of cationic colloidal silica-microbeads are applied to intact cells, forming an ionic interaction with the anionic phospholipid head groups of the membrane. Microbeads are subsequently cross-linked by an anionic polymer and cells are lysed. This results in the formation of a large, open sheet with the associated plasma membrane which can be easily separated from cell debris and lysate by centrifugation. Membranes are then washed and solubilised by sodium dodecyl sulfate (SDS) [274]. The reported enrichment using this technique widely varies, from 16 to 81% and often the total number of plasma membrane proteins identified ranges from less than 100 to just under 400 proteins[275][276][277][278].

Affinity purification

Alternatively, plasma membrane proteins can be extracted from whole cell lysates using affinity purification. Many membrane proteins are glycosylated [279] and can be recognised and captured by immobilised lectins [280]. Overall, the enrichment using this technique has been high (41 to 88%) but similar to the aforementioned techniques, yields a low number of proteins, commonly between 100 and 250 [281][282][283].

Similar to lectin-affinity purification, cell surface proteins can be biotinylated and captured by immobilised streptavidin. Commonly used is the amine-reactive N-hydroxysulfosuccinimydyl-S,S-biotin (NHS-SS-biotin). However, although reported to be membrane impermeable, a few studies have observed the specific-labelling of intracellular proteins suggesting that it at least partially membrane-permeable and as a result, the reported enrichments are highly variable (16 to 67%) [284][285][286].

Cell surface proteins can also be biotinylated using aminooxy-biotin. Aldehydes are introduced onto sialylated plasma membrane glycoproteins by periodate oxidation, subsequently followed by the oxime ligation of the aminooxy-biotin to these aldehydes [284]. Because these sialylated glycoproteins are restricted to the PM and subcellular organelles of the secretory and endocytic pathways of cells and both the periodate and aminooxy-biotin are cell impermeable at 4°C, this technique yields biotin-labelling that is cell surface only [287]. This technique has been optimised by Weekes *et al* and has been coined as plasma membrane profiling (PMP) [288]. This technique not only substantially enriches for plasma membrane proteins (68%), but also identifies upwards of 700 proteins [288]. PMP has already been successfully applied by the Lehner group to elucidate protein interactions [288] and to identify proteins involved in mediating immune evasion [289][290].

1.8.3 Protein quantification

Although mass spectrometry is capable of identifying hundreds to thousands of proteins, it is not inherently quantitative and several strategies can be employed to enable the relative and absolute quantification of identified proteins. Labels can be either incorporated onto peptides before analysis or can be directly quantified using label-free strategies.

Label-free proteomics

Due to their associated low-costs label-free proteomics are becoming increasingly popular. Protein abundance is estimated using either the number of spectra detected for each protein or from the chromatographic peak intensity [291]. Despite recent improvements, these techniques are still considered inaccurate and perform poorly with proteins with low-spectral counts, greatly reducing the quantifiable number of proteins within a sample or resulting in an underestimation of abundance [292][293]. Conversely, label-based techniques are considered to be much more accurate, although potentially at the cost of the total number of proteins identified [293].

Isotope labelling

Traditionally peptides have been labelled using stable isotope labelling by amino acids in cell culture (SILAC). 'Heavy' or 'light' amino acids are introduced into the culture medium and are metabolically incorporated into proteins as cells proliferate and grow [294]. 'Heavy' and 'light' samples are then combined before digestion and further downstream processing. During LC (liquid chromatography)-MS/MS analysis, the labelled peptides elute simultaneously and the relative abundance ratio is used to infer protein abundance. This technique has been utilised in myeloma to elucidate novel signalling proteins and pathways involved in proteasome inhibition [295] and to explore protein-protein interactions [296]. However, it is fairly limited in its use for primary samples that do not grow well *ex vivo* such as myeloma cells and in both of these studies, the authors relied on the use of human myeloma cell lines (HMCLs).

An alternative to metabolic labelling that is amenable to the low-proliferative nature of plasma cells is the labelling of digested peptides using isotope tags, such as ICAT (isotope-coded affinity tag). The ICAT reagent is comprised of three elements, a cysteine reactive group to enable peptide binding, a biotin tag for affinity purification, and an isotopically labelled linker. This linker may be either 'heavy' or 'light' depending on whether it contains eight deuterium or hydrogen atoms. Enriched protein samples are digested, labelled and then combined before MS analysis. Similar to SILAC, 'heavy' and 'light' peptides co-elute following LC and the relative abundance of each sample is determined by the signal intensity ratio of the peptide pair [297]. Although this technique can be used with primary samples that grow poorly *ex vivo*, there are several disadvantages. One common problem with isotope labels is that there is a slight separation of the heavy and light peptides and as a result they

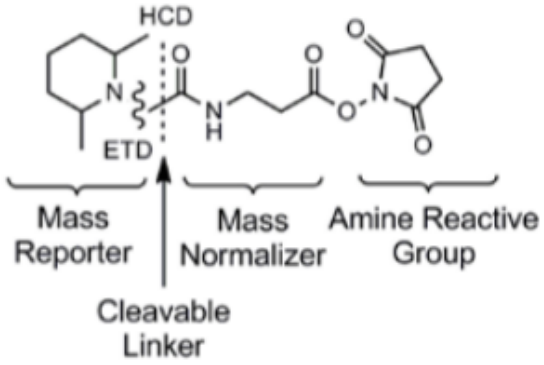

Fig. 1.4 *Overview of the TMT label.* The TMT label consists of a mass reporter, an amine-reactive NHS-ester group and a linker (mass normalizer). All labels within a set share an identical structure but different numbers and combinations of ^{13}C or ^{15}N. (Thermo Fisher Scientific)

may elute as separate fractions compromising sensitivity and accuracy. This can also lead to redundancy, resulting in an under-sampling of the proteome [298]. Additionally, as with SILAC, this technique is limited to just two samples.

Isobaric tags

Unlike isotope tags, isobaric tags have identical mass, resulting in identical mobility and subsequent co-elution during MS analysis. These isobaric tags are comprised of an amine reactive moiety for peptide binding, a mass reporter tag with a unique number of ^{13}C or ^{15}N substitutions and a mass normaliser that balances the tag mass so that all tags within a set have the same mass (fig 1.4). During tandem mass analysis, fragmentation of the label releases the mass reporter tag to produce a unique reporter ion mass. The relative intensities of these reporter ions can be used for relative quantification of the samples [298]. Two commercial tags are available, the isobaric tag for relative and absolute quantitation (iTRAQ) and the tandem mass tag (TMT). Both enable the simultaneously analysis of 4, 6, 8 or 10 biological samples, representing a significant improvement over isotope-labelling techniques. By labelling the peptides directly and not relying on the incorporation of labelled amino acids, freshly isolated myeloma cells can be quantitatively analysed [286][299][261].

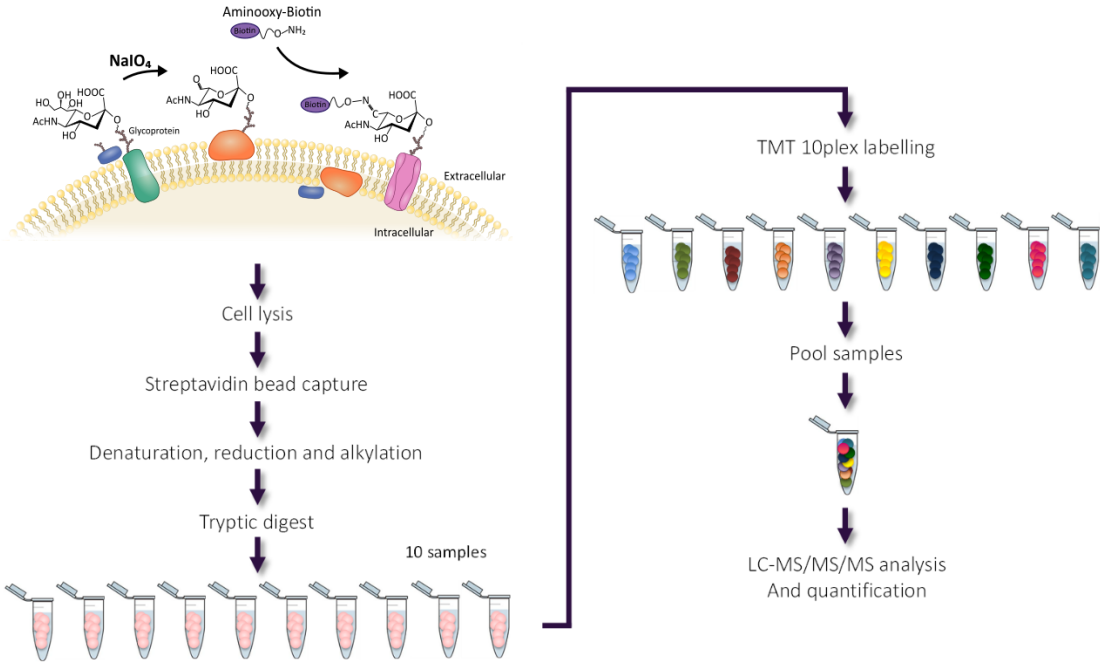

Fig. 1.5 *Overview of the PMP and TMT labelling workflow.* Cell surface proteins are biotinylated and isolated from whole cell extracts using affinity purification before denaturation, reduction, alkylation and digestion. Peptides are then labelled with isobaric mass tags (TMT 10plex) and analysed on a nanoLC-MS3 platform. Spectra are mapped against and annotated using the Uniprot human database.

1.9 Aims

As discussed in section 1.8.2, a number of mass-spectrometry-based approaches have been undertaken to characterise the cell surface proteome. However, the number of proteins identified using these techniques have generally been low, in the range of a few hundred, or have not been quantitative. Furthermore, those few studies that have been undertaken in myeloma have relied on using HMCLs or have not enriched for plasma membrane proteins [261][286][295][299]. Although these studies represent significant improvements over other techniques such as flow cytometry, Western Blot and GEP, the myeloma cell surface proteome is still uncharacterised and there are likely to be many unidentified proteins. As these proteins play an essential role in tumour survival, mediating immune evasion, promoting drug resistance and transducing growth signals, they are of great interest as novel therapeutic targets and prognostic biomarkers.

This thesis is split into three sections, with the overall aim of identifying and characterising a novel antibody drug conjugate target for the treatment of multiple myeloma.

In the first section of this thesis I aim to quantitatively characterise the myeloma cell surface proteome using the relatively novel technique, plasma membrane profiling, in both HMCLs and in primary disease. I then aim to demonstrate this technique provides an accurate and quantitative representation of the plasma membrane by validating this dataset using flow cytometric techniques. As HMCLs are genetically well-characterised, I also aim to compare protein and RNA expression to determine any associations with the underlying genotype that may help elucidate the molecular consequences of these genetic events. Finally, I aim to use this dataset to identify a list of novel candidate ADC targets.

In the second section of this thesis I aim to establish a recombinant protein mammalian expression system to facilitate antibody generation. It is expected that a number of the identified targets will not have commercial or reliable antibodies available and it will be necessary to generate tool antibodies for further characterisation of these top targets.

In the final section of this thesis my aim is to characterise those novel targets that already have commercially available tool antibodies. I will use these antibodies to assess off-tumour expression in healthy tissue and on-tumour expression in a larger sample population. For any candidates that demonstrate an acceptable expression profile, I will assess whether these proteins are internalised to deliver a cytotoxin and trigger myeloma cell death. Finally, I aim to elucidate the function of these targets in myeloma cell biology using RNAi.

Chapter 2

Materials and Methods

2.1 Cell culture

2.1.1 Media

Complete RPMI: Roswell Park Memorial Institute (RPMI) 1640 medium (Life Technologies) supplemented with 10% heat-inactivated fetal bovine serum (FBS, S. American Origin, Life Technologies) and 1% GlutaMax (Life Technologies).
Complete DMEM: Dulbecco's Modified Eagle Medium (DMEM) (Life Technologies high D-glucose (4.5g/L)) supplemented with 10% heat-inactivated FBS and 1% GlutaMax.
Complete IMDM: Iscove's Modified Dulbecco's media (IMDM) (Life technologies) supplemented with 10% heat-inactivated FBS and 1% GlutaMax.
Serum-free media (SFM): DMEM (high glucose) supplemented with 1% GlutaMax without FBS.
All FBS was heat-inactivated by incubating at 56°C for 1h and was identified as tetracycline-free by Life Technologies.

2.1.2 Cell lines

All cells were passaged twice weekly and were grown under normoxic conditions at 37°C, 5% CO_2. Cell counts were performed by trypan-blue exclusion (Corning) using haemocytometers (improved Neubauer).
Suspension cells: The HMCLs (**INA-6**, **JIM3** (ECACC 10081204), **KMS-12-BM** (DMSZ ACC 551), **LP-1** (DMSZ ACC 41), **MM.1S** (ATCC CRL-2974), **NCI-H929** (ATCC CRL-9068), **OCI-My5**, **OCI-My7**, **OPM-2** (DMSZ ACC 50) and **SK-MM-1**) and **K562** (ery-

throleukemic cell line, ATCC CCL-243) were grown in complete RPMI medium, with the exception of OPM-2 which was maintained in complete RPMI supplemented with 5% instead of 10% heat-inactivated FBS. INA-6 were supplemented with 3ng/ml recombinant human interleukin-6 (Roche). Suspension cells were maintained between $3x10^5$ and $1x10^6$ cells/ml.

Adherent cells: **HEK-293T** (human embryonic kidney, ATCC CRL-11268), **HEK-293FT** (derived from 293T, a kind gift from Dr A. Reyes[1]), **hTERT RPE-1** (retina, pigmented epithelium, ATCC-CRL-4000), **CD40L-expressing L cells** (murine fibroblast, ATCC CRL-2648) and **M2-10B4** (murine stromal cell, ATCC CRL-1972) were maintained in complete DMEM media and split when cells reached 80-90% confluency. Both the CD40L- L cells and the M2-10B4 were a generous gift from Dr R. Tooze[2]. For passaging, adherent cells were washed with phosphate buffered saline (PBS, pH 7.4) and detached using trypsin (Thermo Fisher Scientific) at 37°C. Trypsin was neutralised with at least ten times volume of complete DMEM, cells collected and centrifuged at 300g for 5min and seeded at the required dilution (typically 1:25 for routine passaging).
HEK-293FT were maintained in blasticidin (15µg/ml, Invivogen) and zeocin (100µg/ml, Invitrogen) prior to transfection.

2.1.3 Cryopreserving and thawing cells

All cell lines are cryopreserved in 90% FBS with 10% dimethyl sulfoxide (DMSO, Thermo Fisher Scientific) (v/v) at a concentration of $10x10^6$ cells/ml for suspension cells or $1/3$ of a confluent 100mm culture dish for adherent cells. Cells were initially stored at -80°C in a Mr Frosty freezing container (Thermo Fisher Scientific) before being transferred to long term storage at -150°C.

Cells are rapidly thawed by gently agitation in a 37°C water bath before transfer to 10ml of pre-warmed complete media. Cells are then centrifuged at 300g for 5min and re-suspended in complete media. Suspension cells are seeded at $5x10^5$ cells/ml for 24 hours before a viability check and re-seeding at $3x10^5$ cells/ml in fresh complete media. All adherent cells are seeded into 100mm culture dishes and left until confluency.

[1]M Zeviani group, Mitochondrial Biology Unit, University of Cambridge
[2]Faculty of Medicine and Health, University of Leeds

2.1.4 Cell line verification

Cell line identities were verified by genomic DNA sequencing to confirm the presence of mutations known to be unique to each cell line. These were identified from the Keats Lab HMCL preliminary mutations list, which contains all the mutations currently identified to date by exome sequencing (see section 2.16). Genomic DNA was extracted from $5x10^6$ cells from each cell line using the DNeasy blood and tissue kit (Qiagen). Forward and reverse primers were designed to flank each unique mutation (table 2.1) and DNA amplified by polymerase chain reaction (PCR) using BioTaq DNA polymerase (Bioline) following the recommended 3-step PCR protocol (35 cycles). Amplified PCR product was resolved on a 1.5% agarose gel in TAE buffer (40mM Tris, 20mM acetic acid, 1mM EDTA) using 4x loading buffer (250mM Tris-HCl (pH 6.8), 0.0008% bromophenol blue (w/v), 40% glycerol (v/v)) and visualised using GelGreen nucleic acid stain (Biotium). DNA bands were extracted using the QIAquick gel extraction kit (Qiagen) following the manufacturer's instructions. Purified PCR products were then sequenced by Sanger sequencing (Source Bioscience) and results analysed by FinchTV (PerkinElmer).

Target gene	Primer	Sequence (5' to 3')
APC2	APC2_forward_1	GAACTACCTCGCCTCCCTTC
	APC2_reverse_1	GGACACTCACCTAGCTCGTT
APOB	APOB_forward_1	GGTCTCTACGCCACAAATTTCT
	APOB_reverse_1	TTGCAGATCAGAGGTGGAGG
BRCA2	BRCA2_forward_2	GCTGTTCTCCTGTCATCCCT
	BRCA2_reverse_2	TGGGCCTTAACAGCATACCA
DNAH14	DNAH14_forward_1	TCCTTGAGACATTAGCTCCAGG
	DNAH14_reverse_1	GTGTTGGTTTGGAGTGACTTGA
DOCK8	DOCK8_forward_2	ACCATCTGTTGCACTATCCCA
	DOCK8_reverse_2	TTACCTGGGAAGATATGGAAGGA
ELF1	ELF1_forward_1	TGAAGGATGGAGAGGAAGCC
	ELF1_reverse_1	CCCAAGTTCCAGTGGTTGTG
EYS	EYS_forward_1	AGCAATCTCCAGTGCTCTCT
	EYS_reverse_1	TCGTGACCCAGCACAAATTG
IRAK3	IRAK3_forward_1	TGGTGGCAAATCTGAGGCTT
	IRAK3_reverse_1	GGCTTTCATCATCTTCCACTGG
LRP10	LRP10_forward_1	TTTGGCCCTCTGACTCTGAG
	LRP10_reverse_1	CTTCAGGGACAGTAGTGGGG

Table 2.1 *HMCL sequencing primers*

2.1.5 Mycoplasma Testing

All cell lines were tested and confirmed to be mycoplasma free before PMP. Cells were cultured for four days in complete media and supernatant collected and stored at -20°C. Mycoplasma testing was performed using a nested PCR (table 2.2). PCR products were visualised on a 2% agarose TAE gel.

Primer	Sequence (5' to 3')
MycoplasmaF1	ACACCATGGGAGCTGGTAAT
MycoplasmaR1	CTTCWTCGACTTYCAGACCCAAGGCAT
MycoplasmaF2	GTTCTTTGAAAACTGAAT
MycoplasmaR2	GCATCCACCAWAWACTCT

Table 2.2 *Mycoplasma detection primers*

2.2 Primary samples

Patient sample processing and the aminooxy-biotin labelling of MM plasma cells was performed in collaboration with Dr S Surget and Dr J Ballester-Beltran[3]. Bone marrow aspirates (BMA) were obtained from myeloma patients after informed consent (Causes of clonal blood disorders (07/MRE05/44)). Red blood cells (RBC) were lysed using RBC lysis buffer (155mM ammonium chloride, 12mM sodium bicarbonate and 0.1mM EDTA, pH 7.2) and the remaining leukocytes washed and re-suspended in PBS/0.5% (w/v) bovine serum albumin (BSA, Thermo Fisher Scientific). Plasma cell infiltration was determined by flow cytometry (CD138-PE, see table 2.8). Samples with a high infiltration were processed for PMP and remaining samples were either discarded, stored at -150°C or analysed by flow cytometry for target expression using the appropriate antibody in combination with CD138-PE. Additionally, SEMA4A was used in conjunction with CD14, CD19, CD3, CD34 and CD66b for profiling of heematopoietic cell subsets (see section 2.9).

For PMP, plasma cells were isolated using CD138 microbeads (Miltenyi Biotech) on an autoMACS Pro Separator (Miltenyi Biotech) and CD138+ cell purity was confirmed by flow cytometry before proceeding with biotinylation (see section 2.3).

[3]Mike Chapman group, Department of Haematology, University of Cambridge

2.3 Plasma membrane profiling

2.3.1 Biotinylation

$1x10^8$ HMCLs or $1x10^7$ primary myeloma cells were washed four times in ice-cold PBS pH 7.4 before resuspension in an aminooxy-biotin mix (1mM sodium (meta)periodate (Thermo Fisher Scientific), 10mM aniline (Sigma), 100mM aminooxy-biotin (Biotium), PBS, pH 6.7). Samples were incubated with rotation at 4°C for 30min in the dark. Glycerol (Sigma) was added to a final concentration of 1mM and cells were washed a further three times in ice-cold PBS, pH 7.4. $5x10^5$ cells were taken before and after biotinylation to check the biotin labelling efficiency by flow cytometry using streptavidin-APC (table 2.8). Biotinylated cells were pelleted and stored at -20°C until enough samples were collected to perform the pulldown.

2.3.2 Pulldown

Sample were incubated for 30min in PMP lysis buffer (1% Triton X-100 (Thermo Fisher Scientific), 1x protease inhibitor tablet (complete mini, without EDTA, Roche), 150mM sodium chloride, 10 mM Tris-hydrochloride (TRIS-HCl)) at 4°C on rotation. Cell debris was removed by centrifugation at 13,000g for 10min, repeated twice. The total protein concentration was determined using the Pierce™ BCA Protein Assay Kit (Thermo Fisher Scientific) following manufacturer's instructions. Each lysate was adjusted to the same final total protein amount per 10plex before incubation for three hours at 4°C with high affinity streptavidin agarose beads (50µl bead slurry/sample). The beads were washed on SnapCap filter columns on a vacuum manifold as follows (all washes and incubations in 400µl): 20 washes of lysis buffer, then 20 washes of PBS/0.5% (w/v) SDS followed by incubation with PBS/0.5% (w/v) SDS/100mM dithiothreitol (Sigma) for 20min at room temperature (RT) with continuous mixing. Beads were centrifuged at 1,000g for 1min and washed 10 times in urea buffer (6M urea (PlusOne, VWR), 50mM Triethylammonium bicarbonate (TEAB) (Sigma), pH 8.5). Beads were then incubated in urea buffer/50mM iodoacetamide (Sigma) with continuous mixing in the dark for 20min at RT before pelleting by centrifugation (1,000g for 1min). Beads were washed ten times in urea buffer, and five times in 50mM TEAB buffer before resuspension in 50µl of 50mM TEAB/0.5µg trypsin (modified sequencing grade, Promega) and digested overnight with continuous mixing at 37°C. Beads were pelleted by centrifugation, and the supernatant containing the digested peptides collected. Beads were washed in 200µl 50mM TEAB, centrifuged and the supernatant removed and pooled with the

first supernatant.
For the initial PMP, TMTZero and patient sample test runs, samples were processed as described above but were not subjected to a BCA assay and total protein amount adjustment.

2.3.3 Peptide labelling

All individual peptide samples were dried in a vacuum centrifuge, before resuspension in 25µl 50mM TEAB/16% (v/v) acetonitrile (ACN) (Thermo Fisher Scientific). Peptide samples were then either left unlabelled (for initial test runs) or were labelled using TMTZero or TMT10plex (Thermo Fisher Scientific) (annotated in the manuscript).

TMTZero: 5µl of the TMTzero label was resuspended with the LP1 peptide test sample, incubated for 2 hours at RT and then quenched with 21µl 1% trifluoroacetic acid (TFA). Samples were dried in a vacuum centrifuge and resuspended to a final concentration of 10% DMSO/0.5% TFA.

TMT10plex: 5µl of each TMT label reagent from the TMT10plex label reagent set (Thermo Fisher Scientific) was added to each individual peptide sample, incubated for 2 hours at RT and quenched with ammonium formate (final concentration 20mM). Peptide samples were pooled, dried in a vacuum centrifuge and re-suspended in 5% DMSO/0.5% TFA.

2.3.4 High pH Reverse Phase Fractionation

All fractionation, mass spectrometry based acquisition and data processing was performed by Dr J. C. Williams[4].
High pH Reverse Phase Fractionation was conducted on an Ultimate 3000 Ultra-high performance liquid chromatography (UHPLC) system (Thermo Fisher Scientific) equipped with a 2.1mm × 15cm, 1.7µm Aqcuity BEH C18 column (Waters, UK). Solvent A was 3% ACN, Solvent B was 100% ACN, solvent C was 200mM ammonium formate (pH 10). Throughout the analysis solvent C was kept at a constant 10%. The flow rate was 400µL/min and UV was monitored at 280nm. Samples were loaded in 90% A for 10min before a gradient elution of 0–50% B over 36min followed by a 10min wash with 90% B. 100µL fractions were collected throughout the run. Peptide containing fractions were orthogonally recombined into

[4]Paul Lehner group, Department of Medicine, University of Cambridge

12 fractions and dried in a vacuum centrifuge. Fractions were stored at -80°C prior to analysis.

2.3.5 LC-MS Analysis

All samples were resuspended in 5% DMSO/0.5% TFA. Samples were analysed using a nanoLC-MS platform consisting of an Ultimate 3000 RSLC nano UHPLC (Thermo Fisher Scientific) coupled to an Orbitrap Fusion (Thermo Fisher Scientific) instrument. Solvent A was 0.1% formic acid (FA) and solvent B was 80% ACN/0.1% FA. Samples were loaded at 10µL/min for 5min onto an Acclaim PepMap C18 cartridge trap column (300µm x 5mm, 5µm particle size) in 0.1% TFA. After loading a linear gradient of 3-32% solvent B was used for sample separation over a column of the same stationary phase (75µm x 75cm, 2µm particle size) before washing at 95% B and equilibration. Electrospray ionisation was achieved by applying 2.1kV directly to a stainless steel emitter tip.

Analysis was performed using tandem-mass spectrometry (Synchronous precursor selection (SPS)-MS3), in which the parent ion in the MS scan is selected, isolated and further fragmented. A select few of the detected MS2 ions are selected and fragmented again to generate MS3 ions. The instrument settings were as follows: MS1: Quadrupole isolation, 120,000 Resolution, 500,000 automatic gate control (AGC) target, 50ms maximum injection time, ions injected for all parallisable time. MS2: Quadrupole isolation at an isolation width of m/z 1.6, precursors were fragmented by collision-induced dissociation (CID) (normalised collision energy (NCE) of 30%) with ion trap scanning out in rapid mode from m/z 120, AGC target of 5,000 and a 70ms maximum injection time. MS3: In SPS mode the top 10 MS2 ions were selected for Higher-energy collisional dissociation (HCD) fragmentation (65% NCE) and scanned out in the orbitrap at 50,000 resolution with an AGC target of 20,000 and a maximum accumulation time of 120ms, ions were not accumulated for all parallelisable time. The entire MS/MS/MS cycle had a target time of 3s. Dynamic exclusion was set to +/- 10ppm for fragmentation was trigged on precursors 5,000 counts and above.

2.3.6 Data Processing

Spectra were searched by Mascot within Proteome Discoverer 2.1 in two rounds of searching. First search was against the UniProt Human reference proteome and a compendium of common contaminants (Global proteome machine). The second search took all unmatched spectra from the first search and searched against the human trEMBL database (Uniprot).

The following search parameters were applied: peptide and fragment mass tolerances were set to 10ppm and 0.6Da respectively, fixed modifications of carbamidomethyl (C) and TMT (N-term, K) and variable modifications of oxidation (M) and trypsin (/P). MS3 spectra were used for reporter ion based quantitation with a most confident centroid tolerance of 20ppm. Peptide-spectrum match (PSM) false discovery rate (FDR) was calculated using Mascot percolator and was controlled at 0.01% for 'high' confidence PSMs and 0.05% for 'medium' confidence PSMs. For unlabelled samples, the Hi3 method was used for protein quantitation. See section 2.16 for further details on protein annotation and analysis of the dataset.

2.4 Molecular Biology

2.4.1 Preparation of competent cells

A single-use aliquot of one shot Stbl3 chemically competent cells (Thermo Fisher Scientific) were thawed on ice and streaked on a LB/Agar plate without antibiotic and grown overnight. A single colony was picked and grown in 2.5ml of LB broth (typtone 10g/L, sodium chloride 5g/L, yeast extract 5g/L) without antibiotic overnight, shaking at 37°C. This starter culture was then used to inoculate 250ml SOC medium (2% tryptone 0.5% yeast extract, 10mM sodium chloride, 2.5mM potassium chloride, 10mM magnesium chloride, 10mM magnesium sulfate and 20mM glucose). Bacteria were grown at 37°C with shaking until reaching an optical density (OD) of 0.3 to 0.5. Culture media was placed on ice for 10min before centrifugation at 2,880g for 10min at 4°C and the supernatant discarded. Pelleted cells were re-suspended in 100ml cold buffer 1 (30mM potassium acetate, 100mM rubidium chloride, 10mM calcium chloride dihydrate, 50mM manganese(II) chloride tetrahydrate, 15% (v/v) glycerol, pH 5.8) and incubated on ice for 30min before centrifugation (2,880g for 15min at 4°C). Supernatant was removed and cells re-suspended in 10ml cold buffer 2 (10mM MOPS buffer,10mM rubidium chloride, 75mM calcium chloride dihydrate, 15% glycerol, pH 6.5) on ice for 30 minutes. Bacteria were then aliquoted and snap-frozen on dry ice for storage at -80°C until use.

2.4.2 Transformation of competent cells

Aliquots of competent Stbl3 were thawed on ice for 10 minutes. Up to 1/5 of the total volume was added of either ligation mix or plasmid DNA (10pg to 100ng) and cells incubated on ice for 30min. Stbl3 were then heat-shocked at 42°C for 45 seconds before being placed back on ice for 2 minutes. Pre-warmed SOC medium was added and bacteria incubated at 37°C and

225rpm (Thermoshaker, Thermo Fisher Scientific) for 1h. Cells were spread on a LB/agar plate with 100µg/ml ampicillin and cultured overnight at 37°C.

2.4.3 RNA extraction and cDNA synthesis

Cells were collected and RNA extracted using the QIAGEN RNeasy kit, as per the manufacturer's guidelines. Genomic DNA was removed using the recommended gDNA removal spin columns and total RNA was quantified using a NanoDrop Lite Spectrophotometer (Thermo Fisher Scientific). cDNA synthesis was performed from 2µg of total RNA using the High-Capacity cDNA Reverse Transcription Kit (Applied Biosystems). Sequence specific primers (table 2.3) were used to generate cDNA for pcDNA5 constructs, whilst oligo-$dT_{(18)}$ were used for the pcDNA3 and pLenti6.2 constructs. Random hexamers were used for cDNA for qRT-PCR.

Primer	Sequence (5' to 3')
EPHB2_cDNA_F1	GACCTCGCCAAACT
NEO1_cDNA_F1	ATTTTTGGTCTCATTC
PLXNA1_cDNA_F1	CCTTCATTTTCTTGTTCAAA
PLXNC1_cDNA_F1	TTCCATCAAGTCCCT
ROBO1_cDNA_F1	ACTTTTCTGATACCCG
SEMA4A_cDNA_F1	CTTCAATATCAGTGTAGGAG
SEMA4D_cDNA_F1	AATTAAGTGGAAGAAAAGGT

Table 2.3 *Sequence specific primers for cDNA synthesis*

2.4.4 DNA cloning

Specific cloning strategies are described in the relevant sections below. DNA fragments were amplified from cDNA by PCR using Phusion Hot Start II High Fidelity DNA polymerase following the manufacturer's guidelines. Amplified PCR products were resolved on a 0.8% agarose TAE gel and bands were extracted using QIAquick gel extraction kit. Purified PCR products and plasmid backbones were digested for 1-3 hours at the appropriate temperature and buffer for each enzyme (New England Biolabs). Digested plasmids were visualised and extracted from agarose gels in TAE buffer, whilst digested PCR fragments were purified using QIAquick PCR purification kit (Qiagen).

Annealed oligos were prepared as follows: 2µM of oligonucleotides were diluted in buffer 2.1 (New England Biolabs), heated to 98°C, 5min before allowing to gradually cool to room temperature.

Annealed oligos or amplified PCR fragments were ligated into the appopriate digested backbone using T4 DNA ligase (New England Biolabs) following manufacturer's instructions. Ligations were either performed at 16°C overnight or 1-2 hours at room temperature then heat inactivated at 65°C for 10min and transformed in Stbl3 chemically competent cells. Bacteria were plated onto LB/agar plates with ampicillin (100µg/ml) and cultured overnight at 37°C. Several colonies were selected from each construct and grown in LB with ampicillin. Plasmid DNA was extracted using Qiagen's QIAprep spin miniprep kit and the presence of the insert confirmed by Sanger sequencing. For larger amounts of plasmid DNA, Qiagen's plasmid Midi kit was used. DNA concentrations were determined by NanoDrop.

Generation of SEMA4A hairpin constructs

Short hairpins targeting luciferase (control) or SEMA4A were selected from The RNAi Consortium (TRC) library database (Broad Institute) (available from www.portals.broadinstitute.org-/gpp/public). Complementary oligonucleotides containing the hairpin and appropriate restriction enzyme sites were ordered from Sigma (table 2.4) and annealed before insertion into the pLKO.1_puro vector (Addgene 10878), pLKO.1_TET (Addgene 21915) or pLKO.1_GFP at the EcoRI and AgeI restriction sites (see figures 2.1 and 2.2). pLKO.1_GFP was created by Dr M Chapman, replacing the puromycin resistance cassette under the hGPK promoter in the pLKO.1_puro vector with eGFP.

Generation of SEMA4A rescue constructs

Additional restriction enzyme sites (AscI, XmaI, SmaI, PmeI and SalI) were added to the pLenti6.2/V5-DEST vector (Thermo Fisher Scientific) at the EcoRI/BstBI restriction sites using the annealed oligos pLenti_MSC_F/R to generate pLenti6.2_modified_MCS (table 2.5). BFP was cloned from the pKLV_U6_sgRNA(BbsI)-PGKpuro2ABFP vector (a gift from Dr P. Lehner[5] by PCR using the primers pLenti_BFP_F1/R1, including the T2A sequence upstream of the BFP gene and an additional linker (Gly-Ser-Gly) at the N-terminal (table 2.5). The amplified BFP fragment was inserted into pLenti6.2_modified_MCS at

[5]Department of Medicine, University of Cambridge

Oligonucleotide	Sequence (5' to 3')
Luciferase_shRNA_F1	CCGGATGTTTACTACACTCGGATATCTC-GAGATATCCGAGTGTAGTAAACATTTTTTG
Luciferase_shRNA_R1	AATTCAAAAAATGTTTACTACACTCGGAT-ATCTCGAGATATCCGAGTGTAGTAAACAT
SEMA4A_shRNA_136_F1	CCGGGCTCTATTCTGGTACTATGAACTC GAGTTCATAGTACCAGAATAGAGCTTTTTG
SEMA4A_shRNA_136_R1	AATTCAAAAAGCTCTATTCTGGTACTATG AACTCGAGTTCATAGTACCAGAATAGAGC
SEMA4A_shRNA_636_F1	CCGGATGAACACCAAACATCTAAACCTC GAGGTTTAGATGTTTGGTGTTCATTTTTTG
SEMA4A_shRNA_636_R1	AATTCAAAAAATGAACACCAAACATCTA AACCTCGAGGTTTAGATGTTTGGTGTTCAT
SEMA4A_shRNA_567_F1	CCGGGACCTTCATGAAGGACCATTTCTC GAGAAATGGTCCTTCATGAAGGTCTTTTTG
SEMA4A_shRNA_567_R1	AATTCAAAAAGACCTTCATGAAGGACCA TTTCTCGAGAAATGGTCCTTCATGAAGGTC

Table 2.4 *Small hairpin oligonucleotides used for generating pLKO.1 constructs*

the PmeI/BstBI sites to generate pLenti.6.2_T2A_BFP. Using NCI-H929 cDNA (oligodT primers), full-length (wild type, WT) or mutant (SEMA4AΔC) was PCR cloned and inserted into pLenti.6.2_T2A_BFP at the AscI/PmeI sites, immediately upstream of the T2A linker sequence (figure 2.3). The kozak sequence was included for both constructs and the stop codon removed from the 3' end of SEMA4A(WT).

Oligonucleotide/primer	Sequence (5' to 3')
pLenti6_MCS_F	AATTCGGCGCGCCCCCGGGGTTTAAACGTCGACTT
pLenti6_MCS_R	CGAAGTCGACGTTTAAACCCCGGGGGCGCGCCG
pLenti_BFP_F1	CTATCGGTTTAAACGGGTCCGGAGAGGGCAGAG-GAAGTCTCCTAAC
pLenti_BFP_R1	TTCAGTTTCGAATCAATTAAGCTTGTGCCCCAG
pLenti_SEMA4A_F1	TACTATGGCGCGCCGCCAGCATGGCCCTCCCAGCCC
pLenti_SEMA4A_R1 (SEMA4AΔC)	GAATCAGTTTAAACGCCTTCTACGCAATGGGGAGGC-CACGAG
pLenti_SEMA4A_R2 (SEMA4A(wt))	GAATCAGTTTAAACGCCTTCTACGAGCTACCTCAGTG-CCTAGGCAG

Table 2.5 *Primers and oligonucleotides used for generating pLenti6.2 constructs*

Generation of pcDNA5 constructs

The extracellular domains of EPHB2, NEO1, PLXNA1, PLXNC1, ROBO1, SEMA4A and SEMA4D were PCR cloned from HMCL cDNA, see table 2.3 for primers used. These primers were designed to include the kozak sequence at the N-terminal and a TEV protease cleavage site and 6x his-tag followed by a stop codon at the C-terminal. Amplified PCR fragments were inserted at the appropriate restriction enzyme site (see table 2.6 and figure 2.4). The extracellular domain and the full-length SEMA4A were PCR cloned from NCI-H929 cDNA (oligo dT primers) and inserted into pcDNA3.1 (Thermo Fisher Scientific) using SEMA4A_pcDNA5_F1/R1 (1-683, extracellular domain only) and SEMA4A_pcDNA5_F1/R2 (1-761, full-length) (fig 2.5).

Primer	Sequence (5' to 3')	Restriction site
EPHB2_pcDNA5_F1	GGTTCACTCGAGGTTATGGCTCTGCGGAGGCTGG	XhoI/ApaI
EPHB2_pcDNA5_R1	CCGTAGGGGCCCCTAGTGATGGTGATGGTGATGG- CCCTGAAAATACAGGTTTTC	
NEO1_pcDNA5_F1	GAGTGGCAACTTCTCCTGGATGC GGCTCACTCGAGGAGATGGCGGCGGAGCGG	XhoI/ApaI
NEO1_pcDNA5_R1	CCGTAGGGGCCCCTAGTGATGGTGATGGTGATGG- CCCTGAAAATACAGGTTTTC	
PLXNA1_pcDNA5_F1	CAGCATATTACTGTCCAGAGGAGAGGTG GGCTCAAAGCTTGCCATGCCGCTGCCACC	HindIII/NotI
PLXNA1_pcDNA5_R1	CCGTAGGCGGCCGCCTAGTGATGGTGATGGTGATG- GCCCTGAAAATACAGGTTTTC	
PLXNC1_pcDNA5_F1	AGGCAGCGTCAGCAGGC GGCTCACTCGAGAAGATGGAGGTCTCCCGGAGG	XhoI/ApaI
PLXNC1_pcDNA5_R1	CCGTAGGGGCCCCTAGTGATGGTGATGGTGATGGC- CCTGAAAATACAGGTTTTC	
ROBO1_pcDNA5_F1	TGTGGAAGGAACTGACTCCTGC GGCTCACTCGAGACAAAGATGAAATGGAAACATG	XhoI/ApaI
ROBO1_pcDNA5_R1	CCGTAGGGGCCCCTAGTGATGGTGATGGTGATGGC- CCTGAAAATACAGGTTTTC	
SEMA4A_pcDNA5_F1	CGGCTGCTTCACCACATCTG GGCTCAAAGCTTAGCATGGCCCTCCCAGCCCTGG	
SEMA4A_pcDNA5_R1	CCGTAGGCGGCCGCCTAGTGATGGTGATGGTGATG- GCCCTGAAAATACAGGTTTTC	HindIII/NotI
SEMA4A_pcDNA5_R1	GTGGGGCCAGTAGGACTGC CCGTAGGCGGCCGCCTAGTGATGGTGATGGTGATG- GCCCTGAAAATACAGGTTTTCTTAAGCTACCTCAGTGCC	
SEMA4D_pcDNA5_F1	GGCTCAAAGCTTAGCATGAGGATGTGCACC	HindIII/ApaI
SEMA4D_pcDNA5_R1	CCGTAGGGGCCCCTAGTGATGGTGATGGTGATGGCC- CTGAAAATACAGGTTTTC GCGGTTGTCGCTGGACTTA	

Table 2.6 *Primers used for generating pcDNA5 and pcDNA3.1 constructs*

2.5 Transfection

Transient transfection: Per condition, $3.2x10^5$ 293T cells were seeded per well of a 6 well plate in complete DMEM and left overnight to adhere. 1µg of plasmid (pLenti6.2/pcDNA3.1) was combined with 3µl TransIT-LT1 (Mirus Bio) in 250µl of Opti-MEM (Life Technologies) and left at room temperature for 20-30min. Transfection mixture was then added to the cells drop-wise.

Stable transfection of 293FT: $7x10^4$ 293FT cells were seeded per well (6 well plate) per condition in antibiotic-free complete DMEM and left to attach overnight. 150ng of vector (pcDNA5) was combined with 1350ng of pOG44 (Thermo Fisher Scientific) and 6µl TransIT-LT1 in a total volume of 250µl Opti-MEM. DNA was incubated for 20-30min at room temperature and added drop-wise to the cells. Media was changed 24 hours later and replaced with complete DMEM supplemented with blasticidin (15µg/ml). At 48 hours, media was replaced again with complete DMEM, plus blasticidin and hygromycin B Gold (100µg/ml, Invivogen). Media was then changed every two days, maintaining antibiotic selection and surviving colonies redistributed until cells were fully selected. Verification of the tetracycline-inducible expression was confirmed by western-blot using an anti-His-tag antibody (table 2.9)

2.6 Protein production and purification

pcDNA5 construct expressing 293FT cells were seeded at 20-30% confluency and left to adhere overnight. Cells were then switched to SFM with doxycycline (30ng/ml, Sigma). At 72 hours cells were supplemented with additional fresh SFM with doxycyline (1/3 of the initial media volume). Cell culture media containing the secreted recombinant proteins was collected on day 7, clarified by centrifugation at 300g for 5min, and filtered through a 22µm filter.

For protein purification, cell culture media and all buffers were cooled to 4°C and all steps performed in a cold-room. Filtered media was loaded onto a HisTrap Excel column (1ml, GE Healthcare) and washed using 96% buffer A (20mM sodium phosphate and 0.5M sodium chloride, pH 7.4) and 4% buffer B (20mM sodium phosphate, 0.5M sodium chloride and 1M imidazole, pH 7.4). Recombinant proteins were then eluted from the column over 4 to 100% buffer B gradient (final concentration of imidazole: 40mM to 1M) at a flow rate of 1ml/min. 0.5 to 1ml fractions were collected throughout the run. Protein-containing

fractions (as determined by UV absorbance at 280nm) were pooled and buffer exchanged using a Dialyzer Maxi (molecular weight cut-off 12-14kDa, Novagen) into TEV cleavage buffer (50mM Tris-HCl, 0.5M sodium chloride, pH 8.0). The his-tag was cleaved by TEV protease overnight at 4°C (1.25U/µg). The cleaved recombinant protein was loaded back onto the HisTrap column and collected in the flow-through fraction. Bound cleaved his-tag and other contaminants were eluted by a 1M imidazole wash to clean the column. Protein concentration was determined using the NanoDrop. Collected fractions were visualised by SDS-PAGE or western-blot (see section 2.10).

2.7 Lentiviral transduction of suspension cells

Lentivirus was used for stable transduction of suspension cell lines, using a 2^{nd} generation production system. 3.2x10^5 293T cells were seeded per condition per well in a 6 well plate in complete DMEM and left to attach overnight. 1µg of either the pLenti6.2 or pLKO.1 vectors of interest were mixed with 900ng of the packaging plasmid psPAX2 (Addgene 12260) and 100ng of the envelope plasmid pMD2.G (Addgene 12259) with 6µl of TransIT-LT1 in a final volume of 126µl opti-MEM. The DNA mixture was left at room temperature for 30min before adding drop-wise to the adhered 293T cells. Media was changed at 24 hours and the virus-containing media harvest at 40-48 hours. Media was filtered using a 0.45µm filter and either used straight away or stored at -80°C until use.

Cells were re-suspended in the harvested viral supernatant at 8x10^5cells/ml. Polybrene (Sigma) was added to a final concentration of 6µg/ml and cells centrifuged at 750g for 30min at room temperature before overnight culture at 37°C and 5% CO_2. Media was changed and replaced with complete RPMI, with or without antibiotics. Puromycin (Gibco) was added at 2 or 3µg/ml for NCI-H929 and MM.1S respectively and blasticidin at 10µg/ml for both.

2.8 Hairpin competition assay

K562, NCI-H929 and MM.1S were transduced with diluted lentiviral media containing pLKO.1_shLUC_GFP, pLKO.1_shSEMA4A_636_GFP or pLKO.1_shSEMA4A_567_GFP so that only ≈50% of the cell population expressed the hairpin of interest. Cells were maintained in complete RPMI and split to 3x10^5 cells/ml every 4 days. Hairpin expression was confirmed by flow cytometry using GFP expression as a surrogate. SEMA4A knockdown

was also confirmed using SEMA4A-eFlour710 (table 2.8). The proportion of GFP+ cells was measured at day 4, 8, 12 and 16 by flow cytometry.

2.8.1 Knockdown and rescue

SEMA4A(wt) or SEMA4AΔC expressing NCI-H929 and MM.1S cells were generated by lentiviral transduction using the pLenti6.2 constructs: pLenti6.2_hSEMA4AΔC_T2A_BFP and pLenti6.2_hSEMA4A(wt)_T2A_BFP. As a control, cells were also transduced with the empty parental vector pLenti6.2/V5. Following transduction, cells were maintained in blasticidin selection and SEMA4A and BFP expression confirmed by flow cytometry (5E3, table 2.8) and western blot (GeneTex antibody, table 2.9). As described in section 2.8 endogenous SEMA4A was then knocked down by lentiviral transduction of the pLKO.1_GFP constructs and GFP expression monitored by flow cytometry at day 4, 8 and 12.

For the second experiment, pLKO.1_TET_shLUC or pLKO.1_TET_shSEMA4A-636 expressing MM.1S were generated by lentiviral transduction. Following transduction, cells were maintained in puromycin selection before transduction with pLenti6.2_hSEMA4AΔC_T2A_BFP, pLenti6.2_hSEMA4A(wt)_T2A_BFP or the empty parental vector pLenti6.2/V5. 24 hours following transduction, endogenous SEMA4A was knocked down by the introduction of doxycycline to the cell culture media (1μg/ml). SEMA4A expression was monitored by flow cytometry and Flow-Count Fluorospheres (Beckman Coulter) used to determine total cell counts at day 7 and 14.

2.9 Flow cytometry

All immunostainings were performed in PBS at 4°C for 20min for unconjugated antibodies or at room temperature for 13min in the dark for conjugated antibodies. For unconjugated antibodies, unbound antibody was removed by PBS wash before incubation with a fluorescently-labelled secondary antibody for 13min at RT. FC block (Miltenyi Biotech) was included for all patient samples. Sample acquisition was performed on a Gallios Flow Cytometer (Beckman Coulter) and analysed using the Kaluza analysis software (Beckman Coulter, version 1.3). Viable cells were identified and selected for downstream analysis by forward/side scatter profiles and/or, where noted, by the exclusion of a live/dead stain (see table 2.9). Debris and doublets were also excluded from analysis. Compensation was

determined using single stains, prepared from pooled samples, and isotype-matched control antibodies used to determine background fluorescence. The median fluorescence intensity (MFI) was determined as the ratio of median fluorescence of each antibody over its isotype control. All flow cytometry antibodies used are listed in table 2.8.

2.10 Western blot

Collected cells were lysed in RIPA lysis buffer (50mM Tris-HCL (pH 7.4), 150mM sodium chloride, 2mM EDTA, 1% (v/v) IGEPAL CA-630, 0.5% (w/v) sodium deoxycholate, 0.1% (w/v) sodium dodecyl sulfate (SDS) and protease inhibitor (complete mini, without EDTA, Roche)) on ice for 40min, vortexing for 20s every 10 minutes. Cellular debris was removed by centrifugation at 16,000g for 20min at 4°C. The protein concentration of each lysate was determined using the Pierce BCA protein assay kit (Thermo Fisher Scientific). Cell culture media samples were collected at various time points and centrifuged at 400g for 5min to remove cellular debris. Lysate (30µg) and supernatant samples were mixed with 4x NuPAGE LDS Sample Buffer (Thermo Fisher Scientific) at a 3:1 ratio and denatured at 70°C for 10min. Proteins were then resolved on tris-glycine mini gels (cast to a final acrylamide percentage of between 6 and 12%) using a tris/glycine/SDS buffer system (Bio-Rad). Gels were then either transferred to PVDF membrane (Millipore) using the Bio-Rad mini-PROTEAN tetra cell (100v for 1h) or developed in Quick Coomassie (Generon) following manufacturer's guidelines. Membranes were blocked for 1h at room temperature in blocking buffer (0.5% (v/v) gelatin from cold water fish skin (sigma), 0.1% (v/v) Triton x-100, 0.02% (w/v) sodium azide, in PBS) and immunoblotted with primary antibody diluted in blocking buffer overnight at 4°C. Membranes were washed in PBS-Tween-20 (0.1%, w/v) and incubated with the appropriate fluorescently-labelled secondary antibody diluted in blocking buffer plus 0.1% Tween-20 and 0.01% SDS (w/v) for 1h at room temperature. Membranes were washed again and imaged using the Odyssey FC OFC-1095 (LI-COR) imaging system. Protein expression was quantified using the Image Studio Lite software (version 4.0, LI-COR). All western-blot antibodies used are listed in table 2.9.

2.11 Quantitative real time-PCR

Quantitative real time-PCR (qRT-PCR) was performed using BioTaq DNA polymerase in the supplied buffer supplemented with EvaGreen Dye (20x in water, Biotium) in 96-well,

low-profile, semi-skirted, white PCR plates (Starlab). Samples were plated in triplicate and a no-template control well included. Primer efficiency was tested using cDNA serially diluted 1 in 4. Plates were run on a CFX96 machine (Bio-Rad) following a normal three-step PCR protocol (40 cycles) followed by a melt curve from 65 to 95°C. Data was analysed using the Bio-Rad CFX manager software (version 3.1). Relative gene expression was calulated as $E^{(Cq_{exp}-Cq_{ref})}$ where E= $(\frac{\text{primer efficiency}(\%)}{100})+1$, Cq_{exp}= average Cq for experimental sample and Cq_{ref}= average Cq for reference sample and using the housekeeping gene (RPL37a) for normalisation.

Primer	Sequence (5' to 3')
EPHB2_hsqPCR_F1	CTCCATCGGCAGTGTCCATC
EPHB2_hsqPCR_R1	ATGGCTGTGGCGTTGTACTC
NEO1_hsqPCR_F2	TGGAAAACCAACTCCAACTGTGA
NEO1_hsqPCR_R2	TGATTTCACCAGACCCAAAACTTGA
PLXNA1_hsqPCR_F1	CGAGTACTTCCCCACACTGT
PLXNA1_hsqPCR_R1	CGAGGTCAGCTGTGTGTCTA
PLXNC1_hsqPCR_F1	TAACAGCCACAGACCCTCACT
PLXNC1_hsqPCR_R1	TCCAGACGAAATATCCAGCC
RPL37a_hsqPCR_F1	CCTGGACGTACAATACCACTTC
RPL371_hsqPCR_R1	GATGTCTCAAAGAGTAGAGGAGC
SEMA4A_hsqPCR_F2	AGCATGTGAAGGTCCCGTTGA
SEMA4A_hsqPCR_R2	AAATACAGGTTTTCGTGGGGC

Table 2.7 Primers used for real-time PCR

2.12 Antibody internalisation

2.12.1 Flow cytometry

HMCLs were incubated with either an unconjugated antibody directed against SEMA4A, NEO1 or ROBO1 (table 2.8) or an isotype-matched control at 4°C for 30min. Unbound antibody was removed following two PBS (ice-cold) washes and labelled cells split into three groups. The first group were re-suspended in pre-warmed complete RPMI and cultured for 3 hours at 37°C, whilst the second group of cells were re-suspended in ice-cold complete RPMI and kept on ice for 3 hours. The last group was taken as t_0. Samples were taken at hourly intervals and immediately incubated with a PE-conjugated secondary antibody (goat anti-mouse IgG, table 2.9) at room temperature, 13min before fixation (1% formaldehyde

in PBS) at 4°C for 30 minutes. Samples were washed and re-suspended in PBS before analysis by flow cytometry. Internalisation was calculated as the ratio between the remaining surface-bound antibody at t_x compared to t_0.

2.12.2 Microscopy

NCI-H929 were incubated with unconjugated SEMA4A antibody for 30min at 4°C. Unbound antibody was removed by PBS washes and cells were then incubated at 37°C. Samples were removed at t_0 and t_3 and immediately fixed on ice in 4% formaldehyde solution for 30min. Cells were then incubated with an Alexa-Fluor 555 conjugated secondary antibody under permeabilising conditions (2% FBS and 0.1% (w/v) saponin (Sigma) in PBS) for 1h at room temperature. Samples were washed and resuspended in PBS/FBS/saponin with LAMP-1-Alexa-Fluor 488 for 1h at room temperature in the dark. Cells were washed, nuclei stained using DAPI, and attached to poly-L-lysine (Sigma) coated glass slides for 30min at 37°C. Slides were then mounted using Prolong Diamond Antifade Mountant (Life Technologies) and images captured using a Leica DFC7000T microscope and the Leica application suite software (Leica Microsystems). Captured images were analysed by ImageJ (National Institutes of Health).

2.13 ADC cytoxicity assay

Suspension cells ($5x10^3$ per well) or RPE-1 cells ($2.5x10^3$) were seeded in a 96-well flat-bottom plate in complete media. RPE-1 cells were left to adhere for 4-6 hours and treated with 0 or 250µM hydrogen peroxide (Sigma) for 1h at 37°C, 5% CO_2 before media was replaced with fresh complete DMEM. Antibody-ZAP complexes or ADCs (see below) were added to the cells and plates incubated for 72 hours at 37°C and 5% CO_2. Cell viability was determined by adding activated XTT reagent (Biotium) and incubating plates for 2-4 hours at 37°C. Absorbance at 450nm was recorded hourly until the non-treated readings were > 0.3 and background absorbance subtracted from all wells (650nm). Cell viability (%) was calculated as a percentage of the control (media only) wells. EC_{50} values were obtained from sigmoidal dose-response curves using GraphPad Prism software.

Preparation of Fab-ZAP-antibody complexes: Various dilutions of SEMA4A (5E3), ROBO1 (770502) or isotype control antibodies were prepared in complete RPMI containing

2.5mM Fab-ZAP (Advanced Targeting Systems), incubated at room temperature for 20 minutes and subsequently added to the cells.

Preparation of Biotin-ZAP-antibody complexes: SEMA4A antibody was biotinylated using either the Biotin (type A) or (type B) conjugation kit (Abcam) following manufacturer's guidelines. Biotinylation of the antibodies was confirmed by flow cytometry using streptavidin-APC. Biotin-conjugated antibody or un-conjugated antibody were mixed with biotin-ZAP (Advanced Targeting Systems) at 1:4 ratio (antibody:ZAP) and incubated for 20 minutes at room temperature. The antibody:ZAP complex was then diluted in complete RPMI to various dilutions and added to the cells.

SEMA4A direct conjugation: The SEMA4A antibody (5E3) was directly conjugated to either monomethyl auristatin E (MMAE) using a mc-vcPAB linker (malemide-based linker, cysteine linked) or with mertansine (DM1) using a SMCC linker (NHS-ester based, lysine linked) by Abzena, Cambridge. An isotype-matched control directly conjugated to MMAE (mc-vcPAB linker) was also provided by Abzena. Various dilutions of these direct conjugates were diluted in complete RPMI and added directly to the cells.

2.14 *In vivo* xenograft model

All *in vivo* work was performed by Dr G. Giotopoulos[6]. Mice were housed in pathogen free conditions at Central Biomedical Services (University of Cambridge, Cambridge, UK) and were allowed unrestricted access to food and water. All protocols were performed under the Project Licence P846C00DB in accordance with the Animals (scientific procedures) Act 1986 Amendment regulations 2012 and following ethical review by the University of Cambridge Animal Welfare and Ethical Review Body (AWERB).

Establishment of an in vivo xenograft model: Dual GFP/luciferase expressing cell lines (NCI-H929-MAC25 and MM.1S-MAC25) were generated by lentiviral transduction of BLIV301PA-1-MSCV-GFP-T2A-Luciferase (Bioscience). Recipient male SCID (Severe Combined Immunodeficiency) mice were sub-lethally irradiated with a single-dose of 2.5Gy and injected with 0.5, 1 or 2.5x10^6 NCI-H929-MAC25 or MM.1S-MAC25 cells in 200µl in PBS via the tail vein. Tumour establishment and growth was monitored by bioluminescence imaging. Briefly, D-luciferin (100µl of 15mg/ml) was injected i.p., followed by inhalation

[6]Brian Huntly group, Department of Haematology, University of Cambridge

anaesthesia (isoflurane) and after 7.5min, mice were imaged using the IVIS *in vivo* imaging system (PerkinElmer).

Testing 5E3-MMAE activity in vivo: Recipient male NOD SCID gamma (NSG) mice were sub-lethally irradiated as described above and injected with $1x10^6$ MM.1S-MAC25 cells via the tail vein. Tumour establishment and growth was monitored by bioluminescence imaging. Each animal then received a total of four doses (at 4mg/kg for each dose) of either 5E3, 5E3-MMAE or Trastuzumab-MMAE (isotype control) by means of tail vein injection (on day 13, 15, 19 and 22 post transplantation, termed 'Study day' 0, 2, 6 and 9 respectively). Mice were placed on tumour watch and imaging sessions were repeated weekly and at sacrifice.

2.15 B cell to plasma cell generation

Plasma cell generation was performed as described in [94]. CD40L-expressing L cells were gamma-irradiated using the Gammacell1000 and seeded in complete IMDM at $4.2x10^4$ cells/well in a 24 well plate and left to attach overnight. Leukocyte cones were obtained from the NHS Blood and Transport service and diluted in PBS/BSA (0.5% w/v) (1:2). Mononuclear cells were isolated by density gradient centrifugation using lymphocyte separation media (Lymphosep, MP Biomedicals). B cells were isolated using a Human Memory B cell Isolation kit (Miltenyi Biotech) and the autoMACS cell separator following manufacturer's guidelines. For isolating both naïve and memory B cells, the second selection step using CD27 microbeads was not included. Isolated B cells were cultured at $2.5x10^5$ cells/ml with the irradiated CD40L L cells in complete IMDM supplemented with IL-2 (20U/ml, Roche), IL-21 (50ng/ml, Peprotech) and F(ab')2 goat anti-human IgG+IgM (Jackson Labs, 10ug/ml) for 3 days. On day 3, activated B cells were collected from the co-culture and reseeded alone in complete IMDM supplemented with IL-2 (20U/ml), IL-21 (50ng/ml), Lipid mixture 1 (1 in 200 dilution, Sigma), MEM amino acid solution (1 in 50 dilution, Sigma) and TX-HYB hybridoma growth supplement (1 in 91 dilution, Gentaur) at $1x10^5$ cells/ml for a further 3 days. At day 5, M2-10B4 were gamma-irradiated and seeded in complete IMDM at $8.3x10^5$ cells/well in a 12 well plate and left to attach over night. On day 6, plasmablasts were collected and re-seeded with the irradiated M2-10B4 at $5x10^5$ cells/ml in the upper compartment of a transwell (0.4µM pore, Corning) supplemented with IL-21 (50ng/ml), IL-6 (10ng/ml, Peprotech), IFNalpha (100U/ml, Peprotech), MEM amino acid solution, Lipid mixture 1, and TX-HYB in complete IMDM. Media was then refreshed every 3.5 days. From

day 13 onwards, IL-21 was removed from the culture media.

A small sample of cells were taken at day 0 post selection and at day 3, 6, 9.5, 13, 16.5 and 20 to be further analysed for CD38, CD138, CD20 and CD19 (table 2.8) expression by flow cytometry.

2.16 Data repositories and data analysis

Data was analysed using both R (R: A language and environment for statistical computing. R Foundation for Statistical Computing, Vienna, Austria. (URL http://www.R-project.org) (v.3.5.1)) and GraphPad Prism Software (version 5). All statistical tests used are described in the manuscript and where appropriate, multiple testing was corrected for using the Benjamini-Hochberg (BH) method. Statistical significance was determined as a $p<0.05$ and FDR cut-offs are detailed either in the methods or manuscript. Unless otherwise specified, all data is presented as the median $\pm$ standard deviation.

Annotation of plasma membrane proteins: Where detailed plasma membranes were annotated using either Gene Ontology Cellular Component (GOCC) terms (http://www.geneontology.org/) or using a combination of GOCC and UniProt topological domain annotations (http://www.uniprot.org) (see section 3.3.5). For statistical analysis, data generated from the two PMP experiments were processed as follows: any proteins identified by a single, unique peptide or only identified in one dataset were removed before log transformation, column centering and scaling by the median absolute deviation.

Data from public repositories: For normal tissue expression, whole cell proteomic data was taken from the Human Proteome Map (www.humanproteomemap.org) [300]. Expression values were averaged and standardised to a 0 to 1 scale. SEMA4A IHC images and expression values were obtained from The Human Protein Atlas database (www.proteinatlas.org, version 18) [301]. HMCL quantitative transcriptomics data (mRNAseq) and preliminary mutations list (generated using exome sequencing) were downloaded from the Keats Lab data repository (www.keatslab.org/data-repository) and RNA abundance was expressed as FPKM values. A gene-specific RNA-to-protein (RTP) conversion factor for each cell line was determined by calculating the ratio between mRNA and protein abundance following normalisation of the PMP datasets as described above and log10 transformation of the RNA dataset [302]. The average RTP was calculated across 9 of the 10 HMCLs and used to predict

the protein abundance of the tenth cell line from mRNA expression.

Graphical art was obtained from SMART's graphical art (Servier Medical Art by Servier, https://smart.servier.com), licensed under a Creative Commons Attribution 3.0 Unported License and used in the introduction, figure 1.5.

Antibody	Conjugate	Clone	Supplier	Isotype	Dilution
CD138	PE	MI15	Biolegend	Mouse IgG1	1:50
	APC	MI15	Biolegend	Mouse IgG1	1:50
CD16	FITC	3G8	Biolegend	Mouse IgG1	1:33
CD14	APC-eFlour 780	61D3	eBioscience	Mouse IgG1	1:50
CD19	APC	HIB19	Biolegend	Mouse IgG1	1:50
CD20	PE/Cy7	2H7	Biolegend	Mouse IgG2b	1:100
CD220 (INSR)	PE	B6.220	Biolegend	Mouse IgG2b	1:200
CD3	PE/Cy7	OKT3	Biolegend	Mouse IgG2a	1:50
CD333 (FGFR3)	Unconjugated	136334	R&D systems	Mouse IgG1	1:100
CD34	FITC	581	Biolegend	Mouse IgG1	1:50
CD38	APC	HB-7	Biolegend	Mouse IgG1	1:100
	FITC	HB-7	Biolegend	Mouse IgG1	1:50
CD56 (NCAM1)	PE/Cy7	MEM-188	Biolegend	Mouse IgG2a	1:100
CD51 (ITGAV)	PE	NKI-M9	Biolegend	Mouse IgG2a	1:25
CD66b	FITC	G10F5	Biolegend	Mouse IgM	1:50
CD97	PE	VIM3b	Biolegend	Mouse IgG1	1:20
Goat anti-Mouse IgG	PE	Poly4053	Biolegend	Goat IgG polyclonal	1:50
	APC	Poly4053	Biolegend	Goat IgG polyclonal	1:50
NEO1	unconjugated	EPR14696	Abcam	Rabbit monoclonal	1:100
PLXNA1	Alexa 647	708954	R&D systems	Mouse IgG2b	1:200
PLXNC1	unconjugated	1A12	NovusBio	Mouse IgG2b	1:40
	Alexa 647	544232	BD pharmingen	Mouse IgG2b	1:20
ROBO1	unconjugated	770502	R&D systems	Mouse IgG1	1:50
SEMA4A	unconjugated	5E3	Biolegend	Mouse IgG1	1:500
	PE	5E3	Biolegend	Mouse IgG1	1:200
	PerCP-eFlour 710	5E3	Thermo Fisher Scientific	Mouse IgG1	1:24
SEMA4D	PE	A8	Biolegend	Mouse IgG1	1:200
Streptavidin	APC	n/a	Affymetrix	n/a	1:500

Table 2.8 *Antibodies used for flow cytometry.* All dilutions are for 100,000 cells in a 50µl final volume.

Antibody	Conjugate	Clone	Supplier	Isotype	Dilution
Viability stains					
7-AAD	n/a	n/a	Biolegend	n/a	1:100
AnnexinV	APC	n/a	Biolegend	n/a	1:100
DAPI	n/a	n/a	Thermo Fisher Scientific	n/a	1:30000
ZombieAqua	n/a	n/a	Biolegend	n/a	1:100
ZombieRed	n/a	n/a	Biolegend	n/a	1:100
ZombieYellow	n/a	n/a	Biolegend	n/a	1:100
Western-blot					
His	unconjugated	HIS.H8	ThermoFisher	Mouse IgG2b	1:1000
NEO1	unconjugated	EPR14696	Abcam	Rabbit monoclonal	1:1000
SEMA4A	unconjugated	n/a	GeneTex	Rabbit IgG polyclonal	1:700
Goat anti-Mouse IgG	IRDye800CW	n/a	LI-COR Biosciences	Goat IgG polyclonal	1:15000
Goat anti-Mouse IgG	IRDye680RD	n/a	LI-COR Biosciences	Goat IgG polyclonal	1:15000
Immunofluorescence					
Goat anti-Mouse IgG	Alexa 555	A28180	ThermoFisher	Goat IgG polyclonal	1:2000
LAMP-1	Alexa 488	H4A3	Biolegend	Mouse IgG1	1:50

Table 2.9 *Other antibodies/viability dyes used.* All flow cytometry dilutions are for 100,000 cells in a 50µl final volume. Immunofluorescence dilutions are for 200,000 cells in 50µl final volume.

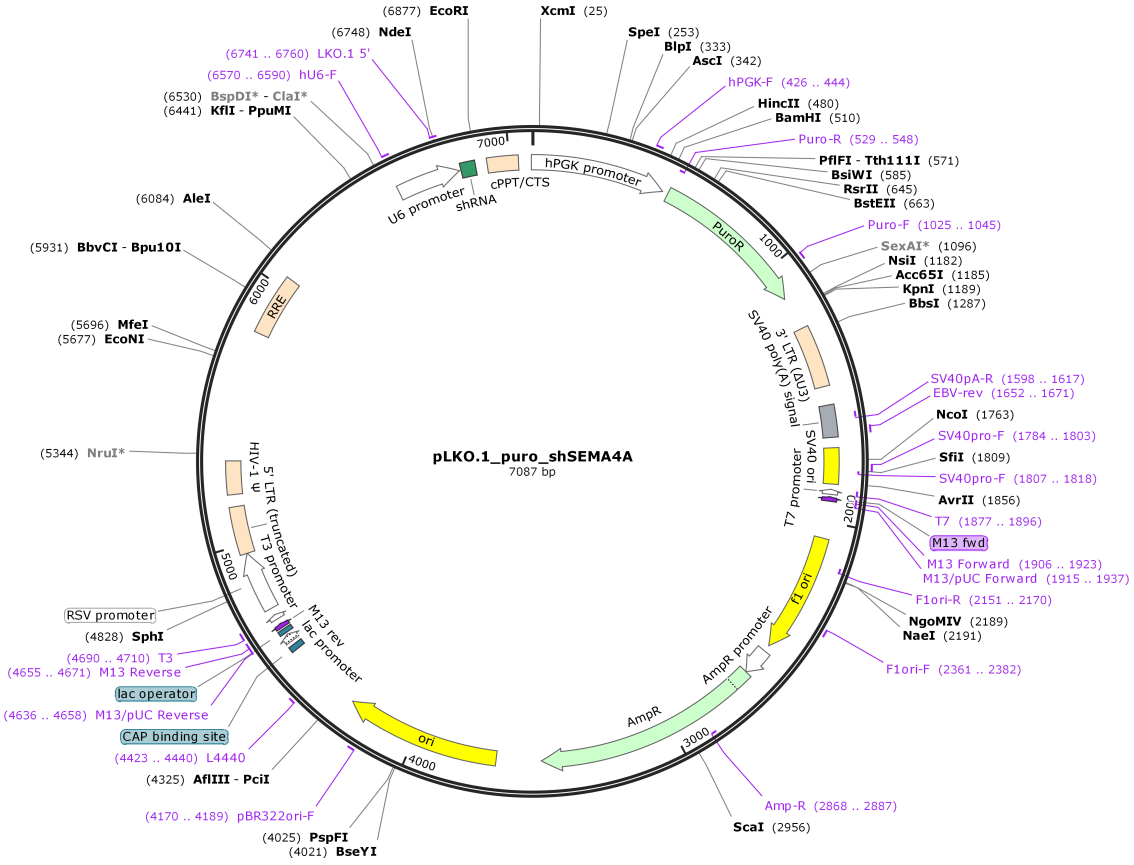

Fig. 2.1 pLKO.1_puro map

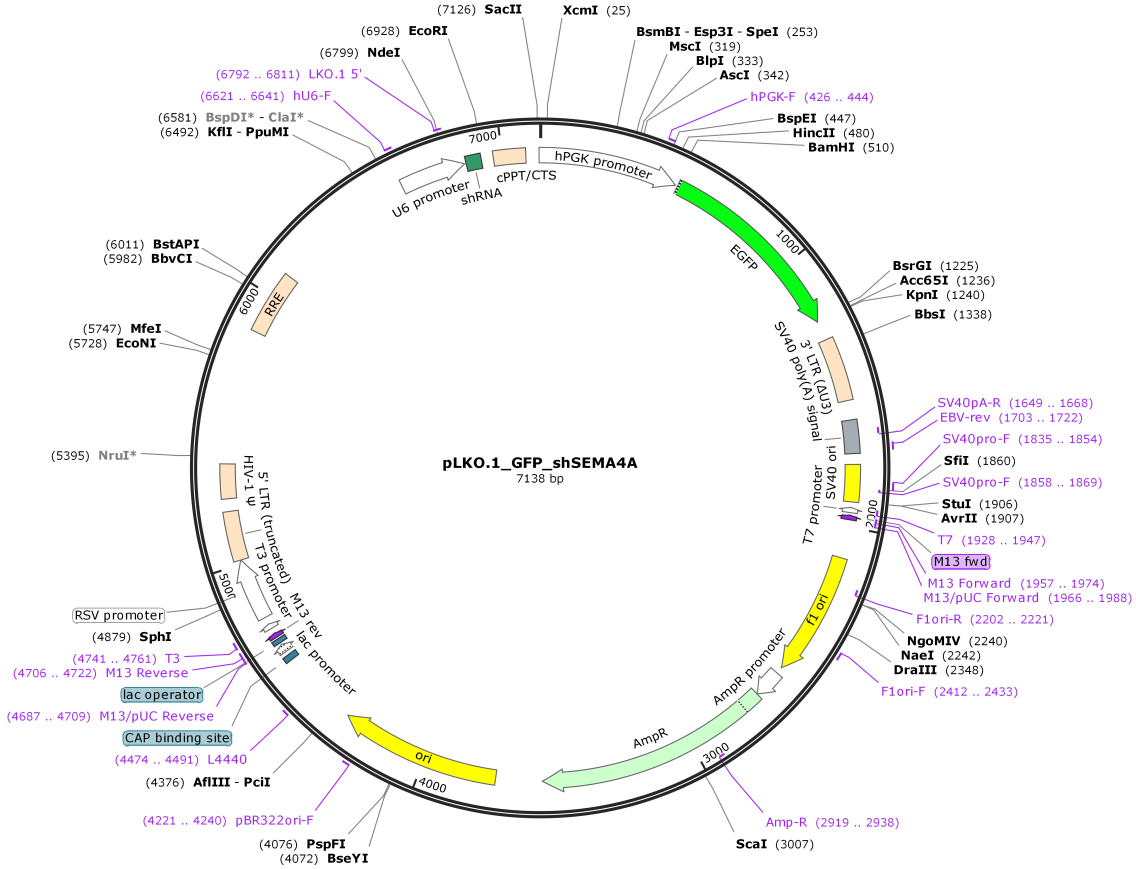

Fig. 2.2 pLKO.1_GFP map

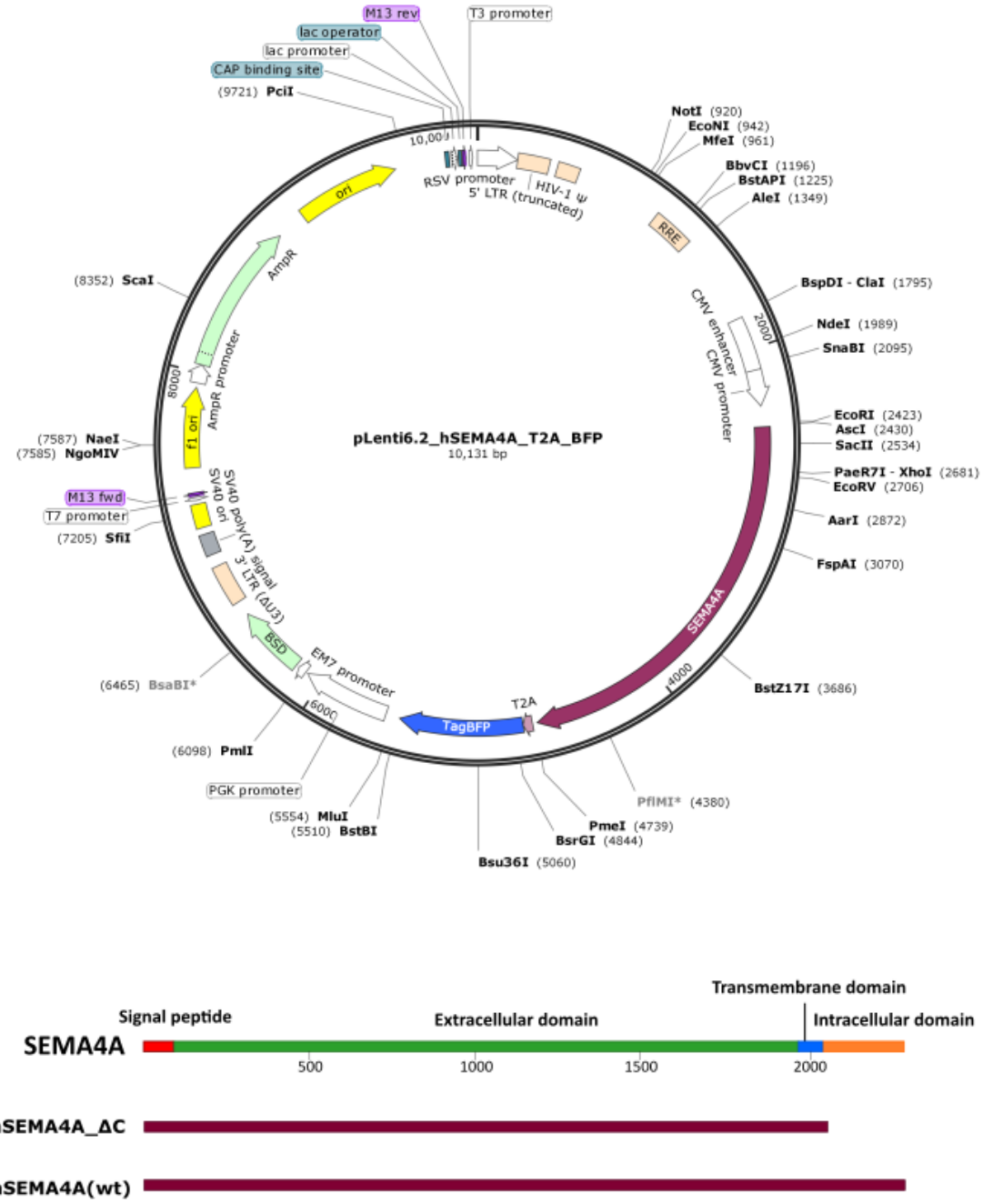

Fig. 2.3 pLenti6.2/SEMA4A_T2A_BFP map. This vector was used for the stable expression of shRNA-resistant mutant SEMA4A (lacking the intracellular domain, SEMA4AΔC) or the full-length SEMA4A (SEMA4A(wt))

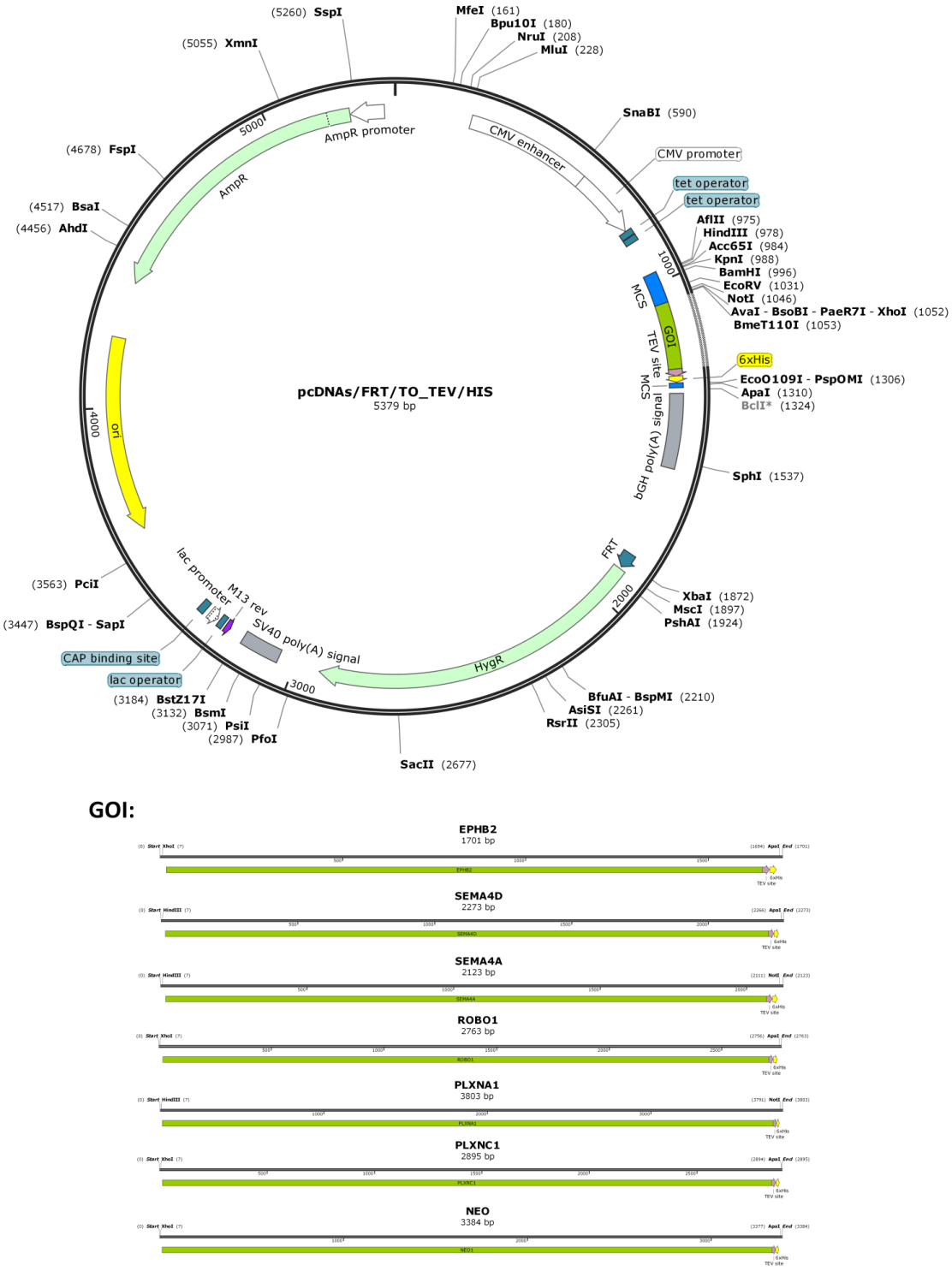

Fig. 2.4 pcDNA5/FRT/TO map. This vector was used to stably express the depicted seven genes of interest (GOI) for recombinant protein production and purification.

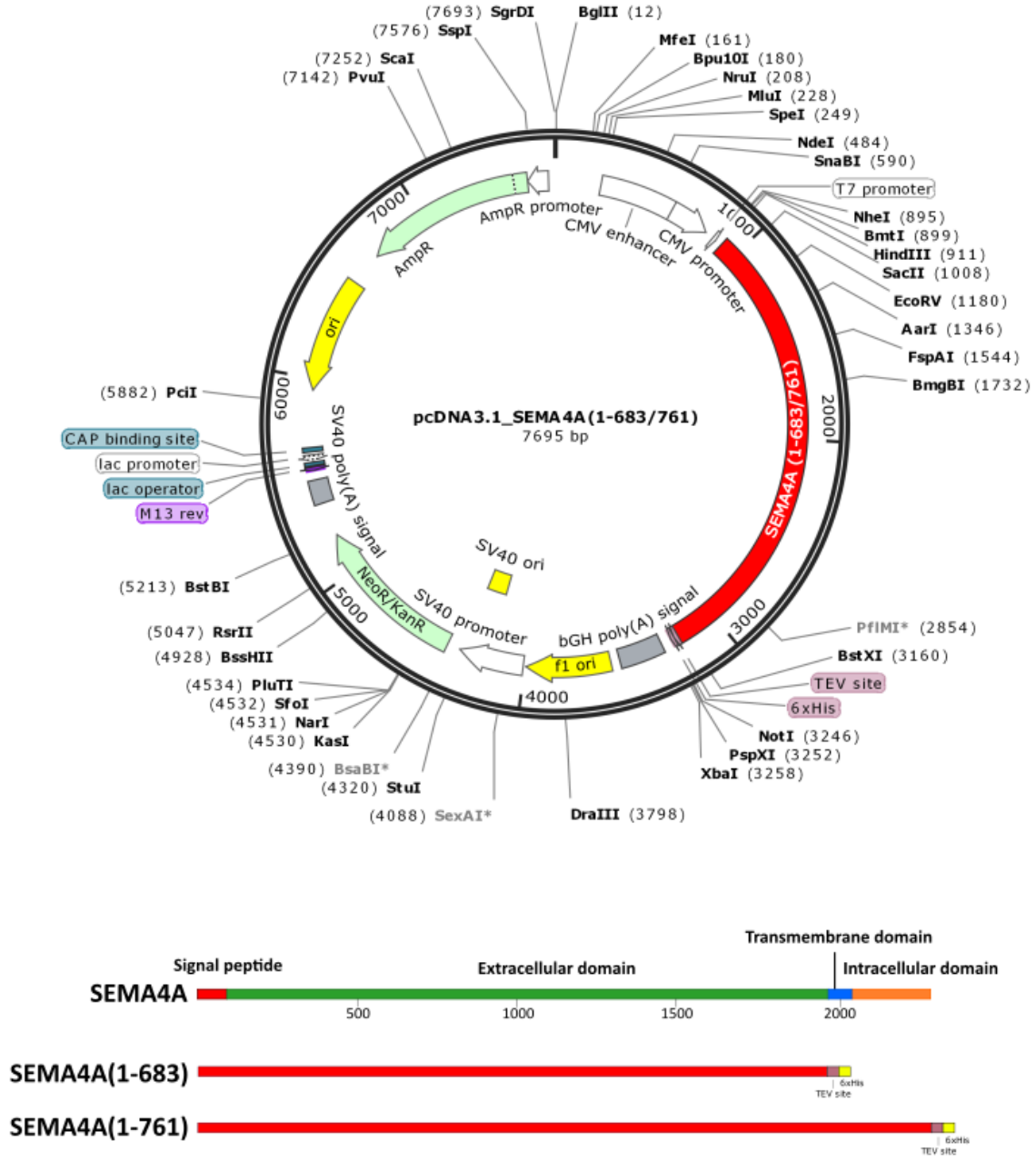

Fig. 2.5 pcDNA3.1_SEMA4A map. This vector was used for the transient expression of truncated SEMA4A (extracellular domain only, amino acids 1-683) or the full-length SEMA4A (1-761).

Chapter 3

Plasma Membrane Profiling

3.1 Introduction

Plasma membrane proteins represent the ideal therapeutic target since they are both easily accessible and involved in mediating numerous biological processes. However, the characterisation of these proteins has been challenging due to their low-abundance and highly hydrophobic nature, frequently leading to under-representation by mass spectrometry-based analysis [266]. A comprehensive profiling of this cellular compartment would provide not only potential therapeutic targets but would also provide valuable diagnostic and prognostic biomarkers. Furthermore, it will increase our understanding of tumorigenesis and the mechanisms of immune evasion. A recent technique, developed by Weekes *et al* [284] (PMP), overcomes the traditional challenges of membrane proteomics. This technique utilises the cell membrane impermeable aminooxy-biotin to tag and specifically isolate these plasma membrane proteins from the contaminating intracellular proteins using immobilised streptavidin. By combining this technique with the isobaric TMT labels, the plasma membrane proteome of up to ten samples can be quantitatively compared at once.

The aim of this chapter is to employ PMP to identify and quantify plasma membrane protein expression in both HMCLs and myeloma patient samples. As the cell surface proteome of primary myeloma cells has not yet been quantitatively analysed, a comprehensive dataset would provide an invaluable tool for the myeloma community. Primary myeloma cells are difficult to maintain in culture and as such HMCLs are an important tool for myeloma researchers. However, there are clear caveats when using these cell lines. For instance, these cell lines are typically obtained from advanced, extramedullary disease and have adapted to survive outside of the tumour microenvironment, which regulates the expression of a number of cell surface proteins (section 1.5). Furthermore, the hyperdiploid subgroup is substantially

under-represented amongst the HMCLs and the method of obtaining these cell lines can have a significant impact on the molecular heterogeneity of these cells [303][304]. Therefore, it is important to profile both HMCLs, which provide a tractable functional model for target validation, and primary cells since it will be of interest to compare the proteomic profile of both groups.

An additional advantage to the profiling of HMCLs is that these cells have been extensively characterised at both the genomic and transcriptomic level. The ten HMCLs used in this thesis were selected to provide the best coverage of all the major chromosomal translocations, copy number variations and other mutational events that occur in MM. By comparing cell surface protein expression with the underlying genotype, I aim to improve our understanding of myeloma cell biology and the downstream *sequelae* of specific mutations. The traditional dogma of proteomics is that RNA is a poor proxy for protein abundance [258]. Interestingly, it has been shown that this may be highly dependent on the gene function and some groups of transcripts may demonstrate a high correlation between RNA and protein abundance [259][260]. It is not yet known if plasma membrane protein expression and RNA abundance follow this tight correlation, although it is expected that this is unlikely to be the case. In addition, Wilhelm and Edfors [302][305] have recently proposed that although the RNA translation and protein degradation rates may vary greatly between different transcripts, these factors remain surprisingly constant for any given protein across multiple tissue types. Therefore, the abundance of any protein could be predicted from transcript expression using a RNA-to-protein (RTP) conversion factor. These reports warrant investigation, and it would be of interest to see if plasma membrane proteins exhibit any correlation with transcript abundance and to determine if a RTP factor can be applied to predict protein abundance.

As well as profiling HMCLs and primary myeloma samples, it is also of interest to profile normal plasma cells. Although not necessary for target identification, this would aid the discovery of proteins involved in promoting tumorigenesis and are essential for myeloma cell survival and growth. However, similarly to malignant plasma cells, it is difficult to obtain sufficient numbers of these cells and there are the ethical considerations in obtaining healthy, age-matched controls. Our initial proposal was to isolate plasma cells from the discarded tops of femurs from total hip arthroplasty procedures. However, following personal communication with CBSB (Cambridge Blood and Stem Cell Biobank), it was advised that this approach would be limited in the isolation of intact and sufficient plasma cell numbers. An alternative solution would be to generate these cells *in vitro* from peripheral blood B cells [94]. Using a combination of cellular and non-cellular components, Cocco *et al* were

able to recapitulate the BM niche and promote the differentiation of long-lived plasma cells. Although these cells clearly exhibit some genetic differences from their BM counterpart, they share a clear common gene expression profile [94] and could be considered representative.

3.1.1 Chapter overview

In this chapter I have addressed the initial concerns in the suitability of using this mass spectrometry technique for the proteomic profiling of primary myeloma cells, confirming biotinylation efficiency and TMT labelling, as well as the demonstrating the consistent enrichment of plasma membrane proteins in both HMCLs and primary samples. Also described is the *in vitro* generation of plasma cells from peripheral blood B cells following the method described by Cocco *et al* [94]. Although I was able to generate cells that phenotypically resembled plasma cells, I was unable to profile these by PMP because of cell-number constraints. However, I report the PMP of ten HMCLs and eight primary patient samples and demonstrate that this dataset provides an accurate and quantitative representation of the myeloma cell surface proteome, using a combination of flow cytometry and repeat profiling to validate this dataset. By comparing RNA and protein abundance, I show that RNA expression alone is insufficient to determine plasma membrane protein expression, but that a RTP factor can be applied, which provides a much more accurate estimation. Finally, applying a bioinformatic approach, I have identified 16 novel potential targets for the treatment of myeloma.

3.2 Results

3.2.1 Authentication of cell lines

To ensure that our results would be reproducible, it was first essential to authenticate the cell lines used in this study and to ensure they were not misidentified. 32 human myeloma cell lines have been extensively characterised at the genomic level by exome sequencing and RNAseq by the Keats Lab[1]. From these publicly available datasets, missense mutations that were unique to each cell line were identified, see table 3.1. The genomic DNA of each cell line was analysed for the absence or presence of these identifying mutations. All cell lines contained only the expected unique mutation, verifying that these cell lines were correctly

[1] Part of the Integrated Cancer Genomics Division at the Translational Genomics Research Institute, Phoenix, AZ. See Materials and methods, section 2.16

identified. The 10 identifying sequencing traces are shown in figure 3.1.

For MM.1S the sequencing trace suggested an issue with cross-contamination due to the difference in intensity for adenine and guanine at the expected mutation site (fig 3.1). These would have been expected to be equal for a heterozygous mutation. However, morphological assessment and all flow cytometry analysis suggests that this is truly a single cell population. This difference may be explained due to the *DNAH14* locus, which is mapped to chromosome 1q42, with 1q amplifications being a common genetic aberration in myeloma.

Cell line	Gene	Amino acid change	Codon change	Heterozygous/ Homozygous
OCI-My7	*APC2*	p.P406L	cCc/cTc	Heterozygous
INA-6	*ELF1*	p.I293L	Att/Ctt	Heterozygous
KMS-12-BM	*DOCK8*	p.P1019L	cCa/cTa	Heterozygous
MM.1S	*DNAH14*	p.K3359R	aAa/aGa	Heterozygous
OCI-My5	*EYS*	p.E1412Q	Gag/Cag	Heterozygous
SK-MM-1	*IRAK3*	p.L399R	cTa/cGa	Heterozygous
NCI-H929	*BRCA2*	p.R2668G	Aga/Gga	Homozygous
JIM3	*LRP10*	p.P614A	Ccc/Gcc	Heterozygous
OPM-2	*APOB*	p.F1480C	tTt/tGt	Heterozygous
LP-1	*LRP10*	p.R554Q	cGa/cAa	Homozygous

Table 3.1 *HMCL identifying missense mutations.* The amino acid and corresponding DNA substitutions for the unique missense mutations used to identify the 10 HMCLs.

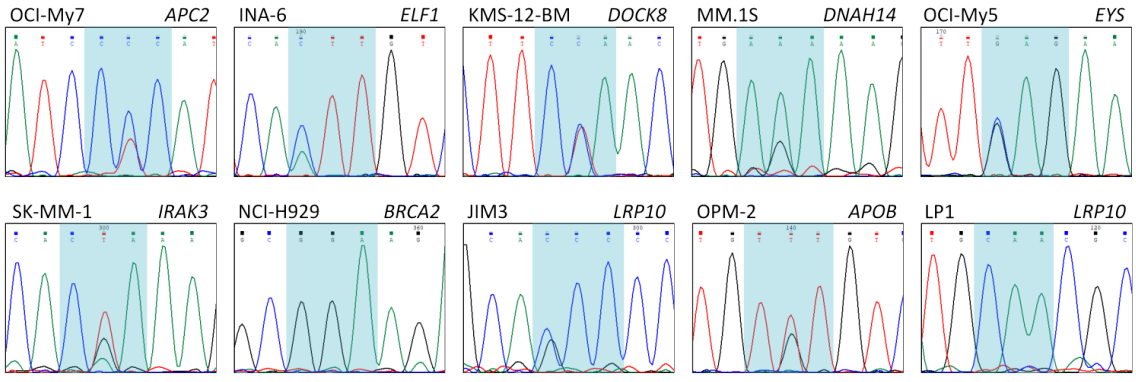

Fig. 3.1 *HMCL sequencing traces.* The genomic DNA sequencing traces for all 10 HMCLs confirm the presence of the expected identifying missense mutation (highlighted in blue).

3.2.2 Isolation of primary myeloma samples

PMP enriches for plasma membrane proteins, a relatively low abundant protein population. Because of this a much larger starting amount of material is required compared to whole cell proteomic techniques. Whilst HMCLs can be grown up accordingly and represent a pure cell population, primary samples are much more complex, comprising a mix of different cell types. The total number of cells obtained in a BMA and the percentage of plasma cells can also be highly variable. The next consideration in this study, therefore, was to ensure that a) enough plasma cells could be extracted from individual samples and that b) they were of a sufficiently high purity for mass spectrometry.

Plasma cells were isolated from bone marrow aspirates using microbeads targeting CD138 (syndecan-1), a plasma cell marker. Samples were analysed by flow cytometry before and after selection to determine sample purity. As shown in figure 3.2 depicting a representative sample, there was a high level of purity for CD138 positive cells following selection. Greater than 98% purity was achieved across all samples analysed which was sufficient for mass spectrometry analysis. Morpholigical assessment by May-Grünwald-Giesma staining was also used to further verify the purity following plasma cell isolation (data not shown). All primary sample processing and biotinylation was performed in collaboration with Dr S Surget and Dr J Ballester Beltran[2].

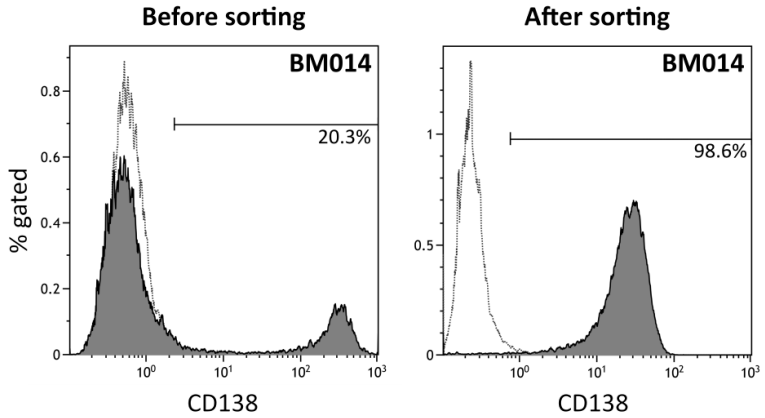

Fig. 3.2 *CD138$^+$ cell purity before and after plasma cell separation.* CD138$^+$ cell purity was assessed by flow cytometry before and after magnetic microbead selection. A representative histogram is shown (BM014) with IgG1 isotype control in white (no fill) and anti-CD138-PE in grey (filled).

[2]Mike Chapman Group, Department of Haematology, University of Cambridge

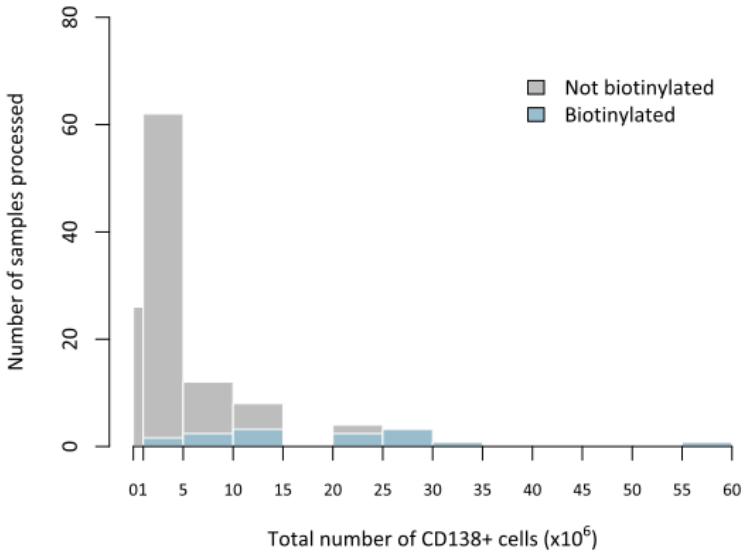

Fig. 3.3 *Total CD138$^+$ cell counts from all samples processed.* The total number of CD138$^+$ cells was determined for each sample based on either cell counts following CD138 selection or estimated by the percentage infiltration determined by flow cytometry. Samples which were biotinylated for PMP are shown in blue.

Following discussions with Dr James Williamson, it was determined that a starting number of $1x10^7$ plasma cells would provide a sufficient quantity of protein following biotinylation. This took into consideration the potential loss of cells during the multiple washing steps whilst remaining within an achievable range. Out of the 117 BMA processed to data, only 17 samples provided $\geq 10x10^6$ CD138$^+$ cells. A total of 17 BMAs were biotinylated, including some samples with less than the required starting number of cells. Figure 3.3 summarises the total number of CD138$^+$ cells per sample and the number of samples biotinylated.

3.2.3 Establishment of PMP

At the start of this project, plasma membrane profiling was a relatively new technique and had not been applied previously to myeloma. In adopting PMP, several pilot experiments were performed to confirm that each step of the protocol was working sufficiently.

One of first potential challenges that could be encountered in applying this technique is the failure of the aminooxy-biotinylation reaction to sufficiently label the cell surface proteins.

In conjunction with this, the acidic conditions required for labelling may be poorly tolerated by the primary samples, which are fragile and can be difficult to handle *ex vivo*. The first initial experiment was therefore to test the efficiency of this reaction in all ten HMCLs and a selected few initial primary samples. Samples were incubated with aminooxy-biotin, sodium periodate and aniline in PBS pH 6.7. The reaction was quenched following the addition of glycerol and the incorporation of the biotin tag into plasma membrane proteins assessed by flow cytometry using a streptavidin-APC conjugate. There was a clear separation between samples before and after biotinylation, with a strong shift in signal intensity (average MFI ratio of 720 $\pm$261 (mean $\pm$SD, n=10), figure 3.4. Primary samples also exhibited a high incorporation of biotin, although there was a greater variability between samples (MFI ratio of 1862 $\pm$672 (mean $\pm$SD, n=4)).

The biotinylation reaction itself was well tolerated, with a mean 12.9% reduction in viability in the HMCLs following aminooxy-biotin labelling. As anticipated, primary cell viability was more affected by the reaction but was still considered to be within an acceptable range (27.6% average loss of viability between before and after biotinylation). Ensuring that all centrifugation steps during the plasma cell isolation were kept at 4°C was found to improve primary cell viability (personal observation).

Having confirmed that there would be no challenges presented by the initial biotinylation step, I next proceeded to confirm that there would also be no technical challenges during the second step (pulldown and labelling) of the PMP workflow and that I would be able to achieve a high level of plasma membrane protein enrichment. This was a particular concern for the primary samples in which I had observed a higher percentage of cell death, which may compromise the cell membrane integrity and impact the amount of intracellular contaminants. To assess the pulldown and labelling, a total of three pilot mass spectrometry runs were performed.

From our preliminary biotinylation experiments, three samples were selected for these pilot runs: two HMCLs and one primary sample. Biotinylated proteins were enriched by affinity-purification before dentaturation, alkylation, reduction and finally digestion with trypsin. Samples were then analysed using a nano LC-MS platform and the subcellular localisation of identified proteins inferred from GOCC terms. The total number of proteins, their relative abundance and subcellular localisation from these pilot studies are summarised in fig 3.5. Protein enrichment was calculated as the percentage abundance.

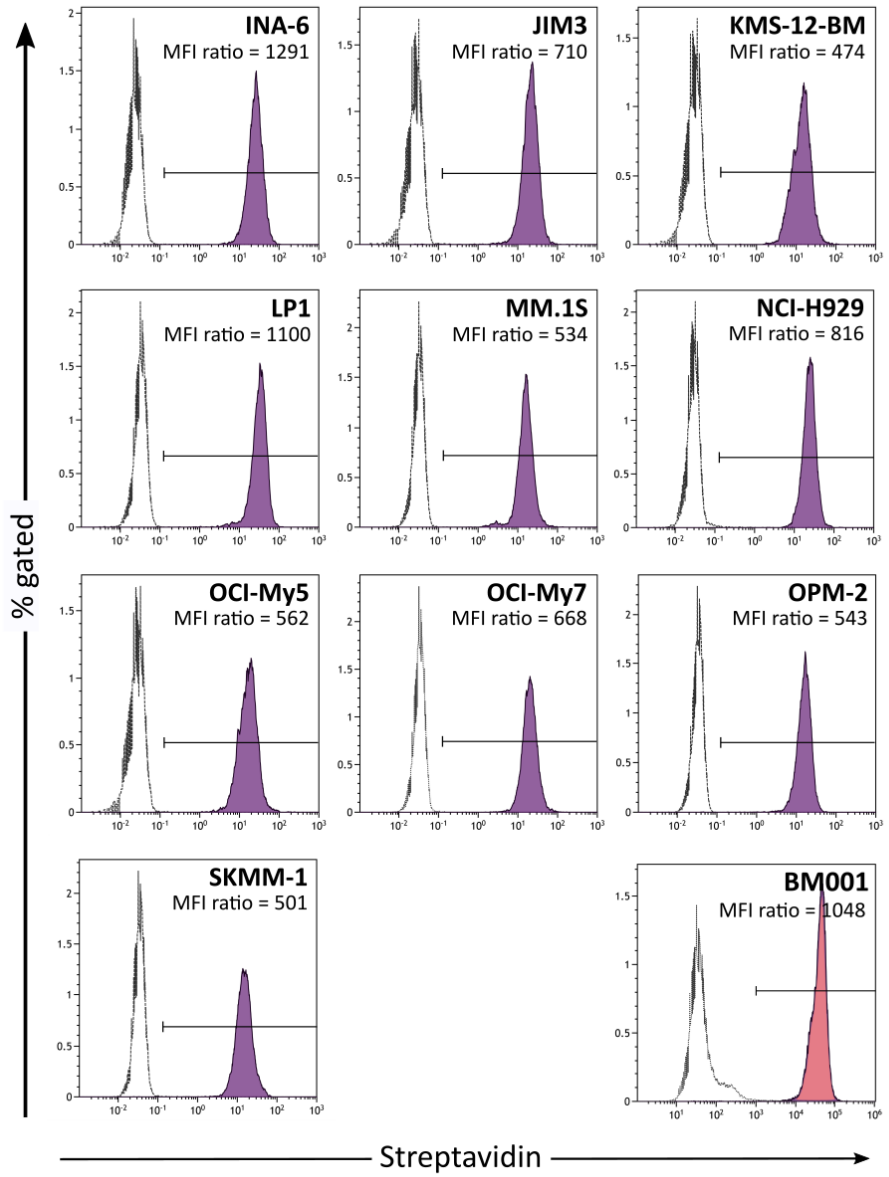

Fig. 3.4 *Labelling of HMCLs and primary MM samples by aminooxy-biotin.* Cells were incubated with 1mM sodium periodate, 10mM aniline and 100mM aminooxy-biotin in PBS pH 6.7 for 30 minutes at 4°C in the dark. A sample population was taken before biotinylation (no fill) and after (fill) and incubated with streptavidin-APC before flow cytometric analysis. A representative patient sample (BM001) is shown in pink.

The first two MS pilot experiments assessed the level of plasma membrane protein enrichment in the HMCL samples. In run one, a total of 413 out of 696 unique proteins were identified as 'plasma membrane' with an enrichment of 87.9%. For run two, sample peptides were labelled using the isobaric TMTZero tag before MS analysis. 114 unique proteins were identified, with 92 annotated as 'plasma membrane' with a respective enrichment of 80.3%. The TMT tag was well incorporated, with 706 out of 718 (98%) peptide-spectrum matches (PSMs) identified as containing a TMT modification. The acquisition method for the TMT label (MS3) in conjunction with the short gradient used meant the total number of proteins identified was much lower than the first run. As this list was smaller, the 'other' proteins were manually annotated and a further seven determined to be plasma membrane proteins due to their possession of an intracellular and extracellular domain as well as a *N*-Acetylglucosamine modification in the later domain. Nine of the remaining 'other' proteins were identified as either naturally biotinylated, such as ACACA, or were environmental contaminants (for example, K1C9 (keratin)). Overall, the plasma membrane protein enrichment may therefore be potentially much greater than what is predicted using GOCC terms.

The final test run was to ensure that I was also able to achieve a high level of enrichment in the primary samples. A total of 988 unique proteins were identified. 438 were classed as 'plasma membrane'. Although the ratio of 'non-PM' to 'PM' was higher compared with the first two runs, the actual enrichment was still relatively high (77.5%). A further assessment of these 'non-PM' proteins revealed 252 were annotated as 'GO_extracellular_vesicular_exosome' or 'GO_extracellular_region', suggesting that these may be potential plasma membrane-associated proteins. Overall, the level of PM protein enrichment across these preliminary studies was consistently high, ranging between 77.5% and 87.9%, consistent with other studies run by the Lehner group (personal communication).

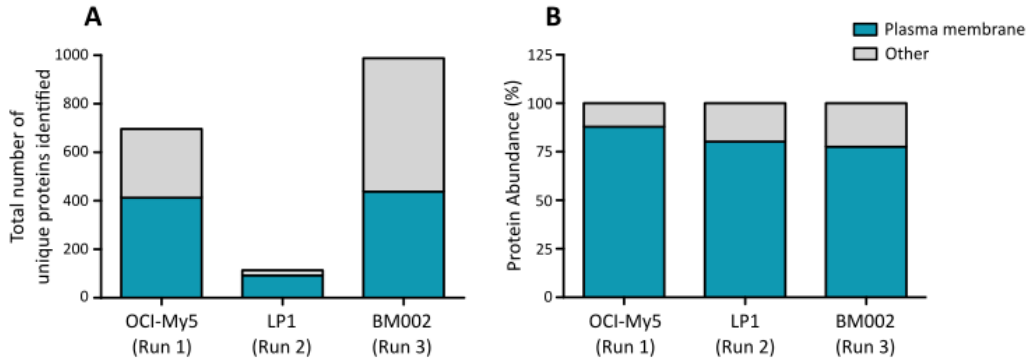

Fig. 3.5 *Total number and enrichment of plasma membrane proteins identified in PMP pilot studies.* Biotinylated proteins from three separate pilot runs (OCI-My5, LP-1 and BM002) were affinity-enriched before denatured, reduced, alkylated and digested with trypsin. Peptides from run two (LP-1) were labelled using the isobaric tag TMTZero. All samples were then analysed using a nanoLC-MS platform. **A** The total number of proteins identified in all three runs. **B** Subcellular localisation enrichment as determined by protein abundance. The number/percentage enrichment for 'plasma membrane proteins' is shown in blue.

3.2.4 *In vitro* generation of healthy plasma cell controls from B cells

Our initial aim was to employ PMP to characterise the cell surface proteome of both malignant and healthy plasma cells. Any proteins that were identified as aberrantly expressed in the myeloma samples would be taken forward as potential monoclonal antibody target candidates. However, there were several challenges associated with obtaining healthy, age-matched samples, including the ethics of obaining BMAs from healthy donors and the rarity of this cell population. A proposed alternative was to use an *in vitro* model of differentiation to generate plasma cells from B cells isolated from the peripheral blood of healthy individuals.

Isolated B cells from healthy donors were stimulated using a combination of CD40L-expressing cells, IL-2, IL-21 and F(ab')$_2$ anti-IgG/IgM over six days to drive differentiation into plasmablasts. These plasmablasts were then further differentiated into a mature plasma cell phenotype over the next seven days using a co-culture system with the stromal cell line M2-10B4 and the addition of IL-21, IL-6 and IFNα. Between day 0 and day 6 I observed a decrease in the expression of the pan B-cell marker CD20, with a concomitant increase in CD38 expression. From day 6 onwards, I observed a further decrease in CD20, and an increase in the expression of CD138 as cells transitioned into a CD20^{neg}CD38^{hi}CD138^{pos}

Sample ID	Cell amplification D0	D3	D6	D10	D13	Comments
LC002(i)	1	0.49	5.9	-	0.24	Starting from naive/memory B cells Contamination of CD16+ cells (27%) between D10 and 13
LC002(ii)	1	0.78	6.06	0.39	0.1	Starting from naive/memory B cells
LC003	1	0.79	5.3	2.1	0.95	Starting from naive/memory B cells
LC004(i)	1	2.6	66	18	2	Starting from memory B cells
LC004(ii)	1	2.8	38	15.4	4.4	Starting from memory B cells

Table 3.2 Cell amplification (fold increase relative to the day 0 B cell input) across the timecourse of the differentiation protocol for each sample.

mature plasma cell phenotype, figure 3.6. CD16 expression was monitored to ensure that the culture was not overtaken by any NK cells that may have been retained following selection, as occurred in our initial test (LC002(i)). By day 13, 70% ±9% (mean ±SD, *n*=4) of the population were $CD38^{hi}CD138^{pos}$.

Mirroring plasma cell differentiation *in vivo*, there was an initial expansion of the B cell population between day 0 and day 6, closely followed by a population contraction. The magnitude of this amplification greatly varied between samples, table 3.2, and our initial experiments provided a low yield of plasma cells (0.1 and 0.95 total cells at day 13 for every 1 B cell seeded on day 0 for LC002(ii) and LC003 respectively). This was much lower than expected based on personal communication with Sophie Stephenson[3] and the available published literature. By selecting only for mature B cells instead of starting with an unsorted mixture of naive and memory B cells, I observed an improvement in the plasma cell yield (2 to 4.4 fold amplification in LC004(i) and (ii) respectively).

Although I was able to successfully generate plasma cells from healthy-donor derived B cells and the cell yield was improving as I gained experience with the technique, the associated costs, culture space and time that would be required to generate $1x10^7$ plasma cells resulted in the discontinuation of this approach. It was then determined to proceed and profile eight primary samples without the normal BM plasma cell controls.

[3]Reuben Tooze's Group, Faculty of Medicine and Health, University of Leeds

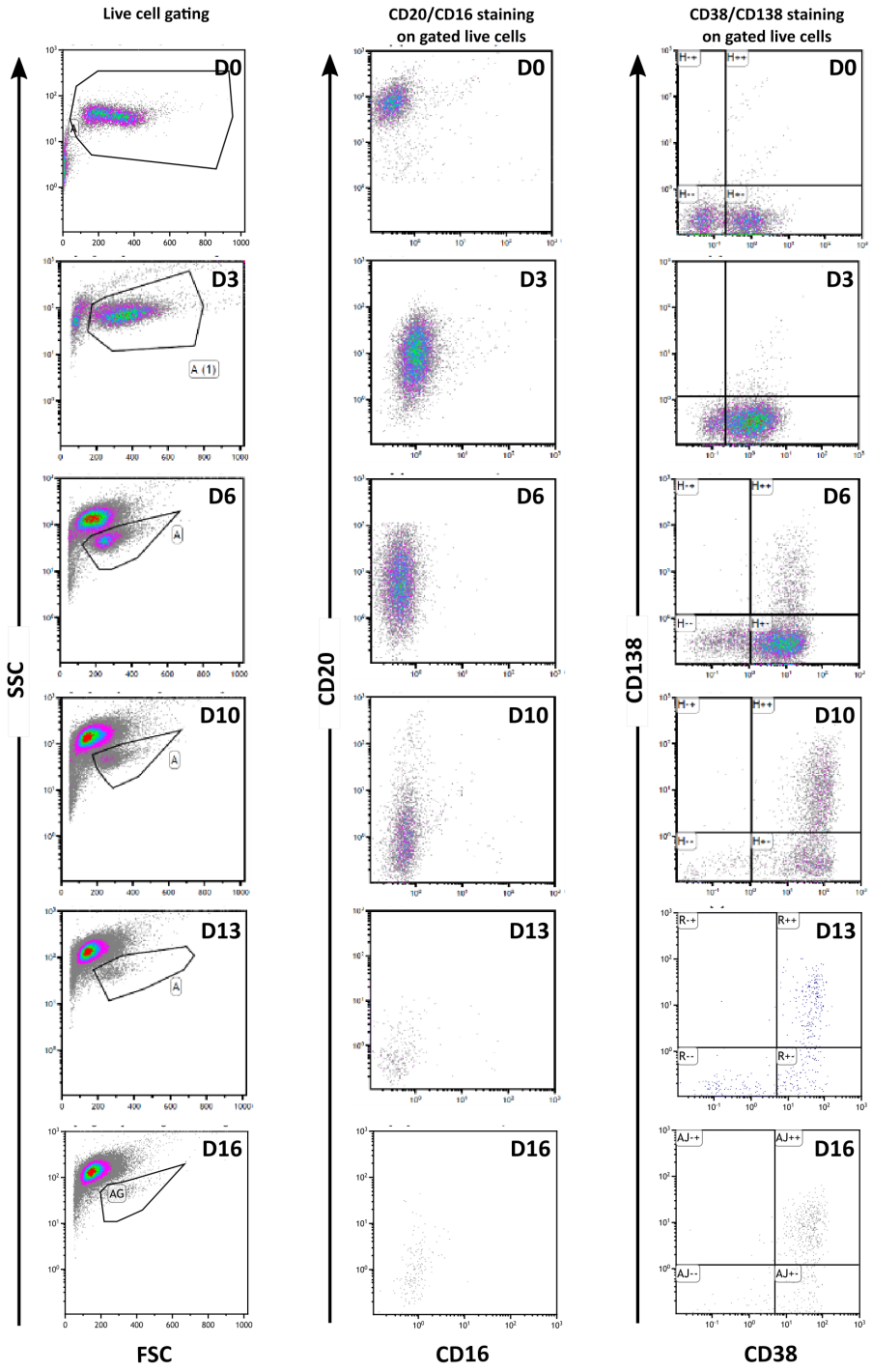

Fig. 3.6 *In vitro generation of healthy plasma cells.* Healthy, peripheral blood B cells were differentiated into plasma cells using a combination of CD40L, IL-2, IL-21, F(ab')$_2$ anti-IgG/IgM Il-6 and IFNalpha over 13 days. The example (LC003) depicted shows the phenotypic changes as cells matured from $CD20^{hi}CD38^{low}CD138^{neg}$ B cells at day 0 to $CD20^{l0w}CD38^{hi}CD138^{neg}$ plasmablasts by day 6 to $CD20^{neg}CD38^{hi}CD138^{pos}$ plasma cells at day 13 and onwards. CD16 was used to monitor NK cell contamination. The forward/side scatter plot exemplifies the extensive cell death I observed during this differentiation.

3.2.5 Plasma membrane profiling of HMCLs and primary myeloma samples

To characterise the cell surface proteome in myeloma, I chose to use two 10-plex experiments to quantitatively compare both HMCL and primary samples. This would enable us to identify proteins that are present in primary disease but also in cell lines, which provide a more tractable model for target validation. Aminooxy-biotinylated proteins were prepared from samples as previously described and captured using streptavidin-agarose beads. Proteins were then denatured, reduced, alkylated and digested with trypsin on-bead. Digested peptides were labelled using tandem mass tags (TMT10plex) to enable the relative quantitation of up to ten samples at once. Following labelling, 3% of each sample per 10-plex was pooled and 50% injected over a 90 minute gradient without fractionation as a test pool to determine if any adjustments in sample quantity would be necessary prior to the final pooling. The final pooled samples were subject to fractionation before MS analysis performed by Dr J Williamson. A total of ten HMCLs and eight primary samples were profiled.

The initial PMP experiment was to characterise the HMCLs. These ten cell lines were chosen to provide the best cover of all the major chromosomal translocations, copy number variations and other mutational events that occur in myeloma (table 3.3). Across the ten samples, 3,131 unique proteins were quantitatively analysed. Using Gene Ontology Cellular Compartment (GOCC) classifications as an estimate of enrichment, 1,159 of these were determined to be 'plasma membrane' proteins with a mean enrichment of 66.9% $\pm$6.6% (SD) across all samples.

The second PMP experiment consisted of eight primary samples and a re-run of two cell lines from the first PMP: KMS-12-BM and JIM3. These two lines were included to provide reference samples for comparisons between the two experiments. KMS-12-BM and JIM3 were chosen as these samples were considered to provide the largest coverage of all proteins identified in the first run. The patient characteristics of the eight samples profiled are detailed in table 3.4. These samples provided a good mix of patient characteristics, with samples taken at both diagnosis (n=5) and at progression/relapse (n=3). A greater total number of proteins were quantitatively analysed in this second run (4,962 unique proteins). The enrichment for plasma membrane proteins was lower compared with the first run (51.8% $\pm$4.2%(mean $\pm$SD)), but still a substantial number of 'plasma membrane proteins' were identified (1,644 proteins). A further 874 proteins were annotated as 'GO_extracellular_region/space/exosome'. The primary samples appeared to be much more sensitive to the biotinylation protocol and so it is unsurprising that there was a higher

Cell line	Primary translocation	Subgroup	*RAS* status	*p53* status
OCI-My7	t(11;14)	*CCND1*	*NRAS* (G61K het)	WT
INA-6	t(11;14)	*CCND1*	*NRAS* (G12D het)	Q331X het + K132M het
KMS-12-BM	t(11;14)	*CCND1*	WT	R337L homo
MM.1S	t(14;16)	*c-MAF*	*KRAS* (G12A het)	WT
SK-MM-1	t(14;20)	*MAFB*	*NRAS* (G12D het)	R175G het
OCI-My5	t(14;16)	*c-MAF*	WT	Frameshift homo
NCI-H929	t(4:14)	*MMSET/FGFR3*	*NRAS* (G13D het)	WT
JIM3	t(4:14)	*MMSET/FGFR3*	*KRAS* (G12D het)	R273C homo
OPM-2	t(4:14)	*MMSET/FGFR3*	WT	R175H homo
LP-1	t(4:14)	*MMSET/FGFR3*	WT	E286K homo

Table 3.3 *Known major genetic events of the HMCLs profiled.* Het=heterozygous. Homo=homozygous. WT=wild-type.

Sample identifier	Age	Sex	Disease status	CD138 infiltration	FISH analysis
BM004	70	M	D	22%	1q amplification and chr.13 deletion
BM014	68	M	D	15%	No IgH rearrangment
BM035	72	F	D	ND	ND
BM040	59	M	P/R	65%	No abnormalities found
BM044(d)	76	M	D	20%	t(14;16), 1q amplification and chr.13 deletion
BM049(d)	62	M	P/R	94%	ND
BM066(d)	88	F	D	27%	1q amplification and chr.13 deletion
BM068	65	F	P/R	65%	1q amplifcation

Table 3.4 *Patient sample characteristics.* CD138 infiltration was determined by flow cytometric analysis of the percentage of CD138+ cells present in each BMA post RBC lysis. M=Male; F=Female; D=diagnostic sample; P/R= progression/relapse sample; ND=not done. (d)=deceased.

number of contaminating intracellular proteins. Protein enrichment by both total unique proteins identified and by the relative abundance in both PMP experiments is shown in figure 3.7.

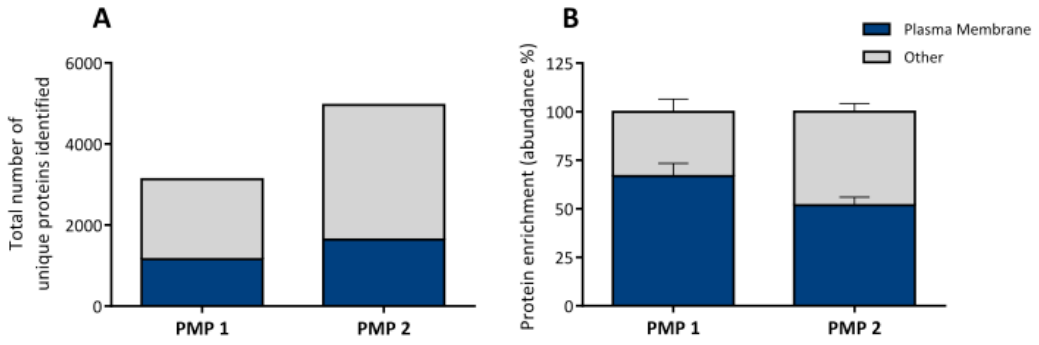

Fig. 3.7 *Total number and enrichment of plasma membrane proteins identified by PMP.* Biotinylated proteins from HMCLs and primary samples were affinity-enriched before denatured, reduced, alkylated and digested on-bead. Peptides were labelled using TMT10-plex before pooling and MS3 analysis on a nanoLC-MS platform. **A** The total number of unique proteins identified in HMCLs (PMP run one) and in primary samples (PMP run two). **B** The relative enrichment of plasma membrane proteins as determined by protein abundance. Proteins were annotated as 'plasma membrane' or 'other' using GOCC annotations.

Data was then processed as follows. Firstly, any proteins identified by only a single, unique peptide were excluded on the basis that these had a high probability of being false positives. These proteins tended to be of very low abundance. Next, as I was only interested in proteins that had been identified in both HMCLs and primary samples, I excluded proteins that were identified by only one PMP 10-plex. These were also proteins of low abundance and were likely to have either been below the threshold of detection for the first run, or were too variable to be detected consistently. Figure 3.8 shows the overlap between the two datasets. Nearly all (2,077 out of 2,356) proteins from the HMCL PMP were identified in the primary cells. Data was then log transformed before column-centering and scaling by the median absolute deviation for all statistical analysis. Except where noted, all data is plotted using the raw values.

Finally, protein subcellular localisation was re-annotated. Although GOCC terms alone can give us a rough prediction as to whether a protein is localised to the 'plasma membrane' or not, these GO terms are highly subject to inaccuracies and the completeness of the literature. Also, the plasma membrane is highly dynamic and proteins can associate with the membrane in various ways. Thus, a more comprehensive annotation was required to

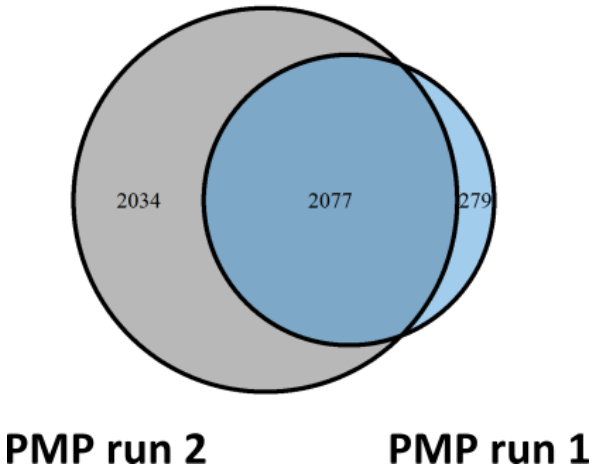

Fig. 3.8 *A venn diagram depicting the overlap of the proteins identified in both runs.* Overall, the majority of proteins identified in PMP run one (2077 out of 2356) were also identified in PMP run two.

discriminate between proteins expressed on the cell surface and therefore 'targetable' by a therapeutic antibody, and those intracellular peripheral proteins which are less so. For this annotation, extracellular and transmembrane domains were identified by Uniprot and used in conjunction with GOCC terms. These domains are either curated by experimental evidence or using topology prediction software. All proteins identified were then grouped into the following five main categories[4]:

- *Extracellular plasma membrane:* Any protein that contained an extracellular *and* transmembrane domain as curated by Uniprot.
- *Other plasma membrane:* Proteins that were annotated as 'plasma membrane' by GO terms but did not contain either an extracellular or transmembrane domain. This group likely contains proteins that are peripheral or lipid-anchored membrane proteins.
- *Secreted:* Any proteins with either an Uniprot or GO annotation for 'secreted', including those annotated as 'extracellular exosome/region' that did not fall into the above two categories.
- *Other membrane*: Proteins that contained *only* a transmembrane domain with no other annotations either by Uniprot or GO to infer plasma membrane localisation.

[4]Protein subcellular localisation strategy designed by Dr M Chapman

- *Non-membrane or unknown localisation:* Any remaining proteins that did not fall into the above categories. This included proteins with no evidence for membrane localisation or those that were unannotated by both databases.

From this classification, a total of 1,319 proteins were classified as plasma membrane or associated proteins with a mean enrichment of 79.5% ±5.59% (±SD, n=20). The summary of the number of proteins identified for each category and their relative abundance is shown in figure 3.9.

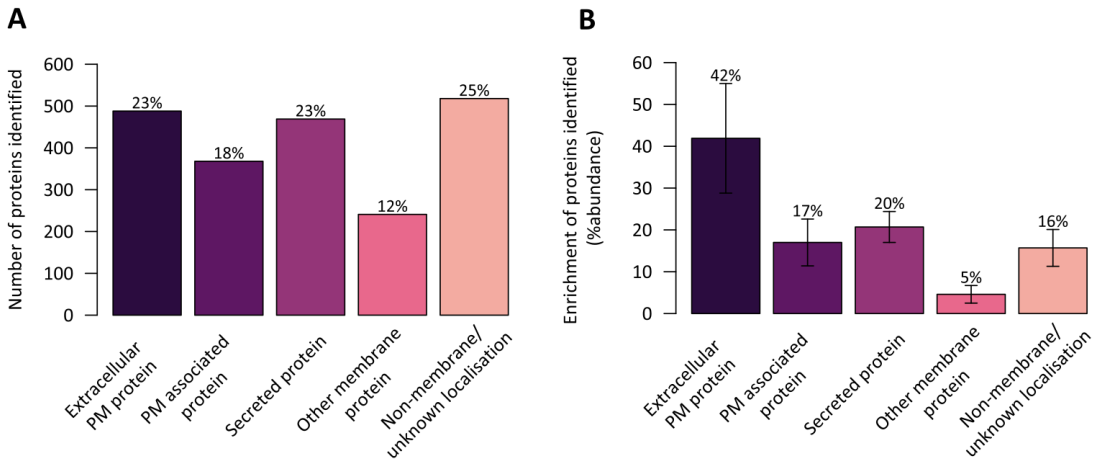

Fig. 3.9 *The subcellular localisation of all proteins commonly identified by PMP*. Using a combination of Uniprot and GO annotations, the 2,077 proteins identified in both PMP experiments were assigned to one of five groups. The total number of proteins **A** and their relative enrichment (determined by protein abundance) **B** for each group is depicted.

To assess the reproducibility of PMP and to confirm it was appropriate to make comparisons between the two datasets, I compared protein expression in both cell lines between the two experiments. There was a high inter-run consistency, with a strong positive correlation for both KMS-12-BM (r(2,077)=0.755, p<0.0001) and JIM3 (r(2,077)=0.692, p<0.0001), figure 3.10. There was a slightly stronger correlation between 'extracellular' and 'other' plasma membrane proteins, r(851)=0.784, p<0.0001 and r(851)=0.727, p<0.0001, for KMS-12-BM and JIM3 respectively. This strong correlation gave us confidence in the dataset generated by PMP.

To further validate our results, I compared the expression of six plasma membrane proteins by flow cytometry (FCM) and PMP. These six antigens were selected as proteins which were well described in the literature for myeloma and were known to have good working

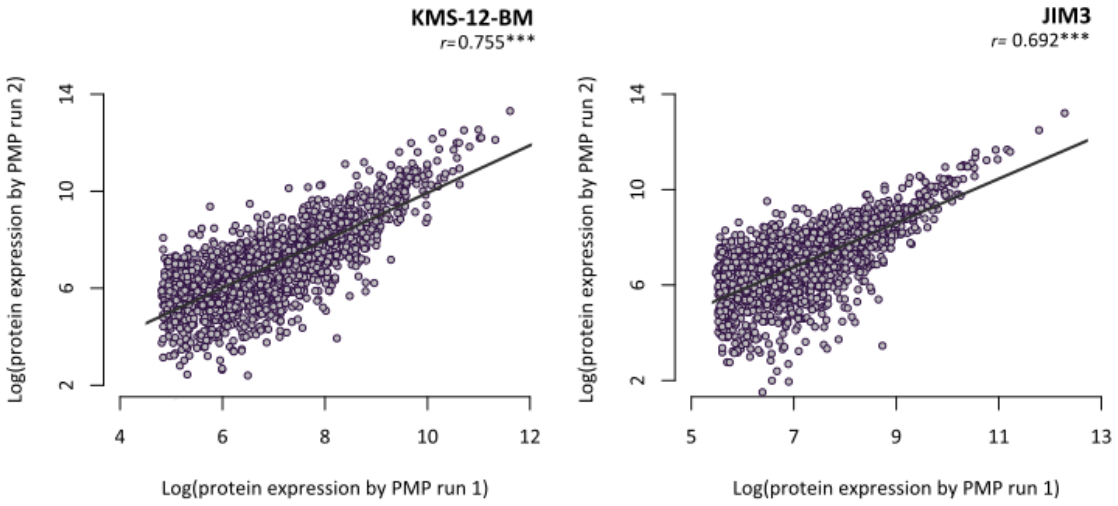

Fig. 3.10 *A comparison between the two HMCLs reveals a high inter-run consistency.* For all proteins identified in both datasets, the relative expression was compared between PMP run one and run two for both KMS-12-BM and JIM3. Correlation is reported as Pearson's correlation coefficient. *=p<0.05, **=p<0.01, ***=p<0.001.

flow cytometry antibodies available. The expression of each protein was measured by FCM across all ten HMCLs and the MFI ratio compared against PMP expression. As seen in figure 3.11, there was a strong positive correlation between PMP and flow cytometry across all six antigens ranging from the lowest correlation with CD38 ($r(10)=0.657$, $p<0.05$) to the highest with FGFR3 ($r(10)=0.993$, $p<0.001$).

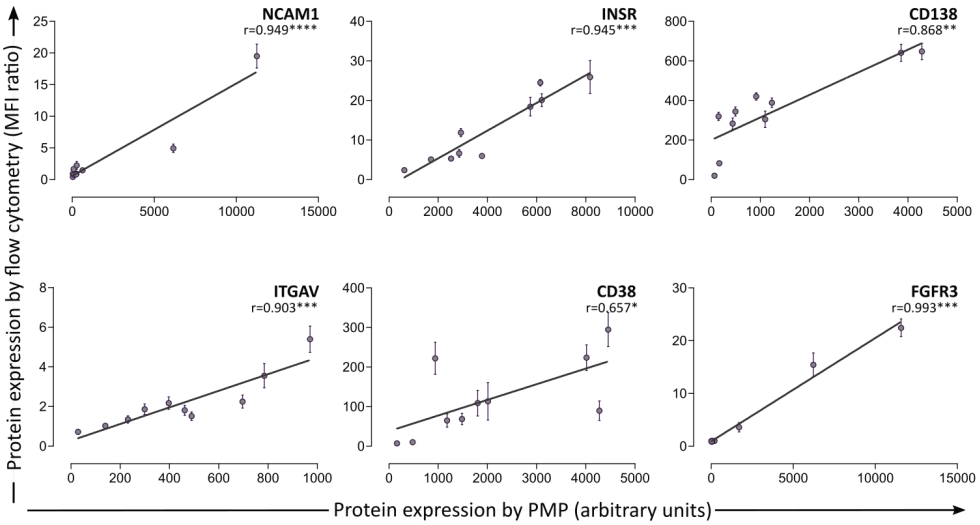

Fig. 3.11 *Protein expression by PMP is correlated with expression by flow cytomery.* Protein expression for the six selected antigens was measured across all ten HMCLs profiled and the MFI ratio compared against the relative expression by PMP. There was a strong positive correlation as determined by Pearson's correlation for all six antigens across the HMCLs. *=p<0.05, **=p<0.01, ***=p<0.001.

Lastly, as a commonly used method of target identification relies on using gene expression profiling, I wanted to assess how well the results of PMP correlated with RNAseq data across the HMCLs. Using the publicly available RNAseq dataset from the Keats Lab, I observed that there was a poor correlation between transcript levels and protein abundance resulting in correlation coefficents ranging from 0.13 to 0.21 (figure 3.12). I next investigated if a conversion factor (RNA-to-protein (RTP)) could be applied to the RNA levels to predict protein abundance. For each gene, a specific RTP factor was calculated using nine of the ten HMCLs as a training set. The RTPs across these nine cell lines were averaged and used to predict protein abundance in the tenth cell line. This was repeated for all the HMCLs profiled. As shown in figure 3.12, by applying a RTP conversion factor, the correlation between RNA and protein expression levels was significantly improved, with correlation coefficients of 0.78 to 0.89.

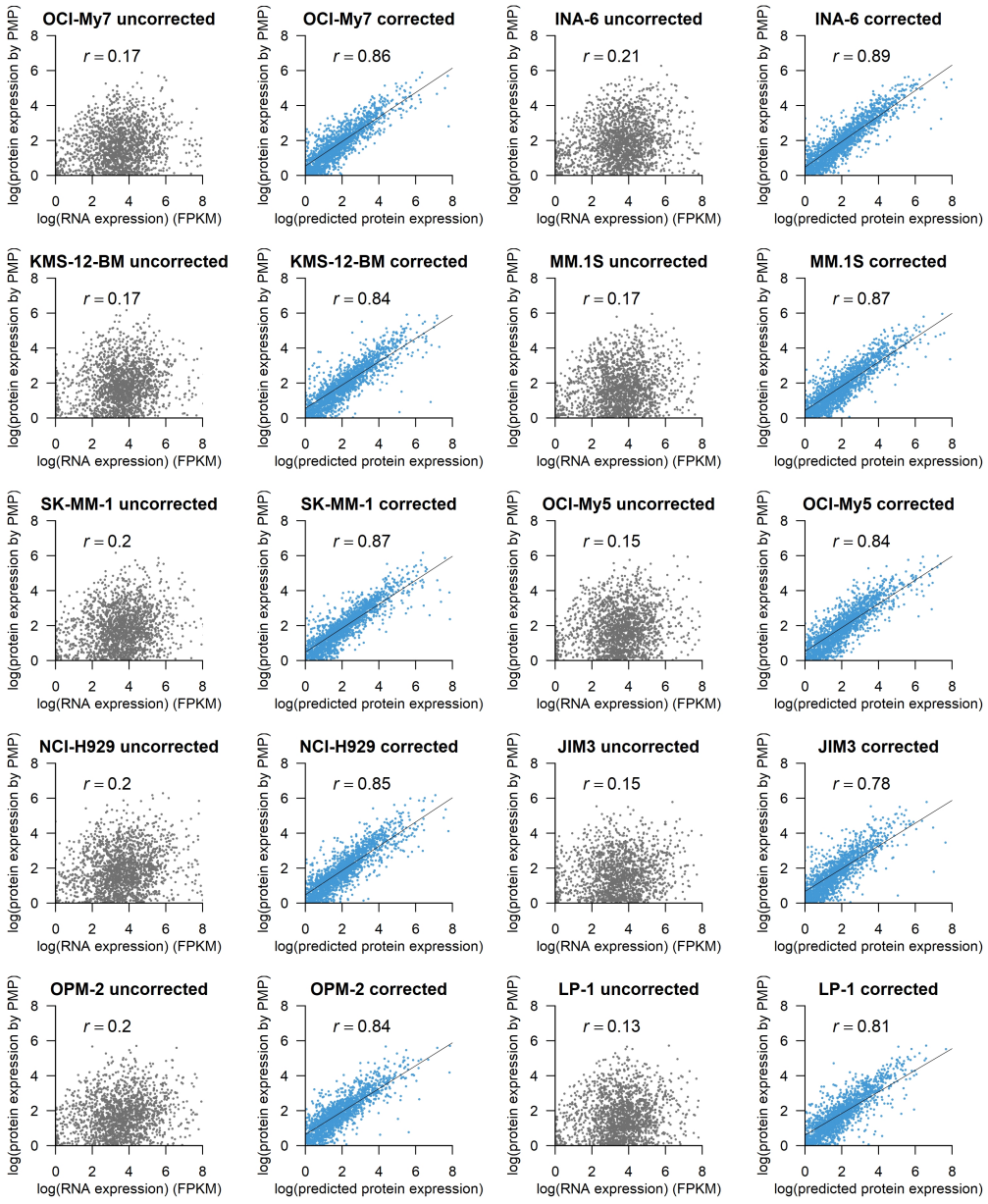

Fig. 3.12 *Protein abundance is poorly correlated with RNA expression but can be predicted by applying a RTP conversion factor.* The total relative protein expression determined by PMP was compared against RNA expression in all ten HMCLs. In grey ('uncorrected') is the direct gene-specific correlation between RNA and protein for each cell line. In blue ('corrected') is the correlation between the predicted protein abundance (determined by applying an averaged RTP conversion factor to RNA levels) and the actual relative protein expression by PMP. Each plotted cell line was excluded from the calculation of the average RTP. Pearson's correlation coefficient are reported.

3.2.6 Identification of proteins associated with underlying genetic aberrations

As these HMCLs profiled are genetically well characterised, our next aim was to identify any plasma membrane proteins whose protein expression is linked to specific mutational events. This may improve our understanding of myeloma cell biology and would enable the identification of markers associated with 'high-risk' cytogenetics.

A student's t-test was carried out to test the difference between protein expression for each subgroup compared with the other HMCLs (see table 3.3). The greatest number of significantly differentially expressed proteins were identified within the t(11;14) subgroup with a total of 11 proteins (SLC22A23, ENTPD1, RELL1, CXADR, HSDB17B11, ABCC4, ST3GAL1, ADCY9, ALG1, SLC25A20 and NDRG3) reported as significant (p<0.01 with a BH-adjusted p value (q value) of less than 0.25). Only one protein associated with the t(MAF) subgroup was reported as significant (STIM1, p<0.001, q=0.226) and none with a q<0.25 were reported for t(4;14). The top 5 differentially expressed proteins for each subgroup (both signficant and non-significant) are shown in figure 3.13.

For the secondary mutations, 11 proteins associated with the *TP53* subgroup were reported as significant: C16orf54, VAV1, CCT7, SLC33A1, EVI2B, REEP5, FDFT1, GNPTAB, ALG2, ERGIC1 and CD58. p<0.01, q<0.25). Only one protein was reported as significant for the *RAS* mutated cell lines (MAP2K3. p<0.001, q=0.242). For both *RAS* and *TP53*, HMCLs were broadly grouped into either WT or mutant. As a result some proteins may have been missed that are associated with specific mutations, such as *KRAS* versus *NRAS*, figure 3.14.

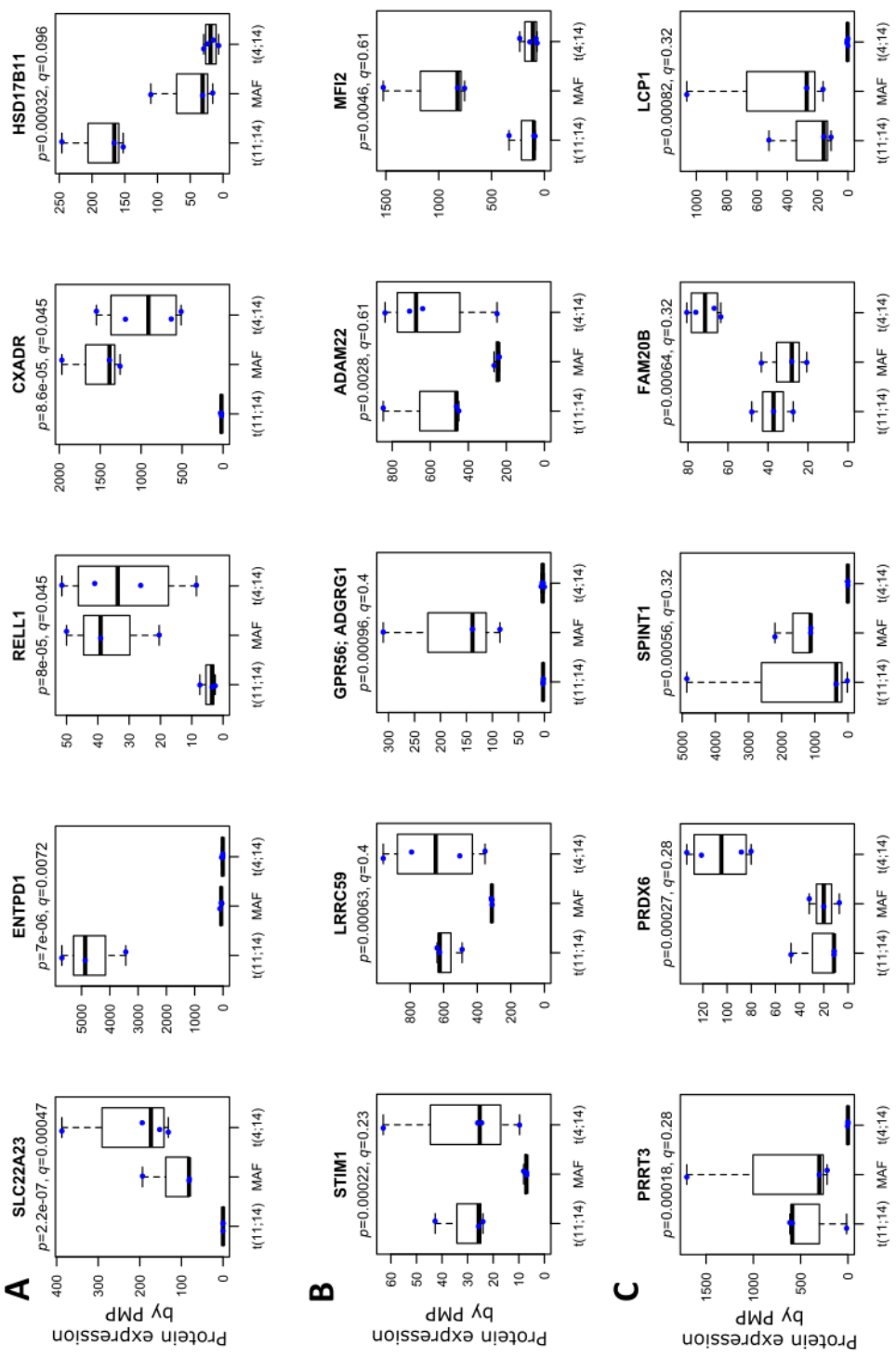

Fig. 3.13 *The top five most differentially expressed proteins for each major primary translocation.* A t-test was performed comparing the relative expression of each protein across the different subgroups to identify proteins associated with primary translocations. The relative expression of the top five most differentially expressed proteins identified for each subgroup are shown, depicted as a box and whiskers plot. **A** t(11;14) associated proteins **B** t(MAF) and **C** t(4;14). The reported and BH-adjusted p values for each t-test are also shown.

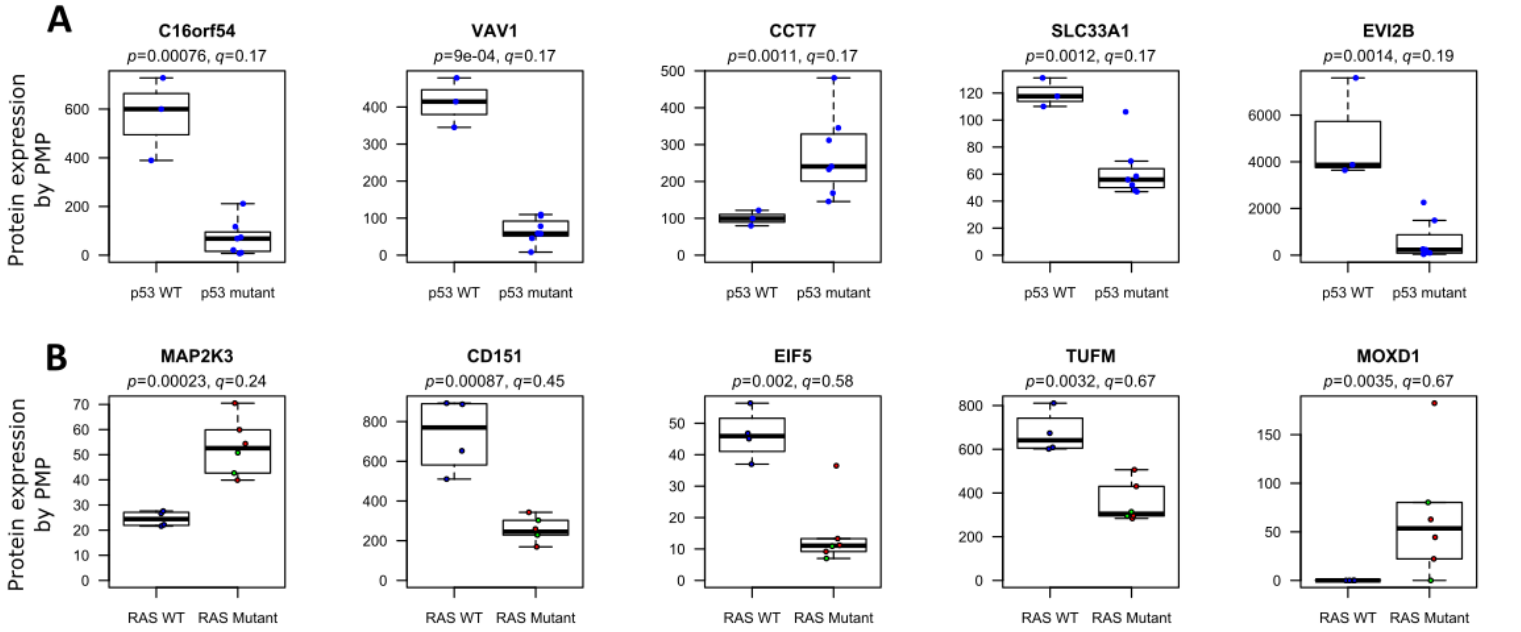

Fig. 3.14 *The top five most differentially expressed proteins for other major mutational events* A t-test was performed comparing the relative expression of each protein between the absence of presence of *TP53* (**A**) or *RAS* (**B**) mutations. The relative expression of the top five most differentially expressed proteins identified for both subgroups are shown, depicted as a box and whiskers plot. The reported and BH-adjusted *p* values for each t-test are also shown. For the *RAS* mutants, *KRAS* mutants are highlighted in green and *NRAS* in red.

Although there appeared to be very few proteins that were significantly associated with specific mutations, unsupervised clustering of the top 100 most variable proteins revealed that there were distinct subgroups within the HMCLs profiled. Consensus clustering of the plasma membrane proteins suggested a stable three-cluster solution (figure 3.15). This three-cluster solution is shown in figure 3.16 as a heatmap of the relative protein expression of the top 100 proteins across the 10 HMCLs (hierarchical clustering (Euclidean distance, average linkage)). Within cluster one was OCI-My5, KMS-12-BM and MM.1S, cluster two contained INA-6, OCI-My7 and SK-MM-1, and cluster three was JIM3, LP-1, NCI-H929 and OPM-2. Cluster three contained solely the t(4;14) cell lines which appeared distinct from the other two subgroups, suggesting that there was a t(4;14) signature at the plasma membrane. Importantly, this cluster was preserved despite the clustering method used, whilst the other two groups appeared to be less stable. For instance, using Ward's hierarchical clustering (Pearson distance) KMS-12-BM was linked with the second cluster containing the other two t(11;14) cell lines and SK-MM-1.

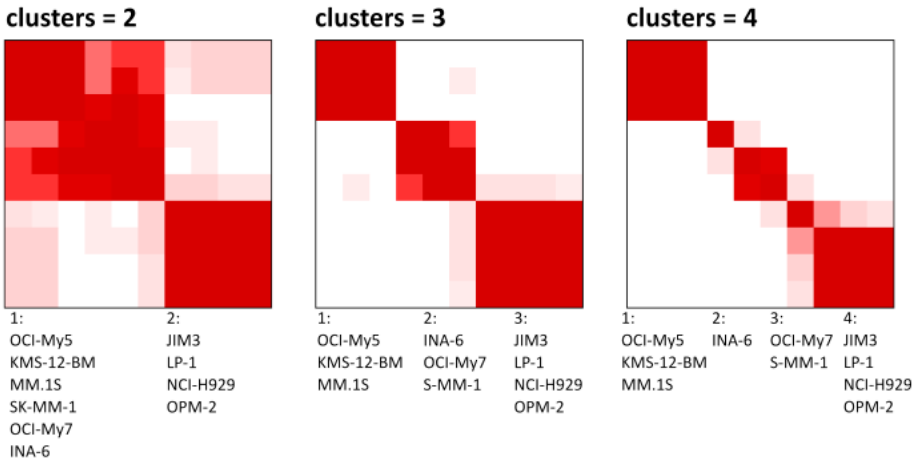

Fig. 3.15 *Consensus clustering reveals three stable clusters within the ten HMCLs profiled.* Colour-coded heatmaps of consensus clustering (Euclidean distance; average linkage) for K=3, 4 or 5 confirms that K=3 as the most stable number of clusters.

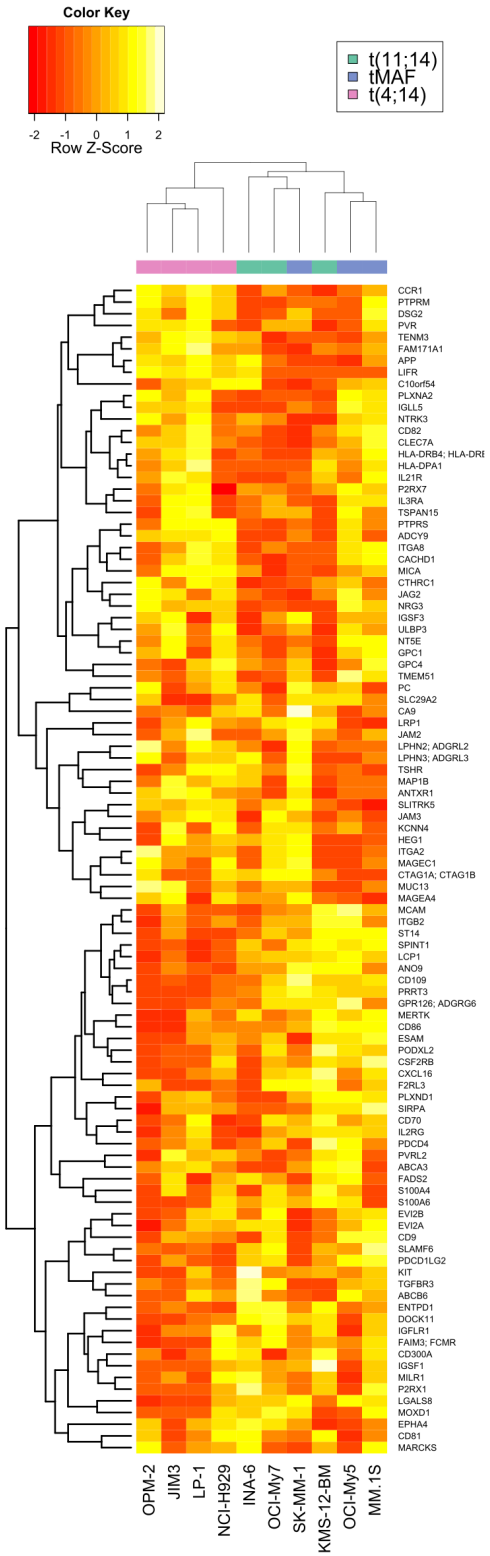

Fig. 3.16 *Unsupervised clustering analysis reveals a t(4;14) signature at the plasma membrane.* A heatmap comparing the relative expression of the top 100 most variable genes. Hierarchical clustering (Euclidean distance, average linkage) of these proteins reveals three subgroups, with one cluster containing solely the t(4;14) cell lines. This suggests that the t(4;14) translocation may dysregulate the expression of a large number of cell surface proteins.

3.2.7 Comparison of protein expression between HMCLs and primary samples

HMCLs are routinely used as functional models in myeloma as an alternative to primary samples. These established cell lines provide a continuous source of cells that are both easier to handle and manipulate. HMCLs have also been shown to recapitulate the molecular heterogeneity of primary disease and can considered to be representative models [303]. Despite this, it is axiomatic that these cells will differ both genetically and phenotypically from primary disease. Having profiled both sample types, I was interested in identifying any proteomic differences between the two.

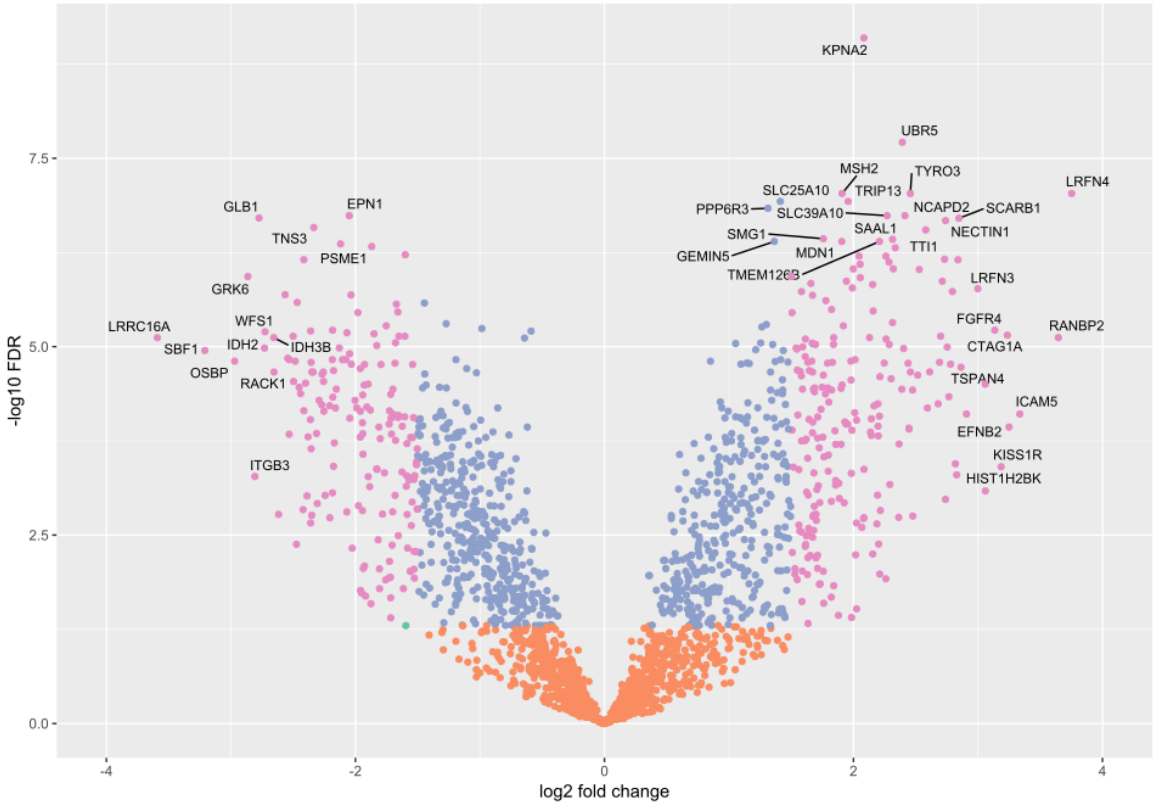

Fig. 3.17 *More than 530 proteins are significantly differentially expressed between HMCLs and primary samples at the cell surface.* A volcano plot representation of the results of a student's t-test caried out, comparing protein expression by PMP between primary samples and HMCLs. A fold change cut off was set at $\pm$ 1.5 and a significance cut-off of of <0.05 using BH-adjusted p values (q values). Significant proteins with a fold change >$\pm$ 1.5 are shown in pink, significant proteins with a fold change of less than $\pm$1.5 shown in purple, non-significant proteins with a fold change greater than $\pm$1.5 are shown in green and the remaining non-significant proteins in orange. Those with a positive fold change are over-expressed in HMCLs compared with primary cells.

A student's t-test was carried out for all 2,077 proteins comparing protein expression between primary cells and myeloma cell lines. 530 proteins were identified as being significantly differentially expressed with a $p<0.001$ ($q<0.001$). There was an even divide between up- and down-regulated proteins, with 276 proteins downregulated and 254 upregulated in HMCLs compared with primary disease. These results are summarised in the volcano plot in figure 3.17. The top five proteins upregulated as ranked by fold change were CTAG1A, EFNB2, ICAM5, RANBP2 and LRFN4. The top five downregulated proteins were LRRC16A, SBF1, OSBP, GRK6, ITGB3. The top 100 most significant proteins and their relative expression across all 20 samples are depicted in the heatmap in figure 3.18. The heatmap reveals clear differences in protein expression between the two sample types. Gene enrichment analysis was performed on these top 100 proteins. The most significantly enriched gene sets are also shown in figure 3.18 alongside the raw and adjusted p values. This analysis revealed an enrichment in cell signalling in primary cells, in particular proteins involved in the negative regulation of the ERBB signalling pathway ($q=2.5\text{x}10^{-5}$) and in the non-canonical Wnt signalling pathway ($q=3.5\text{x}10^{-5}$). In the HMCLs, there was an enrichment for proteins involved in cell replication, such as the cell cycle process ($q= 2.6\text{x}10^{-12}$) and mitotic nuclear division ($q=1.7\text{x}10^{-6}$).

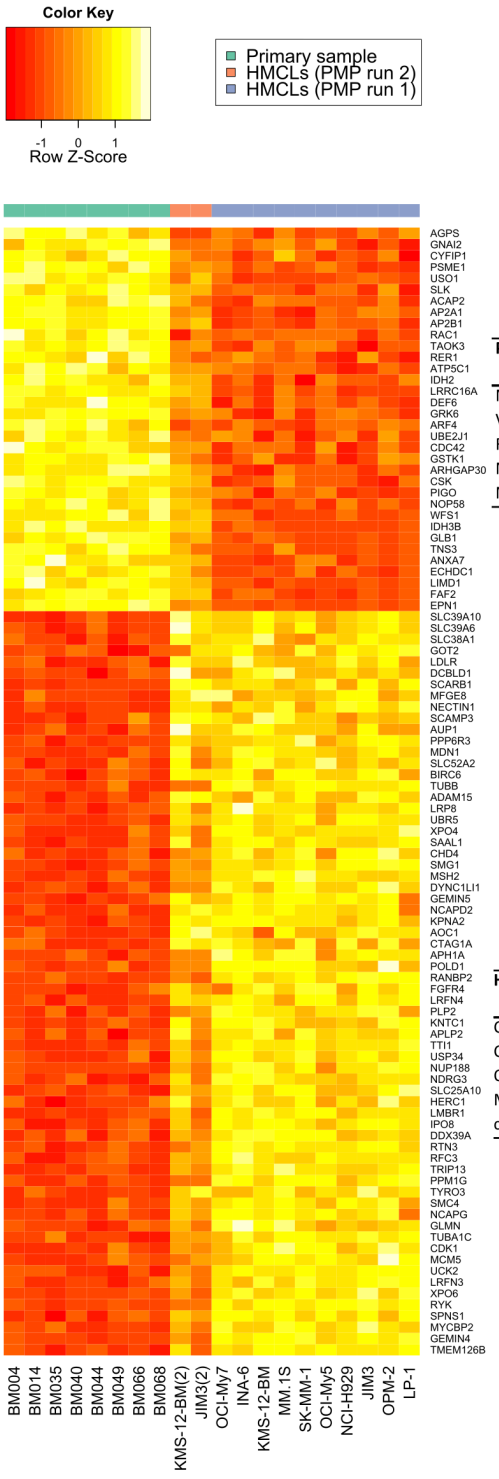

Primary MM upreglated GO terms	p value	q value
Negative regulation of cell communication	5.66E-10	2.51E-06
Vesicle mediated transport	1.42E-08	1.58E-05
Regulation of establishment of planar polarity	1.89E-08	1.67E-05
Negative regulation of ERBB signalling pathway	3.32E-08	2.45E-05
Non-canonical WNT signalling pathway	6.33E-08	3.46E-05

HMCL upregulated GO terms	p value	q value
Cell cycle process	6.19E-16	2.55E-12
Chromosome organisation	3.32E-12	2.94E-09
Organelle fission	4.13E-11	2.29E-08
Mitotic nuclear division	4.9E-09	1.67E-06
cell division	3.69E-09	1.36E-06

Fig. 3.18 *The most significant differentially expressed proteins between HMCLs and primary samples.* The relative expression for the top 100 most significant proteins across all 20 samples profiled by PMP is shown as a heatmap, revealing clear differences between primary samples and HMCLs at the cell surface. The results of the Gene enrichment analysis for proteins upregulated in primary MM and those upregulated in HMCLs is also depicted, alongside the raw and BH adjusted p values (q values)

3.2.8 Identification of novel monoclonal antibody targets

To identify novel monoclonal antibody targets, proteins were prioritised by a number of criteria. The first criteria was exposure at the cell surface and therefore proteins without an annotated extracellular domain were excluded from the starting list of 2,077 proteins. Proteins were then ranked according to a combination of a) high and ubiquitous on-tumour expression, b) low off-tumour expression and c) the size of the extracellular domain. Having observed clear differences between primary cells and cell lines, on-target expression was calculated as the median expression in the primary samples only. Healthy tissue expression was predicted using the publicly available whole-cell proteomics database (The Human Proteome Map [300]). CD38 and SLAMF7 expression (the targets of daratumumab and elotuzumab respectively) were used as a guide for a threshold for tolerable off-tumour expression. Figure 3.19 compares the median expression of each 'extracellular plasma membrane' protein against the normalised length of the extracellular domain, which was used as an approximation of antigenicity. Proteins are also colour-coded by their maximal expression in the lung, liver, heart or kidney. This bioinformatic approach revealed 20 potential monoclonal antibody targets, summarised in table 3.5. Two additional targets, ROBO1 and EPHB2, were initially identified from the first PMP experiment and are discussed in the following chapters. A final extensive literature review revealed that six proteins had already been identified as therapeutic targets for MM and therefore were excluded from our list of top candidates (CD38, SLAMF7, LY75, ITGA4, MERTK and IFNAR1).

The expression of these targets across all healthy tissue is summarised in figure 3.20. Although none of the targets identified exhibited a 'clean' off-tumour expression profile, the majority of these proteins were expressed at low to medium levels in normal tissue. Comparing with CD38, which is well described to be expressed on a multitude of cell types, off-tumour expression at these levels did not appear to be a critical reason for exclusion at this early stage. Importantly, there was no high expression in the heart, kidney, liver or lung.

Using this analytical pipeline, I identified 16 high-ranking candidates to take forward as potential monoclonal antibody targets.

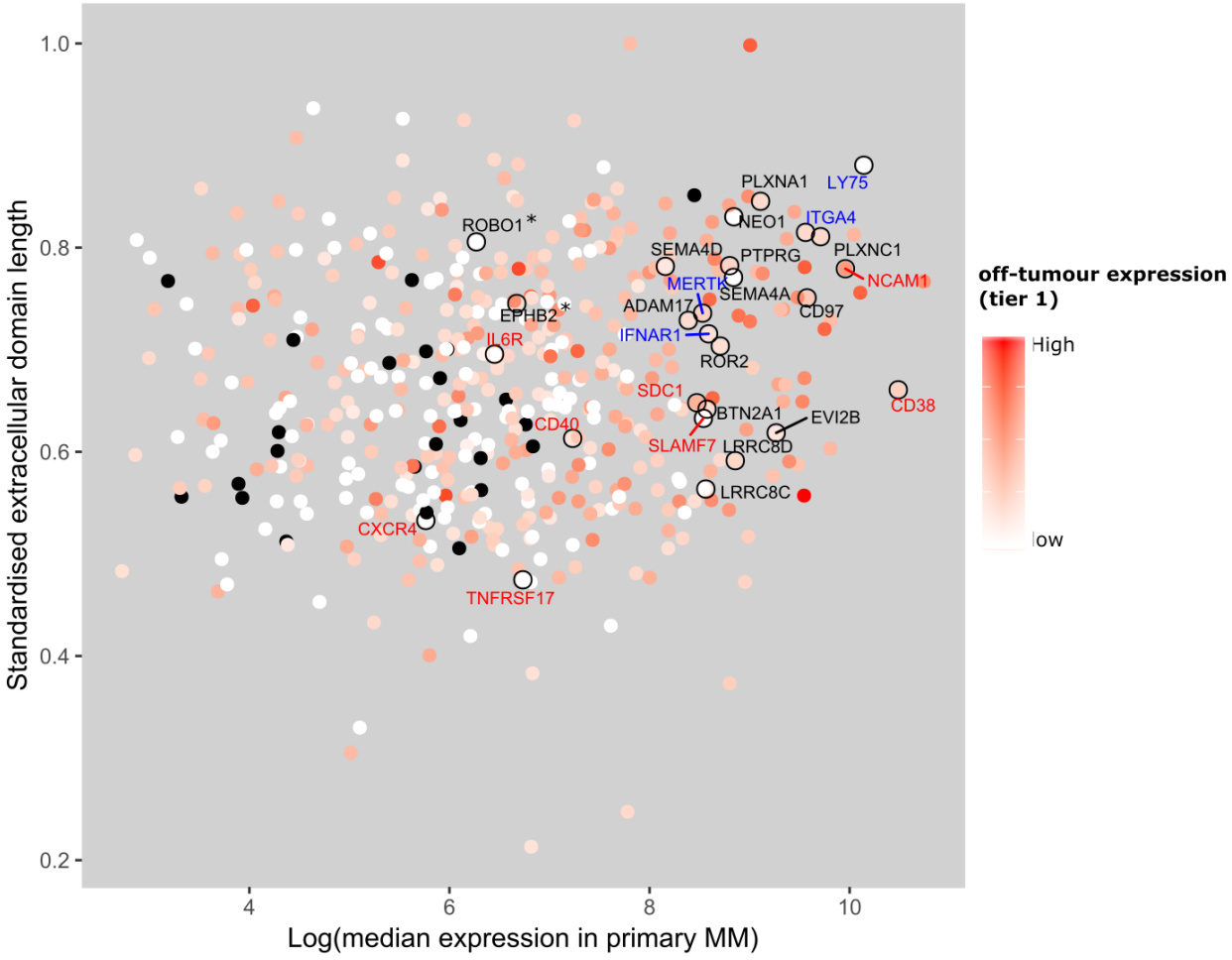

Fig. 3.19 *High ranking monoclonal antibody targets identified by high on-tumour and low off-tumour expression.* A scatterplot comparing the expression of all 'extracellular plasma membrane' proteins by the log median expression in primary cells against the length of their extracellular domain (standardised). Each point (representing an individual protein) is colour-coded according to their maximal expression in high-risk tissue (heart, liver, lungs and kidney). Points in black did not have normal tissue expression data available (The Human Proteome Map) [300]. Protein names highlighted in black are the novel targets identified by the analytical pipeline to be taken further forward. Highlighted in blue are those that were already described in the literature as potential therapeutic candidates. Proteins in red are monoclonal antibody targets that are already FDA approved or are currently in clinical trials for MM. ROBO1 and EPHB2 (*) are two proteins that were identified initially by high expression in HMCLs whilst I was waiting for the primary PMP results and as such are included amongst the novel targets in the next chapter.

Target	Median log normalised expression by PMP		ECD length	Max normalised tier 1 expression	Comments
	Primary	HMCL			
CD38	10.49	9.54	257	0.19	Target of daratumumab
LY75	10.14	9.96	1638	0.00	Already under patent application
PLXNC1	9.71	9.75	909	0.16	
ITGA4	9.56	10.21	942	0.15	Already described as potential MAb target for MM
EVI2B	9.27	8.31	180	0.10	
PLXNA1	9.11	9.83	1217	0.15	
CD97	9.04	9.31	549	0.21	Linked to invase behaviour in solid tumours
LRRC8D	8.86	9.27	143	0.16	
NEO1	8.84	9.78	1071	0.16	Described as potential therapeutic target for medulloblastoma
SEMA4A	8.84	9.11	650	0.00	
PTPRG	8.8	9.03	716	0.16	Candidate breast tumour suppressor protein
ROR2	8.71	6.14	369	0.13	Described as potential therapeutic target for solid tumours Wnt5a/Ror2 pathway implicated in pathophysciology of MM bone disease
IFNAR1	8.59	9.13	408	0.13	Already described as potential MAb target for MM (against Tregs)
BTN2A1	8.57	8.48	219	0.13	
LRRC8C	8.56	8.03	113	0.10	
SLAMF7	8.54	8.56	203	0.00	Target of elotuzumab
MERTK	8.53	7.42	484	0.19	Already described as potential small molecule inhibitor target for MM
ADAM17	8.39	9.39	456	0.14	May be associated with melphalan resistance
SEMA4D	8.16	9.49	712	0.09	Implicated in development of lytic bone disease in MM
EPHB2	6.67	9.62	524	0.13	Originally identified by high expression in HMCLs
ROBO1	6.27	8.81	871	0.00	Originally identified by high expression in HMCLs Described as potential target for osteosarcome

Table 3.5 *Summary of protein characteristics for the top 20 novel target candidates.* Proteins were ranked according to a combination of three variables, median expression in MM, the length of the extracellular domain and the maximum expression in major organs. ROBO1 and EPHB2 wre not included amongst the top 20 hits but were identified initially by high expression in HMCLs whilst I was waiting for the primary PMP results and as such are included amongst the novel targets in the next chapter.

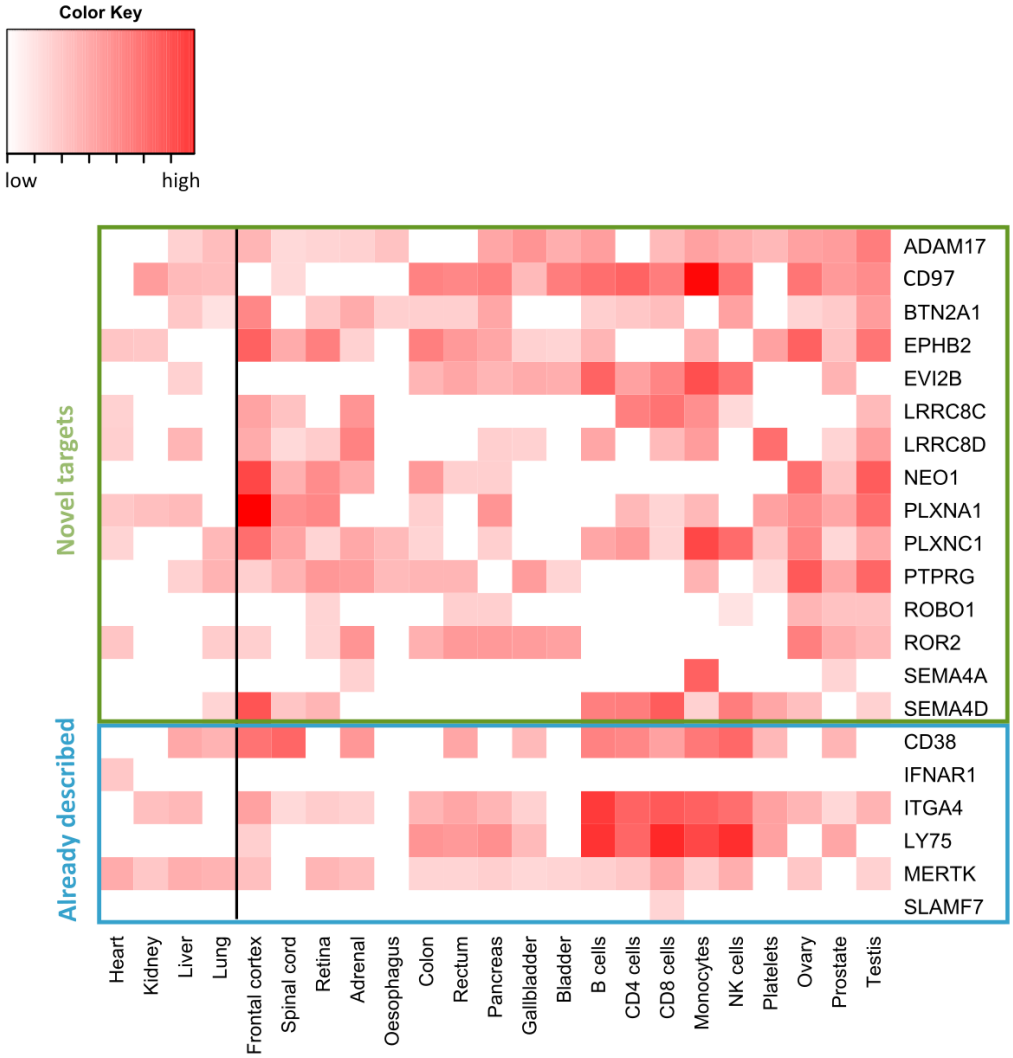

Fig. 3.20 *Expression of the highest ranking candidates in normal tissue.* A whole cell mass spectrometry dataset (The Human proteome Map [300]) was used to determine protein expression of the top 20 hits in healthy, normal tissue. A maximum threshold of expression in the high-risk organs (heart, kidney, liver and lung) was determined by the expression of CD38. Proteins highlighted in green are those novel targets taken forward, whilst those highlighted in blue are proteins that were identified by our analytical pipeline but were already described as therapeutic targets for MM.

3.3 Chapter conclusions

The overall aim of the work presented in this chapter was to establish the PMP technique developed by Professor P Lehner and Dr M Weekes and to use PMP to quantitatively characterise the myeloma cell surface proteome. To this extent, I profiled a total of ten HMCLs and eight primary samples. A total of 2,077 proteins common to both experiments were quantified, of which 1,319 were curated as 'plasma membrane' or 'plasma membrane associated'. From these proteins, I identified 16 monoclonal antibody target candidates to take forward.

3.3.1 *In vitro* generation of plasma cells from B cells

Our initial proposal was to use PMP to quantitatively compare the cell surface proteome between normal plasma cells and malignant cells. Due to the ethical challenges and the potential difficulties in sourcing a sufficient number of cells from healthy donors, especially considering the challenges with isolating enough cells in primary MM (fig 3.3), I considered using an *in vitro* approach to generate plasma cells. Initial attempts at replicating this technique resulted in very low yields of cells, with less than one cell harvested at day 13 for every B cell seeded at day 0. Despite this, there was a clear transition from a B cell to a plasma cell phenotype with a decrease in CD20 and an upregulation in CD38/CD138, two essential markers of plasma cells (fig 3.6). By selecting only for memory B cells, I observed a clear improvement in the number of viable cells at day 13 generated for every B cell seeded (2 to 4.4 cells, table 3.2). After day 13 there was a continued reduction in the number of viable cells, but even at day 20 there was still a small viable population of $CD20^{neg}CD138^{pos}CD38^{hi}$ plasma cells (data not shown). This improvement in cell viability would corroborate with published literature that memory B cells enter the differentiation pathway much more readily than their naïve counterparts [306]. However, this would not have been expected to impact plasmablast numbers at days 3 to 6 [94] and it may be simply due to donor variation as these two experiments were repeats of the same cone. An improvement in cell viability may have also been due to the increased confidence in using this technique.

Despite this, I decided to not include these *in vitro* differentiated plasma cells for PMP for several reasons. Firstly, the number of plasmablasts that would need to be cultured to generate $1x10^7$ plasma cells and the associated costs was considered prohibitive. Especially considering that our amplification counts did not take into account that the final cell population at day 13 is not a $CD138^+$ pure population. In the interests of time, I decided to proceed with the profiling of malignant plasma cells only. Although I would be unable to make comparisons

between healthy and malignant tissue, I would be able to profile a larger number of primary samples and concluded that this would not impact target discovery, although this approach may miss proteins involved in malignant transformation. Many proposed therapeutic targets have not been identified through cross-comparisons and several, including CD38 and CD138 are expressed at comparable levels on normal and malignant plasma cells. Furthermore, it has recently been shown that SLAMF7 (the target of elotuzumab) expression levels may be lower in myeloma compared with normal bone marrow plasma cells and as such would been missed by a straight comparison between normal and malignant cells [307][308][309].

3.3.2 Plasma membrane profiling of MM

Using PMP, 3,131 and 4,962 unique proteins were identified in HMCLs and primary samples respectively, of which 2,714 were common to both datasets (fig 3.8). Although thresholds setting the FDR are applied to peptide identification in mass spectrometry, the sheer number of peptides identified means several false positives may be retained leading to false protein identifications. To reduce the number of false identifications, I excluded proteins identified by only one unique peptide, removing a total of 637 common proteins. This was a highly conservative method and several proteins that have few tryptic peptides may have been lost. However, typically these proteins were of low abundance and the majority were curated as 'non-plasma membrane' and so were unlikely to be of interest for target discovery. They may still represent potential biomarkers of interest though which are typically of low abundance, and this is an important point to note when analysing this dataset. Less stringent methods may be potentially applied to distinguish true and false identifications amongst single-hit proteins [310].

As I was primarily interested in proteins highly expressed in primary MM but also retained in HMCLs to enable later validation work, I focussed only on proteins common to both datasets. As a result, a large number were excluded that were only identified in PMP run one or two, primarily from the primary samples (figure 3.8). It could be considered that these are proteins unique to primary MM but this is unlikely as two HMCLs were included in this second run. Analysis of the GO term enrichment of these excluded proteins indicates these were more commonly low-abundant, non-plasma membrane proteins and it could be possible that these are proteins that were simply missed in the first run due to a higher threshold of detection. Despite the exclusion of these proteins, there was still a large list of potential targets left.

The plasma membrane is highly dynamic, with the continuous recycling, secretion and internalisation of proteins and can be subjective to external factors such as cell density. As such, PMP is only capturing a particular 'snapshot' of the cell surface proteome. Comparing the expression of the commonly-identified proteins between both PMP experiments revealed a strong positive correlation (figure 3.10, correlation coefficient of 0.69 to 0.76). Considering that these HMCLs were profiled almost a year apart, at different passages and from different stocks, our results by PMP appear to be highly representative of the HMCL cell surface proteome. This, in conjunction with the positive correlation between PMP and FC (figure 3.11, correlation coefficients ranging from 0.66 to 0.99), gave us confidence in using this dataset for target discovery.

One of the main arguments for proteomic profiling over the use of gene expression profiling is the highly variable (and often low) correlation between RNA and protein expression at the cell surface. Interested in how the RNA and protein levels compared for the ten HMCLs profiled, I found very poor correlation (coefficients from 0.13 to 0.21) between the two at a global level. Although on a case-by-case basis, I did identify some proteins that were well-correlated with RNA. It could be argued that as the RNAseq was not performed directly on the cells profiled that this may account for the poor correlation, but considering that at least one line (NCI-H929) was derived from stocks from the Keats lab this is unlikely to be the full explanation. This demonstrates that RNA expression alone is a poor proxy for protein abundance and GEP should be used with caution for target discovery. However, similarly to Wilhelm and Edfors [302][305], I demonstrated that by applying a RTP conversion factor, protein abundance could be much more accurately predicted from RNA expression data (figure 3.12). Thus far, I have determined a RTP factor for over 2,000 proteins which may enable the future use of RNAseq data as a less costly approach to plasma membrane proteomics, although it will be important to further validate the preliminary data shown here.

3.3.3 Association of cell surface protein expression with underlying genetic aberrations

As the HMCLs are genetically well profiled, it was of interest to use these lines to determine if there were any associations between the expression of cell surface proteins and major MM mutational events. This was for several reasons. Firstly, an association with high-risk cytogenetics, such as dup(1q) and *TP53* mutations, could help prioritise potential targets. Secondly, this would aid our understanding of myeloma cell biology and help elucidate the

cell-surface consequences of those mutations involved in a) malignant transformation (primary translocations) and b) driving disease progression (secondary mutations). Comparisons may also help identify biomarkers that could be identified by flow cytometry instead of FISH analysis, which is generally more labour-intensive and challenging to perform in very small samples, to help predict a patient's prognosis. Finally, myeloma is know to be genetically diverse and tumours highly heterogenous. If targets are associated with particular mutations, this may help determine if a target is ubiquitously expressed or restricted to a subclone.

Although the ten HMCLs were chosen to represent the major mutational events, the number of cells within each group was small (ranging from n=3 to 4). As a consequence there was limited statistical power in comparing genotype and protein expression and it is unsurprising that I found very few proteins associated with genetic events after correction for multiple testing. Despite this, I did identify several proteins that were reported as significant for the t(11;14) (n=11) and the *TP53* (n=11) subgroups (figure 3.13 and 3.14). For a select few of these proteins, there was a good correlation with RNA and it was possible to look for associations in a larger cohort using the available RNAseq data. An example of this is ENTPD1 which was also found to be significantly upregulated in t(11;14) cell lines at the RNA level, with a mean of 6575.4$\pm$2603.3 (n=13) compared against t(MAF) and t(4;14) (mean= 2603.3$\pm$3351.4, n=31) (t-test, p<0.01). Although not all mutations reported a significant result, these may reveal trends that can be validated in a larger cohort. Interestingly, unsupervised clustering of the HMCLs revealed that there was a distinct t(4;14) signature, with these cell lines strongly clustering together, separate from the other subgroups (figure 3.16). The remaining two clusters were harder to define and appeared to be less stable, with slight modifications to the predicted subgroups depending on the clustering method used. These clusters did not appear to be linked to secondary mutations and may represent the t(11;14) and t(MAF) subgroups.

Between primary cells and HMCLs, a large number of proteins were reported as statistically significant after correcting for multiple testing (n=530, t-test q<0.001, figure 3.17). Some of these reported proteins may be a result of two separate PMP experiments. Despite normalisation, there were some noticeable differences in the tightness of the spread of the data (data not shown). Comparing expression across the 20 samples profiled of the most significant proteins revealed the majority of these are likely to be genuine differences between the two sample types rather than between PMP runs (figure 3.18). GO enrichment analysis revealed that the proteins upregulated in the primary samples were involved in cell signalling pathways, whilst those down-regulated were implicated in cell cycle progression.

The down regulation in cell cycle was unsurprising as human myeloma cell lines are much more proliferative than their primary counterparts. The Wnt signalling pathway has long been recognised as being dysregulated in both HMCLs and primary samples compared with normal BMPCs so it was interesting that it appeared to be upregulated amongst the primary samples. Wnt signalling is known to play a pivotal role within the bone microenvironment in MM and this may in part explain the differences.

3.3.4 Identification of novel targets

One of the biggest challenges faced in this project was determining how to narrow down a list of >2,000 potential targets to a much more manageable list. Having considered several methods, I settled on the following criteria to rank proteins: high on-tumour expression, low off-tumour expression and the length of the extracellular domain.

For on-tumour expression I used the median relative expression in primary cells only. As seen in figure 3.17 there were clear differences between the relative expression of targets in primary samples and HMCLs. Two of the targets (ROBO1 and EPHB2) that are described in the next chapter were in fact initially identified using only the HMCL PMP dataset whilst waiting for the final results of the primary PMP. As clearly seen in figure 3.19, these two proteins were expressed highly in the HMCLs but exhibited much lower expression in the primary samples. Although this didn't discount them as targets, it did reduce their priority. By comparing the median expression rather than the maximum or mean expression in MM, it was hoped that more ubiquitous proteins would be ranked over targets that were highly expressed in only a few samples.

High expression alone does not necessarily translate to a good target. A number of high-ranked proteins were observed to be also highly expressed in normal tissues. To avoid targets that would exhibit unacceptable off-tumour toxicity, proteins were also ranked according to their off-tumour expression as determined by whole-cell proteomics. In addition, these target-expressing cells may act as 'sinks', binding the antibody and reducing the number of therapeutic antibodies that reach the tumour [311]. To compensate, an increased dose is required which may then be associated with an increase in adverse events. As a threshold for off-tumour expression, I examined the normal tissue distribution of several MM therapeutic antibody targets that have either been FDA-approved or are currently in clinical trials. None of our novel targets exhibited 'clean' off-tumour expression profiles but did appear to be within a similar range of known therapeutic targets (figure 3.20).

The last criteria was the length of the extracellular domain. Whilst a protein may be highly expressed in primary MM, it may be completely inaccessible to an antibody if the extracellular domain is too short or steric hindrance prevents binding. As an initial step, all proteins without an extracellular domain were excluded. Using 2D antigen prediction methods to rank proteins was initially proposed. But these sequence-based methods which rely on a combination of residue scoring, hydrophobicity, flexibility as well as other sequence-determined information, are poor at predicting discontinuous epitopes. Considering that >90% of antibody-binding epitopes are estimated to be discontinuous, these sequence-based methods would likely have been uninformative. Structure based methods may be much more informative but are still limited by the number of resolved antigen-antibody structures available [312]. As an alternative, the length of the extracellular domain was used to rank proteins as a surrogate for 'targetability'. Although the length of the domain doesn't directly translate into antigenicity, it could be considered that the longer the extracellular domain is, the greater the chance of containing an antigenic region. Comparing the ranking based on 2D-antigen prediction and the length of the extracellular domain found very little differences between the two methods.

Overall, there were multiple approaches that could have been used to identify novel target candidates, but using this approach resulted in the inclusion of the two FDA-approved antibody targets amongst the top hits.

Chapter 4

Establishment of a recombinant protein production system

4.1 Introduction

In the last chapter I demonstrated that PMP provides an accurate and comprehensive analysis of the cell surface proteome and applied a bioinformatical approach to identify novel therapeutic targets. To identify the best candidate to proceed with, it will be important to verify expression in a large number of patient samples and to determine off-tumour expression. It is expected, however, that the validation of many of these candidates will be hampered by the lack of reliable, commercially available antibodies that recognise the protein's native conformation. As such, it will be necessary to generate tool antibodies for the further characterisation of these targets. Furthermore, it will be imperative to develop a proprietary antibody targeting any lead ADC candidate. To this extent, we have established a few commercial collaborations and will require recombinant protein for antibody generation.

There are numerous expression systems available for recombinant protein production, such as bacterial, insect, yeast and mammalian. There are several advantages and disadvantages to each system. Although bacteria are frequently used as a low-cost system that can generate large amounts of protein in a short period of time, these cells lack the mammalian chaperones and post-translational machinery. Membrane proteins are typically heavily glycosylated and as a result, mammalian proteins produced using these systems may be misfolded or inactive [313][314]. Mammalian systems, on the other hand, provide the required post-translational modifications although at the cost of a lower yield [314]. Other considerations in the establishment of a recombinant protein production system include

transient versus stable transfection and the type of promoter used. Whilst transient systems are initially quicker to establish, the efficiency of transfection is dependent on the cell line used and can be highly variable [314]. Meanwhile, stable over-expression of the recombinant protein under a constitutive promoter may trigger cell stress as a result of the high metabolic burden, affecting protein yield [313]. The use of an inducible promoter can inhibit protein production until an appropriate time. Taking into consideration the advantages of all these respective methodologies, I chose to use the pcDNA5 FRT/TO tetracycline-inducible plasmid (Invitrogen) in a stable mammalian expression system. This vector is stably integrated into the mammalian host genome at a FRT site in a Flp recombinase-dependent manner [315]. The use of this system ensures that the integration site is not random and as such is transcriptionally active and prevents the disruption of other transcripts.

To simplify protein purification, I considered expressing only the extracellular domain of each protein of interest since it represents the region of interest for the targeting antibody. By removing the transmembrane domain and retaining the native signal peptide, the recombinant protein is secreted directly into the cell culture supernatant. This not only reduces the number of purification steps but also segregates these proteins from the cytoplasmic proteases, enhancing stability, and prevents the accumulation of proteins that may trigger cytotoxic stress [316]. The addition of a cleavable His-tag further simplifies purification, enabling the affinity-mediated isolation of these proteins from other cell culture media contaminants [317]. Cleavage of the His-tag enables further purification, separating the cleaved protein from other His-containing proteins. These tags may also provide compositional stability, improving recombinant protein yields [318].

4.1.1 Chapter Overview

In this chapter I describe the establishment of a mammalian recombinant protein production system. I demonstrate that these over-expressed proteins are successfully accumulated within the cell culture media and describe the optimisation of protein yield using valproic acid (VPA). I describe the successful cloning of five of our candidate proteins and the purification of three to homogeneity. Finally, I demonstrate that the difficulties in producing recombinant SEMA4A is likely due to the compositional instability of the truncated protein.

4.2 Results

4.2.1 Establishment of an expression system

To produce protein for antibody generation and subsequent target validation, I have developed an inducible mammalian protein expression system. The extracellular domain of each target was amplified from HMCL cDNA by PCR and fused with a C-terminal 6x His-tag and TEV protease cleavage site before ligation into the pcDNA5/FRT/TO expression vector. Target DNA was then transfected into 293FT and selected using antibiotic resistance to generate stable target-expressing cell lines. The 293FT cell line is derived from the 293T cell line and contains a single integrated flippase recognition target (FRT) site enabling the recombination-mediated integration of the pcDNA5 vector into the genome (generated by Dr A Reyes[1]). To induce protein expression, 293FT were switched to FBS-free media containing doxycycline at 30ng/ml. For the remainder of this section, 293FT cells transfected with the parental, empty vector will be referred to as pcDNA5 and 293FT cells transfected with target DNA will be referred to as pcGOI (gene of interest), e.g. 293FT expressing pcDNA5_EPHB2_HIS are simplified to pcEPHB2.

The inclusion of the native signal peptide and removal of both the intracellular and transmembrane domains ensures that the protein is secreted into the media, simplifying purification and minimising proteolytic degradation. I confirmed that this system was working for all cloned targets by Western Blot. Target-expressing 293FT cells were switched to serum-free media and recombinant protein production induced by the addition of doxycyline (Dox, 30ng/ml). Cell culture media and whole-cell lysates were collected at various time points and analysed by western blot using a poly-His antibody to detect the His-tagged recombinant protein. As shown in figure 4.1 depicting a representative experiment using pcEPHB2, there was an accumulation over time in the cell culture media (lower panel) compared to the whole-cell lysates (upper panel). For all recombinant proteins, the band detected by the poly-His antibody was at the correct predicted molecular weight.

One disadvantage to using a mammalian expression system compared with bacterial and yeast systems, is the limited cell density under standard culture conditions and as a consequence, a reduction in the total amount of recombinant protein produced. The next aim therefore was to optimise the expression system in order to ensure maximal protein production efficiency. Initial experiments were focussed on determining the optimal time for supernatant collection. pcDNA5, pcEPHB2 and pcPLXNC1 were cultured in FBS-free

[1] M Zeviani group, Mitochondrial Biology Unit, University of Cambridge

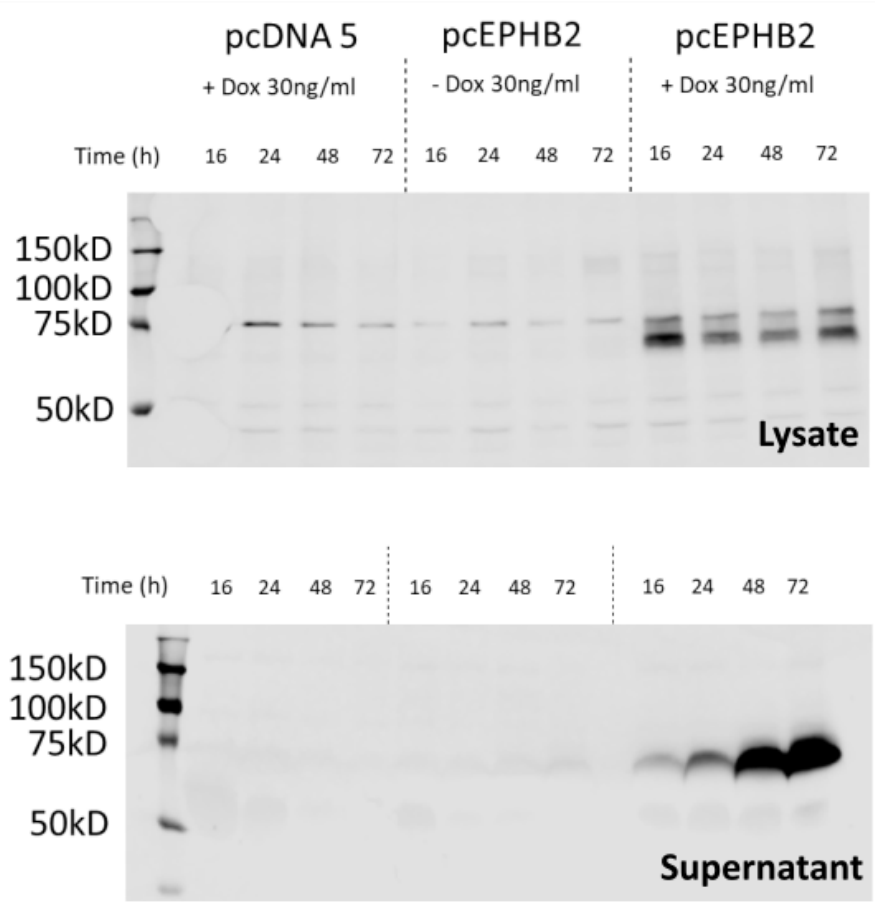

Fig. 4.1 *Recombinant protein is secreted into and accumulates in the cell culture media over time.* pcDNA5 and pcEPHB2 cells were switched to FBS-free media with or without Dox (30ng/ml). Cell lysates and culture media samples were collected at various time points and analysed by Western Blot. Recombinant protein was detected using a poly-His antibody.

media with Dox for three, seven or ten days. At each timepoint, cell viability was assessed by trypan-blue exclusion and a cell culture media sample collected. Recombinant protein was detected by Western Blot using a poly-His antibody and total protein quantified by densitometry and calculated as the fold increase from day 3. As expected, there was an accumulation of protein within the supernatant over time, with a 2.7 and 4.5 fold increase for pcEPHB2 at day 7 and 10 respectively and 3.5 and 4.8 fold increase for pcPLXNC1 (fig 4.2A). For all three transfected cell lines (pcDNA5, pcEPHB2 and pcPLXNC1), there was a clear loss of viability over time from 100% at day 0 to 68% ($\pm$ 2.6% (SD)) at day 3 to 36% ($\pm$ 5.3%) and 12.8% (10.1%) at days 7 and 10 (fig 4.2B). Although the greatest amount of protein was collected at day 10, the accumulation of cell debris, specifically the highly viscous DNA, made the separation of the cell culture from the cell pellet much more difficult. To minimise the contamination of these products and intracellular proteins, day 7 was selected as the optimal day for collection. Analysis of mRNA by qRT-PCR showed that transcript levels began to decrease at 96 hours (data not shown), and so a 72 hour Dox dosing schedule was chosen.

I also analysed the effect of adding a recombinant protein production enhancer to the cell culture media. Valproic acid (VPA) is a histone deacetylase inhibitor that is commonly used in mammalian expression systems to improve the quantity of recombinant protein produced. pcDNA5, pcEPHB2 and pcPLXNC1 were switched to FBS-free media with Dox and with or without VPA (0, 3, 4 and 5mM). At day seven, cell viability was assessed by trypan-blue exclusion and a sample of cell culture supernatant collected and analysed by western blot using an anti-Poly-His antibody. Comparing with and without VPA, there was a clear increase in the quantity of recombinant protein produced, with a 1.6 to 2.1 fold increase in pcEPHB2 compared to without VPA and 2.7 to 3.1 fold increase in pcPLXNC1 (fig 4.2C). This increase in protein production was associated with improved cell viability from 19% ($\pm$ 3% (SD)) with 0mM VPA to 31% ($\pm$ 2%) to 43% ($\pm$ 7%) at 2-5mM VPA (fig 4.2D). From these results, 3mM VPA was selected as the optimal concentration tested. Combining the addition of VPA (3mM) with cell media collection at day 7 resulted in a 5.9 fold increase in the amount of recombinant protein collected compared with 0mM at day 3 (fig 4.2E).

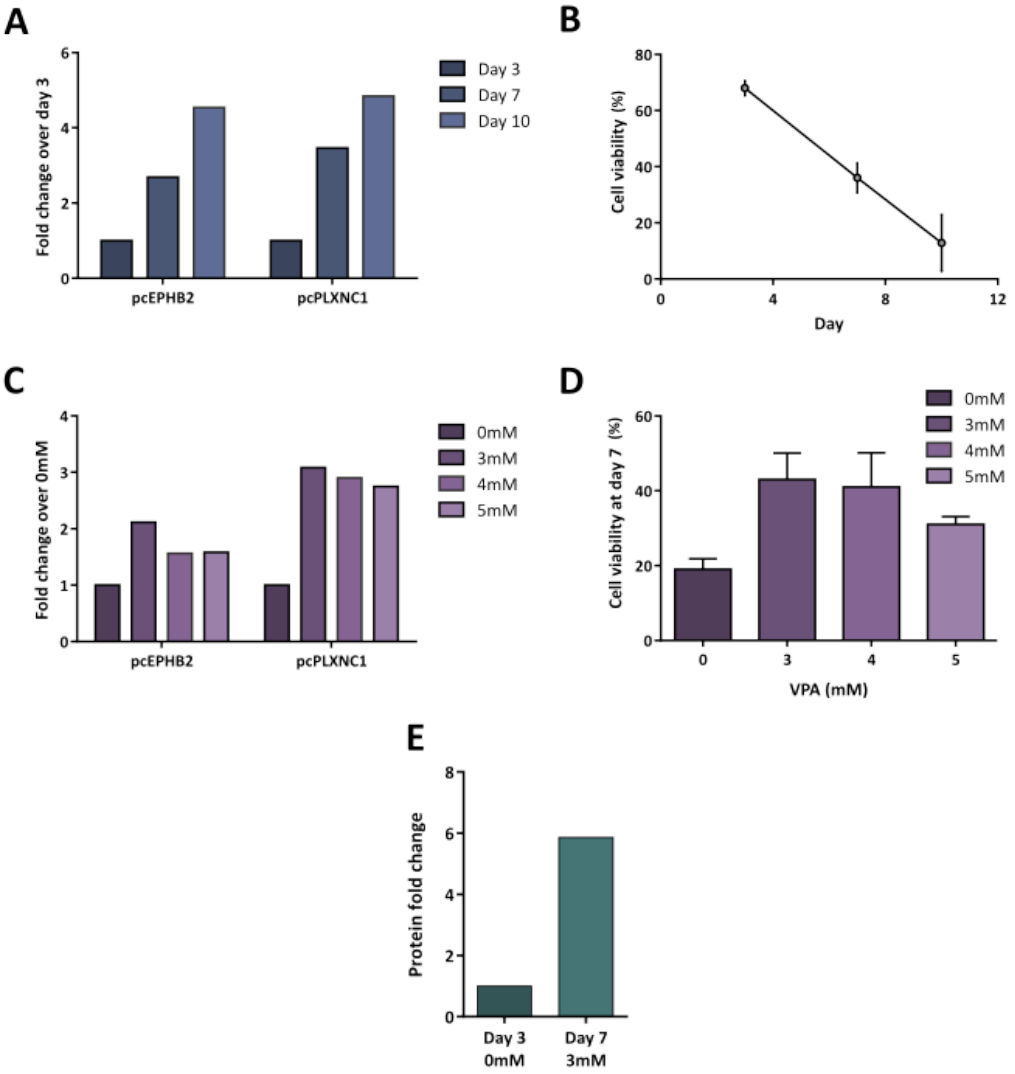

Fig. 4.2 *Optimisation of recombinant protein production using the mammalian expression system.* pcDNA5, pcEPHB2 and pDNA5 were cultured in FBS-free media with Dox (30ng/ml). Cell culture media samples were collected at day 3, 7 and 10 and resolved by Western Blot using a poly-His antibody. **A** Recombinant protein production was quantified by densitometry and calculated as the fold change from day 3. **B** Cell viability was assessed by trypan blue exclusion. pcDNA5, pcEPHB2 and pDNA5 were cultured in FBS-free media with Dox (30ng/ml), without or with VPA (0, 3, 4, and 5mM). Cell culture media samples were collected at day 7 and resolved by Western Blot using a poly-His antibody. **C** Recombinant protein production was quantified by densitometry and calculated as the fold change from day 3. **D** Cell viability was assessed by trypan blue exclusion. Mean $\pm$ SD is plotted, n=3.**E** Fold change of recombinant protein production at day 7 with the addition of VPA (3mM) compared to day 3 (0mM VPA).

4.2.2 Protein purification

Whilst establishing optimisation of the protein production, I proceeded with determining the protein purification protocol. 293FT construct-expressing cells were switched to FBS-free media for seven days with 30ng/ml Dox, without the addition of VPA. Cell culture media was collected and clarified by centrifugation and then filtration. The His-tagged extracellular domains were purified by immobilised metal affinity chromatography (IMAC) on a HisTrap excel column using the ÄKTA purification system. These pre-packed columns are specialised for the purification of recombinant His-tagged proteins from cell culture media. To maximise the purity and quantity of protein recovered, I optimised the imidazole concentration used at various stages during the protocol, settling on a 40mM wash and gradient (40mM to 1M) elution. Protein containing eluate fractions (as determined by absorbance at 280nm) were pooled and dialysed overnight to remove imidazole before cleavage of the His-tag by TEV protease. The cleaved recombinant protein was further purified by re-running the sample through the HisTrap excel column to remove contaminants and the cleaved His-tag. Using this protein production and purification protocol, I have established a protocol for and purified to homogeneity three of our top 16 targets: EPHB2, NEO1 and PLXNC1 (figures 4.3 to 4.5). For pcEPHB2, a total of 195µg His-tagged protein was collected from 64ml of culture media. Following tag cleavage and further purification, 76% of the protein was recovered, as determined by SDS-PAGE (fig 4.3A-D). 96µg of pcPLXNC1 was collected from 50ml of cell culture media with a recovery efficiency of 88.6% (fig 4.5A-D) and 116µg of NEO1 was collected from 64ml of media, of which 60.9% was recovered following tag cleavage and further purification (fig 4.4A-D). Western blot analysis demonstrated that the purified protein was detectable by a NEO1-targeted antibody and also revealed that some of protein was not binding to the column and was being lost in the flow-through (fig 4.4E). The large single peak obtained for all of the purified recombinant proteins in conjunction with the clean bands resolved by SDS-PAGE demonstrates the high-level of purity I achieved using this technique.

I was also able to successfully clone and produce sufficient quantities of protein for both PLXNA1 and ROBO1. PLXNA1 has been IMAC purified (164µg of His-tagged protein from 48ml of culture media) but at the time of writing has not been further purified following tag cleavage (fig 4.6A-B). Due to the decision to not further proceed with ROBO1 as a target (see the next chapter, section 5.2.2), the recombinant protein was not taken forward to protein purification.

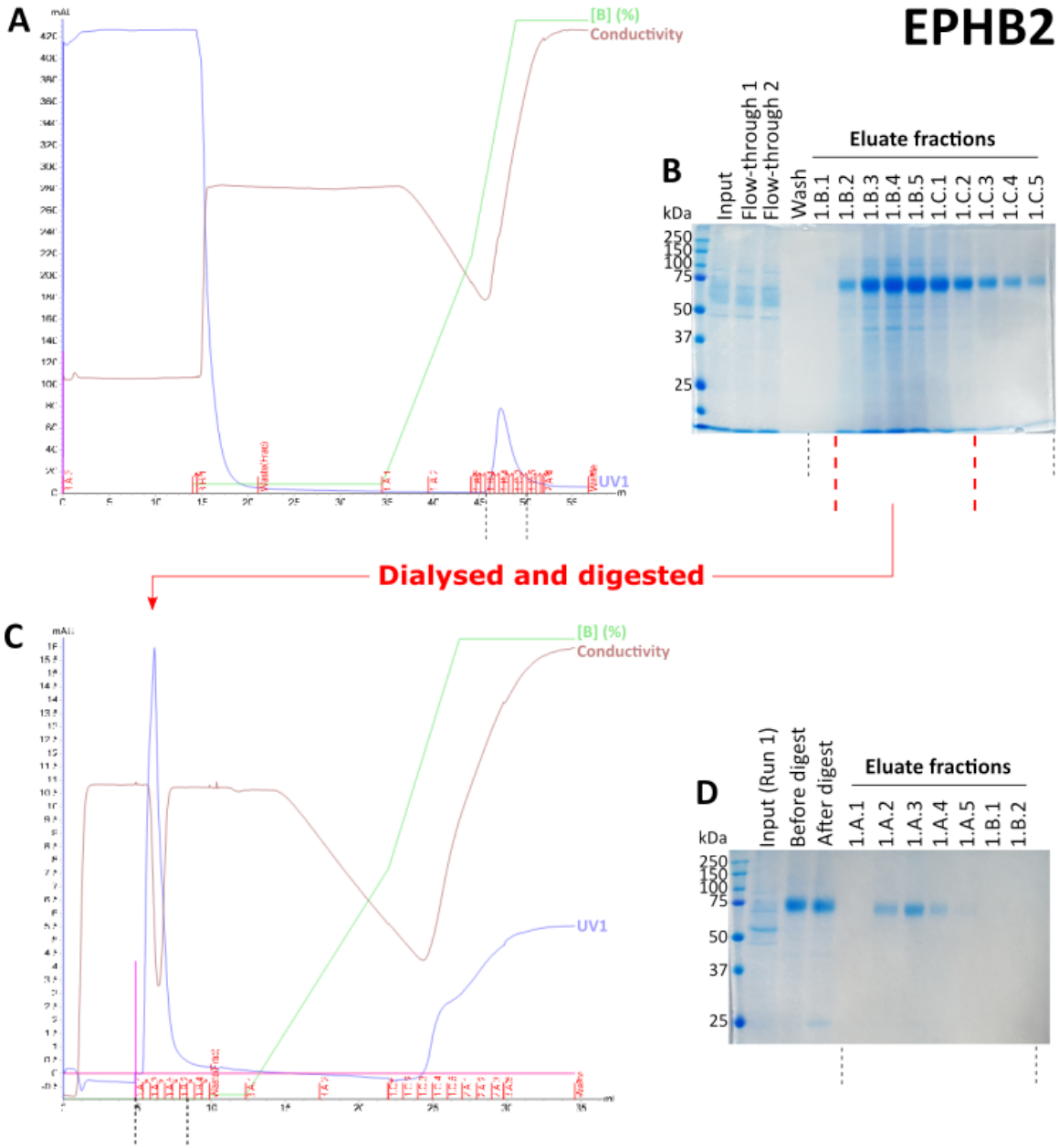

Fig. 4.3 *Purification of EPHB2 by immobilised metal affinity chromatography.* **A** Chromatogram of initial purification of EPHB2 by IMAC from cell culture media using pcEPHB2. The eluate fractions highlighted by the black dotted line were resolved by SDS-PAGE **B**. The eluate fractions highlighted by the red dotted lines were dialysed and the His-tag cleaved by TEV protease digest before further purification. **C** Chromatogram of the second purification step. The flowthrough was collected and the fractions highlighted by black dotted lines resolved by SDS-PAGE (**D**).

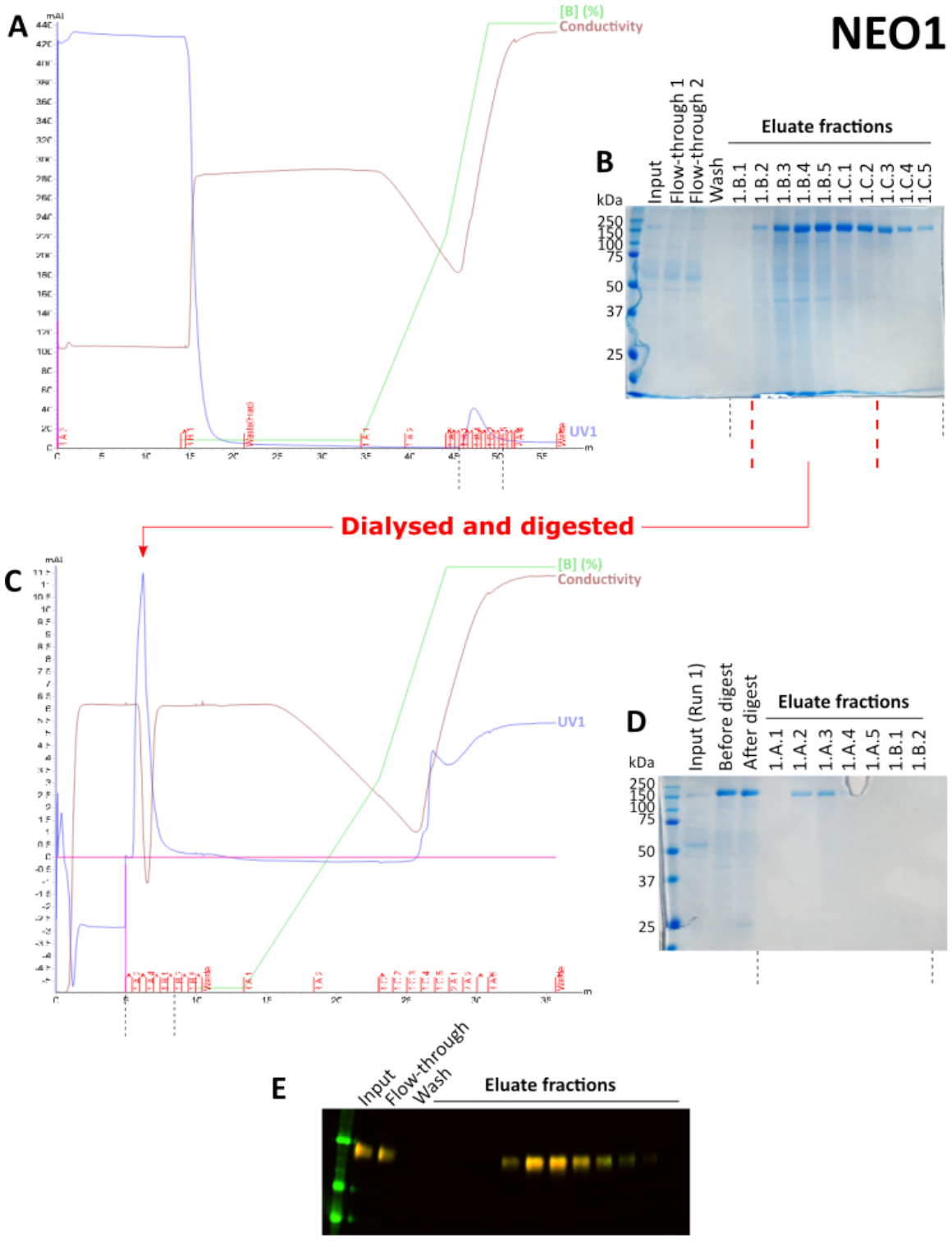

Fig. 4.4 *Purification of NEO1 by immobilised metal affinity chromatography.***A** Chromatogram of initial purification of NEO1 by IMAC from cell culture media using pcNEO1. The eluate fractions highlighted by the black dotted line were resolved by SDS-PAGE **B**. The eluate fractions highlighted by the red dotted lines were dialysed and the His-tag cleaved by TEV protease digest before further purification. **C** Chromatogram of the second purification step. The flowthrough was collected and the fractions highlighted by black dotted lines resolved by SDS-PAGE (**D**). Fractions from the initial column exchange were analysed by Western Blot using an anti-poly-His antibody (green) and an anti-NEO1 antibody (red).

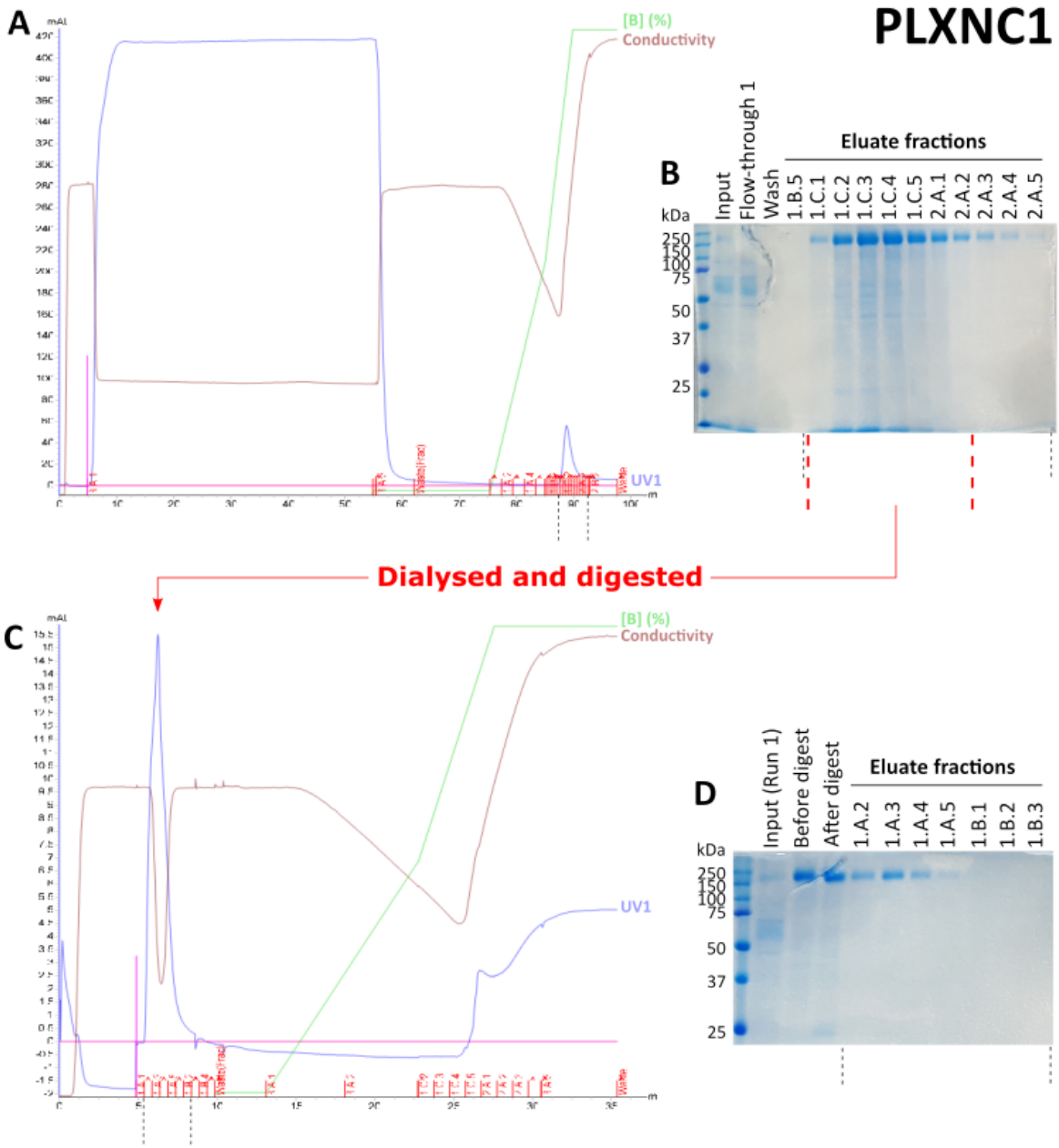

Fig. 4.5 *Purification of PLXNC1 by immobilised metal affinity chromatography.***A** Chromatogram of initial purification of PLXNC1 by IMAC from cell culture media using pc-PLXNC1. The eluate fractions highlighted by the black dotted line were resolved by SDS-PAGE **B**. The eluate fractions highlighted by the red dotted lines were dialysed and the His-tag cleaved by TEV protease digest before further purification. **C** Chromatogram of the second purification step. The flowthrough was collected and the fractions highlighted by black dotted lines resolved by SDS-PAGE (**D**).

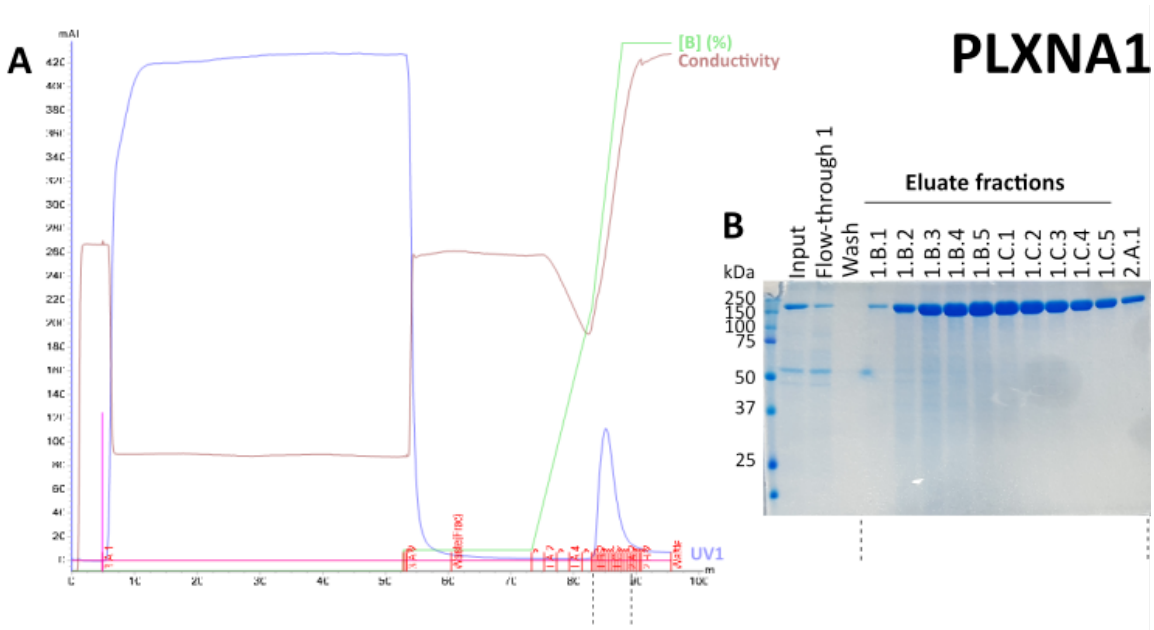

Fig. 4.6 *Purification of PLXNA1 by immobilised metal affinity chromatography.***A** Chromatogram of initial purification of PLXNA1 by IMAC from cell culture media using pcPLXNA1. The eluate fractions highlighted by the black dotted line were resolved by SDS-PAGE (**B**)

Although I was able to successfully clone SEMA4A into the expression vector, the protein production efficiency was very low (fig 4.7A). Western Blot analysis using a SEMA4A-targeted antibody confirmed that this was the correct protein and was the same size as the predicted molecular weight. Transcript expression was assessed by qRT-PCR and revealed that there was a similar fold induction in mRNA with the addition of Dox compared to the other constructs (50.9 $\pm$10.5 fold change with the addition of Dox, n=2. Data not shown). To exclude degradation as a possible mechanism, I analysed SEMA4A protein levels in the supernatant by Western Blot at earlier time points. As seen in figure 4.7B, there was an accumulation in the supernatant over the first 72 hours. There was also no discernible smear or multiple bands in the supernatant. These results suggested that the protein was not being degraded in the media. I hypothesised that this truncated construct was less stable than the wild-type protein and that this was negatively affecting the efficiency of expression. To test this hypothesis, I generated a full-length (wild type) construct of SEMA4A (SEMA4A(1-761)). Both this construct and the extracellular-domain only construct (SEMA4A(1-683)) were fused to a C-terminal His-tag and Tev protease cleavage site, cloned into pcDNA3.1 and transiently transfected into 293T cells. Cells were switched to FBS-free media and cell lysates and cell culture media collected at 72 hours. SEMA4A expression was analysed by Western Blot. As seen in figure 4.7C, the efficiency of expression for the full length

protein was much greater than the truncated recombinant protein although the inclusion of the transmembrane domain inhibited secretion into the cell culture media.

Despite the low yield, I investigated if IMAC purification could be used to purify and concentrate the recombinant protein. As seen in figure 4.8B there was a visible band that matched the expected size of our recombinant protein, but this was not easily discernable from the other contaminating proteins. As a result, I concluded it would be necessary to investigate other SEMA4A constructs to identify more efficiently produced recombinant proteins before proceeding further with protein purification.

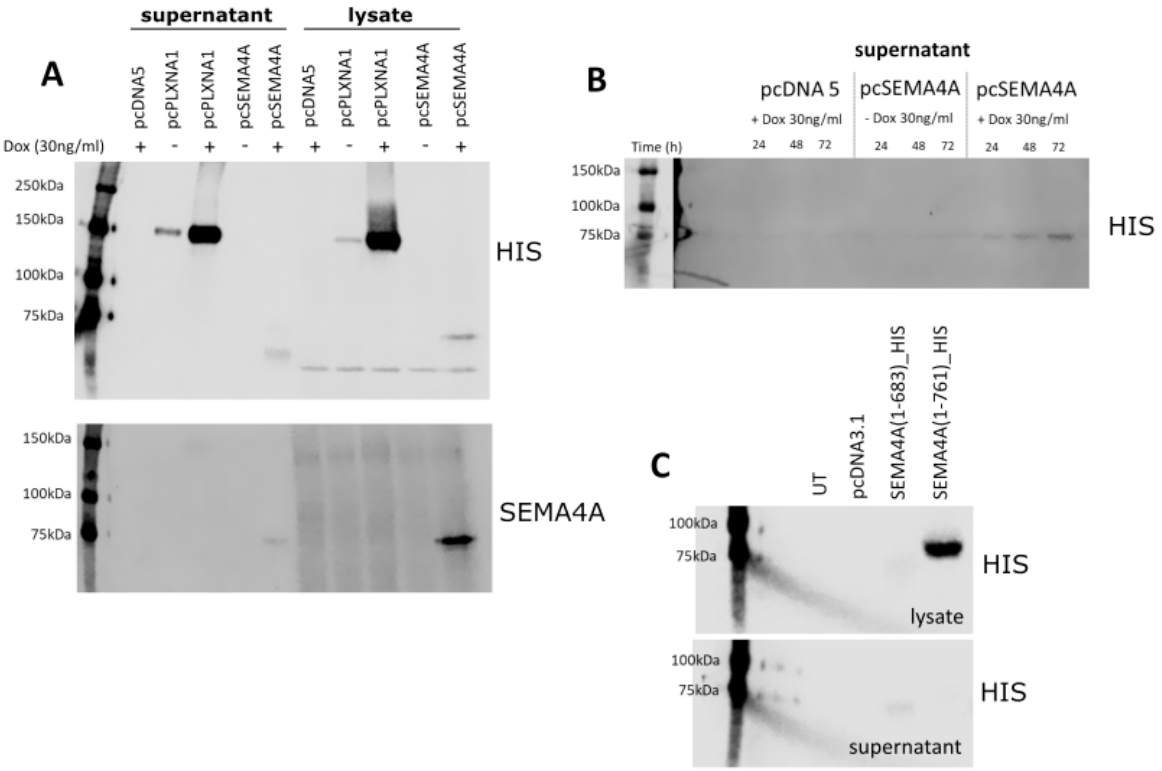

Fig. 4.7 *Expression of recombinant SEMA4A.* **A** pcDNA5, pcPLXNA1, pcSEMA4A were cultured with and without Dox (30ng/ml) for 7 days in FBS-free media. Cell culture media and cell lysates were collected and analysed by Western Blot. **B** pcDNA5 and pcSEMA4A were cultured for 72 hours in FBS-free media with or without Dox. Cell culture media samples were taken at 24, 48 and 72 hours and analysed by Western Blot. **C** Full-length (SEMA4A(1-761)) or the truncated extracellular domain only (SEMA4A(1-683)) SEMA4A was fused with a C-terminal His-tag and Tev protease cleavage site and cloned into pcDNA3.1. 293T were transiently transfected with either construct or the empty parental vector. Cell culture media and cell lysates were collected at 72 hours and analysed by Western Blot. Recombinant proteins were detected using a poly-His antibody (HIS) or an anti-SEMA4A antibody (SEMA4A).

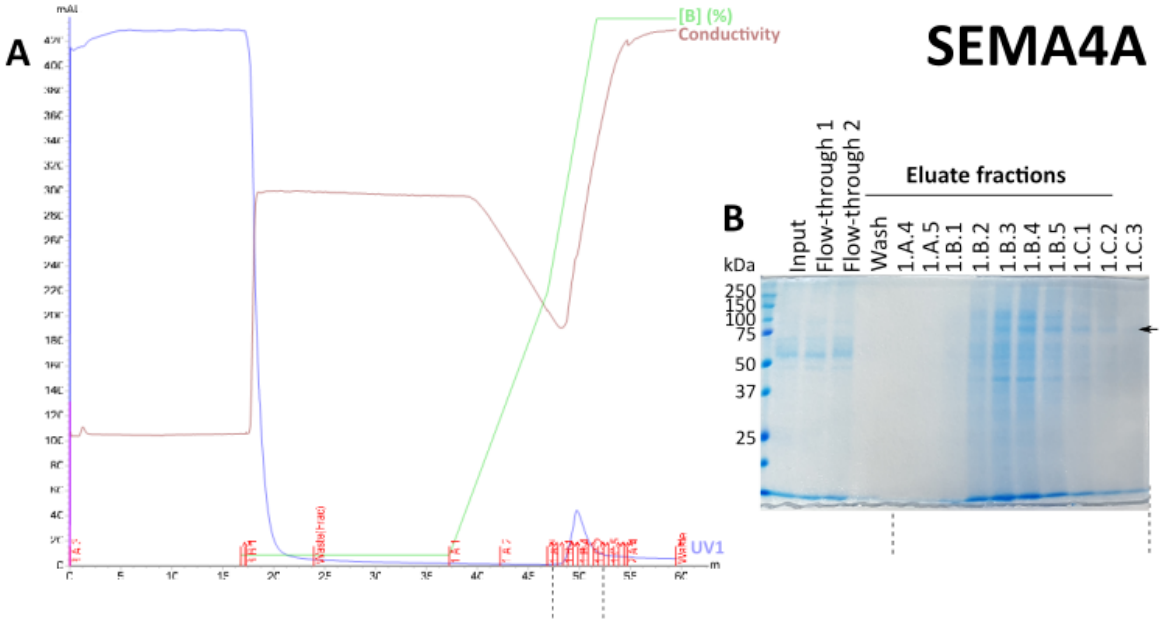

Fig. 4.8 **A** Chromatogram of initial purification of SEMA4A by IMAC from cell culture media using pcSEMA4A. The eluate fractions highlighted by the black dotted line were resolved by SDS-PAGE (**B**). Arrow indicates predicted SEMA4A band as determined by the calculated molecular weight.

4.3 Chapter conclusions

As not all of our candidate proteins will have commercial antibodies available for target validation, it will be necessary to generate proprietary tool antibodies. To produce the protein required for antibody generation, I have established a mammalian expression system in which only the extracellular portion of the protein is secreted into the media for convenient harvesting.

At the time of writing, I have successfully produced four of our top targets (EPHB2, NEO1 PLXNA1, PLXNC1) and purified three to a suitable level of homogeneity (as determined by SDS-PAGE). It was observed for at least one of the targets that there was substantial protein loss in the flow-through (fig 4.4E). Although I observed a good recovery following both purification steps, it may be necessary to adjust the protein purification protocol, either through the addition of a second affinity column or an adjustment to the pH of the cell culture media before purification.

Although I was able to produce SEMA4A, the production efficiency was very low and it was difficult to discern the protein product from contaminating proteins even following purification. As both wild-type and an intracellular-domain lacking mutant had been successfully expressed in three separate cell lines (see Chapter 5), I hypothesised that this was due to a compositional instability of the truncated protein. A direct comparison of the wild-type and truncated protein confirmed that this was the most likely explanation (fig 4.7C) and further investigations will be necessary to assess the efficiency of different SEMA4A constructs. The addition of a second affinity tag, such as maltose-binding protein, may also improve compositional stability [318].

Chapter 5

SEMA4A as a Antibody Drug Conjugate

5.1 Introduction

Whilst establishing a recombinant protein expression system, I next sought to validate those targets for which there were commercially available antibodies, comparing target expression in a larger cohort of patients. This would provide us with a more detailed analysis of target expression within myeloma, comparing expression in newly diagnosed versus relapsed refractory, and to identify any associations with subtype or subclones. Although the use of the publicly available mass spectrometry dataset (The Human Proteome Map) [300] has provided an initial assessment of off-tumour expression, it is possible that the low-abundant plasma membrane proteins were under-sampled because this dataset was generated without subcellular enrichment. Analysis of primary samples will therefore also enable us to determine off-tumour expression within the haematopoietic cell compartment.

Monoclonal antibodies have shown encouraging results thus far in the treatment of both solid and haematological malignancies. However, their low single-agent efficacy often requires the use of combination regimes with chemotherapeutics and as such, there are still some concerns of systemic toxicity. Antibody drug conjugates on the other hand, combine the specificity of antibodies with the cytotoxicity of chemotherapeutics to reduce off-tumour effects [246]. Aside from high on-tumour and low-off tumour expression, an ideal ADC candidate should also be internalised following antibody binding. To induce cell death, the toxin must be released from the targeting-antibody. Non-cleavable linkers rely on complete degradation of the antibody, whilst cleavable linkers rely on either the low pH of the late endosome/lysosome or on lysosomal-specific proteases for cleavage [247]. Regardless of the strategy used for release, nearly all ADCs rely on the intracellular compartment. Internalisation alone, however, is not sufficient and it will be imperative to also assess any

potential candidate antibodies in their ability to specifically deliver a toxin to induce cell-death. The generation of an ADC is a costly and time-consuming process. An alternative approach is to use a secondary antibody already directly conjugated to a toxin that can be used to rapidly screen multiple antibodies ('piggyback' system). These antibodies recognise the Fc domain of the primary targeting antibody and are internalised alongside as part of the immunoglobulin-membrane protein complex. Following internalisation, the secondary antibody is released in the cytosol and triggers cell death [319]. Although this system may not accurately reflect the properties of a lead ADC, they do provide a proof-of-principle that will enable the identification of a lead candidate.

In this chapter I identify SEMA4A as a promising therapeutic target. SEMA4A is a class IV transmembrane Semaphorin, a family of glycoproteins characterised by a conserved Sema domain. With a very short intracellular domain (57 amino acids), SEMA4A primarily functions as a ligand and mediates its signalling through its binding partners, the Plexin and Neuropilin family of receptors [320][321]. Although the Semaphorin family have been classically described as neuronal axon guidance molecules [322], SEMA4A appears to play an important role within the immune system. Initially identified on dendritic cells, SEMA4A functions as a co-stimulator, enhancing the proliferation and differentiation of T helper cells and augmenting IL-2 production *in vitro* [320]. Meanwhile, SEMA4A -/- dendritic cells are markedly impaired in their priming ability [323] and SEMA4A blockade impairs the generation and response of antigen-specific T cells *in vivo* [320]. SEMA4A has also been implicated in immune regulation. Blockade of the SEMA4A-Neuropilin-1 signalling axis attenuated the differentiation, proliferation and suppressive activity of Tregs *in vitro* and significantly reduced tumour growth in WT C57BL/6 mice *in vivo*, suggesting that SEMA4A blockade may reverse immune tolerance [321].

In addition to its role in the immune system, SEMA4A may also play a crucial role in photoreceptor survival. Although SEMA4A -/- mice overall appear to be healthy and phenotypically normal, with no observable defects in the brain, lung, kidney, testis or heart, they do exhibit signs of severe retinal dysfunction [323][324]. At birth these mice have normal retinal development but over time there is a gradual disruption in the outer segment of photoreceptors with a complete loss within 3 to 4 weeks as a result of light-induced apoptosis [324][325]. This anti-apoptotic role for SEMA4A in the retina appears to be mediated by its involvement in endosomal-sorting pathways. Under oxidative stress, one of the major forms of damage from light exposure, SEMA4A in retinal pigment epithelial (RPE) cells prevents the sorting of prosaposin to the lysosomal pathway and instead promotes its exosomal release,

promoting photoreceptor survival [324]. In concordance with these findings, SEMA4A mutations have been subsequently identified in patients with retinal degeneration [326].

Classically considered a ligand, a recent report suggests that SEMA4A may additionally function as a receptor and transduces a 'reverse signal'. Sun *et al* reported that SEMA4A regulates the migration of cancer cells and dendritic cells following the interaction with its ligand PlexinB1. The pro-invasive and migratory behaviour of these cells appeared to be dependent on Scrib, a scaffold protein, which interacts with and regulates the activity of the small GTPases Cdc42 and Rac1 [327].

The role of SEMA4A in myeloma cell biology, and if it possesses reverse signalling capabilities, is currently unknown. One of the reported mechanisms of resistance to antibody therapeutics is target downregulation [328]. Following daratumumab infusion, there is a significant reduction in CD38 cell surface expression on myeloma cells [329]. Whilst this may be a mechanism of tumour escape, it may in fact also promote tumour cell death through the loss of contact with the cellular compartment of the bone marrow niche [329]. It would therefore be of considerable interest to determine if SEMA4A play an essential role in tumour cell biology and if target downregulation is a viable mechanism of resistance.

5.1.1 Chapter Overview

In this chapter I describe the identification of commercial antibodies suitable for target characterisation and the subsequent profiling of these proteins in a larger sample of patients by flow cytometry. From these results, I identify three therapeutic target candidates: ROBO1, NEO1 and SEMA4A, all of which demonstrated rapid receptor internalisation following antibody binding. However, I show that in an *in vitro* ADC cytotoxicity assay, only the SEMA4A antibody demonstrated selective cell killing activity. The SEMA4A-ADC also significantly delayed myeloma growth in an orthometastatic xenograft model. Finally, I show that loss of SEMA4A using RNAi-knockdown conveys a competitive disadvantage, although I am unable to conclude that this is target specific following the failure to reverse the phenotype using shRNA-resistant rescue constructs.

5.2 Results

5.2.1 Characterisation of novel target candidates in primary myeloma samples

In chapter 3 I identified 16 potential monoclonal antibody target candidates: ADAM17, CD97, BTN2A1, EPHB2, EVI2B, LRRC8C, LRRC8D, NEO1, PLXNA1, PLXNC1, PTPRG, ROBO1, ROR2, SEMA4A and SEMA4D (table 3.5). As the number of samples profiled by mass spectrometry was small, the next aim in this project was to characterise tumour expression in a larger cohort of patients as well to compare expression between malignant plasma cells and other leukocyte populations. This would also enable us to analyse the ubiquity of expression within plasma cells to determine if any of these potential target antigens were restricted to particular subclones. In order to do so, it was first necessary to identify commercially available antibodies against our potential targets that were suitable for flow cytometry as well as functional assays for target validation.

Out of 16 targets, 10 had commercially available antibodies that were recommended for flow cytometry (ADAM17, CD97, EVI2B, NEO1, PLXNA1, PLXNC1, ROBO1, ROR2, SEMA4A and SEMA4D). Seven of these were tested by comparing protein expression by flow cytometry against PMP expression across a selection of the HMCLs profiled (figure 5.1A). Five of the antibodies were considered to be target-specific and suitable for further use based on a strong positive correlation between PMP and flow cytometry protein expression, with correlation coefficients ranging from $r(10)=0.849$, $p<0.001$ (NEO1) to $r(10)=0.957$, $p<0.001$ (ROBO1). This included CD97, SEMA4A and SEMA4D. The PLXNA1 antibody exhibited very low MFI ratios across the cell lines tested (1.06 to 1.54, n=5) and a strong negative correlation $r(5)=-0.847$, $p>0.05$ and so was considered unsuitable. Two different antibody clones were tested for PLXNC1 (544232 and 1A12), neither of which exhibited strong, target-specific binding. Despite high PMP expression, the fold change compared with the isotype control was very low and across the HMCLs there was a poor correlation with PMP, $r=0.359$ and 0.292 for clone 544232 and 1A12 respectively, $p>0.05$ for both. As PLXNC1 expression by PMP correlated well with RNA expression by RNAseq (Keats Lab), I confirmed target expression by qRT-PCR. As seen in figure 5.1B comparing PLXNC1 expression by qRT-PCR and PMP, cell line expression of the target had not changed since profiling. Although the antibody targeting ROBO1 exhibited weak signal, it did appear to be highly target specific as determined by correlation with PMP and so was considered suitable for primary sample screening.

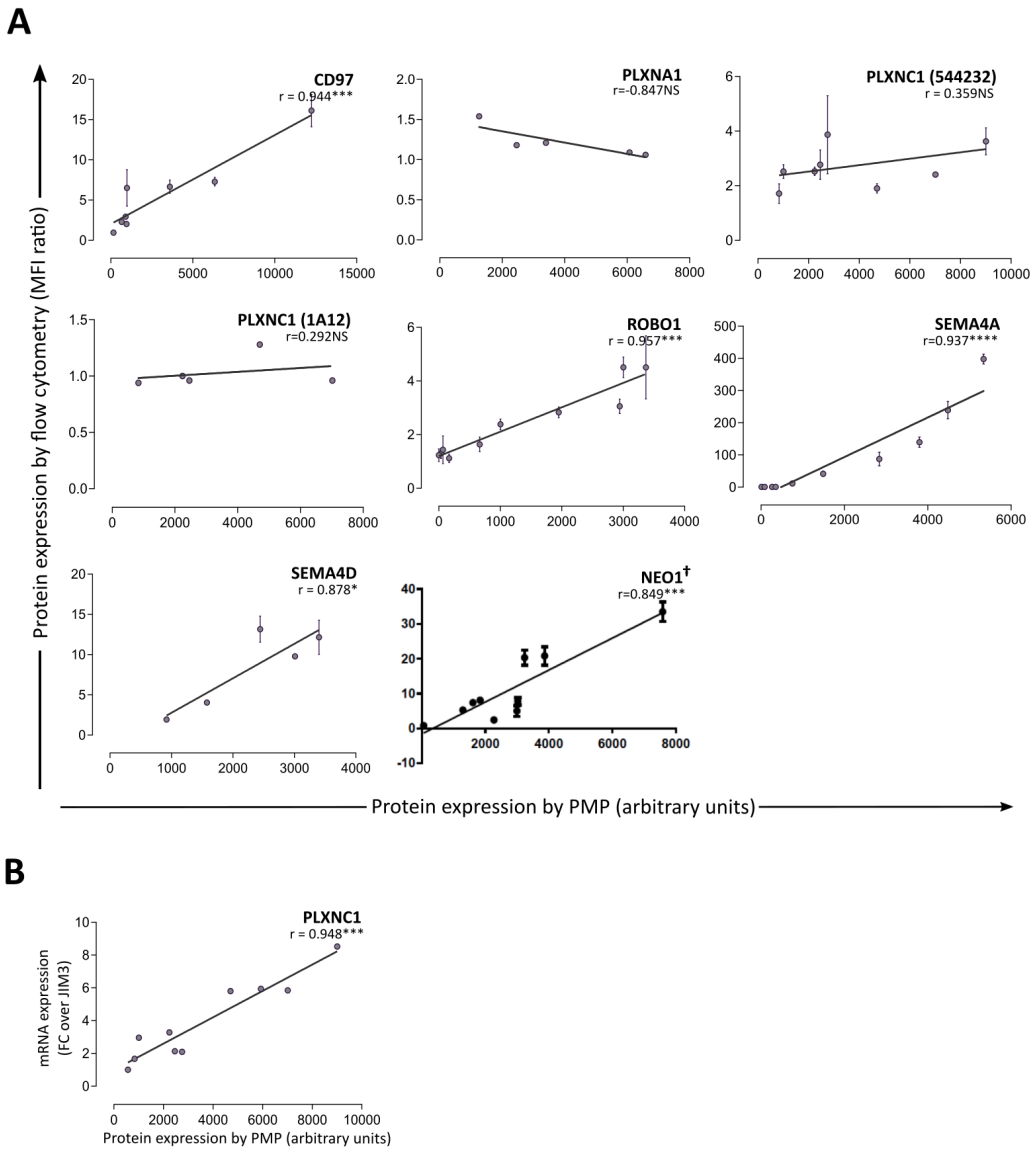

Fig. 5.1 *Five out of 16 novel targets have working, commercially available antibodies suitable for flow cytometry.* To identify working antibodies for the novel targets, target expression across a selection of HMCLs was analysed by flow cytometry (MFI ratio) and compared against protein expression by PMP **A**. For five of the seven targets analysed there was a strong positive correlation with PMP, as determined by Pearson's correlation, validating these antibodies as suitable for primary sample screening. **B** PLXNC1 expression by RNA was quantified in all 10 HMCLs profiled by qPCR and compared with protein expression by PMP to confirm that cell line expression had not changed since profiling, n=1. *=p<0.05, **=p<0.01, ***=p<0.001. † NEO1 staining performed by Dr S. Surget.

These five antibodies were then used to assess target expression in primary myeloma samples by FC. BMA from patients at all stages of disease were processed as described in materials and methods (section 2.2) and target expression by flow cytometry was compared as the fold change between $CD138^{pos}$ and $CD138^{neg}$ leukocytes, figures 5.2 to 5.5. For CD97 and SEMA4A, in which a proportion of $CD138^{neg}$ leukocytes also expressed the target of interest, the mean fold change was calculated between $CD138^{pos}$ and $CD138^{neg}$/$Target^{pos}$ cells. For all samples, a single-sample t-test was performed on log-transformed data.

CD97 was expressed in all HMCLs and primary samples profiled by PMP. In HMCLs, there was a similar median expression (974.15) compared with CD38 (1643.45) and SLAMF7 (612), the targets of daratumumab and elotuzumab respectively. By PMP, CD97 expression was greater in the primary samples compared with HMCLs (fig 5.2A). By flow cytometry, CD97 was highly and uniformly expressed in $CD138^{+}$ cells across all samples analysed. However, there was also high CD97 expression on $CD138^{neg}$ leukocytes and the mean fold change of CD97 expression in $CD138^{+}$ cells over other leukocytes was not significant (1.79 $\pm$2.42 (mean fold change $\pm$SD), t(6)=0.4462, p>0.05) by a one-sample t-test (fig 5.2C). As CD97 was predicted to have a similar level of expression to haematopoeitic cell subsets in a number of other tissues (figure 5.2D), this target was not taken further forward.

By PMP, NEO1 had a similar expression to SLAMF7 in both HMCLs and primary samples but was expressed at a much lower level than CD38 in patient samples (fig 5.3A). Flow cytometric analysis of primary samples revealed that NEO1 expression was largely restricted to $CD138^{+}$ plasma cells, with little to no expression in $CD138^{neg}$ leukocytes. This difference was statistically significant by a one-sample t-test (mean fold change of 4.58 $\pm$3.26 (SD), t(14)=7.323, p<0.0001 (fig 5.3C)). Although NEO1 expression was uniform within each sample across plasma cells, there was clear variability between samples. This variability in expression was independent of disease stage with a mean fold change of 4.996 $\pm$2.34(SD) at diagnosis and 5.09 $\pm$4.272 (SD) at progression/relapse. Analysing the whole-cell mass spectrometry dataset, NEO1 showed low to medium expression in a few tissues (including the frontal cortex, ovary and testis) but importantly was not expressed in tissues associated with severe or lethal toxicities, including the heart, kidney, liver nor lungs (fig 5.3D). Although there was predicted expression in the frontal cortex and spinal cord, it is anticipated that a therapeutic antibody would be unable to cross the blood brain barrier [330].

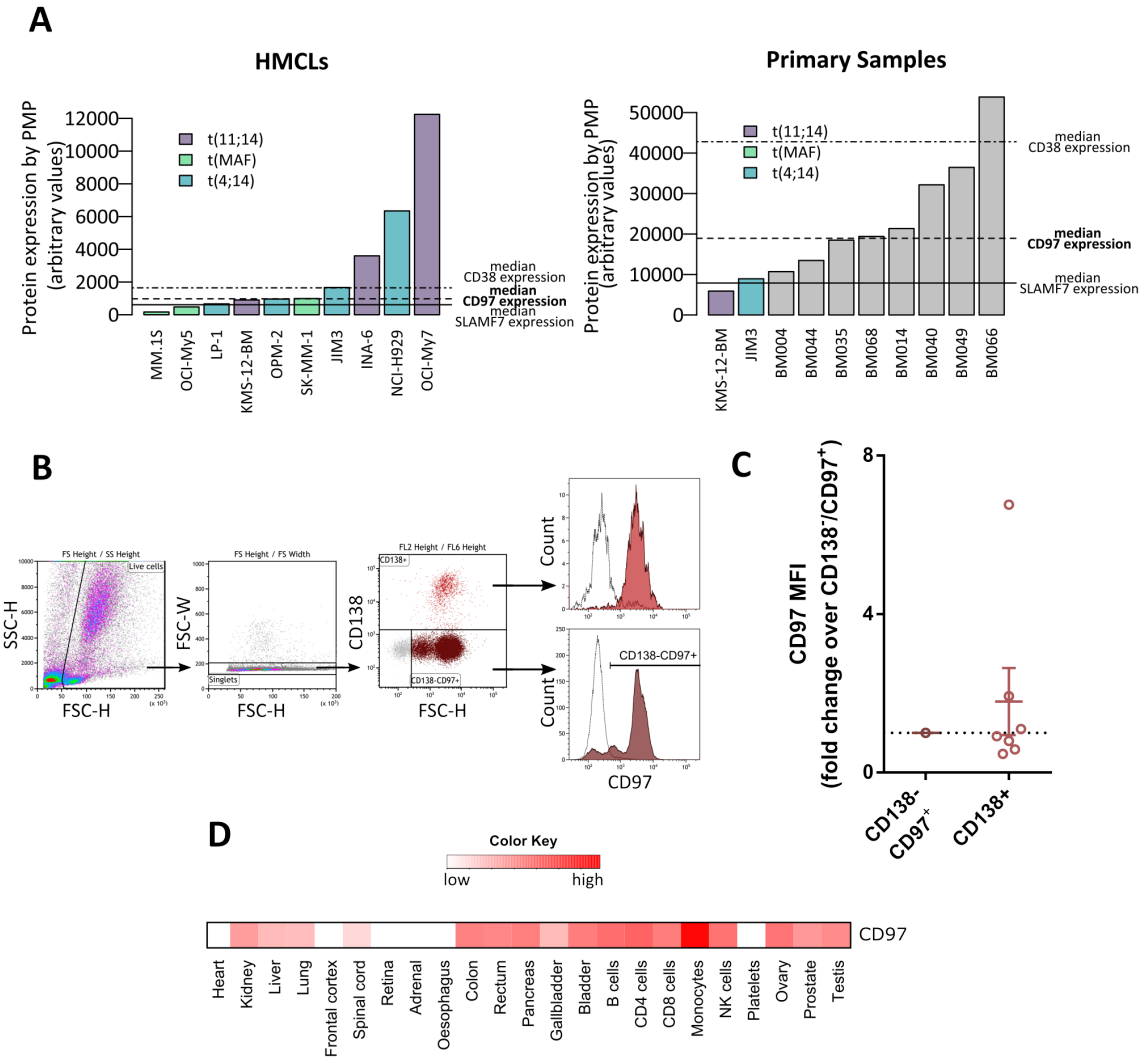

Fig. 5.2 *CD97 is highly expressed in both plasma cells and other CD138^{neg} leukocytes.* **A** CD97 expression in HMCLs and primary samples by PMP. **B** Flow cytometry gating strategy for comparing CD97 expression in primary samples. **C** The fold change of CD97 expression in CD138^{pos} plasma cells over CD138^{neg}/CD97^{pos} leukocytes. CD97 was not signficiantly differentially expressed in plasma cells compared with other CD97^{pos} leukocytes, n=7. **D** Predicted normal tissue expression from The Human Proteome Map [300].

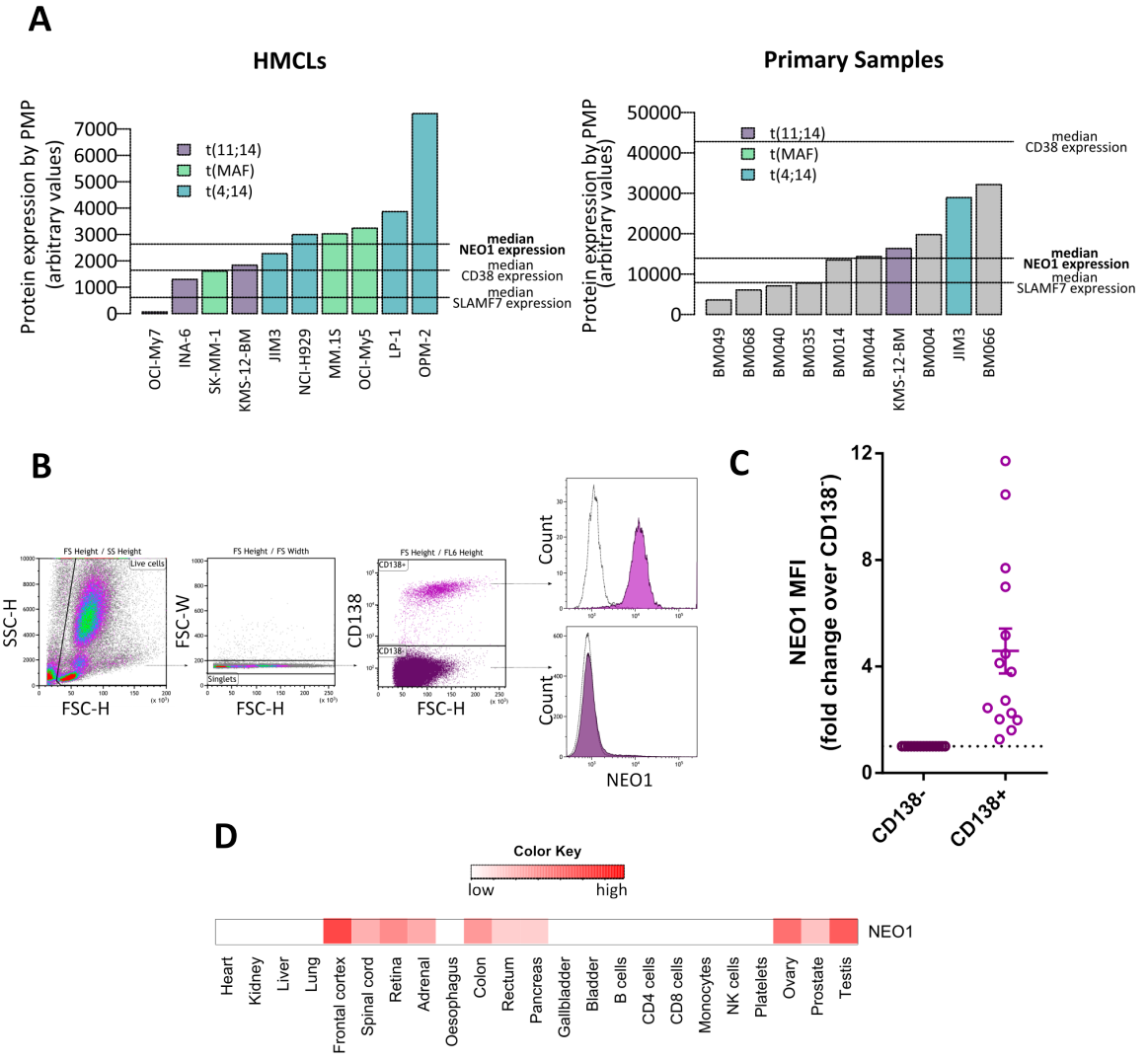

Fig. 5.3 *NEO1 is highly expressed in plasma cells and with little to no expression in CD138^{neg} leukocytes.* **A** NEO1 expression in HMCLs and primary samples by PMP. **B** Flow cytometry gating strategy for comparing NEO1 expression in primary samples. **C** The fold change of NEO1 expression in CD138^{pos} plasma cells over CD138^{neg} leukocytes. NEO1 was expressed at a significantly higher level in in plasma cells compared with other leukocytes, n=15. **D** Predicted normal tissue expression from The Human Proteome Map [300].

As previously discussed, ROBO1 was initially selected as a potential target due to high expression in HMCLs by PMP (fig 5.4A). Despite a similar expression profile to CD38 and SLAMF7 in HMCLs, ROBO1 expression was much lower in primary samples (median expression of 1089.95). Despite the low expression, ROBO1 appeared to be plasma cell restricted amongst all leukocyte subsets by flow cytometry (fig 5.4B and C), with a statistically significant fold change of 1.8 ($\pm$0.689 (SD)), t(14)=5.709, p<0.0001 over CD138^{neg} populations. There were two distinct populations of ROBO1^{hi} and ROBO1^{low}, but similarly to NEO1, these two populations were independent of disease stage with a mean fold change of 1.773($\pm$0.49 (SD)) at diagnosis and 1.879 ($\pm$0.85 (SD)) at progression/relapse.

Compared to ROBO1, SEMA4D was uniformly expressed at a high level across all HMCLs by PMP, with a similar expression to SLAMF7 in primary samples (fig 5.5). By flow cytometry, SEMA4D was consistently expressed by all CD138^{pos} cells, but was also expressed by all other leukocytes, with a mean fold change of 0.873 $\pm$0.912 (SD), t(2)=0.853, p>0.05 (fig5.5C). Even though this was a small sample size, the high leukocyte expression was consistent with the whole cell mass spectrometry dataset (fig 5.5D) and this target was not taken further forward.

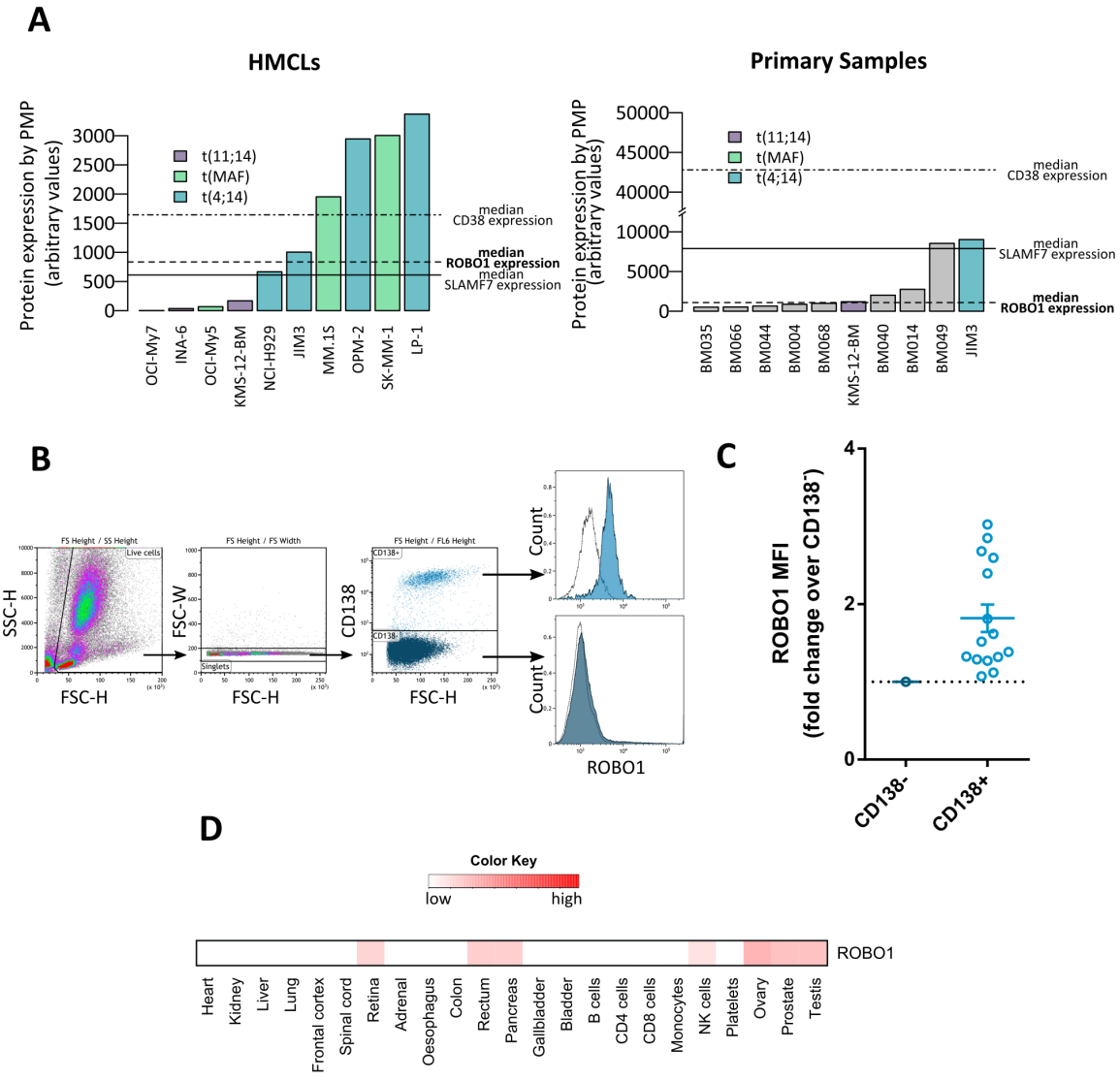

Fig. 5.4 *ROBO1 is more highly expressed in CD138^{pos} plasma cells than other leukocytes* **A** ROBO1 expression in HMCLs and primary samples by PMP. **B** Flow cytometry gating strategy for comparing ROBO1 expression in primary samples. **C** The fold change of ROBO1 expression in CD138^{pos} plasma cells over CD138^{neg} leukocytes. ROBO1 was expressed at a significantly higher level in plasma cells compared with other leukocytes, n=15. **D** Predicted normal tissue expression from The Human Proteome Map [300].

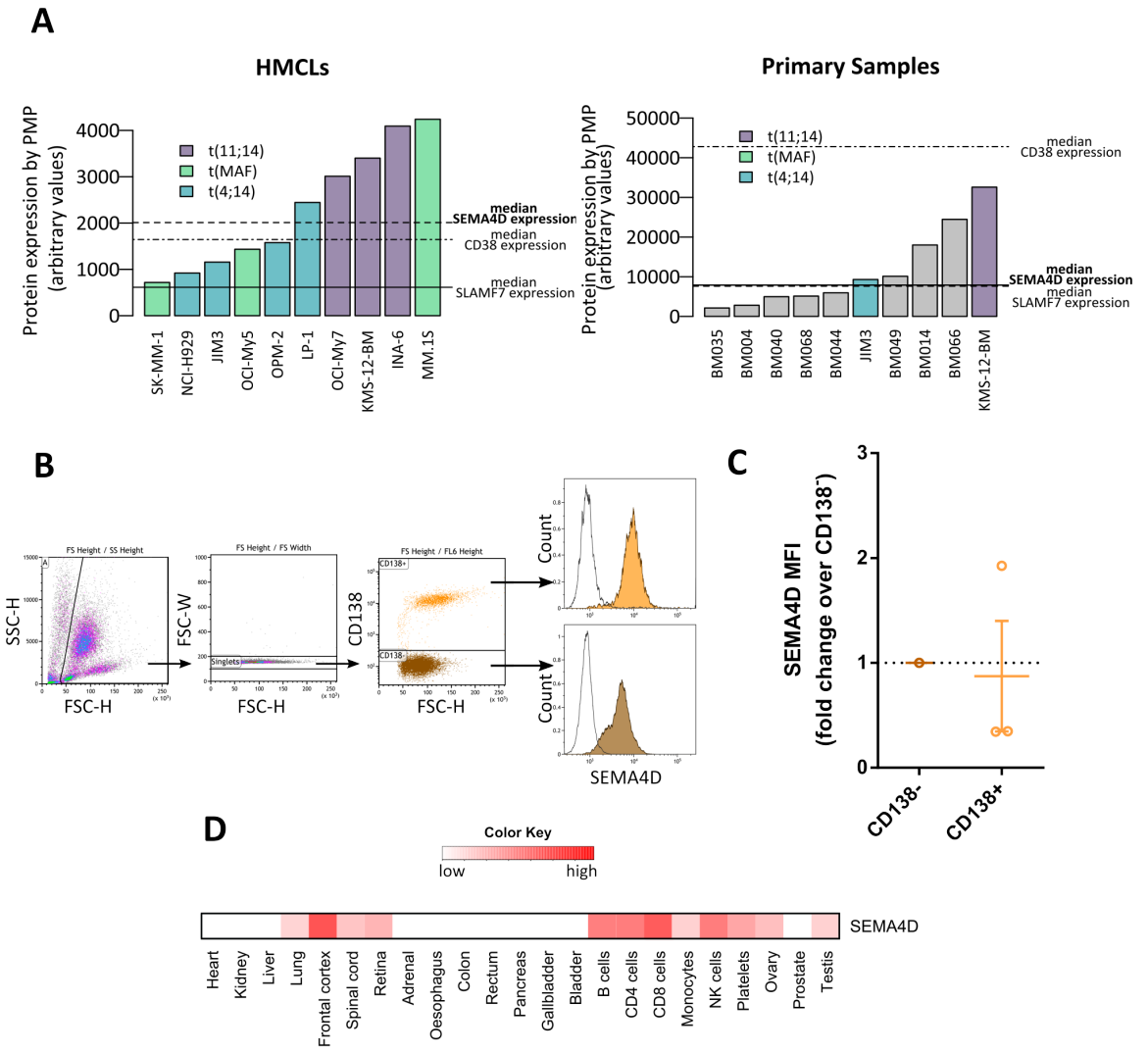

Fig. 5.5 *SEMA4D is more highly expressed in CD138^{neg} leukocytes than plasma cells.* **A** SEMA4D expression in HMCLs and primary samples by PMP. **B** Flow cytometry gating strategy for comparing SEMA4D expression in primary samples. **C** The fold change of SEMA4D expression in CD138^{pos} plasma cells over CD138^{neg} leukocytes, n=3. **D** Predicted normal tissue expression from The Human Proteome Map [300].

SEMA4A was more highly expressed than SLAMF7 in both HMCLs and in primary samples by PMP but was expressed at a lower level than CD38 (fig 5.6A). By flow cytometry, SEMA4A was highly expressed in the majority of primary samples analysed. Although there was a subset of leukocytes that also expressed SEMA4A, SEMA4A expression was greatest in CD138^{pos} plasma cells with a mean fold change of 3.232 $\pm$3.38 (SD) that was statistically significant by a single-sample t-test (t(21)=3.026, p<0.01) (fig 5.6C). SEMA4A expression was independent of disease stage, with a mean fold change at diagnosis of 2.92 $\pm$2.31 (SD) compared to 4.04 $\pm$4.36 (SD) at progression/relapse. Consistent with this, BM068, which exhibited similar SEMA4A expression to KMS-12-BM when profiled by PMP, showed comparable levels by flow cytometry two years later (SEMA4A MFI of 60.2 in plasma cells versus 41.5 $\pm$8.4 (SD) in KMS-12-BM. Overall, SEMA4A was highly expressed in CD138^{+} plasma cells compared with other leukocytes and importantly, had low off-tumour expression outside of haematopoeitc lineages by whole-cell mass spectrometry (fig 5.6D).

To further differentiate SEMA4A expression on normal haematopoeitic cell populations, I utilised a more comprehensive flow cytometry panel to compare levels of SEMA4A between the major subtypes. Samples were processed as previously described for flow cytometry. The following markers were used to identify leukocyte populations: CD66b as a pan-granulocyte marker, CD14 for monocytes and macrophages, CD3 as a T-cell marker, CD19 for B cells and CD34 as a stem-cell marker. SEMA4A expression on CD235a^{+} red blood cells (RBC) was also analysed for one patient sample that was processed without RBC lysis. To enable comparisons between samples, SEMA4A expression on each subtype was calculated as the fold change over CD66b^{+} granulocytes, which appeared to exhibit the most consistent expression. B cells and T cells exhibited minimal expression (mean fold change of 0.13 $\pm$0.07 (SD) and 0.097 $\pm$0.04 (SD) for B and T cells respectively). There was notable relatively higher expression on monocytes (mean fold change 1.15 $\pm$0.38 (SD)) and granulocytes. Importantly, CD34^{+} stem cells exhibited very low SEMA4A expression with a mean fold change of 0.31 $\pm$ 0.26 (SD) and there was also minimal expression on RBC (0.20 fold change, n=1). Overall, SEMA4A expression was still greatest on CD138^{pos} plasma cells in the majority of samples, with a mean fold change of 2.37 $\pm$ 1.82 (SD) (figure 5.7).

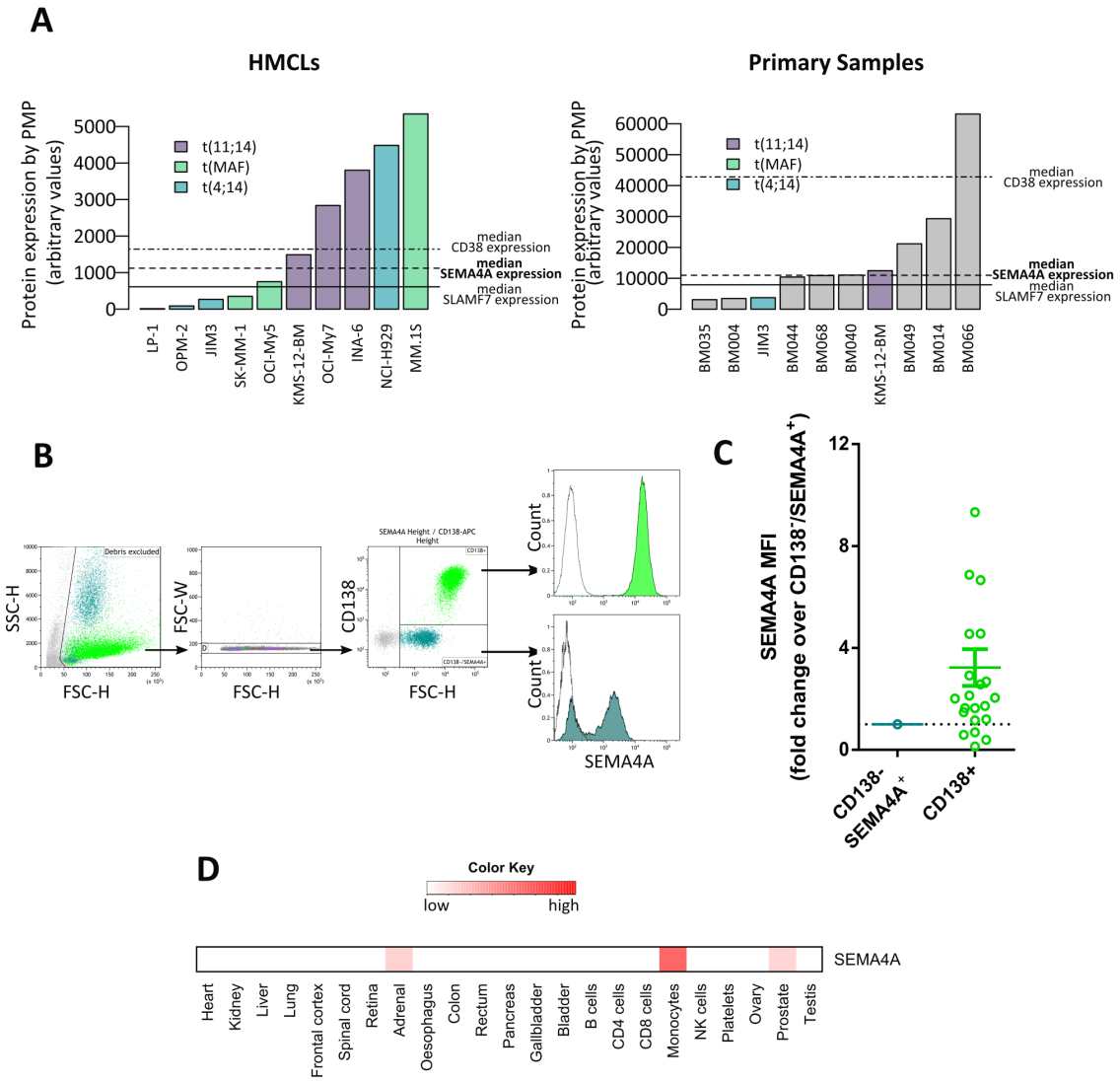

Fig. 5.6 *SEMA4A is more highly expressed in CD138^{pos} plasma cells than other leukocytes* **A** SEMA4A expression in HMCLs and primary samples by PMP. **B** Flow cytometry gating strategy for comparing SEMA4A expression in primary samples. **C** The fold change of SEMA4A expression in CD138^{pos} plasma cells over CD138^{neg}/SEMA4A^{pos} leukocytes. SEMA4A was significantly more highly expressed in plasma cells than other leukocytes, n=22. **D** Predicted normal tissue expression from The Human Proteome Map [300].

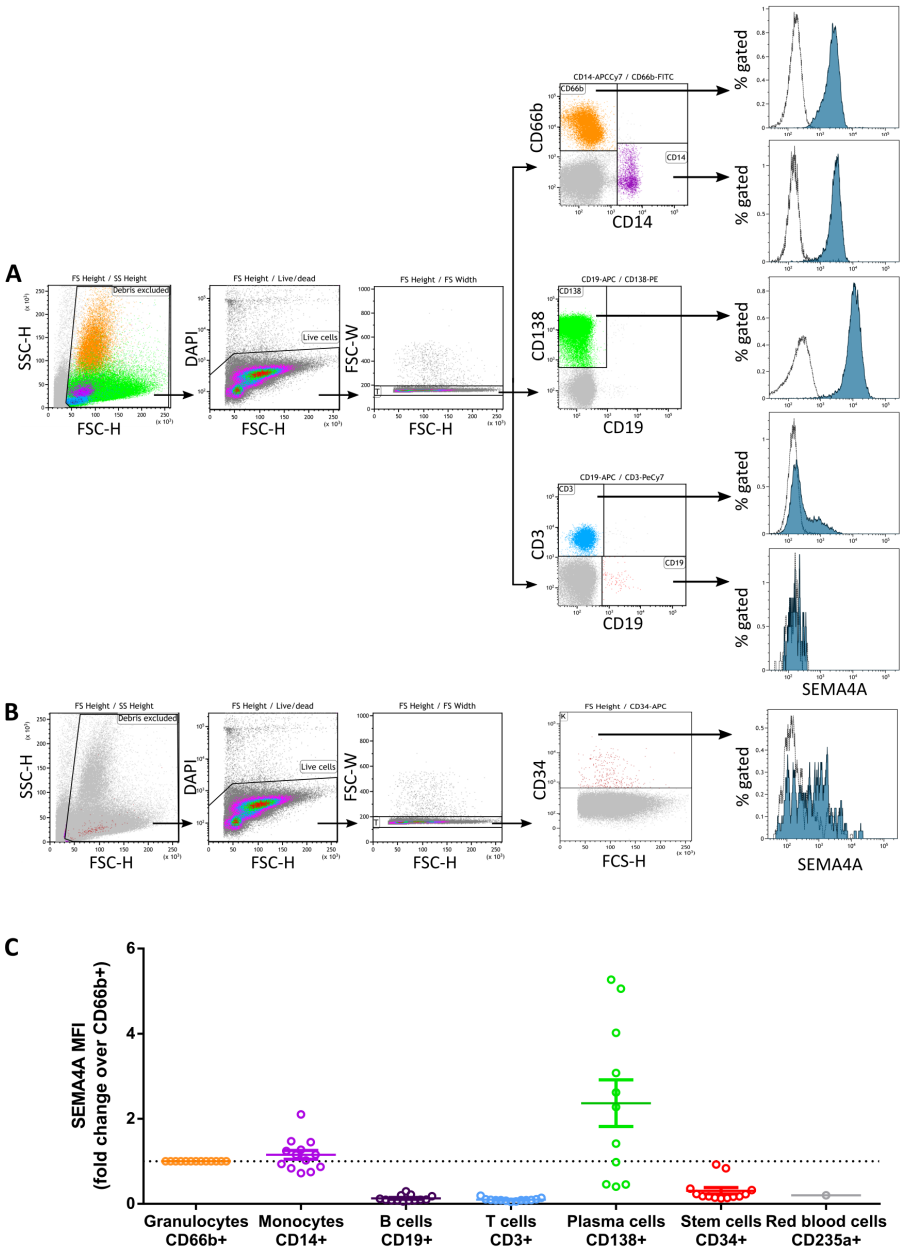

Fig. 5.7 *SEMA4A expression is greatest in CD138^{pos} plasma cells compared with other leukocyte populations* **A** Flow cytometry gating strategy for differentiating SEMA4A expression in normal haematopoietic cell populations. **B** Flow cytometry gating strategy for analysing SEMA4A expresssion on CD34^{+} stem cells. **C** Summary of SEMA4A expression in all patient samples analysed by comparing the mean fold change in each population against CD66b^{+} granulocyte SEMA4A expression, n=13.

5.2.2 Internalisation of targets

As ADC toxicity is directly related to surface expression, I decided to discontinue with both CD97 and SEMA4D as potential targets. Both of these proteins exhibited high off-tumour expression amongst haematopoietic cell subsets and were predicted to be expressed at a substantial level in a number of other, normal tissues.

The cellular internalisation of an ADC is essential for efficacy. Therefore, the next aim of this project was to determine if any of the remaining targets (ROBO1, SEMA4A and NEO1) were suitable as ADCs by assessing internalisation following antibody-binding. Internalisation of the antibody-antigen complex was tracked using a flow-cytometry assay that also enabled analysis of the kinetics of the response.

Surface antigens on live cells were labelled using an unconjugated primary antibody at 4°C before unbound antibody was washed away and cells incubated at either 4 or 37°C for three hours. Samples were taken at various timepoints and any remaining surface-bound primary antibody labelled using a fluorescent-labelled secondary antibody under non-permeabilising conditions before fixation and analysis by flow cytometry. The MFI ratio was used to calculate the proportion of the remaining surface-bound antibody compared with t_0. As membrane trafficking is limited at lower temperatures, internalisation at 4°C was used as a control to prevent receptor endocytosis.

By flow cytometry, both ROBO1 and SEMA4A appeared to be internalised following antibody binding. Incubation of SK-MM-1 with mAb-770502 (targeting ROBO1) at 37 °C was associated with a decrease in surface-bound antibody over time, with a maximal loss of 53.9% by one hour compared with the 4 °C control (fig 5.8). This loss was uniform across all cells. Similarly, there was a loss in surface-bound mAb-5E3 (targeting SEMA4A) in NCI-H929 cells following incubation at 37 °C with max internalisation at two hours (51.4%) (fig 5.9). Again, this was uniform across all cells as shown in the flow cytometry histogram. For both targets there was negligible recycling of antigen-antibody complexes back to the cell surface. NEO1 also appeared to be internalised by flow cytometry with a loss of 44% of surface-bound antibody by two hours (Dr S Surget, personal communication).

Following internalisation, it is also considered essential for ADCs to be trafficked to the late endosome or lysosome for cleavage of the cytotoxic payload from the antibody. Immunofluorescence was used to follow antibody trafficking as well as to confirm that antibody

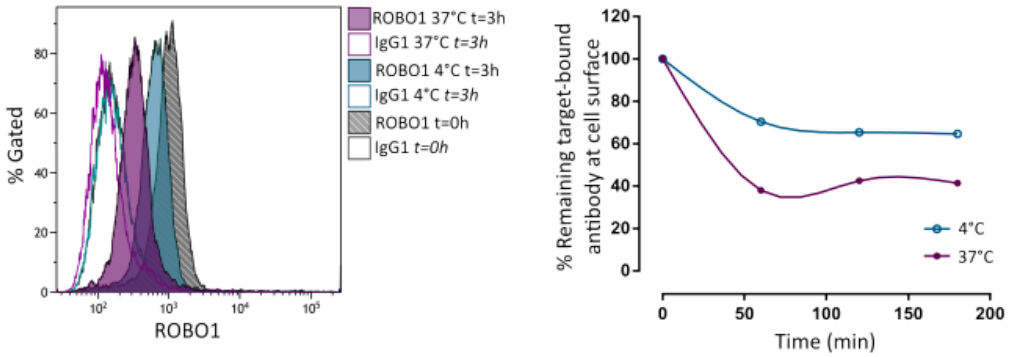

Fig. 5.8 *Cell surface ROBO1 expression is lost following mAb-770502 binding.* SK-MM-1 cells were incubated for 20 minutes at 4°C with mAb-770502 before unbound antibody was washed and cells incubated at 4 or 37°C for three hours. Remaining surface-bound antibody was analysed by flow cytometry **(left panel)** and the proportion of remaining antibody was calculated by the MFI as a proportion of the MFI at t_0. n=1 **(right panel)**.

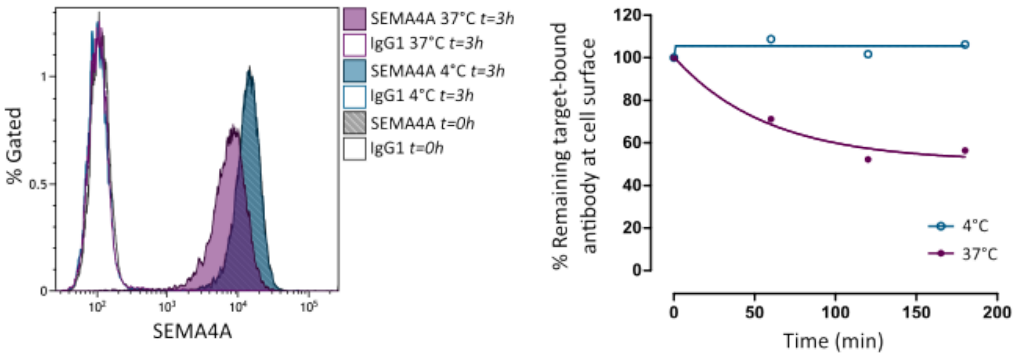

Fig. 5.9 *Cell surface SEMA4A expression is lost following mAb-5E3 binding.* NCI-H929 cells were incubated for 20 minutes at 4°C with mAb-5E3 before unbound antibody was washed and cells incubated at 4 or 37°C for three hours. Remaining surface-bound antibody was analysed by flow cytometry **(left panel)** and the proportion of remaining antibody was calculated by the MFI as a proportion of the MFI at t_0. n=1 **(right panel)**.

loss at the cell-surface was endocytosis-mediated.

Similarly to the flow-cytometry assay, NCI-H929 cells were incubated with the unconjugated primary antibody at 4°C, washed to remove unbound antibody and shifted to 37°C for three hours. Samples were taken before and after incubation at 37°C and cells were fixed on ice. Both internalised and surface-bound antibody were then labelled using a fluorescent-labelled secondary antibody under permeabilising conditions. As seen in figure 5.10, there was clear cell surface localisation of mAb-5E3 at t_0. By three hours, there was a reduction in the remaining surface-bound antibody with a corresponding appearance of antibody-containing vesicles. These vesicles appeared to be localised with LAMP-1 positive lysosomes, as shown by the signal intensity profile overlay (fig 5.10B), suggesting that the antibody-antigen complex is trafficked to the lysosome, the ideal subcellular localisation for ADC delivery.

Although the ROBO1 antibody (mAb-770502) worked well for flow cytometry, the signal couldn't be detected by immunoflourescence (data not shown).

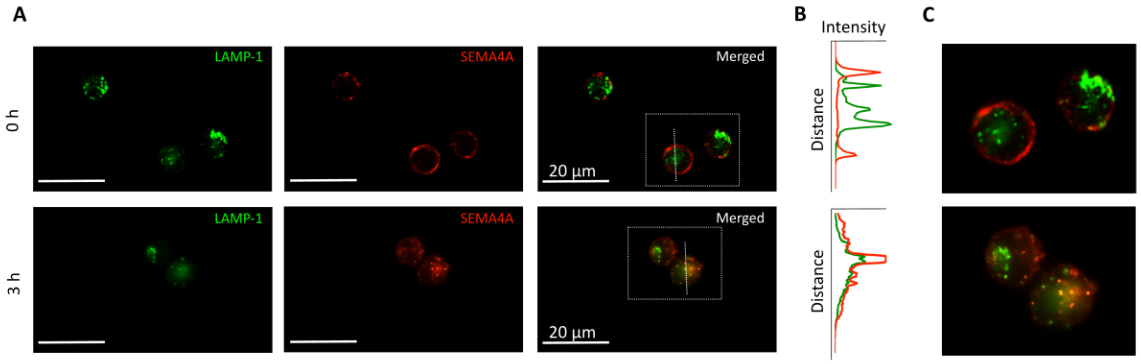

Fig. 5.10 *mAb-5E3 (anti-SEMA4A) is internalised and co-localises with LAMP-1-positive lysosomes.* **A** NCI-H929 cells were incubated for 20 minutes at 4°C with mAb-5E3 before unbound antibody was washed and cells incubated at 37°C for three hours. All primary antibody was labelled using a fluorescent-labelled secondary antibody (red) under permeabilising conditions. LAMP-1 positive lysosomes are green. **B** The image intensity profiles for the dotted line shown in **A**. **C** Enhanced image of the boxed area in **A**. Representative figures are shown for n=3.

5.2.3 mAb-5E3 is effective as an ADC against SEMA4A-expressing cancer cells

Having established that both mAb-770502 (ROBO1) and mAb-5E3 (SEMA4A) were internalised, and in the case of mAb-5E3, trafficked to the lysosome, I next investigated if this internalisation was sufficient to deliver a cytotoxic payload to induce cell death. As the creation of an ADC is both expensive and time-consuming, I used a 'piggyback' system to provide an initial assessment of potential ADC activity. This system utilises a secondary antibody conjugated to a toxin that binds to and is internalised alongside the unconjugated targeting primary antibody. For these experiments, I used an anti-mouse goat antibody chemically linked to saporin, a ribosome inactivating protein that inhibits protein synthesis resulting in cell death. Saporin is cell-membrane impermeable and is therefore only able to induce cell death in cells that successfully internalise the antibody-complex. For both mAb-770502 and mAb-5E3, two target-positive and one target-negative cell lines were tested. Cells were incubated for 72 hours with increasing concentrations of the primary, targeting antibody or an isotype-matched control antibody (mouse IgG1). The secondary antibody concentration remained constant (2.5nM). Cell viability at 72 hours was assessed using a XTT assay, a colourimetric assay in which the tetrazolium derivative (XTT) is reduced by metabolically active cells [331].

Incubation with mAb-770-502 and the secondary antibody did not appear to induce cell death across the three cell lines tested (fig 5.11B). Although there was a reported significant difference in cell viability between mAb-770502 and the isotype control at 1nM for the cell line SK-MM-1 (87.5% $\pm$15.5% (SD) versus 120% $\pm$4.14% (SD), p<0.01 using a student's t-test corrected for multiple testing by BH)), cell viability was not significantly different compared with the secondary antibody alone (77.2% $\pm$0.82% (SD), p<0.05) and it was concluded there was no effect of mAb-770502 (fig 5.11).

In contrast, the co-incubation of mAb-5E3 and the secondary antibody showed strong inhibition of cell viability with an EC_{50} in the picomolar range and no effect with the isotype-matched control or secondary antibody alone (fig 5.12B, (n=3)). This loss of cell viability was observed in the target-expressing cell lines only, with an EC_{50} of 6.02pM in NCI-H929 and 6.75pM in MM.1S. Maximal cell death was observed at the highest concentration tested, 0.1nM, with a mean difference in viability between the isotype control and mAb-5E3 of 56.4% and 47.2% for NCI-H929 and MM.1S respectively. For K562, a SEMA4A^{neg} erythroleukemic cell line, there was no difference in cell viability between the isotype control and mAb-5E3 (fig 5.12).

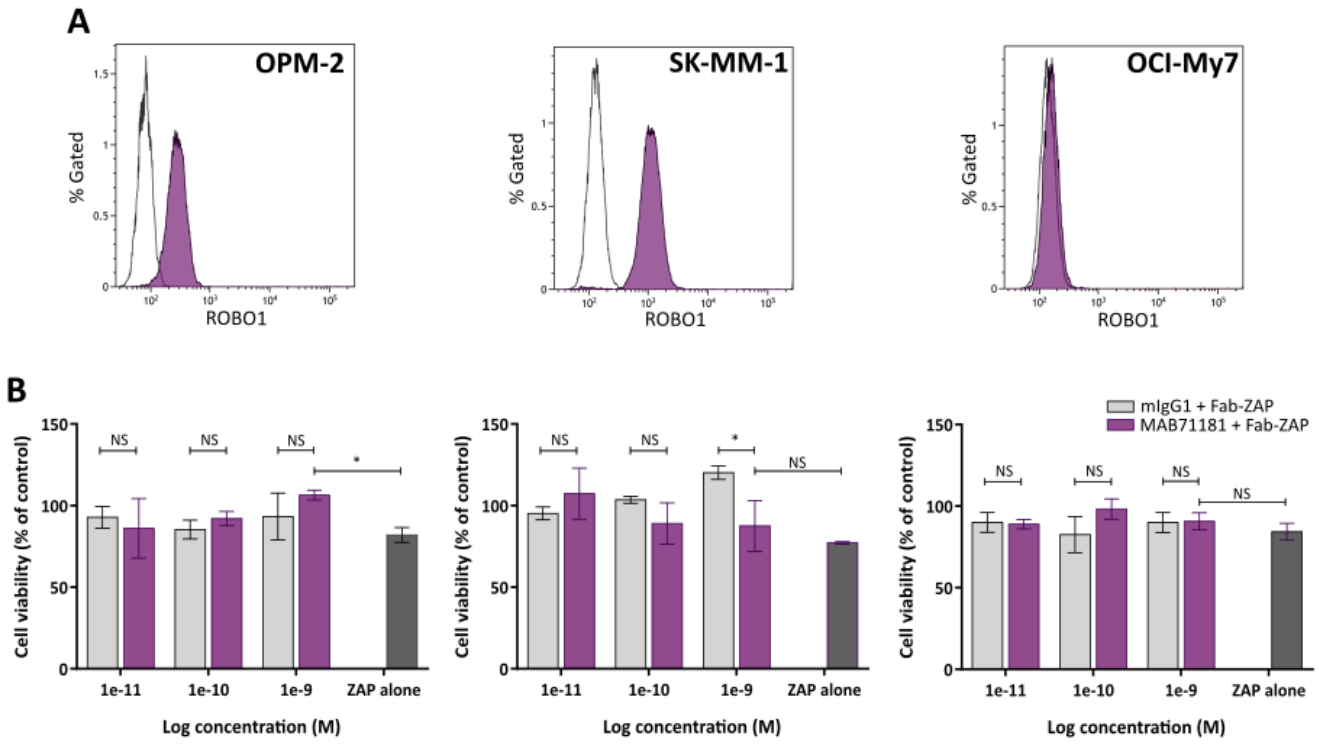

Fig. 5.11 *mAb-770502 (anti-ROBO1) linked to a cytotoxic payload does not trigger cell death.* **A** mAb-770502 binding and ROBO1 expression by flow cytometry in all three cell lines tested. **B** Dose response for mAb-770502 inhibition of cell viability. OPM-2, SK-MM-1 and OCI-My7 were incubated with different concentrations of either mAb-770502 or an isotype-matched control and a saporin-linked secondary antibody (Fab-ZAP, 2.5nM). Cell viability at 72 hours was measured using an XTT assay and calculated as a percentage of a media-only control. n=1, performed in triplicate.

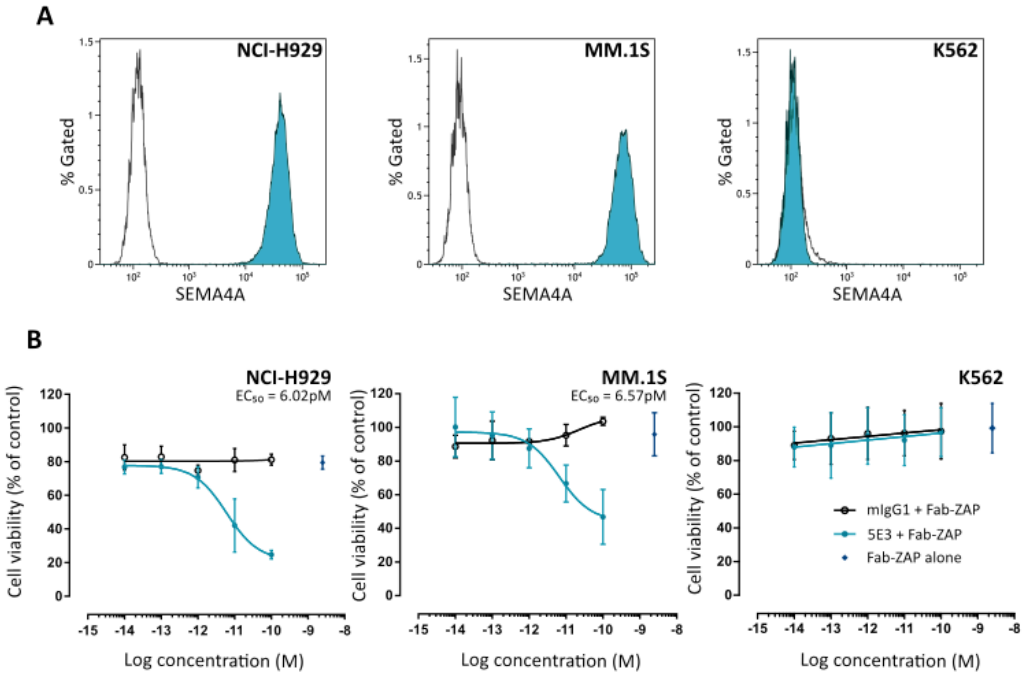

Fig. 5.12 *mAb-5E3 (anti-SEMA4A) linked to a cytotoxic payload induces significant cell killing activity* **A** mAb-5E3 binding and SEMA4A expression by flow cytometry in all three cell lines tested. **B** Dose response for mAb-5E3 inhibition of cell viability. NCI-H929, MM.1S and K562 were incubated with increasing concentrations of either mAb-5E3 or an isotype-matched control and a saporin-linked secondary antibody (Fab-ZAP, 2.5nM). Cell viability at 72 hours was measured using an XTT assay and calculated as a percentage of a media-only control. n=3, each performed in triplicate.

Biotinylated-EPR14696 (NEO1) in combination with a streptavidin-Zap secondary conjugate also failed to demonstrate cell-killing activity across a panel of NEO1-expressing cell lines (personal communication with Dr S Surget).

5.2.4 SEMA4A expression is restricted to immune system organs

Having established that the mAb-5E3 targeting SEMA4A was both rapidly internalised and capable of delivering a toxic payload to target-expressing cells, I decided to further pursue SEMA4A as an ADC target. Aside from high expression and internalisation, another necessary ADC target attribute is low off-tumour expression. Although the whole-cell mass spectrometry dataset used for initial target selection suggested that SEMA4A expression was highly restricted (fig 5.6D), I next sought to obtain additional evidence for off-tumour expression using a second publicly available dataset: The Human Protein Atlas (Tissue Atlas). The Tissue Atlas contains both mRNA and protein expression derived from antibody-

based profiling using immunohistochemistry (IHC) across 44 normal human tissue types (www.proteinatlas.org) [301].

Across the 44 tissues profiled by IHC, SEMA4A expression was only detectable in the lymph nodes and tonsils (fig 5.13). Analysis of the cell types within these tissues revealed medium expression in non-germinal centre and low expression in GC cells. Although SEMA4A was predicted to be expressed at a low level in adrenal gland and prostate by the whole-cell mass spectrometry dataset, there was no detectable expression in these two tissues by IHC.

One tissue that was not curated in either of the two dataset was the retina. SEMA4A mutations in RPE cells have been reported to cause retinitis pigmentosa and cone rode dystrophy through defective endosomal sorting [332]. To investigate SEMA4A expression on RPE cells, I analysed cell surface expression on RPE-1 cells, an immortalised RPE cell line, by flow cytometry. As seen in figure 5.14A, there was no detectable SEMA4A expression on RPE-1 cells (MFI ratio of 0.96). The addition of hydrogen peroxide, which is reported to affect SEMA4A peripheral distribution [333], increased slightly the MFI ratio to 1.01 with 125µM H_2O_2 and 1.09 at 250µM H_2O_2 but was still considered to be negligible expression.

I next confirmed that RPE-1 cells would be unaffected by a SEMA4A ADC. RPE-1 cells were cultured with increasing concentrations of mAb-5E3 and the saporin-linked secondary antibody and cell viability assessed at 72h by XTT. mAb-5E3 did not exhibit cell killing activity in RPE-1 cells, with no difference in viability between mAb-5E3 and the isotype-matched control (99.0% $\pm$ 8.55% (SD) and 101.0% $\pm$ 10.55% (SD) respectively at 0.1nM). The addition of hydrogen peroxide (250µM) also did not affect cell viability, 94.5% $\pm$ 3.28% (SD) for mAb-5E3 and 86.7% $\pm$ 2.28% (SD) for the isotype-matched control at 0.1nM (figure 5.14B). NCI-H929 was included as a positive control, with 10.6% $\pm$ 3.07% for mAb-5E3 at 0.1nM compared to 98.52% $\pm$ 10.77% (SD) for the isotype-matched control (fig 5.14C). Overall, this confirmed that SEMA4A expression in RPE cells would not be a concern in developing SEMA4A as as ADC target.

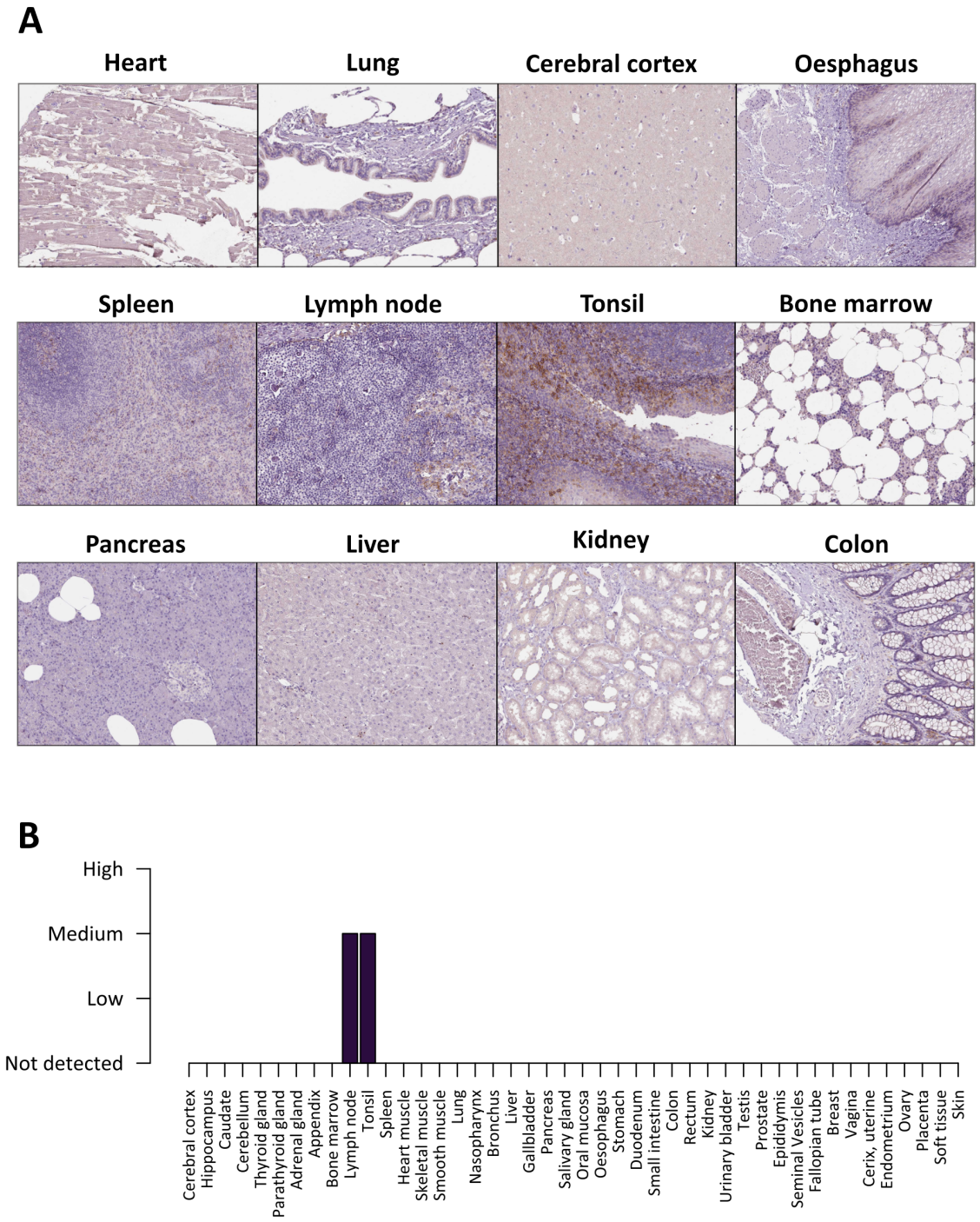

Fig. 5.13 *SEMA4A expression is restricted to immune system organs by IHC* To investigate SEMA4A off-tumour expression, immunohistochemistry data from The Human Protein Atlas [301] was analysed. **A** Representative IHC samples from several normal human tissues **B** Summary of SEMA4A expression across the 44 normal human tissues analysed based on expert-curated annotations of the IHC samples.

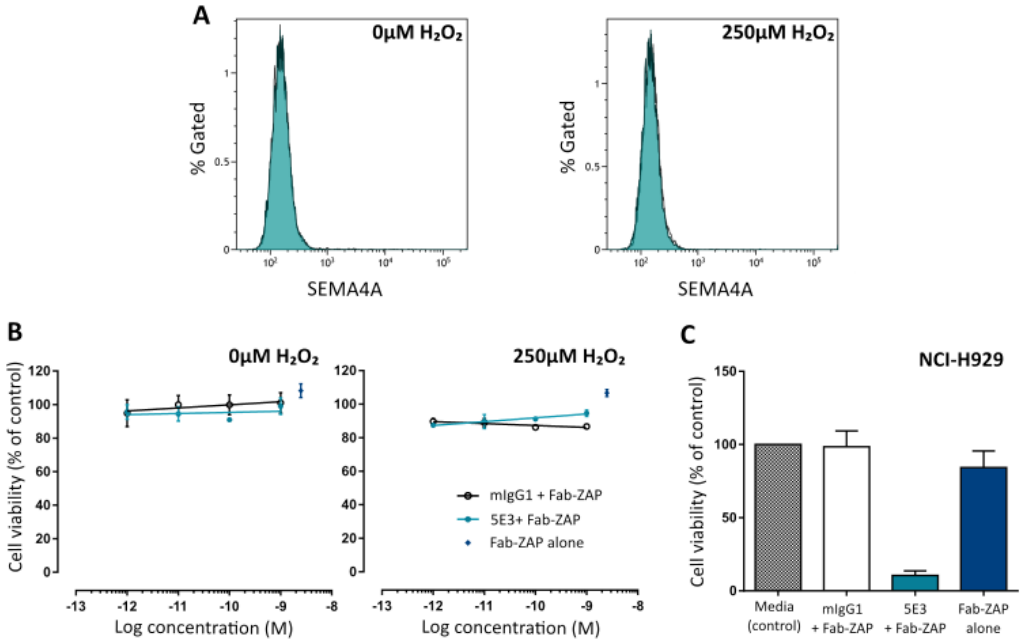

Fig. 5.14 *SEMA4A expression on RPE-1 cells is negligble and insufficient to deliver a cytotoxic payload* **A** SEMA4A expression on RPE-1 in the presence and absence of hydrogen peroxide was analysed by flow cytometry. **B** Dose response for mAb-5E3 inhibition of cell viability. RPE-1 cells were cultured for 72 hours with increasing concentrations of the primary targeting antibody mAb-5E3 or an isotype-matched control and a secondary antibody conjugated to saporin (Fab-ZAP, 2.5nM). **C** As a positive control, NCI-H929 was also cultured for 72 hours with 0.1nM mAb-5E3 or isotype-matched control and 2.5nM Fab-ZAP. Viability was measured by XTT and calculated as a percentage of a media-only control. n=1, performed in triplicate.

5.2.5 Establishment of an ADC mouse model

Our next aim was to investigate the ability of mAb-5E3 to deliver the cytotoxic payload and to eliminate HMCLs *in vivo* in a murine model of myeloma. As the kit used for the initial testing of mAb-5E3 as an ADC (Fab-ZAP) was unsuitable for *in vivo*, I first needed to assess the ability of an alternative kit (Strep-ZAP) to deliver the payload. Instead of a secondary antibody, this kit utilises streptavidin chemically conjugated to saporin which binds to a biotinylated antibody. To biotinylate mAb-5E3 I used two different kits (Abcam), generating (B)-5E3-A and (B)-5E3-B. To confirm biotinylation and to compare binding with the non-biotinylated antibody, MM.1S (SEMA4A^{hi}) and OPM-2 (SEMA4A^{low}) were labelled using all three antibodies and either a fluorescent-labelled secondary antibody or streptavidin-APC. By flow cytometry, both (B)-5E3-A and (B)-5E3-B showed comparable levels of biotinylation (MFI ratio of 23.2 and 17.1 for A and B respectively). Neither of the two biotinylated antibodies exhibited non-specific binding, with no detectable binding to OPM-2 (MFI ratio of 0.95 and 1.03 for A and B). Although they cant be directly compared because of the two different secondaries used for analysis, both biotinylated antibodies did appear to exhibit less binding compared with the non-biotinylated mAb-5E3 (fig 5.15A).

To assess cell killing activity, MM.1S and OPM-2 were cultured with increasing concentrations of (B)-5E3-A/B or the unconjugated mAb-5E3 (negative control) and the streptavidin-ZAP at a 1:4 ratio. Cell viability was measured by XTT at 72 hours. Compared to the non-biotinylated antibody, both (B)-5E3-A and B exhibited cell killing activity with an EC_{50} of 36.6pM and 22.5pM for A and B respectively (fig 5.15B). Maximal cell death was observed at 1nM, with a mean difference in viability between non-biotinylated and biotinylated of 55% and 42.7% for A and B. There appeared to be no significant cell death observed in OPM-2 even at the highest concentration (93.5% ($\pm$19.56%), 98.4% ($\pm$10.38%) and 106.5% ($\pm$ 8.41%) cell viability for A, B and non-biotinylated respectively).

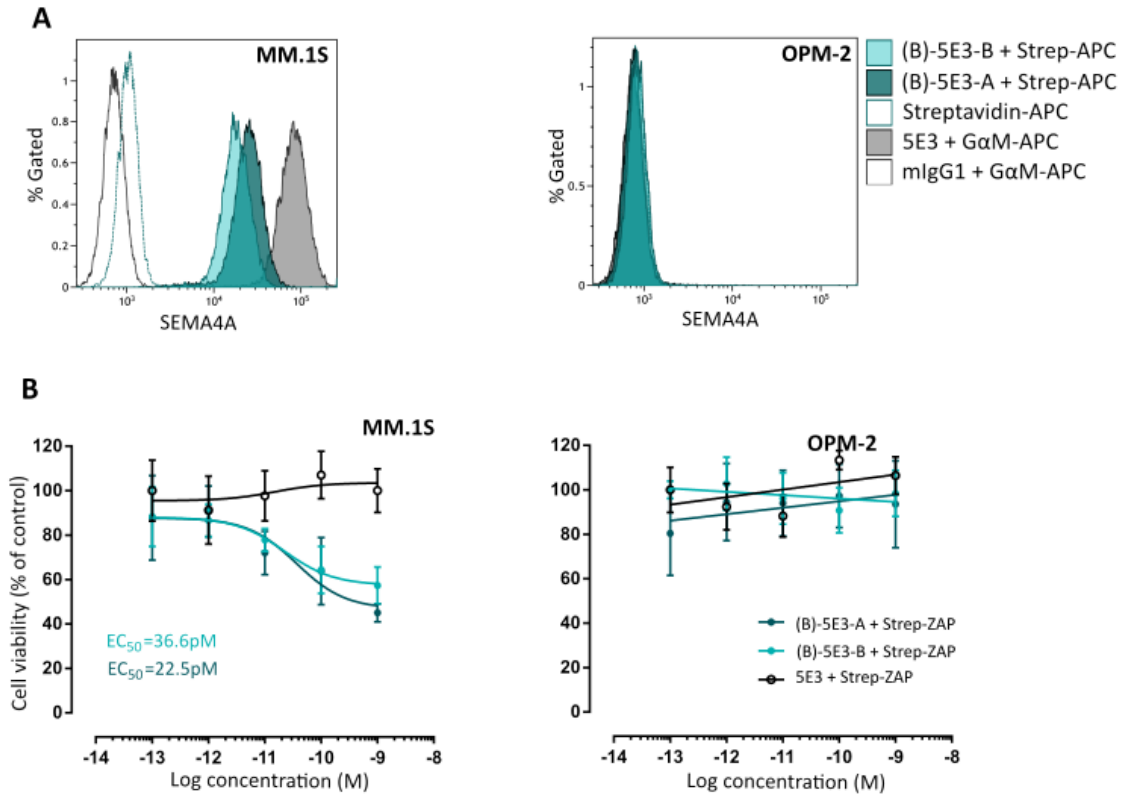

Fig. 5.15 *Biotinylated mAb-5E3 is able to specifically deliver a cytotoxic payload to a target-expressing HMCL.* **A** Flow cytometric analysis of mAb-5E3 binding following biotinylation with fluorescent-labelled streptavidin compared with non-biotinylated mAb-5E3 and a fluorescent-labelled secondary antibody (GαM) **B** Dose response for mAb-5E3 inhibition of cell viability. MM.1S and OPM-2 were incubated for 72 hours with increasing concentrations of the two biotinylated mAb-5E3 ((B)-5E3-A or (B)-5E3-A) or the non-biotinylated mAb. Streptavidin-ZAP was added at all concentrations at a ratio of 1:4 (primary antibody:Strep-ZAP). Cell viability was measured at 72 hours by XTT and calculated as a percentage of a media-only control. n=1, performed in triplicate.

Co-incubation with either mab-5E3 with Fab-ZAP or (B)-5E3-A/B with Strep-ZAP elicited similar maximal killing activity ($\approx$ 45-55% loss of viability). However, using the *in vivo* kit (Strep-ZAP) resulted in a five-fold higher EC_{50} compared with the Fab-ZAP kit. After taking this into consideration and in conjunction with the fact that I was unable to achieve > 56% killing activity using either kit, I decided to proceed with a direct conjugation between two different toxins and mAb-5E3. Two custom ADCs were produced by Abzena Ltd[1]. The first custom conjugate utilised a malemide-based linker (cysteine linked) to conjugate mAb-5E3 to the auristatin MMAE (monomethyl auristatin E, 5E3-MMAE). The second used an NHS-ester based linker (lysine linked) to conjugate mAb-5E3 to the maytansinoid DM1 (mertansine, 5E3-DM1). Unlike saporin, both DM1 and MMAE are routinely used clinically and as such, these direct conjugates are more likely to provide us with a more accurate representation of a lead ADC candidate. The following work is current, on-going work at the time of writing and performed in collaboration with Dr J Ballester Beltran and Dr G Giotopoulos[2].

To establish the xenograft model, male SCID mice were sub-lethally irradiated and injected (i.v.) with two human myeloma cell lines, NCI-H929 and MM.1S. These two cell lines were lentivirally transduced to stably express luciferase using the dual luciferase/GFP vector (BLIV301PA-1-MSCV-GFP-T2A-Luciferase (MAC25)). As these two cell lines have both been used in the literature, our aim was to establish which cell line provided the most representative model and to investigate the disease latency to establish a suitable imaging and dosing schedule. $0.5x10^6$ NCI-H929-MAC25 and MM.1S-MAC25 cells were injected i.v. in male SCID mice and disease monitored using bioluminescence imaging. At day 10 there was no detectable luciferase activity for either cell line (fig 5.16A, no image taken for NCI-H929-MAC25). By day 25, mice injected with MM.1S-MAC25 showed clear engraftment that was localised to the bone. NCI-H929-MAC25 did not engraft and even by day 42, there was no discernable bioluminescence activity. A second experiment investigated a larger starting dose of both MM.1S-MAC25 and NCI-H929-MAC25 (1 and $2.5x10^6$ starting cells), fig 5.16B. Even at the higher concentrations there was minimal engraftment for NCI-H929-MAC25 and only one mouse ($2.5x10^6$ cells) exhibited discernable signal localised to the bone at day 21. By day 12 there was detectable signal for both doses for MM.1S-MAC25. Although there was a strong bioluminescent signal for the higher starting number of cells, both doses showed similar disease latency. As a result, it was concluded to proceed with only MM.1S-MAC25 at $1x10^6$ cells.

[1]Babraham Research Campus, Cambidge, UK
[2]Brian Huntly group, Department of Haematology, University of Cambridge

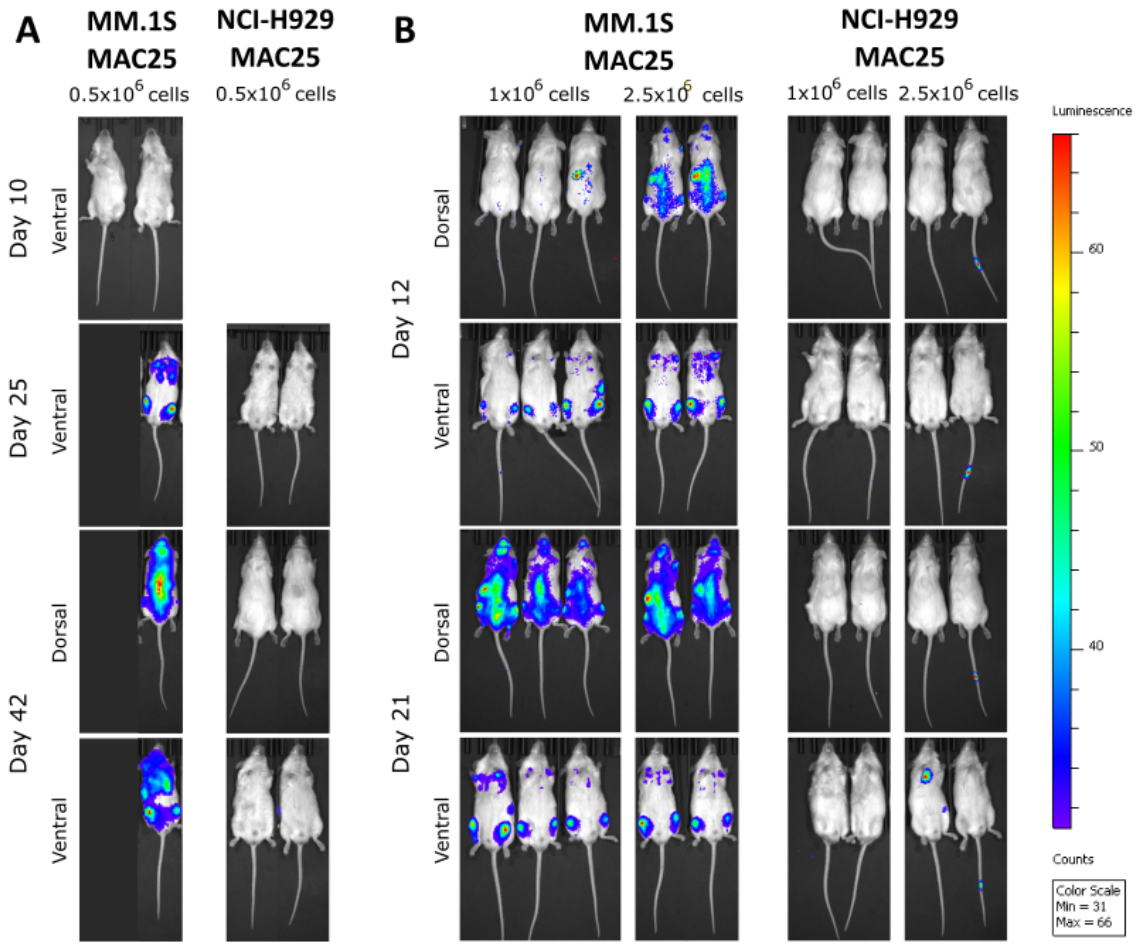

Fig. 5.16 *Establishment of an orthometastatic xenograft model.* **A** 0.5x10^6 or **B** 1 and 2.5x10^6 MM.1S-MAC25 or NCI-H929-MAC25 were injected i.v. into male SCID mice and disease establishment monitored by bioluminescence imaging.

Having established MM.1S as the cell line that will be used for the xenograft model, I next investigated the cell killing activity of the two direct conjugates on it. Both conjugates exhibited similar binding profiles to the unconjugated mAb-5E3 by flow cytometry (fig 5.17A), confirming that the addition of the toxin did not impair antigen-antibody binding. Next MM.1S-MAC25 cells were incubated with increasing concentrations of either 5E3-DM1 or 5E3-MMAE and cell viability measured by XTT at 72 hours. Both 5E3-DM1 and 5E3-MMAE induced extensive cell death, with a loss in cell viability from 0.01pM to 10nM of 86.63% and 96.6% for DM1 and MMAE respectively. 5E3-MMAE (EC_{50} of 44.7pM) appeared to be more potent compared to DM1 (100pM EC_{50}) (fig 5.17B).

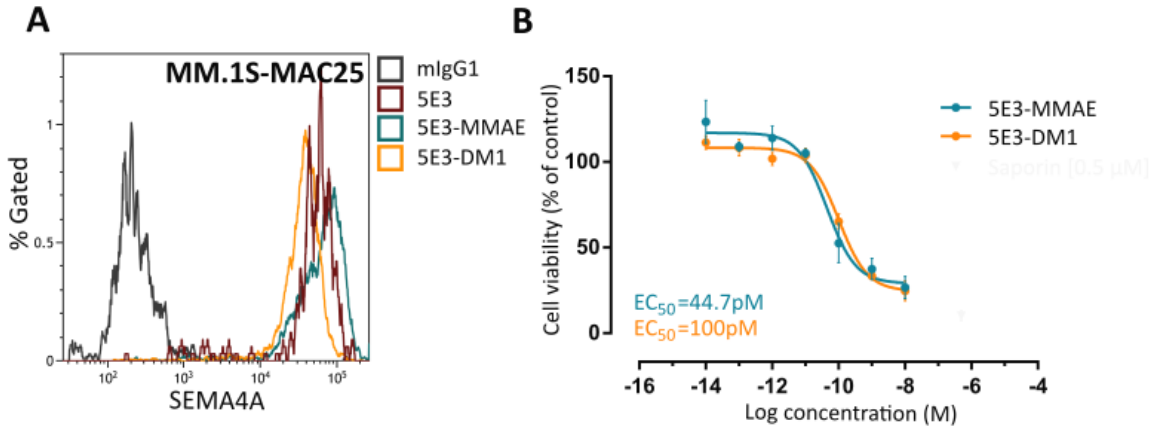

Fig. 5.17 *5E3-MMAE ADC is more potent than 5E3-DM1.* **A** Flow cytometric analysis of antibody binding of 5E3-DM1 and 5E3-MMAE compared with the unconjugated mAb-5E3 using a fluorescent-labelled secondary antibody. **B** Dose response for 5E3-ADC inhibition of cell viability. MM.1S-MAC25 were incubated with increasing concentrations of two ADCs (5E3-DM1 and 5E3-MMAE) to compare the two different conjugates. Cell viability was measured at 72 hours by XTT and calculated as a percentage of a media-only control. n=1, performed in triplicate.

I next tested these two ADCs on a panel of human myeloma cell lines, as well as on the SEMA4A^{neg} cell lines, K562 and RPE-1 cells (fig 5.18). Across the highest SEMA4A-expressing cell lines, 5E3-MMAE demonstrated substantial cell killing activity with an EC_{50} range of 53.7pM to 1.5nM. 5E3-DM1 appeared to be less potent, with an EC_{50} range of 129.9pM to 17.8µM. Unexpectedly, OCI-My7 appeared to be unaffected by the MMAE-conjugate, despite a higher SEMA4A expression compared with KMS-12-BM. As this cell line was still sensitive to the DM1 conjugate, this cell line is possibly less sensitive to the MMAE toxin. Amongst the lower SEMA4A-expressing cell lines and the two SEMA4A negative cell lines I did not observe any effect of 5E3-MMAE or 5E3-DM1. Although more

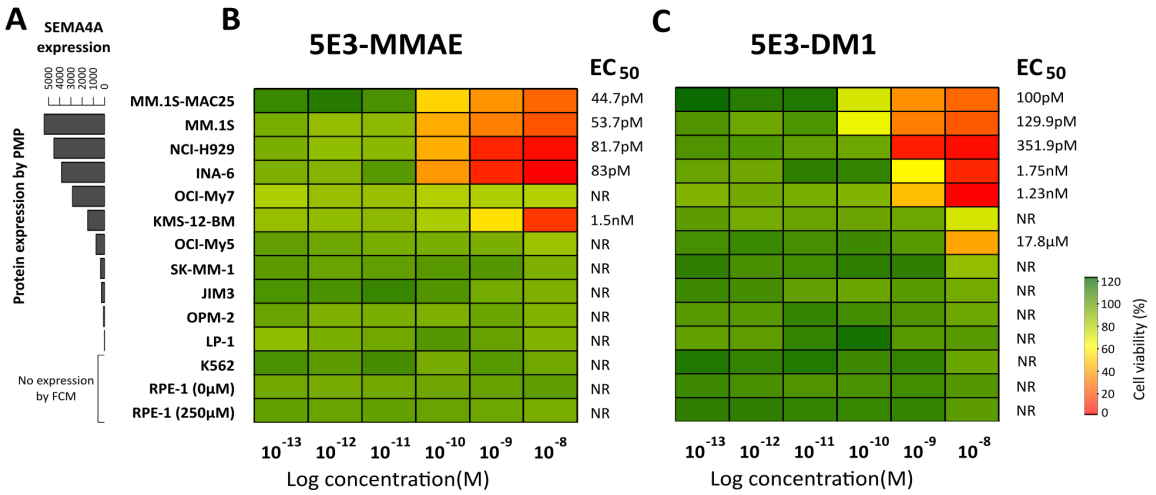

Fig. 5.18 *Comparison of 5E3-MMAE and 5E3-DM1 potency across a panel of cell lines.* **A** SEMA4A expression by mass spectrometry for those HMCLs profiled by PMP. **B** Dose response for 5E3-MMAE in HMCLs, K562 and RPE-1 (with and without H_2O_2) after a 72 hour incubation. **C** Dose response for 5E3-DM1. Cell viability was measured by XTT and calculated as a percentage of a media-only control. n=1, performed in triplicate. NR=EC_{50} not reached. FCM=Flow cytometry.

cell lines appeared to be sensitive to the DM1 toxin, the MMAE conjugate appeared to demonstrate an enhanced potency in the SEMA4A^{hi} cell lines and so I decided to proceed with this conjugate.

5.2.6 5E3-MMAE significantly delays myeloma growth in an orthometastatic xenograft model

I next sought to establish the efficacy of 5E3-MMAE *in vivo*. Male NSG mice were sub-lethally irradiated and injected (i.v) with MM.1S-MAC25 and disease establishment confirmed by bioluminescence imaging. Mice received a total of four doses at 4mg/kg of either the naked antibody (5E3), 5E3-MMAE or an isotype control (mIgG1-MMAE), administered biweekly for two weeks (fig 5.19A). Disease activity was monitored by weekly bioluminescence imaging. For 5E3-MMAE there was an initial near-complete elimination of bioluminescence activity (fig 5.19B and C). However, following cessation of treatment these mice relapsed (week 3) and all eventually succumbed to disease. Meanwhile, there was no effect on tumour growth for either 5E3 alone or the isotype control. Overall, 5E3-MMAE significantly improved survival compared with the two control groups (p=0.0004), demonstrating the potent activity of 5E3-MMAE *in vivo* (fig 5.19D).

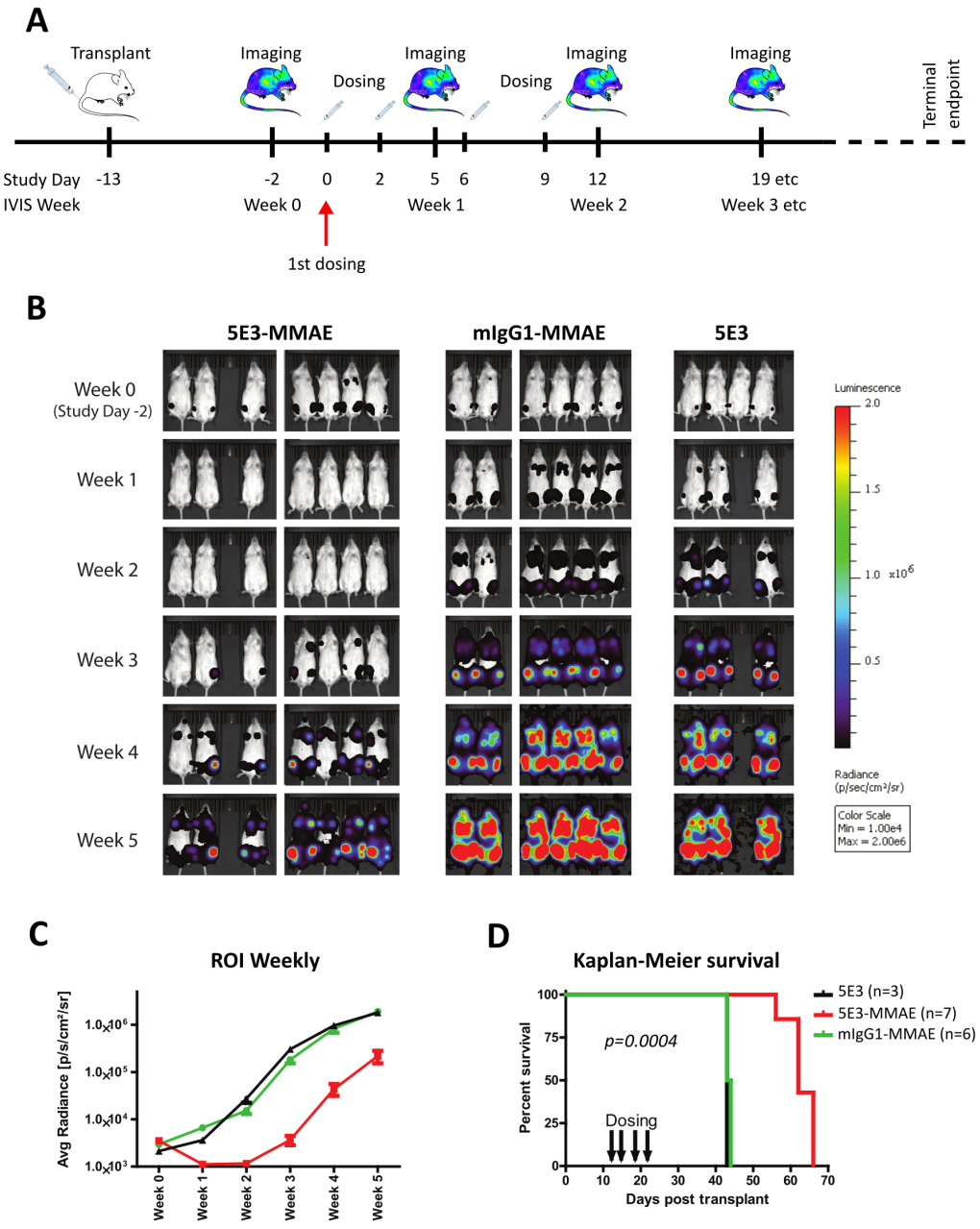

Fig. 5.19 *5E3-MMAE anti-myeloma activity in a myeloma orthometastatic xenograft model.* **A** Study treatment outline. 1x10^6 MM1S-MAC25 were injected i.v into sub-lethally irradiated male NSG mice and disease establishment confirmed by bioluminescence imaging. Each animal then received a total of four doses (i.v., at 4mg/kg for each dose) of either 5E3, 5E3-MMAE or mIgG1-MMAE (on day 13, 15, 19 and 22 post transplantation, termed 'Study day' 0, 2, 6 and 9 respectively). Disease was monitored by weekly bioluminescence imaging. **B** Bioluminescence imaging of the NSG xenografts showing the initial reduction in tumour burden in the 5E3-MMAE treated mice compared with the mIgG1-MMAE and 5E3 alone groups. **C** The average radiance of each mouse (region of interest (ROI)) for each treatment group at each weekly imaging session. **D** Kaplan-Meier survival curves of NSG xenografts in response to treatment. Graphs are shown as mean ± SEM.

5.2.7 SEMA4A may play an essential role in myeloma cell biology

As discussed in the introduction, one of the potential mechanisms for resistance towards targeted therapeutics is downregulation of the target. The role of SEMA4A as a ligand has been extensively characterised. It's role as a receptor, however, has been largely unexplored. Recently, Sun *et al* reported that SEMA4A does exhibit signalling functionality and is involved in regulating cell migration [327]. Our next aim was to investigate the functional role of SEMA4A in myeloma cell biology and to determine if loss of this protein would provide a viable mechanism for tumour escape.

To initially investigate the role of SEMA4A, I performed a stable RNA-mediated knock-down of SEMA4A in the myeloma cell line, NCI-H929. NCI-H929 were lentivirally transduced with one of three SEMA4A-targeting hairpins (shSEMA4A-136, shSEMA4A-636 and shSEMA4A-567) or with a luciferase-targeting hairpin (shLUC, non-targeting control). Interestingly, despite the maintenance of antibiotic selection, I observed the emergence of a small population of SEMA4A^{pos} cells for all three hairpins (10.05%, 9.68% and 21.42% for shSEMA4A-136, shSEMA4A-636 and shSEMA4A-567 respectively at day 80, fig 5.20A). The emergence of this SEMA4A^{pos} population, despite an antibiotic selection pressure, suggested that loss of SEMA4A may be detrimental to cell viability. To further investigate, I performed a RNAi competition assay in which SEMA4A was knocked-down in $\approx$ 50% of the cell population and the proportion of remaining GFP+ cells analysed over time. The two hairpins which provided the greatest knock-down (98% and 96% loss in MFI compared to shLUC for shSEMA4A-636 and shSEMA4A-567 respectively) were cloned into pLKO.1_GFP. The puromycin resistance gene in this vector has been replaced with a GFP reporter to monitor hairpin expression by flow cytometry.

For both NCI-H929 and MM.1S there was an observed rapid decrease in the proportion of GFP$^+$ cells over time, with a decrease from 1.0 at day 4 to 0.29 ($\pm$0.034) and 0.16 ($\pm$0.007) at day 16 for shSEMA4A-636 and -567 in NCI-H929 and to 0.082 ($\pm$ 0.004) and 0.104 ($\pm$0.05) for MM.1S at day 16 (fig 5.20C). There was minimal to no loss in the proportion of GFP$^+$ cells in the SEMA4A^{neg} cell line K562, 0.710 ($\pm$ 0.021) and 0.939 ($\pm$ 0.053) for shSEMA4A-636 or -567 respectively at day 16 compared to day 4. For both NCI-H929 and K562 there was no effect of the non-targeting control (1.17 $\pm$ 0.049 and 1.071 $\pm$ 0.017 for NCI-H929 and K562 respectively), whilst there was a modest loss of GFP$^+$ cells in MM.1S (0.716 $\pm$ 0.045) (fig 5.20C, n=3).

Overall these results suggested that loss of SEMA4A conferred a competitive disadvantage and that SEMA4A may play an essential role within myeloma cell biology. This loss of fitness appeared to be at least partly mediated through loss of viability, with an increased proportion of dead cells amongst the GFP^{+} population for both NCI-H929 and MM.1S compared to the shLUC control as determined by flow cytometry (fig 5.21, n=1).

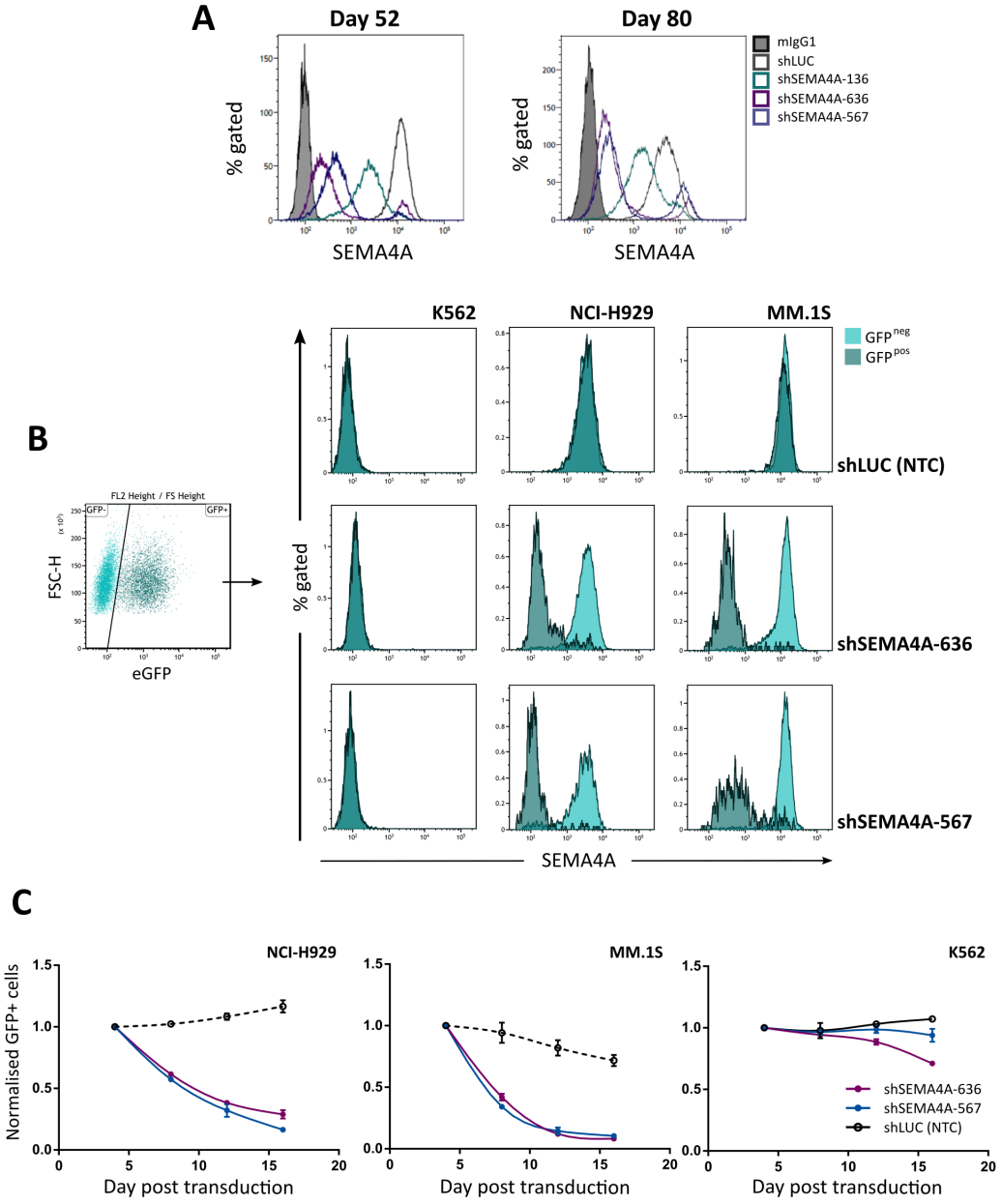

Fig. 5.20 *RNAi mediated knockdown of SEMA4A in HMCLs is associated with a competitive disadvantage.* **A** SEMA4A expression by flow cytometry at 52 and 80 days post viral transduction for the four hairpins in antibiotic selection. **B** RNAi mediated knockdown competition assay. NCI-H929, MM.1S and K562 were lentivirally transduced with two SEMA4A hairpins or a control shRNA targeting luciferase. Representative histograms showing SEMA4A expression by flow cytometry at day 8 in both the GFP^+ and GFP^- populations. **C** The proportion of GFP^+ cells was monitored over time by flow cytometry and compared to the proportion of GFP^+ cells present at day 4 post transduction (mean $\pm$ SD, n=3).

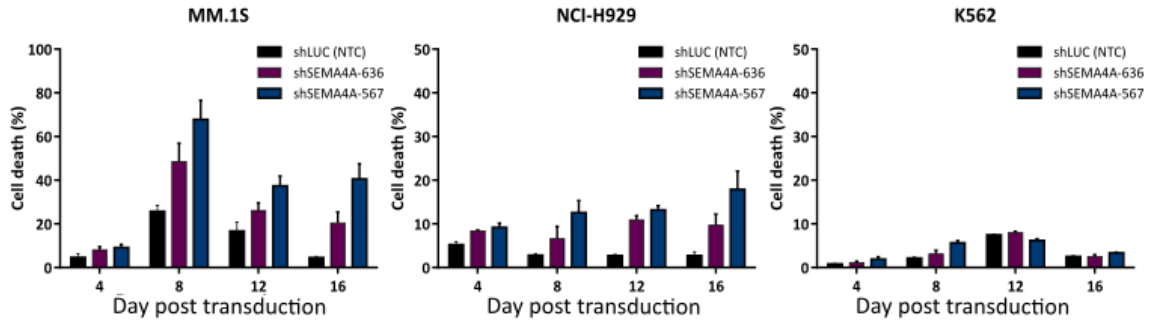

Fig. 5.21 *RNAi mediated knockdown of SEMA4A in HMCLs is associated with a decrease in cell viability* RNAi mediated knockdown competition assay. NCI-H929, MM.1S and K562 were lentivirally transduced with two SEMA4A hairpins or a control shRNA targeting luciferase. GFP^+ cell viability was analysed by flow cytometry using 7-AAD to discriminate between live and dead cells over the timecourse of the competition assay.

5.2.8 Rescue of SEMA4A expression does not restore cell fitness

I next investigated whether re-expression of SEMA4A could restore cell fitness in SEMA4A shRNA-expressing cells. I generated two bi-cistronic vectors, expressing either the wild-type (WT) (pLenti6.2_hSEMA4A(wt)) or truncated SEMA4A (pLenti6.2_hSEMA4AΔC) and a fluorescent reporter (blue fluorescent protein (BFP)) separated by a small T2A peptide sequence. This truncated mutant lacks the intracellular domain, which has been shown by Sun *et al* to be required for signal transduction [327]. These two constructs were designed to investigate whether a) over-expression of the wild-type SEMA4A was sufficient to reverse the observed phenotype and therefore that the shRNA effect was target-specific and b) whether SEMA4A was acting as a receptor with intracellular domain-mediated signalling in myeloma cells.

NCI-H929 and MM.1S were stably transduced with either the WT or mutant (SEMA4AΔC) over-expression vectors or the empty parental vector (pLenti6.2/V5) before transduction with a SEMA4A- or luciferase-shRNA vector. The SEMA4A shRNA used for this experiment was shSEMA4A-636, which targets the three prime untranslated region (3'-UTR) and therefore does not target the exogenous SEMA4A. As with the competition assay described above, the proportion of GFP+ cells was monitored by flow cytometry over time. As seen in figure 5.22A, both constructs restored SEMA4A expression at the cell surface following knock-down. Although both constructs were expressed at a high level in both cell lines, SEMA4A expression was only completely restored to the endogenous levels in NCI-H929. The MFI ratio of endogenous SEMA4A in pLenti6.2/V5 expressing GFP^- NCI-H929 cells

was 86.6 ± 1.1 compared to 123.3 ± 10.22 for the mutant-expressing GFP^+ cells and 163.0 ± 16.02 (SD) for WT-expressing GFP^+ cells. For MM.1S both WT (MFI ratio of 190.9 ± 45.96 (SD)) and mutant SEMA4A (80.38 ± 8.95) were expressed at a lower level than endogenous SEMA4A (227.4 ± 7.51) in the cells transduced with the empty parental vector.

I expected rescue of WT SEMA4A expression at the cell surface would prevent the loss of GFP^+ cells. Contrary to this, I did not observe any differences between the three constructs and all of the groups exhibited a competitive disadvantage following hairpin transduction compared to their non-hairpin expressing counterparts (GFP^-) (fig 5.22B, n=2).

To generate the bi-cistronic vector, I used the T2A peptide sequence to mediate 'cleavage' between our SEMA4A construct and the fluorescent reporter. This 'cleavage' is mediated by a ribosomal skip mechanism [334]. One consideration in using this method is that the T2A peptide sequence may be insufficiently 'cleaved', resulting in a SEMA4A-BFP fusion construct that may interfere with signal transduction [334]. Although I had confirmed that T2A was efficiently cleaved in 293T when initially generating the constructs, 2A 'cleavage' is cell-type dependent [335] and I therefore hypothesised that the failure of the rescue of the phenotype may be caused by insufficient T2A cleavage. Analysis of NCI-H929 lysates by Western Blot revealed that a large proportion of the mutant SEMA4A was insufficiently cleaved (fig 5.23). For both cell lines, however, WT SEMA4A appeared to be efficiently cleaved from BFP.

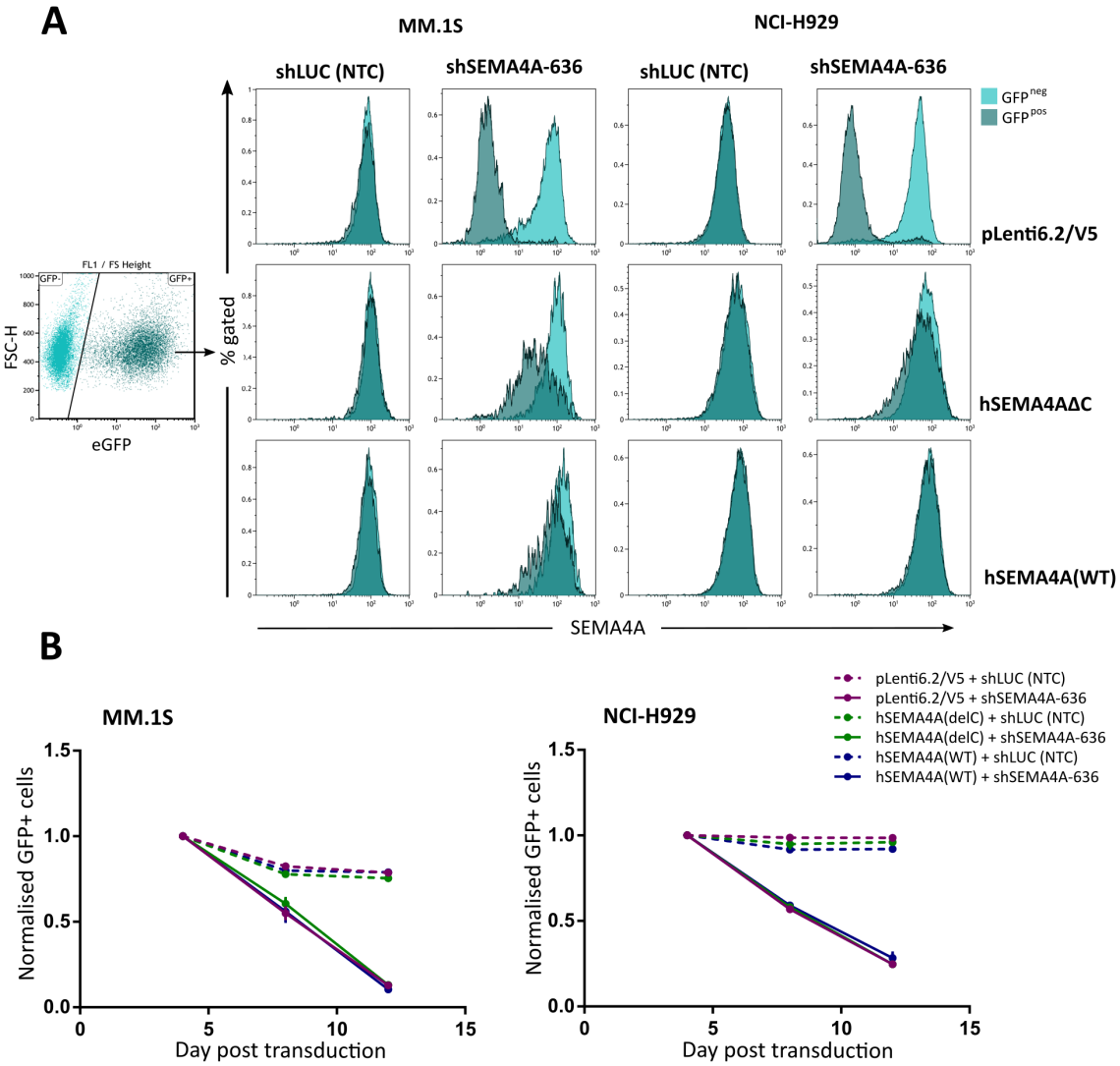

Fig. 5.22 *Rescue of SEMA4A expression does not revert competitive disadvantage following RNA-mediated loss of endogenous SEMA4A* **A** RNAi mediated knock-down competition assay. Empty vector (pLenti6.2/V5), SEMA4A WT or mutant (ΔC) transduced NCI-H929 and MM.1S were lentivirally transduced with shSEMA4A-636 or a control shRNA targeting luciferase. Representative histograms showing SEMA4A expression by flow cytometry at day 8 in both the GFP^+ and GFP^- populations. **B** The proportion of GFP^+ cells was monitored over time by flow cytometry and compared to the proportion of GFP^+ cells present at day 4 post transduction (mean ± SD, n=3).

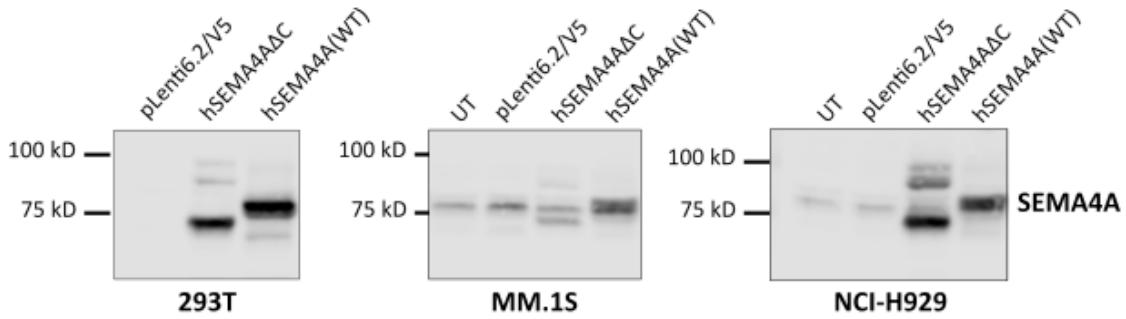

Fig. 5.23 *WT and mutant SEMA4A expression by Western Blot.* Expression of the three constructs (pLenti6.2/V5, hSEMA4AΔC and hSEMA4A(WT)) was analysed by Western Blot to assess the efficiency of the T2A cleavage.

Another hypothesis for the failure of the rescue experiment was that the prolonged over-expression of the rescue constructs prior to knockdown had a detrimental effect on cell growth. As a result, the cells may have down-regulated the expression of downstream signalling molecules, preventing the reversal of the competitive disadvantage. I therefore next investigated whether the simultaneous expression of the rescue constructs and the SEMA4A-targeting hairpins could prevent the loss of cell fitness observed previously (section 5.2.7). MM.1S were stably transduced with one of two doxycyline-inducible hairpin constructs (pLKO.1_TET _shLUC or pLKO.1_TET _shSEMA4A-636). Following antibiotic selection, cells were lentivirally transduced with either the WT or mutant (SEMA4AΔC) over-expression vectors or the empty parental vector (pLenti6.2/V5). Hairpin expression was subsequently induced by the addition of doxycyline (1μg/ml) to the cell culture media and the total cell counts were measured at days 7 and 14 by flow cytometry.

As seen in figure 5.24A both of the over-expression constructs restored SEMA4A expression at the cell surface following knockdown of endogenous SEMA4A (shSEMA4A-636 +Dox). Although expression of the mutant construct was similar to endogenous SEMA4A (MFI ratio of 169.3 for MM1S_shSEMA4A-636 + hSEMA4AΔC versus 193.6 for MM1S_shLUC + pLenti6.2/V5), expression of the WT SEMA4A was much greater (MFI ratio of 646.8 for MM1S_shSEMA4A-636 + hSEMA4A(WT)). Despite rescue of cell surface expression, neither WT nor mutant SEMA4A could restore cell fitness. Instead, both constructs appeared to be highly cytotoxic, with a clear detrimental effect on cell growth that was independent of endogenous SEMA4A knockdown (fig 5.24B and C). As a result, I was unable to conclude that the observed hairpin effects were target-specific and as such the essentiality of SEMA4A remains unclear.

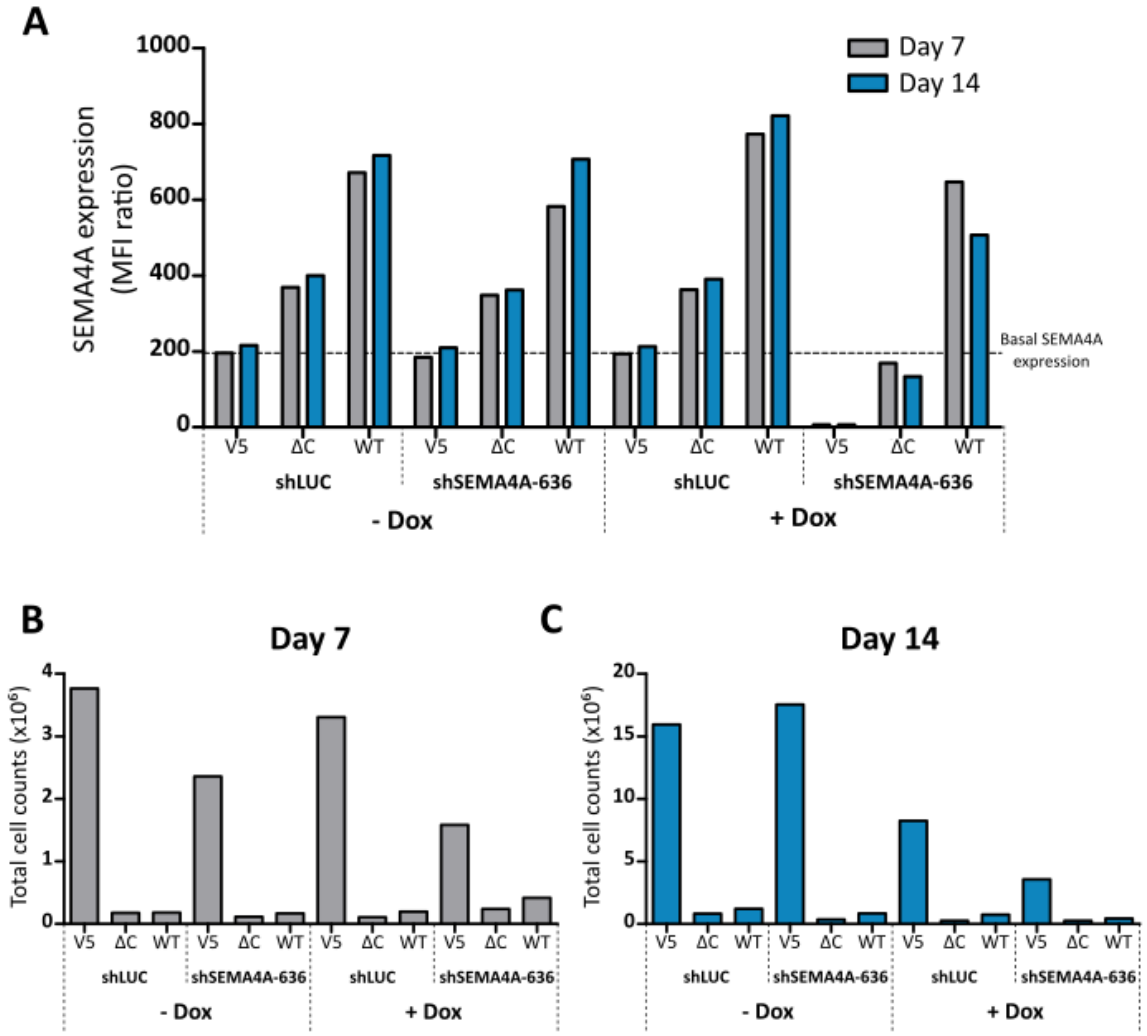

Fig. 5.24 *Expression of exogenous SEMA4A is highly detrimental to cell growth.*
A pLKO.1_TET _shLUC or shSEMA4A-636 expressing MM.1S cells were lentivirally transduced with either an empty vector (V5), WT SEMA4A (WT) or mutant SEMA4A (ΔC). 24 hours later, hairpin expression was induced with the addition of 1μg/ml doxycycline to the cell culture media (+Dox). SEMA4A expression at days 7 and 14 was measured by flow cytometry and expressed as the MFI ratio over the isotype control. **B** The total number of cells in culture was determined by flow cytometry using fluorescent microbeads at day 7 **C** and day 14. n=1.

5.3 Chapter conclusions

Having identified a list of 16 potential monoclonal antibody targets, the aim of this chapter was to further characterise these targets in order to identify a lead candidate. With an interest in generating an ADC, I focussed on identifying a therapeutic target that was both highly expressed on malignant plasma cells relative to other normal tissue and also rapidly internalised to deliver a cytotoxic payload. From these investigations I identified SEMA4A as a promising novel ADC target for the treatment of multiple myeloma.

5.3.1 Identification of a lead candidate

Multiple myeloma is a highly heterogenous disease, both at the inter-patient level but also within the tumour, with numerous subclones present at all stages of disease [21]. Although I had identified a number of potential targets by PMP, the number of samples profiled was relatively small (n=8). The first aim of this chapter was to therefore characterise target expression in a larger cohort of myeloma patients and to compare expression between malignant plasma cells and other normal hematopoietic cells. This would enable us to not only determine if the target is most highly expressed by plasma cells amongst all normal tissue but also if any of the target antigens were restricted to a particular subclone.

The characterisation of some targets was hampered by the lack of commercially available FCM antibodies, such as was the case for BTN2A1, EPHB2, LRRC8C, LRRC8D and PTRPG for which there were no flow cytometry antibodies available. For PLXNA1 and PLXNC1, the three antibodies tested exhibited weak target binding that was likely to be non-specific (fig 5.1A) and so were determined to be unsuitable for target characterisation. In the case of PLXNC1, it was confirmed that the poor correlation between flow cytometry and PMP was not caused by a change in target expression by analysis of mRNA expression (fig 5.1B). Three targets had suitable antibodies available but were not tested (ADAM17, EVI2B and ROR2). Following patient sample analysis by flow cytometry, CD97 and SEMA4D expression was determined to be similar or greater in normal leukocytes compared to malignant plasma cells in the majority of samples (fig 5.2 and 5.5). One of the critical factors in target selection for an ADC is tumour over-expression relative to other, normal tissue, reducing the likelihood of off-tumour toxicities [336] and any potential 'sink' effects [311]. For these reasons, I did not pursue the two candidates which exhibited high levels of off-tumour expression.

Two of the potential targets (NEO1 and ROBO1) exhibited highly restricted plasma cell expression, with minimal to no expression in other immune cell subsets (fig 5.3 and 5.4).

Although ROBO1 expression in primary samples was low both by PMP and flow cytometry, because of the clean target expression profile amongst leukocyte subsets by flow cytometry and other normal tissue by mass spectrometry I further pursued this antigen as a potential therapeutic target. Both ROBO1 and NEO1 appeared to be internalised by flow cytometry, another critical factor for the development of an ADC, but did not induce cell death when linked to a cytotoxic compound (fig 5.11). This may be explained by several reasons. The most likely hypothesis for ROBO1 is that because the antibody used in this study exhibited very weak binding, very few antibody-toxin conjugates were taken up by the cell, which would have resulted in minimal cell death. Alternatively, the target antigen may not have been internalised but was instead lost at the cell surface through other means, such as cleavage. A third hypothesis is that the antigen-antibody complex was internalised but failed to traffic to a suitable intracellular location. Finally, the secondary antibody itself may have dissociated from the primary antibody or inhibited internalisation of the antigen-antibody complex. As ADC internalisation is highly dependent on the properties of a specific antibody clone, the failure of one clone to induce cell death does not discount a plasma membrane protein as an ADC candidate and NEO1 still remains of interest. ROBO1, however, was discontinued as a potential target following re-evaluation of target expression in both primary samples and HMCLs in conjunction with the failure to induce cell death.

5.3.2 SEMA4A as an ADC candidate

By flow cytometry analysis, SEMA4A expression was highest in plasma cells in the majority of samples. Although there was relatively high expression on monocytes and granulocytes, there was no discernible expression on B cells and low to minimal expression on T lymphocytes, protecting the adaptive immune system from any on-target cytotoxic effects. Importantly, SEMA4A was not highly expressed on $CD34^{+}$ stem cells (fig 5.7C). Therefore, if there were any ADC-related toxicities to the $SEMA4A^{pos}$ haematopoeitic cells, these pluripotent stem cells would be able to reconstitute the bone marrow. For one of the patients profiled by PMP, I was able to obtain a second BMA sample two years later. Flow-cytometric analysis of this sample suggested that SEMA4A expression was relatively unchanged over the course of disease progression. This was consistent with our observations in the flow cytometry profiling of samples with no notable difference in the mean expression at diagnosis compared with relapse and progression (fig 5.6). IHC revealed that SEMA4A exhibited clean off-tumour expression with no detectable expression in normal, healthy tissue except within the lymph node and tonsil. From this, it was concluded that SEMA4A was most likely restricted to immune cell populations (fig 5.13B). Although SEMA4A mutations have been reported to be involved in retinitis pigmentosa, a genetic disease associated with loss

of vision, I was unable to detect cell surface SEMA4A expression in the RPE-1 cell line. This is in accordance with other published reports that suggest that under normal conditions, SEMA4A in RPE cells is localised intracellularly and under oxidative stress is secreted via exosomal release [324]. As expected, these cells were unaffected by a SEMA4A-targeted ADC (fig 5.14).

Similarly to NEO1 and ROBO1, SEMA4A was rapidly internalised following antigen binding, with 50% loss of cell surface SEMA4A over two hours. Importantly the antibody-antigen complex was not recycled back to the cell surface (fig 5.9). Antigen internalisation was confirmed by immunofluorescence and the antigen-Ig complex appeared to be partially localised with LAMP-1 positive lysosomes (fig 5.10) suggesting that the internalised antibody is trafficked to the lysosome. This is considered to be an ideal subcellular localisation for ADCs as a number of cytotoxin linkers rely on either the acidic environment of the late endosome/lysosome or lysosomal-specific proteases for degradation [247]. Using a 'piggy back' system, a SEMA4A-targeting antibody in conjunction with a saporin-linked secondary antibody induced extensive cell death (47 to 56% over 72 hours) in two antigen-expressing cell lines. Importantly, a third cell line that did not express SEMA4A was unaffected (fig 5.12).

Having characterised SEMA4A as a promising target *in vitro*, the next aim of this chapter was to investigate the potential of SEMA4A as an ADC candidate *in vivo*. Whilst the use of a 'piggy back' system enables the rapid screening of antibody clones *in vitro* for preliminary proof of principle, there are several disadvantages to this system [337] and I was unable to achieve greater than 56% loss of viability in NCI-H929 and MM.1S (at 1nM) using either the Fab-ZAP or Strep-ZAP kit. This was likely because I was unable to increase the primary antibody concentration above 1nM as the ratio of unbound primary antibody began to out-compete secondary-bound-primary antibody for SEMA4A. Saporin is also not used clinically and so in order to have greater understanding of the properties of a lead SEMA4A-targeting ADC, I opted for a directly conjugated ADC to evaluate activity *in vivo*. Using the direct conjugates, I was able to test the antibody at a higher dose and achieved greater maximal cell death (66 to 92% cell death at 0.1nM in MM.1S and NCI-H929 respectively) (fig 5.18). As 5E3-MMAE was more potent *in vitro* and did not appear to exhibit any non-specific activity, I decided to proceed with this conjugate. *In vivo* 5E3-MMAE showed promising anti-tumour activity with an initial reduction in tumour burden during dosing and overall significantly improved survival for treated mice compared with both control groups (fig 5.19).

Finally, I have begun to investigate the role of SEMA4A in myeloma cell biology. An initial stable RNAi-mediated knock-down experiment suggested that loss of SEMA4A may be detrimental to HMCL fitness with the emergence of a SEMA4A^{pos} population (fig 5.20A). A competitive disadvantage following loss of SEMA4A in SEMA4A^{hi} cell lines was confirmed using a competition assay, in which I observed the rapid decline in proportion of SEMA4A-hairpin expressing cells compared to shLUC expressing cells (fig 5.20C) that was associated with an increase in cell death (fig 5.21). To confirm that this observed phenotype was not the result of a hairpin off-target effect, I performed a rescue experiment in which endogenous SEMA4A was knocked-out and shRNA-resistant wild-type or mutant (intracellular domain deficient) SEMA4A re-expressed. Unexpectedly, I failed to observe a reversion of the competitive disadvantage following rescue of SEMA4A expression (fig 5.22). This was unlikely to be due to insufficient rescue of expression (fig 5.22B) or cleavage of the BFP reporter (fig 5.23). Instead, the failure to reverse the observed phenotype may be due to the apparent toxicity of the rescue constructs, with both WT and mutant SEMA4A having a detrimental effect on cell growth (fig 5.24B and C). From these experiments, I was unable to conclude that SEMA4A plays an essential role in myeloma biology.

Chapter 6

Discussion and Future Perspectives

Despite the recent improvements in patient survival due to novel therapeutics, it is still largely considered that myeloma is incurable, and patients will eventually relapse. Recently, the focus of future myeloma treatment has shifted towards more targeted therapeutics, such as monoclonal antibodies. These antibodies are a promising strategy for the treatment of malignancies and have demonstrated significant successes in a wide range of both solid and haematological cancers. Although there are a few proteins that have been well characterised as potential targets, it is likely that there are many more novel targets that have not yet been identified due to the limitations of currently available techniques. These limitations include their low abundance, the difficulty in isolating these proteins from the membrane and the limited availability of antibodies for characterisation. The overall aim of this thesis was to use PMP to identify a novel antibody drug conjugate target for the treatment of myeloma.

6.1 The myeloma cell surface proteome

The first aim of this thesis was to characterise the myeloma cell surface proteome using PMP. Although this technique has been used successfully in the past on cell lines [288][338], our initial concerns were that the mildly acidic conditions required for PMP would be highly detrimental to the viability of the fragile myeloma cells *ex vivo*. Despite the challenges faced in obtaining a sufficient number of patient samples, I observed no technical difficulties applying this technique to primary myeloma cells. Using PMP, I quantified a total of 2,714 proteins across the 18 samples, 2,077 of which were identified by two or more unique peptides (fig 3.8). Of these proteins, 1,319 were determined to be plasma membrane proteins using a combination of gene ontology and UniProt annotations (79.5% enrichment as determined by protein abundance). 488 had an extracellular domain and therefore represented potential

monoclonal antibody targets of interest. Although I have tried to be as inclusive as possible using both the GOCC and UniProt databases for protein annotations, it is highly possible that there are several plasma membrane proteins missed. As discussed in the introduction, membrane proteomics has been traditionally challenging, and the number of plasma membrane proteins identified have been both small and highly variable. Using PMP, I was able to consistently achieve a high level of enrichment over both cell lines and primary samples. Although several MS analyses have been undertaken in myeloma, the number of plasma membrane proteins identified has been typically low, and few have been quantitative. Dytfeld *et al* [299][261] also used isobaric tags for mass spectrometry multiplex analysis of primary samples, quantifying 399 to 944 total proteins across several studies. However, Dytfeld *et al* did not enrich for the PM, and it is highly possible that less than 15% of these proteins are plasma membrane proteins [284]. Whilst Xie *et al* [339] did enrich for the plasma membrane, using biotin for affinity-purification, they only reported the identification of 156 proteins using two cell lines. Using a similar technique, Zhao *et al* reported the identification of 663 plasma membrane proteins in a human lung epithelial cell, but this was not quantitative [286]. The results presented in this thesis, therefore, represent the first quantitative analysis of the whole myeloma cell surface proteome, providing a substantial improvement over other published reports (including studies undertaken in other cell types), both in terms of the enrichment and in the total numbers of plasma membrane proteins identified and quantified. This dataset represents an invaluable tool to aiding target discovery, as well as our understanding of myeloma cell biology.

However, it should be noted that there are a few caveats to this dataset. Firstly, although the majority of cell surface proteins are predicted to be glycosylated, not all are [279], and these may have been excluded from our dataset. Secondly, although I was able to select HMCLs that represent the majority of the genetic events that occur in myeloma, because nearly all cell lines are of the non-hyperdiploid subgroup, the hyperdiploid group (which comprises nearly half of the myeloma cell population) is not represented at all in our HMCL PMP. Conversely, thus far, only one of the patients profiled by PMP exhibits an IgH rearrangement by FISH analysis (6 out of 8 analysed to date). Finally, because of the difficulties in obtaining healthy, age-matched BMAs or sufficient PC numbers from the *in vitro* differentiation of B cells, I was unable to profile normal plasma cells. Although I concluded that this would not hinder target discovery significantly, it may limit the identification of biomarkers that are associated with plasma cell transformation or disease progression. In lieu of this, I have used the extensively characterised HMCLs to identify proteins that are associated with high-risk cytogenetics and may be involved in driving the disease. By comparing protein expression

between subgroups, I identified 11 proteins associated with del(17p)/TP53 mutations, including VAV1. Interestingly, VAV1 was reported as playing a dual pro- and anti-apoptotic role that was dependent on p53 availability and it may be possible there is a feedback loop for this protein [340]. I also observed several proteins linked with the t(11;14) subgroup, including ENTPD1 (p=7e-6, q=0.0072, fig 3.13) which was validated in a larger sample of HMCLs by RNA expression analysis. Overall though, the total number of proteins associated with underlying genetic perturbations was low, most likely as a result of the limited number of samples for each subgroup. For seven out of the eight patients profiled by PMP we have banked CD138+ cells and it is hoped it will be possible to use these for gene expression profiling. Using this additional data, it will be possible to expand the number of samples within each sub-type and enable the identification of other plasma membrane proteins associated with high-risk cytogenetics. These proteins not only represent potential biomarkers for high-risk that are more accessible than FISH analysis or GEP but may help elucidate the downstream *sequelae* of common genetic events.

Interestingly, although I failed to identify any proteins significantly associated with the t(4;14) subgroup, using unsupervised clustering I identified a clear t(4;14) plasma membrane protein signature (fig 3.16). Meanwhile, the t(11;14) and t(MAF) subgroups were less well defined, possible because these subgroups were smaller (only 1 sample for t(14;20)) but also because cyclin D and c-Maf are frequently dysregulated in a translocation-independent manner [34][35]. Aside from subtype, I also observed a clear contrast between HMCLs and primary samples, with upwards of 500 proteins identified as significantly differentially expressed with a FDR of 0.01% (fig 3.18). This was not entirely unexpected. Although these cells recapitulate the major mutational events in myeloma, they represent advanced relapsed/refractory disease and are highly proliferative in comparison to their primary counterparts, as shown by the gene enrichment analysis performed (fig 3.18). Furthermore, as discussed, cell lines are typically non-hyperdiploid and represent those patients with a poorer prognosis. Whilst this doesn't detract from using HMCLs as a model for myeloma, it should be noted that there are limitations to using these cell lines for target discovery. This was highlighted by ROBO1 and EPHB2, both of which were predicted to be highly expressed in myeloma by the HMCL PMP. Subsequent analysis of patient samples revealed that these were in fact not so highly expressed in primary disease.

One of the predominant arguments for the use of proteomic profiling over RNA analysis is the poor correlation between transcript and protein levels. As anticipated, I observed a very poor correlation between RNA and protein abundance across the ten cell lines (ranging

from 0.13 to 0.21 across all proteins, (fig 3.12)), corresponding with what has been reported previously [258]. However, both Wilhelm and Edfors [302][305] have recently proposed that although the RNA translation and protein degradation rates may vary greatly between different transcripts, these factors remain surprisingly constant for any given protein across multiple tissue types. Therefore, using a RNA-to-protein (RTP) conversion factor, the abundance of any protein can be predicted from transcript expression. Using a training set of nine of the ten HMCLs, I determined a RTP factor for each protein quantified by PMP and demonstrated that this factor could accurately predict the abundance of any given protein in the tenth HMCL using only RNAseq data (Pearson correlation coefficient of 0.78 to 0.89, fig 3.12). Using a combination of our results obtainined by PMP and the publicly available RNAseq dataset, I have determined a RTP conversion factor for over 2,000 proteins.

Whilst mass spectrometry analysis has provided substantial insight into our understanding of the myeloma cell proteome, these techniques are still limited by both the associated prohibitive costs and the large number of cells required per analysis. Comparatively, next generation sequencing is not only cheaper but also requires considerably fewer cells and is better suited for high-throughput analysis. During this project, one of the challenges faced was obtaining a suitable number of CD138+ cells for PMP analysis and many samples were discarded because of low cell counts. Although it would be imperative to first validate these values, it would be possible to use a combination of RNAseq data and the RTP ratios to analyse the cell surface proteome of a much greater cohort of patient samples in an unbiased and comprehensive manner. These low CD138+ samples are also likely to be of considerable interest, representing MGUS, SMM or early-stage myeloma patients with low infiltration and those patients that have recently undergone treatment but have retained a small population of therapeutic-resistant cells. In addition, it would be possible to profile the cell surface proteome of normal plasma cells, enabling the identification of proteins involved in plasma cell transformation. Furthermore, myeloma is a highly heterogenous sub-clonal disease. Because of the large sample size requirements, analysis by mass spectrometry only informs us of the population-average and subsequent studies are required to determine sub-clonal protein expression. Single-cell proteomic techniques are beginning to emerge but are still very much in their infancy. Although, Budnik recently reported the mass spectrometry-based profiling of a single cell [341], the majority of single-cell techniques rely on antibodies to target specific proteins and are limited to the detection of tens to hundreds of proteins [342]. In comparison, single cell RNA sequencing (scRNAseq) is now a well-established technique and is comparatively low-cost. In combination with the RTP factor, scRNAseq could be used to accurately predict the myeloma cell surface proteome on a sub-clonal scale. This would

enable us to track the clonal evolution of the tumour over the course of the disease and to identify biomarkers associated with the drug-resistant minor sub-clones.

Aside from profiling the myeloma tumour on a sub-clonal and high-throughput scale, the calculated RTP factors could be used to characterise the plasma membrane proteome in other cell types. Although I was initially interested in using the *in vitro* plasma cell differentiation protocol to generate normal controls for our study, I also considered the possibility of using PMP to quantify cell surface protein expression changes during plasma cell differentiation. However, as discussed, the low cell counts associated with this protocol meant I did not proceed with this. Using our calculated RTP ratios, it would now be possible to predict protein abundance from transcript levels using much fewer cells. This would provide further insight into plasma cell generation, which to our knowledge has not yet been performed on a proteomic scale (excluding one study which used cell lines to represent different stages of plasma cell differentiation [343]). This may also help elucidate the mechanisms involved in determining the longevity of a plasma cell. In addition, because the RTP factor has been shown to be considerably stable over multiple tissue types [305], this may allow the direct comparison of off-tumour expression between targets instead of relying on whole-cell proteomic data, which although useful for this study, is limited by the low number of proteins and tissue types profiled.

Overall, I have profiled a total of 18 samples and consider that this dataset provides us with a comprehensive analysis of the myeloma cell surface proteome. The fact that only a few changes occurred between the first and second PMP of the two cell lines (fig 3.10), which were profiled more than a year apart, and that I was able to correlate this data with flow cytometry (fig 3.11), suggests that this data can be considered to be highly representative of the cell surface proteome. Through the combined analysis of our PMP dataset and other whole-cell proteomic databases, I identified 20 plasma membrane proteins that represented potential monoclonal antibody targets, four of which had already been described as therapeutic targets for myeloma (table 3.5). This approach also identified the two monoclonal antibody targets currently FDA approved for the treatment of myeloma (CD38 and SLAMF7), giving us confidence in this technique and our analytical approach. Several of these top hits were proteins that have already been identified in other malignancies, both solid and haematological. CD97, for instance, has been shown to promote the migration and invasiveness of hepatocellular carcinoma [344]. While EPHB2 is associated with a poor prognosis in breast cancer [345] and ROBO1 has been reported to be promote the proliferation and survival of osteosarcoma [346]. Interestingly, the SLIT2/ROBO1 axis has been

implicated in the inhibition of osteoblast differentiation and was identified in two separate studies as a candidate gene in myeloma, associated with a t(4;14) subgroup and mutated in 5 out of 67 patients [22][347]. NEO1 dysregulation has been reported in a number of human tumours, including glioma, medulloblastoma, breast cancer, cervix cancer, pancreas cancer and colorectal [348]. Other proteins have been associated with regulation of the immune system and may promote tumour evasion, including BTN2A1 which has been identified as a ligand for dendritic cells [349] and ADAM17 which may be involved in the shedding of immune-regulating proteins, such as MICA [350].

6.2 Recombinant protein production and purification of remaining targets

As it was anticipated that not all of our candidate proteins would have reliable antibodies available, the second aim of this thesis was to establish a recombinant protein mammalian expression system. This would enable the production of the protein required for the generation of key, proprietary antibodies for target validation but also for any potential lead candidates to take forward into pre-clinical testing. Thus far, I have successfully cloned five proteins and purified three to homogeneity. Despite successfully cloning and expressing full-length SEMA4A in both HEK-293T and HMCLs (fig 5.23), I experienced difficulties expressing high levels of truncated SEMA4A in the cell culture media (fig 4.7). This is likely due to the compositional instability of this construct, which may improve with the addition of a stabilising tag. Alternatively, as I plan to use this recombinant protein for phage-display, it may be simpler to use target-expressing cell lines instead of purified protein.

6.3 SEMA4A as a novel myeloma target

From our list of 16 novel targets, I was only able to characterise a few because of the limited availability and reliability of commercial antibodies. Of those that were characterised, only three exhibited comparatively higher expression on myeloma cells and were assessed as ADCs.

Although naked antibodies have demonstrated clinical success, these antibodies are frequently used in combination with chemotherapy to achieve therapeutic efficacy. Elotuzumab,

for instance, fails to demonstrate any single agent activity but does act synergistically with lenalidomide and dexamethasone to significantly improve both progression-free and overall survival [241]. ADCs, which combine the specificity of unconjugated antibodies with the cytotoxicity of chemotherapeutics, are becoming increasingly popular. Out of the three proteins I assessed, SEMA4A, which met the ideal properties of an ADC target, was identified as a lead candidate. By flow cytometry, SEMA4A was determined to be highly expressed in nearly all patient samples and did not appear to be expressed outside of the lymphoid organs by IHC (fig 5.13). Furthermore, following antibody binding, SEMA4A was rapidly internalised to deliver a cytotoxic agent in a target-specific manner (fig 5.12). Although SEMA4A mutations are associated with retinitis pigmentosa, I did not observe any expression on RPE-1 cells, despite the addition of oxidative stress (fig 5.14). Notably, I did observe SEMA4A expression on monocytes and granulocytes and a small subset of T cells, although in nearly all cases SEMA4A expression was greater on myeloma cells (fig 5.7). ADC toxicity is directly proportional to target expression. The higher the expression, the more ADC can be internalised to deliver the toxin. Only the highest SEMA4A-expressing cell lines were sensitive to 5E3-MMAE (fig 5.18). Based on our observations with BM068, which showed similar expression to KMS-12-BM, I would expect monocyte and granulocyte expression levels to be comparable to the cell lines in which I did not observe any ADC cytotoxic activity. Of course this is highly dependent on the sensitivity of the cell type to the conjugated toxin and it may be that similar to alemtuzumab [351], a naked antibody for the treatment of chronic lymphocytic leukaemia, a prophylactic antibiotic will be necessary with this antibody. Importantly, I observed minimal SEMA4A expression on CD34+ cells and therefore, if there were any ADC-related toxicities to the SEMA4A^{pos} haematopoeitic cells, these pluripotent stem cells would be left untouched and would be able to reconstitute the bone marrow. CD46 was recently reported as a potential ADC target for myeloma [223]. Similar to SEMA4A, they observed notable expression on monocytes and granulocytes. Reassuringly, they observed no off-tumour toxicity within the haematopoietic compartment, and this target is now set to enter human clinical trials in spring 2019 (NCT03650491, [221]).

Having confirmed the selective and potent activity of the SEMA4A-ADC *in vitro*, I also tested 5E3-MMAE activity *in vivo* in an orthometastatic xenograft model. NSG mice bearing luciferase-expressing MM.1S tumours received one of three treatments: 5E3-MMAE, isotype control (mIgG1-MMAE) or the unconjugated antibody (5E3) for a total of four doses at 4mg/kg (i.v.). 5E3-MMAE demonstrated potent activity *in vivo*, with a near-complete elimination of bioluminescence activity during treatment, although all mice did subsequently relapse and eventually succumb to disease. This delay in tumour growth translated to a

significant improvement in survival for all 5E3-MMAE treated mice over the control groups. These results are highly promising and demonstrate the potential for a SEMA4A-targeting antibody for the treatment of myeloma. As the mice used in this study are immune-deficient, the effects of a SEMA4A-targeting ADC on the haematopoeitic compartment is currently unknown. As such, a future tolerability study in immunocompetent mice is planned. Because 5E3 exhibits cross-reactivity, targeting both human and murine SEMA4A, this will enable us to assess any off-tumour target-specific toxicity, such as on monocytes and granulocytes as well as on retinal tissue.

Interestingly, SEMA4A is located at 1q22, within the predicted minimally amplified region for gain 1q. It would be of considerable interest to determine if myeloma cells with dup(1q), a poor prognostic marker associated with relapsed/refractory disease, also exhibit SEMA4A gene amplification. As the 1q amplification is routinely assessed by FISH during patient diagnosis, this would prove an invaluable marker for patient stratification and personalised medicine. Although I have the FISH results for six of the eight patients profiled by PMP confirming dup(1q), I do not have exact copy numbers and have not yet been able to determine a correlation between copy number gains and SEMA4A expression, although the highest expressing patient sample by PMP was positive for 1q amplification. There are a few datasets available, including the CoMMpass Study (https://research.themmrf.org), which would enable us to correlate 1q gains with SEMA4A gene amplification in a much larger cohort than our eight samples.

Several reports have suggested that monoclonal antibody resistance can in part be mediated through target downregulation, as is seen for both rituximab (CD20) in B lymphoid malignancies and daratumumab (CD38) for myeloma [328][329]. CD38 expression strongly correlates with ADCC and CDC activity, and cell surface downregulation provides a mechanism for tumour escape from immune-mediated killing. However, some patients with CD38 downregulation are still responders, and it has been hypothesised that loss of CD38 reduces myeloma cell contact with the BM stromal cells and may contribute to reduced growth and survival [329]. The report that SEMA4A can function as a receptor [327] led us to hypothesise that dysregulated SEMA4A may contribute to myeloma cell biology and that loss of this protein may not represent a viable mechanism of resistance.

RNA-interference (RNAi) is a frequently used method for RNA knock-down. However, it can also be highly non-specific, and off-target effects are a common problem, requiring the use of multiple targeting hairpins as well as control hairpins. Using two targeting hairpins, I

observed that loss of SEMA4A conveyed a substantial competitive disadvantage and these cells were rapidly lost in a co-culture with SEMA4A-expresssing cells. This effect appeared to be target specific as I did not observe the same effect using a control hairpin (shLuciferase) or in a third SEMA4A^{neg} cell line (K562) (fig 5.20). To further prove that these effects were target-specific, I attempted a knockdown and rescue experiment, in which the endogenous SEMA4A is knocked-down and exogenous, shRNA-resistant SEMA4A is re-introduced to reverse the phenotype. Unfortunately, I was unable to reverse the competitive disadvantage, with either mutant or WT SEMA4A and I was unable to conclude that the observed phenotype was SEMA4A-specific (fig 5.22B). Although expression rescue experiments can be considered the ultimate proof for an observed shRNA effect, these experiments are not without limitations, including the challenges involved in expressing the correct level of exogenous protein and the presence of splice variants. Datler *et al* were similarly unable to reverse the observed phenotype following RNAi, despite using a total of 19 hairpins to demonstrate that mitochondrial depolarisation only occurred in the presence of CKMT1 gene silencing [352]. I confirmed that exogenous SEMA4A was expressed at the cell surface of the rescue cells and although it was lower than endogenous SEMA4A for MM.1S, it was similar for NCI-H929 and this is unlikely to be the reason behind the failure to rescue the phenotype. I also demonstrated that at least the WT SEMA4A was completely cleaved from the BFP reporter. However, following T2A cleavage, some additional residues are left on the first protein [353]. The loss of as few as four amino acids from the termini of a receptor can completely abolish receptor signalling [354] and it may be that these additional amino acids interfered with correct protein folding and signal transduction. In addition, it can't be excluded that there is an un-described alternatively spliced transcript that is dissimilar to our rescue constructs but is essential for myeloma cell survival.

Another possible reason for the failure of the rescue experiment was that the prolonged over-expression of the rescue constructs prior to knockdown had a detrimental effect on cell growth. To test this hypothesis, I used doxycycline-inducible hairpins to induce the simultaneous knockdown of endogenous SEMA4A and over-expression of the WT or mutant SEMA4A constructs. Following transduction, there was a substantial reduction in cell growth for both the WT and mutant SEMA4A-expressing cells compared to the cells transduced with the empty parental vector (fig 5.24). This observed effect was independent of hairpin expression. The results of this experiment may explain why the initial knockdown and rescue experiment failed and suggests that the over-expression of SEMA4A is highly toxic. Protein over-expression may negatively impact cell viability and/or growth for several reasons. One reason is that the over-expression of protein overwhelms the cell with the high resource

burden required for protein production. Alternatively, high expression of the protein may modulate numerous signalling pathways, over-stimulating the normal physiological pathway and promoting promiscuous interactions and sequestration of essential proteins [355]. As a result, I am unable to conclude that the observed phenotype reported in this thesis is the result of an on-target effect. As an alternative, I have begun to investigate a CRISPR/Cas9-mediated knockout of SEMA4A which may help elucidate the essentiality of SEMAA in myeloma cell lines.

6.4 Conclusion

- Using plasma membrane profiling to selectively enrich for an quantify cell surface proteins, I have quantified over 1,300 plasma-membrane or associated proteins. This represents a substantial improvement over other published studies, both in the total number of identified membrane proteins but also in the number of cell surface proteomes quantitatively analysed. From this unique dataset, I have identified 16 novel myeloma therapeutic targets.
- I have established a recombinant protein production system that will enable us to generate the tool antibodies necessary to validate these proteins and have successfully purified protein for three of our candidates.
- From this dataset, I identified SEMA4A as a lead candidate based on a combination of high on-tumour and low off-tumour expression. Furthermore, an ADC against this target has been shown to be highly efficacious in high SEMA4A-expressing cell lines both *in vitro* and *in vivo*. The work presented in this thesis supports further investigation into SEMA4A as a novel target for the treatment of myeloma and to this extent, we have established an ongoing collaboration with CMAL (Cancer Research UK-Medimmune Alliance Laboratory).

References

[1] A. Palumbo and K. Anderson. Multiple myeloma. *N. Engl. J. Med.*, 364(11):1046–1060, Mar 2011.

[2] Cancer Research UK. http://www.cancerresearchuk.org/health-professional/cancer-statistics/statistics-by-cancer-type/myeloma. Accessed July 2015.

[3] O. Landgren, R. A. Kyle, R. M. Pfeiffer, J. A. Katzmann, N. E. Caporaso, R. B. Hayes, A. Dispenzieri, S. Kumar, R. J. Clark, D. Baris, R. Hoover, and S. V. Rajkumar. Monoclonal gammopathy of undetermined significance (MGUS) consistently precedes multiple myeloma: a prospective study. *Blood*, 113(22):5412–5417, May 2009.

[4] S. V. Rajkumar, M. A. Dimopoulos, A. Palumbo, J. Blade, G. Merlini, et al. International Myeloma Working Group updated criteria for the diagnosis of multiple myeloma. *Lancet Oncol.*, 15(12):e538–548, Nov 2014.

[5] I. Turesson, S. A. Kovalchik, R. M. Pfeiffer, S. Y. Kristinsson, L. R. Goldin, M. T. Drayson, and O. Landgren. Monoclonal gammopathy of undetermined significance and risk of lymphoid and myeloid malignancies: 728 cases followed up to 30 years in Sweden. *Blood*, 123(3):338–345, Jan 2014.

[6] S. V. Rajkumar, R. A. Kyle, T. M. Therneau, L. J. Melton, A. R. Bradwell, R. J. Clark, D. R. Larson, M. F. Plevak, A. Dispenzieri, and J. A. Katzmann. Serum free light chain ratio is an independent risk factor for progression in monoclonal gammopathy of undetermined significance. *Blood*, 106(3):812–817, Aug 2005.

[7] R. A. Kyle, E. D. Remstein, T. M. Therneau, A. Dispenzieri, P. J. Kurtin, J. M. Hodnefield, D. R. Larson, M. F. Plevak, D. F. Jelinek, R. Fonseca, L. J. Melton, and S. V. Rajkumar. Clinical course and prognosis of smoldering (asymptomatic) multiple myeloma. *N. Engl. J. Med.*, 356(25):2582–2590, Jun 2007.

[8] S. V. Rajkumar, O. Landgren, and M. V. Mateos. Smoldering multiple myeloma. *Blood*, 125(20):3069–3075, May 2015.

[9] M. A. Dimopoulos, E. Kastritis, L. Rosinol, J. Blade, and H. Ludwig. Pathogenesis and treatment of renal failure in multiple myeloma. *Leukemia*, 22(8):1485–1493, Aug 2008.

[10] B. O. Oyajobi. Multiple myeloma/hypercalcemia. *Arthritis Res. Ther.*, 9 Suppl 1:S4, 2007.

[11] A. Hameed, J. J. Brady, P. Dowling, M. Clynes, and P. O'Gorman. Bone disease in multiple myeloma: pathophysiology and management. *Cancer Growth Metastasis*, 7:33–42, 2014.

[12] K. Podar. MM-associated anemia: more than "crowding out" HSPCs. *Blood*, 120(13):2539–2540, Sep 2012.

[13] S. V. Rajkumar and S. Kumar. Multiple Myeloma: Diagnosis and Treatment. *Mayo Clin. Proc.*, 91(1):101–119, Jan 2016.

[14] C. S. Chim, S. K. Kumar, R. Z. Orlowski, G. Cook, P. G. Richardson, M. A. Gertz, S. Giralt, M. V. Mateos, X. Leleu, and K. C. Anderson. Management of relapsed and refractory multiple myeloma: novel agents, antibodies, immunotherapies and beyond. *Leukemia*, 32(2):252–262, Feb 2018.

[15] C. Touzeau and P. Moreau. How I treat extramedullary myeloma. *Blood*, 127(8):971–976, Feb 2016.

[16] M. Chesi and P. L. Bergsagel. Molecular pathogenesis of multiple myeloma: basic and clinical updates. *Int. J. Hematol.*, 97(3):313–323, 2013.

[17] C. Fernandez de Larrea, R. A. Kyle, B. G. Durie, H. Ludwig, S. Usmani, et al. Plasma cell leukemia: consensus statement on diagnostic requirements, response criteria and treatment recommendations by the International Myeloma Working Group. *Leukemia*, 27(4):780–791, Apr 2013.

[18] A. M. Rajan and S. V. Rajkumar. Interpretation of cytogenetic results in multiple myeloma for clinical practice. *Blood Cancer J*, 5:e365, Oct 2015.

[19] J. R. Mikhael, D. Dingli, V. Roy, C. B. Reeder, F. K. Buadi, et al. Management of newly diagnosed symptomatic multiple myeloma: updated Mayo Stratification of Myeloma and Risk-Adapted Therapy (mSMART) consensus guidelines 2013. *Mayo Clin. Proc.*, 88(4):360–376, Apr 2013.

[20] J. G. Lohr, P. Stojanov, S. L. Carter, P. Cruz-Gordillo, M. S. Lawrence, et al. Widespread genetic heterogeneity in multiple myeloma: implications for targeted therapy. *Cancer Cell*, 25(1):91–101, Jan 2014.

[21] B. A. Walker, C. P. Wardell, L. Melchor, A. Brioli, D. C. Johnson, et al. Intraclonal heterogeneity is a critical early event in the development of myeloma and precedes the development of clinical symptoms. *Leukemia*, 28(2):384–390, Feb 2014.

[22] N. Bolli, H. Avet-Loiseau, D. C. Wedge, P. Van Loo, L. B. Alexandrov, et al. Heterogeneity of genomic evolution and mutational profiles in multiple myeloma. *Nat Commun*, 5:2997, 2014.

[23] J. J. Keats, M. Chesi, J. B. Egan, V. M. Garbitt, S. E. Palmer, et al. Clonal competition with alternating dominance in multiple myeloma. *Blood*, 120(5):1067–1076, Aug 2012.

[24] Y. Furukawa and J. Kikuchi. Molecular pathogenesis of multiple myeloma. *Int. J. Clin. Oncol.*, 20(3):413–422, Jun 2015.

[25] J. B. Egan, C. X. Shi, W. Tembe, A. Christoforides, A. Kurdoglu, et al. Whole-genome sequencing of multiple myeloma from diagnosis to plasma cell leukemia reveals genomic initiating events, evolution, and clonal tides. *Blood*, 120(5):1060–1066, Aug 2012.

[26] F. Magrangeas, H. Avet-Loiseau, W. Gouraud, L. Lode, O. Decaux, et al. Minor clone provides a reservoir for relapse in multiple myeloma. *Leukemia*, 27(2):473–481, Feb 2013.

[27] C. Pawlyn and G. J. Morgan. Evolutionary biology of high-risk multiple myeloma. *Nat. Rev. Cancer*, 17(9):543–556, Aug 2017.

[28] R. Fonseca, P. L. Bergsagel, J. Drach, J. Shaughnessy, N. Gutierrez, et al. International Myeloma Working Group molecular classification of multiple myeloma: spotlight review. *Leukemia*, 23(12):2210–2221, Dec 2009.

[29] M. L. Chretien, J. Corre, V. Lauwers-Cances, F. Magrangeas, A. Cleynen, et al. Understanding the role of hyperdiploidy in myeloma prognosis: which trisomies really matter? *Blood*, 126(25):2713–2719, Dec 2015.

[30] J. D. Hoyer, C. A. Hanson, R. Fonseca, P. R. Greipp, G. W. Dewald, and P. J. Kurtin. The (11;14)(q13;q32) translocation in multiple myeloma. A morphologic and immunohistochemical study. *Am. J. Clin. Pathol.*, 113(6):831–837, Jun 2000.

[31] M. C. Casimiro, M. Crosariol, E. Loro, Z. Li, and R. G. Pestell. Cyclins and cell cycle control in cancer and disease. *Genes Cancer*, 3(11-12):649–657, Nov 2012.

[32] E. M. Sewify, O. A. Afifi, E. Mosad, A. H. Zaki, and S. A. El Gammal. Cyclin D1 amplification in multiple myeloma is associated with multidrug resistance expression. *Clin Lymphoma Myeloma Leuk*, 14(3):215–222, Jun 2014.

[33] Y. W. Qiang, S. Ye, Y. Chen, A. F. Buros, R. Edmonson, et al. MAF protein mediates innate resistance to proteasome inhibition therapy in multiple myeloma. *Blood*, 128(25):2919–2930, 12 2016.

[34] P. L. Bergsagel, W. M. Kuehl, F. Zhan, J. Sawyer, B. Barlogie, and J. Shaughnessy. Cyclin D dysregulation: an early and unifying pathogenic event in multiple myeloma. *Blood*, 106(1):296–303, Jul 2005.

[35] E. M. Hurt, A. Wiestner, A. Rosenwald, A. L. Shaffer, E. Campo, T. Grogan, P. L. Bergsagel, W. M. Kuehl, and L. M. Staudt. Overexpression of c-maf is a frequent oncogenic event in multiple myeloma that promotes proliferation and pathological interactions with bone marrow stroma. *Cancer Cell*, 5(2):191–199, Feb 2004.

[36] M. Santra, F. Zhan, E. Tian, B. Barlogie, and J. Shaughnessy. A subset of multiple myeloma harboring the t(4;14)(p16;q32) translocation lacks FGFR3 expression but maintains an IGH/MMSET fusion transcript. *Blood*, 101(6):2374–2376, Mar 2003.

[37] E. Martinez-Garcia, R. Popovic, D. J. Min, S. M. Sweet, P. M. Thomas, L. Zamdborg, A. Heffner, C. Will, L. Lamy, L. M. Staudt, D. L. Levens, N. L. Kelleher, and J. D. Licht. The MMSET histone methyl transferase switches global histone methylation

and alters gene expression in t(4;14) multiple myeloma cells. *Blood*, 117(1):211–220, Jan 2011.

[38] J. Lauring, A. M. Abukhdeir, H. Konishi, J. P. Garay, J. P. Gustin, Q. Wang, R. J. Arceci, W. Matsui, and B. H. Park. The multiple myeloma associated MMSET gene contributes to cellular adhesion, clonogenic growth, and tumorigenicity. *Blood*, 111(2):856–864, Jan 2008.

[39] M. Y. Shah, E. Martinez-Garcia, J. M. Phillip, A. B. Chambliss, R. Popovic, T. Ezponda, E. C. Small, C. Will, M. P. Phillip, P. Neri, N. J. Bahlis, D. Wirtz, and J. D. Licht. MMSET/WHSC1 enhances DNA damage repair leading to an increase in resistance to chemotherapeutic agents. *Oncogene*, 35(45):5905–5915, 11 2016.

[40] H. Pei, L. Zhang, K. Luo, Y. Qin, M. Chesi, F. Fei, P. L. Bergsagel, L. Wang, Z. You, and Z. Lou. MMSET regulates histone H4K20 methylation and 53BP1 accumulation at DNA damage sites. *Nature*, 470(7332):124–128, Feb 2011.

[41] Y. W. Qiang, S. Ye, Y. Huang, Y. Chen, F. Van Rhee, J. Epstein, B. A. Walker, G. J. Morgan, and F. E. Davies. MAFb protein confers intrinsic resistance to proteasome inhibitors in multiple myeloma. *BMC Cancer*, 18(1):724, Jul 2018.

[42] L. H. Gallo, K. N. Nelson, A. N. Meyer, and D. J. Donoghue. Functions of Fibroblast Growth Factor Receptors in cancer defined by novel translocations and mutations. *Cytokine Growth Factor Rev.*, 26(4):425–449, Aug 2015.

[43] S. Trudel, A. K. Stewart, E. Rom, E. Wei, Z. H. Li, S. Kotzer, I. Chumakov, Y. Singer, H. Chang, S. B. Liang, and A. Yayon. The inhibitory anti-FGFR3 antibody, PRO-001, is cytotoxic to t(4;14) multiple myeloma cells. *Blood*, 107(10):4039–4046, May 2006.

[44] S. Trudel, S. Ely, Y. Farooqi, M. Affer, D. F. Robbiani, M. Chesi, and P. L. Bergsagel. Inhibition of fibroblast growth factor receptor 3 induces differentiation and apoptosis in t(4;14) myeloma. *Blood*, 103(9):3521–3528, May 2004.

[45] E. E. Plowright, Z. Li, P. L. Bergsagel, M. Chesi, D. L. Barber, D. R. Branch, R. G. Hawley, and A. K. Stewart. Ectopic expression of fibroblast growth factor receptor 3 promotes myeloma cell proliferation and prevents apoptosis. *Blood*, 95(3):992–998, Feb 2000.

[46] M. Chesi, L. A. Brents, S. A. Ely, C. Bais, D. F. Robbiani, E. A. Mesri, W. M. Kuehl, and P. L. Bergsagel. Activated fibroblast growth factor receptor 3 is an oncogene that contributes to tumor progression in multiple myeloma. *Blood*, 97(3):729–736, Feb 2001.

[47] A. Gabrea, P. Leif Bergsagel, and W. Michael Kuehl. Distinguishing primary and secondary translocations in multiple myeloma. *DNA Repair (Amst.)*, 5(9-10):1225–1233, Sep 2006.

[48] B. A. Walker, P. E. Leone, L. Chiecchio, N. J. Dickens, M. W Jenner, et al. A compendium of myeloma-associated chromosomal copy number abnormalities and their prognostic value. *Blood*, 116(15):56–65, Oct 2010.

[49] L. Lopez-Corral, N. C. Gutierrez, M. B. Vidriales, M. V. Mateos, A. Rasillo, R. Garcia-Sanz, B. Paiva, and J. F. San Miguel. The progression from MGUS to smoldering myeloma and eventually to multiple myeloma involves a clonal expansion of genetically abnormal plasma cells. *Clin. Cancer Res.*, 17(7):1692–1700, Apr 2011.

[50] I. Hanamura, J. P. Stewart, Y. Huang, F. Zhan, M. Santra, et al. Frequent gain of chromosome band 1q21 in plasma-cell dyscrasias detected by fluorescence in situ hybridization: incidence increases from MGUS to relapsed myeloma and is related to prognosis and disease progression following tandem stem-cell transplantation. *Blood*, 108(5):1724–1732, Sep 2006.

[51] K. D. Boyd, F. M. Ross, B. A. Walker, C. P. Wardell, W. J. Tapper, et al. Mapping of chromosome 1p deletions in myeloma identifies FAM46C at 1p12 and CDKN2C at 1p32.3 as being genes in regions associated with adverse survival. *Clin. Cancer Res.*, 17(24):7776–7784, Dec 2011.

[52] Balárková J., Urbánková H., Scudla V., Holzerová M., Bacovský J., Indrák K., and Jarosová M. Gain of chromosome arm 1q in patients in relapse and progression of multiple myeloma. *Cancer Genet Cytogenet.*, 192(2):68–72, Jul 2009.

[53] A. Tagde, H. Rajabi, A. Bouillez, M. Alam, R. Gali, S. Bailey, Y. T. Tai, T. Hideshima, K. Anderson, D. Avigan, and D. Kufe. MUC1-C drives MYC in multiple myeloma. *Blood*, 127(21):2587–2597, May 2016.

[54] J. Inoue, T. Otsuki, A. Hirasawa, I. Imoto, Y. Matsuo, S. Shimizu, M. Taniwaki, and J. Inazawa. Overexpression of PDZK1 within the 1q12-q22 amplicon is likely to be associated with drug-resistance phenotype in multiple myeloma. *Am. J. Pathol.*, 165(1):71–81, Jul 2004.

[55] S. Wuilleme-Toumi, N. Robillard, P. Gomez, P. Moreau, S. Le Gouill, H. Avet-Loiseau, J. L. Harousseau, M. Amiot, and R. Bataille. Mcl-1 is overexpressed in multiple myeloma and associated with relapse and shorter survival. *Leukemia*, 19(7):1248–1252, Jul 2005.

[56] M. Chin, J. I. Sive, C. Allen, C. Roddie, S. J. Chavda, D. Smith, P. Blombery, K. Jones, G. L. Ryland, R. Popat, A. Rismani, S. D'Sa, N. Rabin, R. E. Gale, and K. L. Yong. Prevalence and timing of TP53 mutations in del(17p) myeloma and effect on survival. *Blood Cancer J*, 7(9):e610, Sep 2017.

[57] D. Hofste op Bruinink, H. Remco, M. Sanders, C. Wardell, C. Ashby, et al. Multiple myeloma with a deletion of chromosome 17p: Tp53 mutations are highly prevalent and negatively affect prognosis. *Blood*, 128(22):3271–3271, 2016.

[58] P. J. Teoh and W. J. Chng. p53 abnormalities and potential therapeutic targeting in multiple myeloma. *Biomed Res Int*, 2014:717919, 2014.

[59] J. Ishizawa, K. Nakamaru, T. Seki, K. Tazaki, K. Kojima, D. Chachad, R. Zhao, L. Heese, W. Ma, M. C. J. Ma, C. DiNardo, S. Pierce, K. P. Patel, A. Tse, R. E. Davis, A. Rao, and M. Andreeff. Predictive Gene Signatures Determine Tumor Sensitivity to MDM2 Inhibition. *Cancer Res.*, 78(10):2721–2731, May 2018.

[60] A. Neri, L. Baldini, D. Trecca, L. Cro, E. Polli, and A. T. Maiolo. p53 gene mutations in multiple myeloma are associated with advanced forms of malignancy. *Blood*, 81(1):128–135, Jan 1993.

[61] T. Rasmussen, M. Kuehl, M. Lodahl, H. E. Johnsen, and I. M. Dahl. Possible roles for activating RAS mutations in the MGUS to MM transition and in the intramedullary to extramedullary transition in some plasma cell tumors. *Blood*, 105(1):317–323, Jan 2005.

[62] A. Fernandez-Medarde and E. Santos. Ras in cancer and developmental diseases. *Genes Cancer*, 2(3):344–358, Mar 2011.

[63] W. J. Chng, N. Gonzalez-Paz, T. Price-Troska, S. Jacobus, S. V. Rajkumar, M. M. Oken, R. A. Kyle, K. J. Henderson, S. Van Wier, P. Greipp, B. Van Ness, and R. Fonseca. Clinical and biological significance of RAS mutations in multiple myeloma. *Leukemia*, 22(12):2280–2284, Dec 2008.

[64] P. Roy, U. A. Sarkar, and S. Basak. The NFkB Activating Pathways in Multiple Myeloma. *Biomedicines*, 6(2), May 2018.

[65] J. Hsu, Y. Shi, S. Krajewski, S. Renner, M. Fisher, J. C. Reed, T. F. Franke, and A. Lichtenstein. The AKT kinase is activated in multiple myeloma tumor cells. *Blood*, 98(9):2853–2855, Nov 2001.

[66] A. Dib, A. Gabrea, O. K. Glebov, P. L. Bergsagel, and W. M. Kuehl. Characterization of MYC translocations in multiple myeloma cell lines. *J. Natl. Cancer Inst. Monographs*, (39):25–31, 2008.

[67] H. W. Schroeder and L. Cavacini. Structure and function of immunoglobulins. *J. Allergy Clin. Immunol.*, 125(2 Suppl 2):41–52, Feb 2010.

[68] Thermo Fisher Scientific. https://www.thermofisher.com/uk/en/home/life-science/antibodies/antibodies-learning-center/antibodies-resource-library/antibody-methods/immunoglobulin-structure-classes.html. Accessed September 2018.

[69] D. B. Roth. V(D)J Recombination: Mechanism, Errors, and Fidelity. *Microbiol Spectr*, 2(6), Dec 2014.

[70] J. Stavnezer, J. E. Guikema, and C. E. Schrader. Mechanism and regulation of class switch recombination. *Annu. Rev. Immunol.*, 26:261–292, 2008.

[71] D. D. Chaplin. Overview of the immune response. *J. Allergy Clin. Immunol.*, 125(2 Suppl 2):3–23, Feb 2010.

[72] David Zahavi, Dalal AlDeghaither, Allison O'Connell, and Louis M Weiner. Enhancing antibody-dependent cell-mediated cytotoxicity: a strategy for improving antibody-based immunotherapy. *Antibody Therapeutics*, 1(1):7–12, 2018.

[73] M. S. Braza, B. Klein, G. Fiol, and J. F. Rossi. Î³Î´ T-cell killing of primary follicular lymphoma cells is dramatically potentiated by GA101, a type II glycoengineered anti-CD20 monoclonal antibody. *Haematologica*, 96(3):400–407, Mar 2011.

[74] M. Naradikian, J. Scholz, M. Oropallo, and M. Cancro. Understanding B cell Biology. In X. Bosch, M. Ramos-Carlos, and M. Khamashta, editors, *Drugs targeting B-cells in Autoimmune Disease*, chapter 2, pages 11–35. Springer Basel, Basel, 2014.

[75] K. Chen and A. Cerutti. The function and regulation of immunoglobulin D. *Curr. Opin. Immunol.*, 23(3):345–352, Jun 2011.

[76] T. L. Rothstein, D. O. Griffin, N. E. Holodick, T. D. Quach, and H. Kaku. Human B-1 cells take the stage. *Ann. N. Y. Acad. Sci.*, 1285:97–114, May 2013.

[77] M. Zouali and Y. Richard. Marginal zone B-cells, a gatekeeper of innate immunity. *Front Immunol*, 2:63, 2011.

[78] H. Song and J. Cerny. Functional heterogeneity of marginal zone B cells revealed by their ability to generate both early antibody-forming cells and germinal centers with hypermutation and memory in response to a T-dependent antigen. *J. Exp. Med.*, 198(12):1923–1935, Dec 2003.

[79] S. A. Oracki, J. A. Walker, M. L. Hibbs, L. M. Corcoran, and D. M. Tarlinton. Plasma cell development and survival. *Immunol. Rev.*, 237(1):140–159, Sep 2010.

[80] Y. Zhang, L. Garcia-Ibanez, and K. M. Toellner. Regulation of germinal center B-cell differentiation. *Immunol. Rev.*, 270(1):8–19, 03 2016.

[81] J. Lian and A. D. Luster. Chemokine-guided cell positioning in the lymph node orchestrates the generation of adaptive immune responses. *Curr. Opin. Cell Biol.*, 36:1–6, Oct 2015.

[82] S. Crotty. T follicular helper cell differentiation, function, and roles in disease. *Immunity*, 41(4):529–542, Oct 2014.

[83] C. G. Vinuesa, M. A. Linterman, C. C. Goodnow, and K. L. Randall. T cells and follicular dendritic cells in germinal center B-cell formation and selection. *Immunol. Rev.*, 237(1):72–89, Sep 2010.

[84] I. C. MacLennan, K. M. Toellner, A. F. Cunningham, K. Serre, D. M. Sze, E. Zuniga, M. C. Cook, and C. G. Vinuesa. Extrafollicular antibody responses. *Immunol. Rev.*, 194:8–18, Aug 2003.

[85] T. Yoshida, H. Mei, T. Dorner, F. Hiepe, A. Radbruch, S. Fillatreau, and B. F. Hoyer. Memory B and memory plasma cells. *Immunol. Rev.*, 237(1):117–139, Sep 2010.

[86] D. C. Hargreaves, P. L. Hyman, T. T. Lu, V. N. Ngo, A. Bidgol, G. Suzuki, Y. R. Zou, D. R. Littman, and J. G. Cyster. A coordinated change in chemokine responsiveness guides plasma cell movements. *J. Exp. Med.*, 194(1):45–56, Jul 2001.

[87] A. Kallies, J. Hasbold, D. M. Tarlinton, W. Dietrich, L. M. Corcoran, P. D. Hodgkin, and S. L. Nutt. Plasma cell ontogeny defined by quantitative changes in blimp-1 expression. *J. Exp. Med.*, 200(8):967–977, Oct 2004.

[88] X. Yu, T. Tsibane, P. A. McGraw, F. S. House, C. J. Keefer, et al. Neutralizing antibodies derived from the B cells of 1918 influenza pandemic survivors. *Nature*, 455(7212):532–536, Sep 2008.

[89] O. J. Landsverk, O. Snir, R. B. Casado, L. Richter, J. E. Mold, et al. Antibody-secreting plasma cells persist for decades in human intestine. *J. Exp. Med.*, 214(2):309–317, Feb 2017.

[90] J. M. van Laar, M. Melchers, Y. K. Teng, B. van der Zouwen, R. Mohammadi, R. Fischer, L. Margolis, W. Fitzgerald, J. C. Grivel, F. C. Breedveld, P. E. Lipsky, and A. C. Grammer. Sustained secretion of immunoglobulin by long-lived human tonsil plasma cells. *Am. J. Pathol.*, 171(3):917–927, Sep 2007.

[91] T. Tsubaki, S. Takegawa, H. Hanamoto, N. Arita, J. Kamogawa, et al. Accumulation of plasma cells expressing CXCR3 in the synovial sublining regions of early rheumatoid arthritis in association with production of Mig/CXCL9 by synovial fibroblasts. *Clin. Exp. Immunol.*, 141(2):363–371, Aug 2005.

[92] A. Radbruch, G. Muehlinghaus, E. O. Luger, A. Inamine, K. G. Smith, T. Dorner, and F. Hiepe. Competence and competition: the challenge of becoming a long-lived plasma cell. *Nat. Rev. Immunol.*, 6(10):741–750, Oct 2006.

[93] Z. Xiang, A. J. Cutler, R. J. Brownlie, K. Fairfax, K. E. Lawlor, E. Severinson, E. U. Walker, R. A. Manz, D. M. Tarlinton, and K. G. Smith. FcgammaRIIb controls bone marrow plasma cell persistence and apoptosis. *Nat. Immunol.*, 8(4):419–429, Apr 2007.

[94] M. Cocco, S. Stephenson, Ma. Care, D. Newton, N. Barnes, et al. In vitro generation of long-lived human plasma cells. *The Journal of Immunology*, 189(12):5773–5785, 2012.

[95] A. Bortnick and D. Allman. What is and what should always have been: long-lived plasma cells induced by T cell-independent antigens. *J. Immunol.*, 190(12):5913–5918, Jun 2013.

[96] H. A. Minges Wols, G. H. Underhill, G. S. Kansas, and P. L. Witte. The role of bone marrow-derived stromal cells in the maintenance of plasma cell longevity. *J. Immunol.*, 169(8):4213–4221, Oct 2002.

[97] G. Cassese, S. Arce, A. E. Hauser, K. Lehnert, B. Moewes, M. Mostarac, G. Muehlinghaus, M. Szyska, A. Radbruch, and R. A. Manz. Plasma cell survival is mediated by synergistic effects of cytokines and adhesion-dependent signals. *J. Immunol.*, 171(4):1684–1690, Aug 2003.

[98] M. Okada, N. Sakaguchi, N. Yoshimura, H. Hara, K. Shimizu, N. Yoshida, K. Yoshizaki, S. Kishimoto, Y. Yamamura, and T. Kishimoto. B cell growth factors and B cell differentiation factor from human T hybridomas. Two distinct kinds of B cell growth factor and their synergism in B cell proliferation. *J. Exp. Med.*, 157(2):583–590, Feb 1983.

[99] M. Kawano, T. Hirano, T. Matsuda, T. Taga, Y. Horii, K. Iwato, H. Asaoku, B. Tang, O. Tanabe, and H. Tanaka. Autocrine generation and requirement of BSF-2/IL-6 for human multiple myelomas. *Nature*, 332(6159):83–85, Mar 1988.

[100] E. Roldan and J. A. Brieva. Terminal differentiation of human bone marrow cells capable of spontaneous and high-rate immunoglobulin secretion: role of bone marrow stromal cells and interleukin 6. *Eur. J. Immunol.*, 21(11):2671–2677, Nov 1991.

[101] D. Chauhan, S. Kharbanda, A. Ogata, M. Urashima, G. Teoh, M. Robertson, D. W. Kufe, and K. C. Anderson. Interleukin-6 inhibits Fas-induced apoptosis and stress-activated protein kinase activation in multiple myeloma cells. *Blood*, 89(1):227–234, Jan 1997.

[102] M. A. Frassanito, A. Cusmai, G. Iodice, and F. Dammacco. Autocrine interleukin-6 production and highly malignant multiple myeloma: relation with resistance to drug-induced apoptosis. *Blood*, 97(2):483–489, Jan 2001.

[103] N. Giuliani, P. Storti, M. Bolzoni, B. D. Palma, and S. Bonomini. Angiogenesis and multiple myeloma. *Cancer Microenviron*, 4(3):325–337, Dec 2011.

[104] B. Dankbar, T. Padro, R. Leo, B. Feldmann, M. Kropff, R. M. Mesters, H. Serve, W. E. Berdel, and J. Kienast. Vascular endothelial growth factor and interleukin-6 in paracrine tumor-stromal cell interactions in multiple myeloma. *Blood*, 95(8):2630–2636, Apr 2000.

[105] A. Vacca, D. Ribatti, L. Roncali, G. Ranieri, G. Serio, F. Silvestris, and F. Dammacco. Bone marrow angiogenesis and progression in multiple myeloma. *Br. J. Haematol.*, 87(3):503–508, Jul 1994.

[106] D. Gupta, S. P. Treon, Y. Shima, T. Hideshima, K. Podar, et al. Adherence of multiple myeloma cells to bone marrow stromal cells upregulates vascular endothelial growth factor secretion: therapeutic applications. *Leukemia*, 15(12):1950–1961, Dec 2001.

[107] S. Le Gouill, K. Podar, M. Amiot, T. Hideshima, D. Chauhan, K. Ishitsuka, S. Kumar, N. Raje, P. G. Richardson, J. L. Harousseau, and K. C. Anderson. VEGF induces Mcl-1 up-regulation and protects multiple myeloma cells against apoptosis. *Blood*, 104(9):2886–2892, Nov 2004.

[108] M. Urashima, A. Ogata, D. Chauhan, M. Hatziyanni, M. B. Vidriales, D. A. Dedera, R. L. Schlossman, and K. C. Anderson. Transforming growth factor-beta1: differential effects on multiple myeloma versus normal B cells. *Blood*, 87(5):1928–1938, Mar 1996.

[109] R. Castriconi, C. Cantoni, M. Della Chiesa, M. Vitale, E. Marcenaro, R. Conte, R. Biassoni, C. Bottino, L. Moretta, and A. Moretta. Transforming growth factor beta 1 inhibits expression of NKp30 and NKG2D receptors: consequences for the NK-mediated killing of dendritic cells. *Proc. Natl. Acad. Sci. U.S.A.*, 100(7):4120–4125, Apr 2003.

[110] S. Huber, C. Schramm, H. A. Lehr, A. Mann, S. Schmitt, C. Becker, M. Protschka, P. R. Galle, M. F. Neurath, and M. Blessing. Cutting edge: TGF-beta signaling is required for the in vivo expansion and immunosuppressive capacity of regulatory CD4+CD25+ T cells. *J. Immunol.*, 173(11):6526–6531, Dec 2004.

[111] K. Takeuchi, M. Abe, M. Hiasa, A. Oda, H. Amou, S. Kido, T. Harada, O. Tanaka, H. Miki, S. Nakamura, A. Nakano, K. Kagawa, K. Yata, S. Ozaki, and T. Matsumoto. Tgf-Beta inhibition restores terminal osteoblast differentiation to suppress myeloma growth. *PLoS ONE*, 5(3):e9870, Mar 2010.

[112] J. Moreaux, E. Legouffe, E. Jourdan, P. Quittet, T. Reme, C. Lugagne, P. Moine, J. F. Rossi, B. Klein, and K. Tarte. BAFF and APRIL protect myeloma cells from apoptosis induced by interleukin 6 deprivation and dexamethasone. *Blood*, 103(8):3148–3157, Apr 2004.

[113] B. P. O'Connor, V. S. Raman, L. D. Erickson, W. J. Cook, L. K. Weaver, C. Ahonen, L. L. Lin, G. T. Mantchev, R. J. Bram, and R. J. Noelle. BCMA is essential for the survival of long-lived bone marrow plasma cells. *J. Exp. Med.*, 199(1):91–98, Jan 2004.

[114] M. J. Benson, S. R. Dillon, E. Castigli, R. S. Geha, S. Xu, K. P. Lam, and R. J. Noelle. Cutting edge: the dependence of plasma cells and independence of memory B cells on BAFF and APRIL. *J. Immunol.*, 180(6):3655–3659, Mar 2008.

[115] T. Matthes, I. Dunand-Sauthier, M. L. Santiago-Raber, K. H. Krause, O. Donze, J. Passweg, T. McKee, and B. Huard. Production of the plasma-cell survival factor a proliferation-inducing ligand (APRIL) peaks in myeloid precursor cells from human bone marrow. *Blood*, 118(7):1838–1844, Aug 2011.

[116] F. Melchers. Actions of BAFF in B cell maturation and its effects on the development of autoimmune disease. *Ann. Rheum. Dis.*, 62 Suppl 2:i25–27, Nov 2003.

[117] J. Quinn, J. Glassford, L. Percy, P. Munson, T. Marafioti, M. Rodriguez-Justo, and K. Yong. APRIL promotes cell-cycle progression in primary multiple myeloma cells: influence of D-type cyclin group and translocation status. *Blood*, 117(3):890–901, Jan 2011.

[118] Y. T. Tai, X. F. Li, I. Breitkreutz, W. Song, P. Neri, et al. Role of B-cell-activating factor in adhesion and growth of human multiple myeloma cells in the bone marrow microenvironment. *Cancer Res.*, 66(13):6675–6682, Jul 2006.

[119] G. An, C. Acharya, X. Feng, K. Wen, M. Zhong, L. Zhang, N. C. Munshi, L. Qiu, Y. T. Tai, and K. C. Anderson. Osteoclasts promote immune suppressive microenvironment in multiple myeloma: therapeutic implication. *Blood*, 128(12):1590–1603, Sep 2016.

[120] Y. T. Tai, L. Lin, L. Xing, S. F. Cho, T. Yu, C. Acharya, K. Wen, P. A. Hsieh, J. Dulos, A. van Elsas, N. Munshi, P. Richardson, and K. C. Anderson. APRIL signaling via TACI mediates immunosuppression by T regulatory cells in multiple myeloma: therapeutic implications. *Leukemia*, Aug 2018.

[121] K. Tokoyoda, T. Egawa, T. Sugiyama, B. I. Choi, and T. Nagasawa. Cellular niches controlling B lymphocyte behavior within bone marrow during development. *Immunity*, 20(6):707–718, Jun 2004.

[122] M. Drew, H. F. Barker, J. Ball, C. Pearson, G. Cook, and I. Franklin. Very late antigen (VLA) expression by normal and neoplastic human plasma cells; including an assessment of antibodies submitted to the Vth International Workshop on Leucocyte Differentiation Antigens using human myeloma cell lines. *Leuk. Res.*, 20(7):619–624, Jul 1996.

[123] G. H. Underhill, H. A. Minges Wols, J. L. Fornek, P. L. Witte, G. S. Kansas, and H. A. Minges-Wols. IgG plasma cells display a unique spectrum of leukocyte adhesion and homing molecules. *Blood*, 99(8):2905–2912, Apr 2002.

[124] Y. Nefedova, T. H. Landowski, and W. S. Dalton. Bone marrow stromal-derived soluble factors and direct cell contact contribute to de novo drug resistance of myeloma cells by distinct mechanisms. *Leukemia*, 17(6):1175–1182, Jun 2003.

[125] K. Noborio-Hatano, J. Kikuchi, M. Takatoku, R. Shimizu, T. Wada, M. Ueda, M. Nobuyoshi, I. Oh, K. Sato, T. Suzuki, K. Ozaki, M. Mori, T. Nagai, K. Muroi, Y. Kano, Y. Furukawa, and K. Ozawa. Bortezomib overcomes cell-adhesion-mediated drug resistance through downregulation of VLA-4 expression in multiple myeloma. *Oncogene*, 28(2):231–242, Jan 2009.

[126] R. Schmidmaier, P. Baumann, M. Simsek, F. Dayyani, B. Emmerich, and G. Meinhardt. The HMG-CoA reductase inhibitor simvastatin overcomes cell adhesion-mediated drug resistance in multiple myeloma by geranylgeranylation of Rho protein and activation of Rho kinase. *Blood*, 104(6):1825–1832, Sep 2004.

[127] V. T. Chu, A. Frohlich, G. Steinhauser, T. Scheel, T. Roch, S. Fillatreau, J. J. Lee, M. Lohning, and C. Berek. Eosinophils are required for the maintenance of plasma cells in the bone marrow. *Nat. Immunol.*, 12(2):151–159, Feb 2011.

[128] F. Davoine and P. Lacy. Eosinophil cytokines, chemokines, and growth factors: emerging roles in immunity. *Front Immunol*, 5:570, 2014.

[129] T. W. Wong, H. Kita, C. A. Hanson, D. K. Walters, B. K. Arendt, and D. F. Jelinek. Induction of malignant plasma cell proliferation by eosinophils. *PLoS ONE*, 8(7):e70554, 2013.

[130] S. Zehentmeier, K. Roth, Z. Cseresnyes, O. Sercan, K. Horn, R. A. Niesner, H. D. Chang, A. Radbruch, and A. E. Hauser. Static and dynamic components synergize to form a stable survival niche for bone marrow plasma cells. *Eur. J. Immunol.*, 44(8):2306–2317, Aug 2014.

[131] C. Yu, A. B. Cantor, H. Yang, C. Browne, R. A. Wells, Y. Fujiwara, and S. H. Orkin. Targeted deletion of a high-affinity GATA-binding site in the GATA-1 promoter leads to selective loss of the eosinophil lineage in vivo. *J. Exp. Med.*, 195(11):1387–1395, Jun 2002.

[132] D. Wong, O. Winter, C. Hartig, S. Siebels, M. Szyska, B. Tiburzy, L. Meng, U. Kulkarni, A. Fahnrich, K. Bommert, R. Bargou, C. Berek, V. T. Chu, B. Bogen, F. Jundt, and R. A. Manz. Eosinophils and megakaryocytes support the early growth of murine MOPC315 myeloma cells in their bone marrow niches. *PLoS ONE*, 9(10):e109018, 2014.

[133] R. R. Redfield, E. Rodriguez, Y. Luo, S. Rostami, R. F. Parsons, H. Noorchashm, P. L. Abt, and A. Naji. Interleukin 5 immunotherapy depletes alloreactive plasma cells. *J. Surg. Res.*, 187(1):310–315, Mar 2014.

[134] P. Cravedi, D. A. Lessman, and P. S. Heeger. Eosinophils are not required for the induction and maintenance of an alloantibody response. *Am. J. Transplant.*, 13(10):2696–2702, Oct 2013.

[135] A. Bortnick, I. Chernova, S. P. Spencer, and D. Allman. No strict requirement for eosinophils for bone marrow plasma cell survival. *Eur. J. Immunol.*, 48(5):815–821, May 2018.

[136] K. Haberland, J. A. Ackermann, N. Ipseiz, S. Culemann, K. Pracht, M. Englbrecht, H. M. Jack, G. Schett, W. Schuh, and G. Kronke. Eosinophils are not essential for maintenance of murine plasma cells in the bone marrow. *Eur. J. Immunol.*, 48(5):822–828, May 2018.

[137] Y. Nei, K. Obata-Ninomiya, H. Tsutsui, K. Ishiwata, M. Miyasaka, K. Matsumoto, S. Nakae, H. Kanuka, N. Inase, and H. Karasuyama. GATA-1 regulates the generation and function of basophils. *Proc. Natl. Acad. Sci. U.S.A.*, 110(46):18620–18625, Nov 2013.

[138] A. Straumann. Antieosinophil Therapeutics. In J. Lee and H. Rosenberg, editors, *Eosinophils in Health and Disease*, chapter 2, pages 11–35. Springer Basel, Basel, 2014.

[139] E. Belnoue, C. Tougne, A. F. Rochat, P. H. Lambert, D. D. Pinschewer, and C. A. Siegrist. Homing and adhesion patterns determine the cellular composition of the bone marrow plasma cell niche. *J. Immunol.*, 188(3):1283–1291, Feb 2012.

[140] S. Wichert, A. Pettersson, T. Hellmark, A. Johansson, and M. Hansson. Bone marrow eosinophils in plasma cell disorders. *Exp. Hematol.*, 66:27–31, Oct 2018.

[141] K. Beider, H. Bitner, M. Leiba, O. Gutwein, M. Koren-Michowitz, O. Ostrovsky, M. Abraham, H. Wald, E. Galun, A. Peled, and A. Nagler. Multiple myeloma cells recruit tumor-supportive macrophages through the CXCR4/CXCL12 axis and promote their polarization toward the M2 phenotype. *Oncotarget*, 5(22):11283–11296, Nov 2014.

[142] C. Scavelli, B. Nico, T. Cirulli, R. Ria, G. Di Pietro, D. Mangieri, A. Bacigalupo, G. Mangialardi, A. M. Coluccia, T. Caravita, S. Molica, D. Ribatti, F. Dammacco, and A. Vacca. Vasculogenic mimicry by bone marrow macrophages in patients with multiple myeloma. *Oncogene*, 27(5):663–674, Jan 2008.

[143] Y. Li, Y. Zheng, T. Li, Q. Wang, J. Qian, Y. Lu, M. Zhang, E. Bi, M. Yang, F. Reu, Q. Yi, and Z. Cai. Chemokines CCL2, 3, 14 stimulate macrophage bone marrow homing, proliferation, and polarization in multiple myeloma. *Oncotarget*, 6(27):24218–24229, Sep 2015.

[144] L. Freire-de Lima, A. F. F. R. Nardy, E. S. Ramos-Junior, L. Conde, J. Santos Lemos, L. M. da Fonseca, J. E. Lima, A. Maiolino, and A. Morrot. Multiple Myeloma Cells Express Key Immunoregulatory Cytokines and Modulate the Monocyte Migratory Response. *Front Med (Lausanne)*, 4:92, 2017.

[145] D. Kim, J. Wang, S. B. Willingham, R. Martin, G. Wernig, and I. L. Weissman. Anti-CD47 antibodies promote phagocytosis and inhibit the growth of human myeloma cells. *Leukemia*, 26(12):2538–2545, Dec 2012.

[146] X. Liu, H. Kwon, Z. Li, and Y. X. Fu. Is CD47 an innate immune checkpoint for tumor evasion? *J Hematol Oncol*, 10(1):12, Jan 2017.

[147] Y. Zheng, Z. Cai, S. Wang, X. Zhang, J. Qian, S. Hong, H. Li, M. Wang, J. Yang, and Q. Yi. Macrophages are an abundant component of myeloma microenvironment and protect myeloma cells from chemotherapy drug-induced apoptosis. *Blood*, 114(17):3625–3628, Oct 2009.

[148] K. Anton, D. Banerjee, and J. Glod. Macrophage-associated mesenchymal stem cells assume an activated, migratory, pro-inflammatory phenotype with increased IL-6 and CXCL10 secretion. *PLoS ONE*, 7(4):e35036, 2012.

[149] A. Ponzetta, G. Benigni, F. Antonangeli, G. Sciume, E. Sanseviero, A. Zingoni, M. R. Ricciardi, M. T. Petrucci, A. Santoni, and G. Bernardini. Multiple Myeloma Impairs Bone Marrow Localization of Effector Natural Killer Cells by Altering the Chemokine Microenvironment. *Cancer Res.*, 75(22):4766–4777, Nov 2015.

[150] Y. Zheng, J. Yang, J. Qian, P. Qiu, S. Hanabuchi, Y. Lu, Z. Wang, Z. Liu, H. Li, J. He, P. Lin, D. Weber, R. E. Davis, L. Kwak, Z. Cai, and Q. Yi. PSGL-1/selectin and ICAM-1/CD18 interactions are involved in macrophage-induced drug resistance in myeloma. *Leukemia*, 27(3):702–710, Mar 2013.

[151] O. Winter, K. Moser, E. Mohr, D. Zotos, H. Kaminski, M. Szyska, K. Roth, D. M. Wong, C. Dame, D. M. Tarlinton, H. Schulze, I. C. MacLennan, and R. A. Manz. Megakaryocytes constitute a functional component of a plasma cell niche in the bone marrow. *Blood*, 116(11):1867–1875, Sep 2010.

[152] M. V. Dhodapkar, K. M. Dhodapkar, and A. K. Palucka. Interactions of tumor cells with dendritic cells: balancing immunity and tolerance. *Cell Death Differ.*, 15(1):39–50, Jan 2008.

[153] D. Chauhan, A. V. Singh, M. Brahmandam, R. Carrasco, M. Bandi, et al. Functional interaction of plasmacytoid dendritic cells with multiple myeloma cells: a therapeutic target. *Cancer Cell*, 16(4):309–323, Oct 2009.

[154] P. Leone, S. Berardi, M. A. Frassanito, R. Ria, V. De Re, et al. Dendritic cells accumulate in the bone marrow of myeloma patients where they protect tumor plasma cells from CD8+ T-cell killing. *Blood*, 126(12):1443–1451, Sep 2015.

[155] N. Robillard, G. Jego, C. Pellat-Deceunynck, D. Pineau, D. Puthier, et al. CD28, a marker associated with tumoral expansion in multiple myeloma. *Clin. Cancer Res.*, 4(6):1521–1526, Jun 1998.

[156] J. R. Nair, L. M. Carlson, C. Koorella, C. H. Rozanski, G. E. Byrne, P. L. Bergsagel, J. P. Shaughnessy, L. H. Boise, A. Chanan-Khan, and K. P. Lee. CD28 expressed on malignant plasma cells induces a prosurvival and immunosuppressive microenvironment. *J. Immunol.*, 187(3):1243–1253, Aug 2011.

[157] C. Orabona, U. Grohmann, M. L. Belladonna, F. Fallarino, C. Vacca, R. Bianchi, S. Bozza, C. Volpi, B. L. Salomon, M. C. Fioretti, L. Romani, and P. Puccetti. CD28 induces immunostimulatory signals in dendritic cells via CD80 and CD86. *Nat. Immunol.*, 5(11):1134–1142, Nov 2004.

[158] R. D. Brown, B. Pope, A. Murray, W. Esdale, D. M. Sze, et al. Dendritic cells from patients with myeloma are numerically normal but functionally defective as they fail to up-regulate CD80 (B7-1) expression after huCD40LT stimulation because of inhibition by transforming growth factor-beta1 and interleukin-10. *Blood*, 98(10):2992–2998, Nov 2001.

[159] L. Martinez-Lostao, A. Anel, and J. Pardo. How Do Cytotoxic Lymphocytes Kill Cancer Cells? *Clin. Cancer Res.*, 21(22):5047–5056, Nov 2015.

[160] C. Zelle-Rieser, S. Thangavadivel, R. Biedermann, A. Brunner, P. Stoitzner, E. Willenbacher, R. Greil, and K. Johrer. T cells in multiple myeloma display features of exhaustion and senescence at the tumor site. *J Hematol Oncol*, 9(1):116, 11 2016.

[161] R. D. Brown, B. Pope, E. Yuen, J. Gibson, and D. E. Joshua. The expression of T cell related costimulatory molecules in multiple myeloma. *Leuk. Lymphoma*, 31(3-4):379–384, Oct 1998.

[162] J. Liu, A. Hamrouni, D. Wolowiec, V. Coiteux, K. Kuliczkowski, D. Hetuin, A. Saudemont, and B. Quesnel. Plasma cells from multiple myeloma patients express B7-H1 (PD-L1) and increase expression after stimulation with IFN-gamma and TLR ligands via a MyD88-, TRAF6-, and MEK-dependent pathway. *Blood*, 110(1):296–304, Jul 2007.

[163] A. Facciabene, G. T. Motz, and G. Coukos. T-regulatory cells: key players in tumor immune escape and angiogenesis. *Cancer Res.*, 72(9):2162–2171, May 2012.

[164] K. Giannopoulos, W. Kaminska, I. Hus, and A. Dmoszynska. The frequency of T regulatory cells modulates the survival of multiple myeloma patients: detailed characterisation of immune status in multiple myeloma. *Br. J. Cancer*, 106(3):546–552, Jan 2012.

[165] A. Glatman Zaretsky, C. Konradt, F. Depis, J. B. Wing, R. Goenka, et al. T Regulatory Cells Support Plasma Cell Populations in the Bone Marrow. *Cell Rep*, 18(8):1906–1916, Feb 2017.

[166] R. H. Prabhala, D. Pelluru, M. Fulciniti, H. K. Prabhala, P. Nanjappa, et al. Elevated IL-17 produced by TH17 cells promotes myeloma cell growth and inhibits immune function in multiple myeloma. *Blood*, 115(26):5385–5392, Jul 2010.

[167] K. Noonan, L. Marchionni, J. Anderson, D. Pardoll, G. D. Roodman, and I. Borrello. A novel role of IL-17-producing lymphocytes in mediating lytic bone disease in multiple myeloma. *Blood*, 116(18):3554–3563, Nov 2010.

[168] G. Di Lullo, M. Marcatti, S. Heltai, E. Brunetto, C. Tresoldi, A. Bondanza, C. Bonini, M. Ponzoni, G. Tonon, F. Ciceri, C. Bordignon, and M. P. Protti. Th22 cells increase in poor prognosis multiple myeloma and promote tumor cell growth and survival. *Oncoimmunology*, 4(5):e1005460, May 2015.

[169] H. J. Pegram, D. M. Andrews, M. J. Smyth, P. K. Darcy, and M. H. Kershaw. Activating and inhibitory receptors of natural killer cells. *Immunol. Cell Biol.*, 89(2):216–224, Feb 2011.

[170] V. Jurisic, T. Srdic, G. Konjevic, O. Markovic, and M. Colovic. Clinical stage-depending decrease of NK cell activity in multiple myeloma patients. *Med. Oncol.*, 24(3):312–317, 2007.

[171] R. T. Costello, A. Boehrer, C. Sanchez, D. Mercier, C. Baier, T. Le Treut, and G. Sebahoun. Differential expression of natural killer cell activating receptors in blood versus bone marrow in patients with monoclonal gammopathy. *Immunology*, 139(3):338–341, Jul 2013.

[172] D. M. Benson, C. E. Bakan, A. Mishra, C. C. Hofmeister, Y. Efebera, et al. The PD-1/PD-L1 axis modulates the natural killer cell versus multiple myeloma effect: a therapeutic target for CT-011, a novel monoclonal anti-PD-1 antibody. *Blood*, 116(13):2286–2294, Sep 2010.

[173] D. M. Benson, C. E. Bakan, A. Mishra, C. C. Hofmeister, Y. Efebera, et al. The PD-1/PD-L1 axis modulates the natural killer cell versus multiple myeloma effect: a therapeutic target for CT-011, a novel monoclonal anti-PD-1 antibody. *Blood*, 116(13):2286–2294, Sep 2010.

[174] M. J. Scott, J. J. Hoth, M. Turina, D. R. Woods, and W. G. Cheadle. Interleukin-10 suppresses natural killer cell but not natural killer T cell activation during bacterial infection. *Cytokine*, 33(2):79–86, Jan 2006.

[175] L. Cifaldi, G. Prencipe, I. Caiello, C. Bracaglia, F. Locatelli, F. De Benedetti, and R. Strippoli. Inhibition of natural killer cell cytotoxicity by interleukin-6: implications for the pathogenesis of macrophage activation syndrome. *Arthritis Rheumatol*, 67(11):3037–3046, Nov 2015.

[176] E. Carbone, P. Neri, M. Mesuraca, M. T. Fulciniti, T. Otsuki, D. Pende, V. Groh, T. Spies, G. Pollio, D. Cosman, L. Catalano, P. Tassone, B. Rotoli, and S. Venuta. HLA class I, NKG2D, and natural cytotoxicity receptors regulate multiple myeloma cell recognition by natural killer cells. *Blood*, 105(1):251–258, Jan 2005.

[177] M. Jinushi, M. Vanneman, N. C. Munshi, Y. T. Tai, R. H. Prabhala, J. Ritz, D. Neuberg, K. C. Anderson, D. R. Carrasco, and G. Dranoff. MHC class I chain-related protein A antibodies and shedding are associated with the progression of multiple myeloma. *Proc. Natl. Acad. Sci. U.S.A.*, 105(4):1285–1290, Jan 2008.

[178] J. Krejcik, T. Casneuf, I. S. Nijhof, B. Verbist, J. Bald, et al. Daratumumab depletes CD38+ immune regulatory cells, promotes T-cell expansion, and skews T-cell repertoire in multiple myeloma. *Blood*, 128(3):384–394, Jul 2016.

[179] L. Zhang, Y. T. Tai, M. Ho, L. Xing, D. Chauhan, A. Gang, L. Qiu, and K. C. Anderson. Regulatory B cell-myeloma cell interaction confers immunosuppression and promotes their survival in the bone marrow milieu. *Blood Cancer J*, 7(3):e547, Mar 2017.

[180] U. Lerner. Osteoblasts, Osteoclasts, and Osteocytes: Unveiling Their Intimate-Associated Responses to Applied Orthodontic Forces. *Seminars in Orthodontics*, 18(4):237–248, Dec 2012.

[181] M. Bolzoni, D. Toscani, F. Costa, E. Vicario, F. Aversa, and N. Giuliani. The link between bone microenvironment and immune cells in multiple myeloma: Emerging role of CD38. *Immunol. Lett.*, Apr 2018.

[182] N. Raje and G. D. Roodman. Advances in the biology and treatment of bone disease in multiple myeloma. *Clin. Cancer Res.*, 17(6):1278–1286, Mar 2011.

[183] E. Tian, F. Zhan, R. Walker, E. Rasmussen, Y. Ma, B. Barlogie, and J. D. Shaughnessy. The role of the Wnt-signaling antagonist DKK1 in the development of osteolytic lesions in multiple myeloma. *N. Engl. J. Med.*, 349(26):2483–2494, Dec 2003.

[184] A. Kukreja, S. Radfar, B. H. Sun, K. Insogna, and M. V. Dhodapkar. Dominant role of CD47-thrombospondin-1 interactions in myeloma-induced fusion of human dendritic cells: implications for bone disease. *Blood*, 114(16):3413–3421, Oct 2009.

[185] M. Attal, J. L. Harousseau, A. M. Stoppa, J. J. Sotto, J. G. Fuzibet, et al. A prospective, randomized trial of autologous bone marrow transplantation and chemotherapy in multiple myeloma. Intergroupe Français du Myélome. *N. Engl. J. Med.*, 335(2):91–97, Jul 1996.

[186] I. M. Konstantinova, A. S. Tsimokha, and A. G. Mittenberg. Role of proteasomes in cellular regulation. *Int Rev Cell Mol Biol*, 267:59–124, 2008.

[187] L. Kubiczkova, L. Pour, L. Sedlarikova, R. Hajek, and S. Sevcikova. Proteasome inhibitors - molecular basis and current perspectives in multiple myeloma. *J. Cell. Mol. Med.*, 18(6):947–961, Jun 2014.

[188] S. Meister, U. Schubert, K. Neubert, K. Herrmann, R. Burger, M. Gramatzki, S. Hahn, S. Schreiber, S. Wilhelm, M. Herrmann, H. M. Jack, and R. E. Voll. Extensive immunoglobulin production sensitizes myeloma cells for proteasome inhibition. *Cancer Res.*, 67(4):1783–1792, Feb 2007.

[189] P. G. Richardson, P. Sonneveld, M. Schuster, D. Irwin, E. Stadtmauer, et al. Extended follow-up of a phase 3 trial in relapsed multiple myeloma: final time-to-event results of the APEX trial. *Blood*, 110(10):3557–3560, Nov 2007.

[190] E. A. Zaal, W. Wu, G. Jansen, S. Zweegman, J. Cloos, and C. R. Berkers. Bortezomib resistance in multiple myeloma is associated with increased serine synthesis. *Cancer Metab*, 5:7, 2017.

[191] A. K. Stewart, S. V. Rajkumar, M. A. Dimopoulos, T. Masszi, I. Spicka, et al. Carfilzomib, lenalidomide, and dexamethasone for relapsed multiple myeloma. *N. Engl. J. Med.*, 372(2):142–152, Jan 2015.

[192] J. J. Shah, A. J. Jakubowiak, O. A. O'Connor, R. Z. Orlowski, et al. Phase I Study of the Novel Investigational NEDD8-Activating Enzyme Inhibitor Pevonedistat (MLN4924) in Patients with Relapsed/Refractory Multiple Myeloma or Lymphoma. *Clin. Cancer Res.*, 22(1):34–43, Jan 2016.

[193] K. B. OLSON, T. C. HALL, J. HORTON, C. L. KHUNG, and H. F. HOSLEY. THALIDOMIDE (N-PHTHALOYLGLUTAMIMIDE) IN THE TREATMENT OF ADVANCED CANCER. *Clin. Pharmacol. Ther.*, 6:292–297, 1965.

[194] S. Singhal, J. Mehta, R. Desikan, D. Ayers, P. Roberson, P. Eddlemon, N. Munshi, E. Anaissie, C. Wilson, M. Dhodapkar, J. Zeddis, and B. Barlogie. Antitumor activity of thalidomide in refractory multiple myeloma. *N. Engl. J. Med.*, 341(21):1565–1571, Nov 1999.

[195] F. E. Davies, N. Raje, T. Hideshima, S. Lentzsch, G. Young, et al. Thalidomide and immunomodulatory derivatives augment natural killer cell cytotoxicity in multiple myeloma. *Blood*, 98(1):210–216, Jul 2001.

[196] C. Galustian, B. Meyer, M. C. Labarthe, K. Dredge, D. Klaschka, et al. The anti-cancer agents lenalidomide and pomalidomide inhibit the proliferation and function of T regulatory cells. *Cancer Immunol. Immunother.*, 58(7):1033–1045, Jul 2009.

[197] T. Hideshima, D. Chauhan, Y. Shima, N. Raje, F. E. Davies, et al. Thalidomide and its analogs overcome drug resistance of human multiple myeloma cells to conventional therapy. *Blood*, 96(9):2943–2950, Nov 2000.

[198] Y. Liu, X. Huang, X. He, Y. Zhou, X. Jiang, S. Chen-Kiang, S. R. Jaffrey, and G. Xu. A novel effect of thalidomide and its analogs: suppression of cereblon ubiquitination enhances ubiquitin ligase function. *FASEB J.*, 29(12):4829–4839, Dec 2015.

[199] J. Kronke, N. D. Udeshi, A. Narla, P. Grauman, S. N. Hurst, et al. Lenalidomide causes selective degradation of IKZF1 and IKZF3 in multiple myeloma cells. *Science*, 343(6168):301–305, Jan 2014.

[200] P. G. Richardson, D. S. Siegel, R. Vij, C. C. Hofmeister, R. Baz, et al. Pomalidomide alone or in combination with low-dose dexamethasone in relapsed and refractory multiple myeloma: a randomized phase 2 study. *Blood*, 123(12):1826–1832, Mar 2014.

[201] Chad C Bjorklund, Jian Kang, Ling Lu, Michael Amatangelo, Hsiling Chiu, Patrick Hagner, Anita K. Gandhi, Michael Pourdehnad, Anke Klippel, and Anjan Thakurta. Cc-122 is a cereblon modulating agent that is active in lenalidomide-resistant and lenalidomide/dexamethasone-double-resistant multiple myeloma pre-clinical models. *Blood*, 128(22):1592–1592, 2016.

[202] J. Waldenstroem. MELPHALAN THERAPY IN MYELOMATOSIS. *Br Med J*, 1(5387):859–865, Apr 1964.

[203] B. L. Samuels and J. D. Bitran. High-dose intravenous melphalan: a review. *J. Clin. Oncol.*, 13(7):1786–1799, Jul 1995.

[204] U. D. Bayraktar, Q. Bashir, M. Qazilbash, R. E. Champlin, and S. O. Ciurea. Fifty years of melphalan use in hematopoietic stem cell transplantation. *Biol. Blood Marrow Transplant.*, 19(3):344–356, Mar 2013.

[205] S. Ito, T. Oyake, K. Murai, and Y. Ishida. Successful use of cyclophosphamide as an add-on therapy for multiple myeloma patients with acquired resistance to bortezomib or lenalidomide. *Case Rep Hematol*, 2013:651902, 2013.

[206] M. Cives, S. Ciavarella, F. M. Rizzo, M. De Matteo, F. Dammacco, and F. Silvestris. Bendamustine overcomes resistance to melphalan in myeloma cell lines by inducing cell death through mitotic catastrophe. *Cell. Signal.*, 25(5):1108–1117, May 2013.

[207] L. M. Leoni, B. Bailey, J. Reifert, H. H. Bendall, R. W. Zeller, J. Corbeil, G. Elliott, and C. C. Niemeyer. Bendamustine (Treanda) displays a distinct pattern of cytotoxicity and unique mechanistic features compared with other alkylating agents. *Clin. Cancer Res.*, 14(1):309–317, Jan 2008.

[208] W. Ponisch, B. Holzvogt, M. Plotze, M. Andrea, M. Bourgeois, et al. Bendamustine and prednisone in combination with bortezomib (BPV) in the treatment of patients with newly diagnosed/untreated multiple myeloma. *J. Cancer Res. Clin. Oncol.*, 140(11):1947–1956, Nov 2014.

[209] I. J. Lau, D. Smith, R. Aitchison, N. Blesing, P. Roberts, and others. Bendamustine in combination with thalidomide and dexamethasone is a viable salvage option in myeloma relapsed and/or refractory to bortezomib and lenalidomide. *Ann. Hematol.*, 94(4):643–649, Apr 2015.

[210] A. A. Lopez-Iglesias, A. B. Herrero, M. Chesi, L. San-Segundo, L. Gonzalez-Mendez, et al. Preclinical anti-myeloma activity of EDO-S101, a new bendamustine-derived molecule with added HDACi activity, through potent DNA damage induction and impairment of DNA repair. *J Hematol Oncol*, 10(1):127, Jun 2017.

[211] J. P. Laubach, C. J. Liu, N. S. Raje, A. J. Yee, P. Armand, et al. A Phase 1/2 Study of evofosfamide, A Hypoxia-Activated Prodrug with or without Bortezomib in Subjects with Relapsed/Refractory Multiple Myeloma. *Clin. Cancer Res.*, Oct 2018.

[212] M. Mateos, J. Bladé, A. Larocca, A. Oriol, P. Rodriguez, et al. Melflufen therapy for relapsed refractory multiple myeloma (rrmm) patients refractory to daratumumab and/or pomalidomide: A report on early efficacy. *Blood*, 130(Suppl 1):1841–1841, 2017.

[213] S. Sharma and A. Lichtenstein. Dexamethasone-induced apoptotic mechanisms in myeloma cells investigated by analysis of mutant glucocorticoid receptors. *Blood*, 112(4):1338–1345, Aug 2008.

[214] R. V. Sionov. MicroRNAs and Glucocorticoid-Induced Apoptosis in Lymphoid Malignancies. *ISRN Hematol*, 2013:348212, 2013.

[215] B. Sanchez-Vega, N. Krett, S. T. Rosen, and V. Gandhi. Glucocorticoid receptor transcriptional isoforms and resistance in multiple myeloma cells. *Mol. Cancer Ther.*, 5(12):3062–3070, Dec 2006.

[216] S. K. Kumar, J. H. Lee, J. J. Lahuerta, G. Morgan, P. G. Richardson, et al. Risk of progression and survival in multiple myeloma relapsing after therapy with IMiDs and bortezomib: a multicenter international myeloma working group study. *Leukemia*, 26(1):149–157, Jan 2012.

[217] J. F. San-Miguel, V. T. Hungria, S. S. Yoon, M. Beksac, M. A. Dimopoulos, and others. Overall survival of patients with relapsed multiple myeloma treated with panobinostat or placebo plus bortezomib and dexamethasone (the PANORAMA 1 trial): a randomised, placebo-controlled, phase 3 trial. *Lancet Haematol*, 3(11):e506–e515, Nov 2016.

[218] H. N. Abramson. The Multiple Myeloma Drug Pipeline-2018: A Review of Small Molecules and Their Therapeutic Targets. *Clin Lymphoma Myeloma Leuk*, 18(9):611–627, Sep 2018.

[219] A. Im and S. Z. Pavletic. Immunotherapy in hematologic malignancies: past, present, and future. *J Hematol Oncol*, 10(1):94, Apr 2017.

[220] H. M. Knochelmann, A. S. Smith, C. J. Dwyer, M. M. Wyatt, S. Mehrotra, and C. M. Paulos. CAR T Cells in Solid Tumors: Blueprints for Building Effective Therapies. *Front Immunol*, 9:1740, 2018.

[221] www.ClinicalTrials.gov. Accessed November 2018.

[222] Jesus G. Berdeja, Yi Lin, Noopur Raje, Nikhil Munshi, David Siegel, Michaela Liedtke, et al. Durable clinical responses in heavily pretreated patients with relapsed/refractory multiple myeloma: Updated results from a multicenter study of bb2121 anti-bcma car t cell therapy. *Blood*, 130(Suppl 1):740–740, 2017.

[223] D. W. Sherbenou, B. T. Aftab, Y. Su, C. R. Behrens, A. Wiita, and others. Antibody-drug conjugate targeting CD46 eliminates multiple myeloma cells. *J. Clin. Invest.*, 126(12):4640–4653, Dec 2016.

[224] C. M. Calton, K. R. Kelly, F. Anwer, J. S. Carew, and S. T. Nawrocki. Oncolytic Viruses for Multiple Myeloma Therapy. *Cancers (Basel)*, 10(6), Jun 2018.

[225] G. Salles, M. Barrett, R. Foa, J. Maurer, S. O'Brien, N. Valente, M. Wenger, and D. G. Maloney. Rituximab in B-Cell Hematologic Malignancies: A Review of 20 Years of Clinical Experience. *Adv Ther*, 34(10):2232–2273, Oct 2017.

[226] M. Suzuki, C. Kato, and A. Kato. Therapeutic antibodies: their mechanisms of action and the pathological findings they induce in toxicity studies. *J Toxicol Pathol*, 28(3):133–139, Jul 2015.

[227] A. L. Catapano and N. Papadopoulos. The safety of therapeutic monoclonal antibodies: implications for cardiovascular disease and targeting the PCSK9 pathway. *Atherosclerosis*, 228(1):18–28, May 2013.

[228] Kewal K. Jain. Aactions and Uses of Monoclonal Antibodies in Cancer. In Kewal K. Jain, editor, *Applications of Biotechnology in Oncology*, chapter 8, pages 371–391. Springer, Berlin, 2014.

[229] F. Malavasi, S. Deaglio, A. Funaro, E. Ferrero, A. L. Horenstein, E. Ortolan, T. Vaisitti, and S. Aydin. Evolution and function of the ADP ribosyl cyclase/CD38 gene family in physiology and pathology. *Physiol. Rev.*, 88(3):841–886, Jul 2008.

[230] M. de Weers, Y. T. Tai, M. S. van der Veer, J. M. Bakker, T. Vink, et al. Daratumumab, a novel therapeutic human CD38 monoclonal antibody, induces killing of multiple myeloma and other hematological tumors. *J. Immunol.*, 186(3):1840–1848, Feb 2011.

[231] M. B. Overdijk, S. Verploegen, M. Bogels, M. van Egmond, J. J. Lammerts van Bueren, and others. Antibody-mediated phagocytosis contributes to the anti-tumor activity of the therapeutic antibody daratumumab in lymphoma and multiple myeloma. *MAbs*, 7(2):311–321, 2015.

[232] S. Z. Usmani, B. M. Weiss, T. Plesner, N. J. Bahlis, A. Belch, et al. Clinical efficacy of daratumumab monotherapy in patients with heavily pretreated relapsed or refractory multiple myeloma. *Blood*, 128(1):37–44, Jul 2016.

[233] A. Spencer, S. Lentzsch, K. Weisel, H. Avet-Loiseau, T. M. Mark, et al. Daratumumab plus bortezomib and dexamethasone versus bortezomib and dexamethasone in relapsed or refractory multiple myeloma: updated analysis of CASTOR. *Haematologica*, Sep 2018.

[234] NICE. https://www.nice.org.uk/guidance/ta510/chapter/1-recommendations. Accessed October 2018.

[235] F. Costa, D. Toscani, A. Chillemi, V. Quarona, M. Bolzoni, et al. Expression of CD38 in myeloma bone niche: A rational basis for the use of anti-CD38 immunotherapy to inhibit osteoclast formation. *Oncotarget*, 8(34):56598–56611, Aug 2017.

[236] J. Deckert, M. C. Wetzel, L. M. Bartle, A. Skaletskaya, V. S. Goldmacher, and others. SAR650984, a novel humanized CD38-targeting antibody, demonstrates potent antitumor activity in models of multiple myeloma and other CD38+ hematologic malignancies. *Clin. Cancer Res.*, 20(17):4574–4583, Sep 2014.

[237] Ravi Vij, Nikoletta Lendvai, Thomas G. Martin, Rachid C. Baz, Frank Campana, Florent Mazuir, Eric Charpentier, and Don M. Benson. A phase ib dose escalation trial of isatuximab (sar650984, anti-cd38 mab) plus lenalidomide and dexamethasone (len/dex) in relapsed/refractory multiple myeloma (rrmm): Interim results from two new dose cohorts. *Journal of Clinical Oncology*, 34(15_suppl):8009–8009, 2016.

[238] E. D. Hsi, R. Steinle, B. Balasa, S. Szmania, A. Draksharapu, et al. CS1, a potential new therapeutic antibody target for the treatment of multiple myeloma. *Clin. Cancer Res.*, 14(9):2775–2784, May 2008.

[239] T. Pazina, A. M. James, A. W. MacFarlane, N. A. Bezman, K. A. Henning, C. Bee, R. F. Graziano, M. D. Robbins, A. D. Cohen, and K. S. Campbell. The anti-SLAMF7 antibody elotuzumab mediates NK cell activation through both CD16-dependent and -independent mechanisms. *Oncoimmunology*, 6(9):e1339853, 2017.

[240] J. A. Zonder, A. F. Mohrbacher, S. Singhal, F. van Rhee, W. I. Bensinger, et al. A phase 1, multicenter, open-label, dose escalation study of elotuzumab in patients with advanced multiple myeloma. *Blood*, 120(3):552–559, Jul 2012.

[241] M. A. Dimopoulos, S. Lonial, D. White, P. Moreau, A. Palumbo, J. San-Miguel, et al. Elotuzumab plus lenalidomide/dexamethasone for relapsed or refractory multiple myeloma: ELOQUENT-2 follow-up and post-hoc analyses on progression-free survival and tumour growth. *Br. J. Haematol.*, 178(6):896–905, Sep 2017.

[242] NICE. https://www.nice.org.uk/guidance/ta434. Accessed October 2018.

[243] Alexander M. Lesokhin, Stephen M. Ansell, Philippe Armand, Emma C. Scott, Ahmad Halwani, Martin Gutierrez, Michael M. Millenson, et al. Preliminary results of a phase i study of nivolumab (bms-936558) in patients with relapsed or refractory lymphoid malignancies. *Blood*, 124(21):291–291, 2014.

[244] Jesus San Miguel, Maria-Victoria Mateos, Jatin J. Shah, Enrique M. Ocio, Paula Rodriguez-Otero, et al. Pembrolizumab in combination with lenalidomide and low-dose dexamethasone for relapsed/refractory multiple myeloma (rrmm): Keynote-023. *Blood*, 126(23):505–505, 2015.

[245] Misty Jenkins, Rachael Canfield, Michael Robbins, David S. Ritchie, Joe Trapani, and Paul Neeson. Targeting mechanisms for natural killer cell dysfunction in patients with multiple myeloma. *Blood*, 126(23):4237–4237, 2015.

[246] E. G. Kim and K. M. Kim. Strategies and Advancement in Antibody-Drug Conjugate Optimization for Targeted Cancer Therapeutics. *Biomol Ther (Seoul)*, 23(6):493–509, Nov 2015.

[247] N. Jain, S. W. Smith, S. Ghone, and B. Tomczuk. Current adc linker chemistry. *Pharm. Res.*, 32(11):3526–3540, Nov 2015.

[248] L. Wang, G. Amphlett, W. A. Blattler, J. M. Lambert, and W. Zhang. Structural characterization of the maytansinoid-monoclonal antibody immunoconjugate, huN901-DM1, by mass spectrometry. *Protein Sci.*, 14(9):2436–2446, Sep 2005.

[249] H. Perez, P. Cardarelli, S. Deshpande, S. Gangwar, G Schroeder, et al. Antibody–drug conjugates: current status and future directions. *Drug Discovery Today*, 19(7):869–881, Jul 2014.

[250] J. Berdeja, F. Hernandez-Ilizaliturri, A. Chanan-Khan, M. Patel, K.. Kelly, K. Running, et al. Phase i study of lorvotuzumab mertansine (lm, imgn901) in combination with lenalidomide (len) and dexamethasone (dex) in patients with cd56-positive relapsed or relapsed/refractory multiple myeloma (mm). *Blood*, 120(21):728–728, 2012.

[251] A. Chanan-Khan, J. Wolf, J. Garcia, M. Gharibo, S. Jagannath, D. Manfredi, et al. Efficacy analysis from phase i study of lorvotuzumab mertansine (imgn901), used as monotherapy, in patients with heavily pre-treated cd56-positive multiple myeloma - a preliminary efficacy analysis. *Blood*, 116(21):1962–1962, 2010.

[252] L. Heffner, S. Jagannath, T. Zimmerman, K. Lee, J. Rosenblatt, and others. Bt062, an antibody-drug conjugate directed against cd138, given weekly for 3 weeks in each 4 week cycle: Safety and further evidence of clinical activity. *Blood*, 120(21):4042–4042, 2012.

[253] K. Kelly, D. Siegel, A. Chanan-Khan, G. Somlo, L. Heffner, et al. Indatuximab ravtansine (bt062) in combination with low-dose dexamethasone and lenalidomide or pomalidomide: Clinical activity in patients with relapsed / refractory multiple myeloma. *Blood*, 128(22):4486–4486, 2016.

[254] S. Trudel, N. Lendvai, R. Popat, P. Voorhees, B. Reeves, et al. Deep and durable responses in patients (pts) with relapsed/refractory multiple myeloma (mm) treated with monotherapy gsk2857916, an antibody drug conjugate against b-cell maturation antigen (bcma): Preliminary results from part 2 of study bma117159. *Blood*, 130(Suppl 1):741–741, 2017.

[255] M. Pick, V. Vainstein, N. Goldschmidt, D. Lavie, D. Libster, and others. Daratumumab resistance is frequent in advanced-stage multiple myeloma patients irrespective of CD38 expression and is related to dismal prognosis. *Eur. J. Haematol.*, 100(5):494–501, May 2018.

[256] J. P. Overington, B. Al-Lazikani, and A. L. Hopkins. How many drug targets are there? *Nat Rev Drug Discov*, 5(12):993–996, Dec 2006.

[257] My Cancer Genome. https://www.mycancergenome.org/content/molecular-medicine/overview-of-targeted-therapies-for-cancer/. Accessed September 2018.

[258] R. de Sousa Abreu, L. O. Penalva, E. M. Marcotte, and C. Vogel. Global signatures of protein and mRNA expression levels. *Mol Biosyst*, 5(12):1512–1526, Dec 2009.

[259] Y. Guo, P. Xiao, S. Lei, F. Deng, G. G. Xiao, et al. How is mRNA expression predictive for protein expression? A correlation study on human circulating monocytes. *Acta Biochim. Biophys. Sin. (Shanghai)*, 40(5):426–436, May 2008.

[260] U. T. Shankavaram, W. C. Reinhold, S. Nishizuka, S. Major, D. Morita, et al. Transcript and protein expression profiles of the NCI-60 cancer cell panel: an integromic microarray study. *Mol. Cancer Ther.*, 6(3):820–832, Mar 2007.

[261] D. Dytfeld, S. Rosebeck, M. Kandarpa, A. Mayampurath, D. Mellacheruvu, et al. Proteomic profiling of naïve multiple myeloma patient plasma cells identifies pathways associated with favourable response to bortezomib-based treatment regimens. *Br. J. Haematol.*, 170(1):66–79, Jul 2015.

[262] N. Jackson, N. R. Ling, J. Ball, E. Bromidge, P. D. Nathan, and I. M. Franklin. An analysis of myeloma plasma cell phenotype using antibodies defined at the IIIrd International Workshop on Human Leucocyte Differentiation Antigens. *Clin. Exp. Immunol.*, 72(3):351–356, Jun 1988.

[263] N. Hosen, H. Ichihara, A. Mugitani, Y. Aoyama, Y. Fukuda, et al. CD48 as a novel molecular target for antibody therapy in multiple myeloma. *Br. J. Haematol.*, 156(2):213–224, Jan 2012.

[264] V. E. Muccio, E. Saraci, M. Gilestro, V. Gattei, A. Zucchetto, M. Astolfi, M. Ruggeri, E. Marzanati, R. Passera, A. Palumbo, M. Boccadoro, and P. Omede. Multiple myeloma: New surface antigens for the characterization of plasma cells in the era of novel agents. *Cytometry B Clin Cytom*, 90(1):81–90, Jan 2016.

[265] G. Giorgi. Mass spectrometry and high resolution mass spectrometry: An overview. In Banoub J. and Caprioli R., editors, *Molecular Technologies for Detection of Chemical and Biological Agents. NATO Science for Peace and Security Series A: Chemistry and Biology.*, chapter 5, pages 89–101. Springer, Dordrecht, 2017.

[266] W. Dormeyer, D. van Hoof, C. L. Mummery, J. Krijgsveld, and A. J. Heck. A practical guide for the identification of membrane and plasma membrane proteins in human embryonic stem cells and human embryonal carcinoma cells. *Proteomics*, 8(19):4036–4053, Oct 2008.

[267] S. Magdeldin, S. Enany, Y. Yoshida, B. Xu, Y. Zhang, Z. Zureena, I. Lokamani, E. Yaoita, and T. Yamamoto. Basics and recent advances of two dimensional- polyacrylamide gel electrophoresis. *Clin Proteomics*, 11(1):16, 2014.

[268] A. E. Speers and C. C. Wu. Proteomics of integral membrane proteins–theory and application. *Chem. Rev.*, 107(8):3687–3714, Aug 2007.

[269] K. Chandramouli and P. Y. Qian. Proteomics: challenges, techniques and possibilities to overcome biological sample complexity. *Hum Genomics Proteomics*, 2009, Dec 2009.

[270] R. Cao, X. Li, Z. Liu, X. Peng, W. Hu, X. Wang, P. Chen, J. Xie, and S. Liang. Integration of a two-phase partition method into proteomics research on rat liver plasma membrane proteins. *J. Proteome Res.*, 5(3):634–642, Mar 2006.

[271] L. J. Zhang, X. E. Wang, X. Peng, Y. J. Wei, R. Cao, Z. Liu, J. X. Xiong, X. F. Yin, C. Ping, and S. Liang. Proteomic analysis of low-abundant integral plasma membrane proteins based on gels. *Cell. Mol. Life Sci.*, 63(15):1790–1804, Aug 2006.

[272] Mark Holland, Fernanda V Castro, Seema Alexander, Duncan Smith, Jizhong Liu, et al. Rac2, aep, and icam1 expression are associated with cns disease in a mouse model of pre-b childhood acute lymphoblastic leukemia. *Blood*, 2011.

[273] A. R. Blackler, A. E. Speers, M. S. Ladinsky, and C. C. Wu. A shotgun proteomic method for the identification of membrane-embedded proteins and peptides. *J. Proteome Res.*, 7(7):3028–3034, Jul 2008.

[274] Y. Kim, S. Elschenbroich, P. Sharma, L. Sepiashvili, A. O. Gramolini, and T. Kislinger. Use of colloidal silica-beads for the isolation of cell-surface proteins for mass spectrometry-based proteomics. *Methods Mol. Biol.*, 748:227–241, 2011.

[275] W. Choksawangkarn, S. K. Kim, J. R. Cannon, N. J. Edwards, S. B. Lee, and C. Fenselau. Enrichment of plasma membrane proteins using nanoparticle pellicles: comparison between silica and higher density nanoparticles. *J. Proteome Res.*, 12(3):1134–1141, Mar 2013.

[276] E. Durr, J. Yu, K. M. Krasinska, L. A. Carver, J. R. Yates, et al. Direct proteomic mapping of the lung microvascular endothelial cell surface in vivo and in cell culture. *Nat. Biotechnol.*, 22(8):985–992, Aug 2004.

[277] A. M. Rahbar and C. Fenselau. Integration of Jacobson's pellicle method into proteomic strategies for plasma membrane proteins. *J. Proteome Res.*, 3(6):1267–1277, 2004.

[278] W. Choksawangkarn, N. Edwards, Y. Wang, P. Gutierrez, and C. Fenselau. Comparative study of workflows optimized for in-gel, in-solution, and on-filter proteolysis in the analysis of plasma membrane proteins. *J. Proteome Res.*, 11(5):3030–3034, May 2012.

[279] K. B. Chandler and C. E. Costello. Glycomics and glycoproteomics of membrane proteins and cell-surface receptors: Present trends and future opportunities. *Electrophoresis*, 37(11):1407–1419, Jun 2016.

[280] Y. Liu, J. He, and D. Lubman. Characterization of membrane-associated glycoproteins using lectin affinity chromatography and mass spectrometry. In Kohler J. and Patrie S., editors, *Mass Spectrometry of Glycoproteins. Methods in Molecular Biology (Methods and Protocols)*, pages 69–77. Humana Press, Totowa, NJ, 2013.

[281] H. Zhang, X. J. Li, D. B. Martin, and R. Aebersold. Identification and quantification of N-linked glycoproteins using hydrazide chemistry, stable isotope labeling and mass spectrometry. *Nat. Biotechnol.*, 21(6):660–666, Jun 2003.

[282] J. Li, J. Gao, M. Jiang, J. Chen, Z. Liu, et al. Rat liver sinusoidal surface N-linked glycoproteomic analysis by affinity enrichment and mass spectrometric identification. *Biochemistry Mosc.*, 80(3):260–275, Mar 2015.

[283] D. Ghosh, R. C. Beavis, and J. A. Wilkins. The identification and characterization of membranome components. *J. Proteome Res.*, 7(4):1572–1583, Apr 2008.

[284] M. P. Weekes, R. Antrobus, J. R. Lill, L. M. Duncan, S. Hor, and P. J. Lehner. Comparative analysis of techniques to purify plasma membrane proteins. *J Biomol Tech*, 21(3):108–115, Sep 2010.

[285] Y. Zhao, W. Zhang, M. A. White, and Y. Zhao. Capillary high-performance liquid chromatography/mass spectrometric analysis of proteins from affinity-purified plasma membrane. *Anal. Chem.*, 75(15):3751–3757, Aug 2003.

[286] Yingxin Zhao, Wei Zhang, Yoonjung Kho, and Yingming Zhao. Proteomic analysis of integral plasma membrane proteins. *Analytical Chemistry*, 76(7):1817–1823, 2004. PMID: 15053638.

[287] Y. Zeng, T. N. Ramya, A. Dirksen, P. E. Dawson, and J. C. Paulson. High-efficiency labeling of sialylated glycoproteins on living cells. *Nat. Methods*, 6(3):207–209, Mar 2009.

[288] M. P. Weekes, R. Antrobus, S. Talbot, S. Hor, N. Simecek, et al. Proteomic plasma membrane profiling reveals an essential role for gp96 in the cell surface expression of LDLR family members, including the LDL receptor and LRP6. *J. Proteome Res.*, 11(3):1475–1484, Mar 2012.

[289] M. P. Weekes, S. Y. Tan, E. Poole, S. Talbot, R. Antrobus, D. L. Smith, C. Montag, S. P. Gygi, J. H. Sinclair, and P. J. Lehner. Latency-associated degradation of the MRP1 drug transporter during latent human cytomegalovirus infection. *Science*, 340(6129):199–202, Apr 2013.

[290] J. L. Hsu, D. J. van den Boomen, P. Tomasec, M. P. Weekes, R. Antrobus, et al. Plasma membrane profiling defines an expanded class of cell surface proteins selectively targeted for degradation by HCMV US2 in cooperation with UL141. *PLoS Pathog.*, 11(4):e1004811, Apr 2015.

[291] M. Wang, J. You, K. G. Bemis, T. J. Tegeler, and D. P. Brown. Label-free mass spectrometry-based protein quantification technologies in proteomic analysis. *Brief Funct Genomic Proteomic*, 7(5):329–339, Sep 2008.

[292] E. L. Hendrickson, Q. Xia, T. Wang, J. A. Leigh, and M. Hackett. Comparison of spectral counting and metabolic stable isotope labeling for use with quantitative microbial proteomics. *Analyst*, 131(12):1335–1341, Dec 2006.

[293] T. S. Collier, P. Sarkar, W. L. Franck, B. M. Rao, R. A. Dean, and D. C. Muddiman. Direct comparison of stable isotope labeling by amino acids in cell culture and spectral counting for quantitative proteomics. *Anal. Chem.*, 82(20):8696–8702, Oct 2010.

[294] In T. Letzel and E. Smith, editors, *Protein and peptide analysis by LC-MS: experimental strategies (RSC Chromatography Monographs).* Royal Society of Chemistry, Cambridge, 2011.

[295] F. Ge, C. L. Xiao, L. J. Bi, S. C. Tao, S. Xiong, et al. Quantitative phosphoproteomics of proteasome inhibition in multiple myeloma cells. *PLoS ONE*, 5(9), Sep 2010.

[296] F. Ge, W. L. Li, L. J. Bi, S. C. Tao, Z. P. Zhang, and X. E. Zhang. Identification of novel 14-3-3Î¶ interacting proteins by quantitative immunoprecipitation combined with knockdown (QUICK). *J. Proteome Res.*, 9(11):5848–5858, Nov 2010.

[297] Y. Shiio and R. Aebersold. Quantitative proteome analysis using isotope-coded affinity tags and mass spectrometry. *Nat Protoc*, 1(1):139–145, 2006.

[298] A. Thompson, J. Schafer, K. Kuhn, S. Kienle, J. Schwarz, G. Schmidt, T. Neumann, R. Johnstone, A. K. Mohammed, and C. Hamon. Tandem mass tags: a novel quantification strategy for comparative analysis of complex protein mixtures by MS/MS. *Anal. Chem.*, 75(8):1895–1904, Apr 2003.

[299] D. Dytfeld, M. Hari, J. Strahler, D. Mellacheruvu, S. Subramani, et al. Proteomic profiling of multiple myeloma using itraq labeling followed by multidimensional liquid chromatography and tandem mass spectrometry. *Blood*, 114(22):4865–4865, 2009.

[300] M. S. Kim, S. M. Pinto, D. Getnet, R. S. Nirujogi, S. S. Manda, and others. A draft map of the human proteome. *Nature*, 509(7502):575–581, May 2014.

[301] M. Uhlen, L. Fagerberg, B. M. Hallstrom, C. Lindskog, P. Oksvold, et al. Proteomics. Tissue-based map of the human proteome. *Science*, 347(6220):1260419, Jan 2015.

[302] M. Wilhelm, J. Schlegl, H. Hahne, A. M. Gholami, M. Lieberenz, et al. Mass-spectrometry-based draft of the human proteome. *Nature*, 509(7502):582–587, May 2014.

[303] J. Moreaux, B. Klein, R. Bataille, G. Descamps, S. Maïga, D Hose, et al. A high-risk signature for patients with multiple myeloma established from the molecular classification of human myeloma cell lines. *Haematologica*, 96(4):574–582, 2011.

[304] X. Li, A. Pennisi, F. Zhan, J. R. Sawyer, J. D. Shaughnessy, and S. Yaccoby. Establishment and exploitation of hyperdiploid and non-hyperdiploid human myeloma cell lines. *Br. J. Haematol.*, 138(6):802–811, Sep 2007.

[305] F. Edfors, F. Danielsson, B. M. Hallstrom, L. Kall, E. Lundberg, F. Ponten, B. Forsstrom, and M. Uhlen. Gene-specific correlation of RNA and protein levels in human cells and tissues. *Mol. Syst. Biol.*, 12(10):883, Oct 2016.

[306] K. L. Good, D. T. Avery, and S. G. Tangye. Resting human memory B cells are intrinsically programmed for enhanced survival and responsiveness to diverse stimuli compared to naive B cells. *J. Immunol.*, 182(2):890–901, Jan 2009.

[307] S Szmania, B Balasa, P. Malaviarachchi, F. Zhan, Y. Huang, et al. CS1 is expressed on myeloma cells from early stage, late stage, and drug-treated multiple myeloma patients, and is selectively targeted by the Huluc63 Antibody. *Blood*, 108(11):660–660, 2006.

[308] R de Tute. CD319/CS1 expression patterns in WM, myeloma and MGUS: implications for antibody therapy. Poster presented at: the Eighth International Workshop on Waldenström's Macroglobulinemia. August 13-17, 2014. London, UK.

[309] Katharina Lisenko, Stefan Schönland, Ute Hegenbart, Katrin Wallenwein, Ute Braun, Elias K. Mai, Jens Hillengass, Hartmut Goldschmidt, Anna Jauch, Anthony D. Ho, Marc Raab, and Michael Hundemer. Potential therapeutic targets in plasma cell disorders: A flow cytometry study. *Cytometry Part B: Clinical Cytometry*, 92(2):145–152, 2015.

[310] Roger Higdon and Eugene Kolker. A predictive model for identifying proteins by a single peptide match. *Bioinformatics*, 23(3):277–280, 2007.

[311] M. A. Tabrizi, C. M. Tseng, and L. K. Roskos. Elimination mechanisms of therapeutic monoclonal antibodies. *Drug Discov. Today*, 11(1-2):81–88, Jan 2006.

[312] P. Haste Andersen, M. Nielsen, and O. Lund. Prediction of residues in discontinuous B-cell epitopes using protein 3D structures. *Protein Sci.*, 15(11):2558–2567, Nov 2006.

[313] C. G. Tate, J. Haase, C. Baker, M. Boorsma, F. Magnani, Y. Vallis, and D. C. Williams. Comparison of seven different heterologous protein expression systems for the production of the serotonin transporter. *Biochim. Biophys. Acta*, 1610(1):141–153, Feb 2003.

[314] J. Andrell and C. G. Tate. Overexpression of membrane proteins in mammalian cells for structural studies. *Mol. Membr. Biol.*, 30(1):52–63, Feb 2013.

[315] B. Sauer. Site-specific recombination: developments and applications. *Curr. Opin. Biotechnol.*, 5(5):521–527, Oct 1994.

[316] L. Bryant, O. Lozynska, G. Han, J. I. W. Morgan, X. Gai, A. M. Maguire, T. Aleman, and J. Bennett. On variants and disease-causing mutations: Case studies of a SEMA4A variant identified in inherited blindness. *Ophthalmic Genet.*, 39(1):144–146, 2018.

[317] J. Porath, J. Carlsson, I. Olsson, and G. Belfrage. Metal chelate affinity chromatography, a new approach to protein fractionation. *Nature*, 258(5536):598–599, Dec 1975.

[318] M. C. Deller, L. Kong, and B. Rupp. Protein stability: a crystallographer's perspective. *Acta Crystallogr F Struct Biol Commun*, 72(Pt 2):72–95, Feb 2016.

[319] M. D. Kohls and D. A. Lappi. Mab-ZAP: a tool for evaluating antibody efficacy for use in an immunotoxin. *BioTechniques*, 28(1):162–165, Jan 2000.

[320] A. Kumanogoh, S. Marukawa, K. Suzuki, N. Takegahara, C. Watanabe, E. Ch'ng, I. Ishida, H. Fujimura, S. Sakoda, K. Yoshida, and H. Kikutani. Class IV semaphorin Sema4A enhances T-cell activation and interacts with Tim-2. *Nature*, 419(6907):629–633, Oct 2002.

[321] G. M. Delgoffe, S. R. Woo, M. E. Turnis, D. M. Gravano, C. Guy, A. E. Overacre, M. L. Bettini, P. Vogel, D. Finkelstein, J. Bonnevier, C. J. Workman, and D. A. Vignali. Stability and function of regulatory T cells is maintained by a neuropilin-1-semaphorin-4a axis. *Nature*, 501(7466):252–256, Sep 2013.

[322] A. L. Kolodkin, D. J. Matthes, and C. S. Goodman. The semaphorin genes encode a family of transmembrane and secreted growth cone guidance molecules. *Cell*, 75(7):1389–1399, Dec 1993.

[323] A. Kumanogoh, T. Shikina, K. Suzuki, S. Uematsu, K. Yukawa, S. Kashiwamura, H. Tsutsui, M. Yamamoto, H. Takamatsu, E. P. Ko-Mitamura, N. Takegahara, S. Marukawa, I. Ishida, H. Morishita, D. V. Prasad, M. Tamura, M. Mizui, T. Toyofuku, S. Akira, K. Takeda, M. Okabe, and H. Kikutani. Nonredundant roles of Sema4A in the immune system: defective T cell priming and Th1/Th2 regulation in Sema4A-deficient mice. *Immunity*, 22(3):305–316, Mar 2005.

[324] T. Toyofuku, S. Nojima, T. Ishikawa, H. Takamatsu, T. Tsujimura, et al. Endosomal sorting by Semaphorin 4A in retinal pigment epithelium supports photoreceptor survival. *Genes Dev.*, 26(8):816–829, Apr 2012.

[325] D. S. Rice, W. Huang, H. A. Jones, G. Hansen, G. L. Ye, N. Xu, E. A. Wilson, K. Troughton, K. Vaddi, R. C. Newton, B. P. Zambrowicz, and A. T. Sands. Severe retinal degeneration associated with disruption of semaphorin 4A. *Invest. Ophthalmol. Vis. Sci.*, 45(8):2767–2777, Aug 2004.

[326] A. Abid, M. Ismail, S. Q. Mehdi, and S. Khaliq. Identification of novel mutations in the SEMA4A gene associated with retinal degenerative diseases. *J. Med. Genet.*, 43(4):378–381, Apr 2006.

[327] T. Sun, L. Yang, H. Kaur, J. Pestel, M. Looso, H. Nolte, C. Krasel, D. Heil, R. K. Krishnan, M. J. Santoni, J. P. Borg, M. Bunemann, S. Offermanns, J. M. Swiercz, and T. Worzfeld. A reverse signaling pathway downstream of Sema4A controls cell migration via scrib. *J. Cell Biol.*, 216(1):199–215, Jan 2017.

[328] M Smida, V Kozlova, V Vakulova, A Ledererova, M Doubek, J Mayer, and S Pospisilova. Cellular mechanisms regulating cd20 as a target of monoclonal antibody therapy in b-lymphoid malignancies. *Blood*, 128(22):3968–3968, 2016.

[329] I. Nijhof, T Casneuf, J van Velzen, B van Kessel, A Axel, et al. Cd38 expression and complement inhibitors affect response and resistance to daratumumab therapy in myeloma. *Blood*, 128(7):959–970, 2016.

[330] V. Neves, F. Aires-da Silva, S. Corte-Real, and M. Castanho. Antibody approaches to treat brain diseases. *Cell Press*, 34(1):36–48, Jan 2016.

[331] T. Mosmann. Rapid colorimetric assay for cellular growth and survival: application to proliferation and cytotoxicity assays. *J. Immunol. Methods*, 65(1-2):55–63, Dec 1983.

[332] A. Abid, M. Ismail, S. Q. Mehdi, and S. Khaliq. Identification of novel mutations in the SEMA4A gene associated with retinal degenerative diseases. *J. Med. Genet.*, 43(4):378–381, Apr 2006.

[333] T. Toyofuku, S. Nojima, T. Ishikawa, H. Takamatsu, T. Tsujimura, A. Uemura, J. Matsuda, T. Seki, and A. Kumanogoh. Endosomal sorting by Semaphorin 4A in retinal pigment epithelium supports photoreceptor survival. *Genes Dev.*, 26(8):816–829, Apr 2012.

[334] A. L. Szymczak-Workman, K. M. Vignali, and D. A. Vignali. Design and construction of 2A peptide-linked multicistronic vectors. *Cold Spring Harb Protoc*, 2012(2):199–204, Feb 2012.

[335] Z. Liu, O. Chen, B. Wall, M. Zheng, Y. Zhou, et al. Systematic comparison of 2A peptides for cloning multi-genes in a polycistronic vector. *Scientific Reports*, 7(1):1, May 2017.

[336] N. H. Bander. Antibody-drug conjugate target selection: critical factors. *Methods Mol. Biol.*, 1045:29–40, 2013.

[337] K. C. Catcott, M. A. McShea, C. U. Bialucha, K. L. Miller, S. W. Hicks, P. Saxena, T. G. Gesner, M. Woldegiorgis, M. E. Lewis, C. Bai, M. S. Fleming, S. A. Ettenberg, H. K. Erickson, and N. C. Yoder. Microscale screening of antibody libraries as maytansinoid antibody-drug conjugates. *MAbs*, 8(3):513–523, 2016.

[338] C. A. Fielding, M. P. Weekes, L. V. Nobre, E. Ruckova, G. S. Wilkie, et al. Control of immune ligands by members of a cytomegalovirus gene expansion suppresses natural killer cell activation. *Elife*, 6, 02 2017.

[339] Z. Xie, J. Gunaratne, L. L. Cheong, S. C. Liu, T. L. Koh, G. Huang, W. P. Blackstock, and W. J. Chng. Plasma membrane proteomics identifies biomarkers associated with MMSET overexpression in T(4;14) multiple myeloma. *Oncotarget*, 4(7):1008–1018, Jul 2013.

[340] S. Sebban, M. Farago, D. Gashai, L. Ilan, E. Pikarsky, I. Ben-Porath, and S. Katzav. Vav1 fine tunes p53 control of apoptosis versus proliferation in breast cancer. *PLoS ONE*, 8(1):e54321, 2013.

[341] B. Budnik, E. Levy, G. Harmange, and N. Slavov. SCoPE-MS: mass spectrometry of single mammalian cells quantifies proteome heterogeneity during cell differentiation. *Genome Biol.*, 19(1):161, Oct 2018.

[342] P. Zhao, S. Bhowmick, J. Yu, and J. Wang. Highly Multiplexed Single-Cell Protein Profiling with Large-Scale Convertible DNA-Antibody Barcoded Arrays. *Adv Sci (Weinh)*, 5(9):1800672, Sep 2018.

[343] J. Salonen, G. Ronnholm, N. Kalkkinen, and M. Vihinen. Proteomic changes during B cell maturation: 2D-DIGE approach. *PLoS ONE*, 8(10):e77894, 2013.

[344] Y. Yin, X. Xu, J. Tang, W. Zhang, G. Zhangyuan, et al. CD97 Promotes Tumor Aggressiveness Through the Traditional G Protein-Coupled Receptor-Mediated Signaling in Hepatocellular Carcinoma. *Hepatology*, 68(5):1865–1878, Nov 2018.

[345] A. M. Husa, Z. Magic, M. Larsson, T. Fornander, and G. Perez-Tenorio. EPH/ephrin profile and EPHB2 expression predicts patient survival in breast cancer. *Oncotarget*, 7(16):21362–21380, Apr 2016.

[346] S. J. Zhao, Y. F. Shen, Q. Li, Y. J. He, Y. K. Zhang, and others. SLIT2/ROBO1 axis contributes to the Warburg effect in osteosarcoma through activation of SRC/ERK/c-MYC/PFKFB2 pathway. *Cell Death Dis*, 9(3):390, Mar 2018.

[347] S. P. Wu, R. M. Pfeiffer, I. E. Ahn, S. Mailankody, P. Sonneveld, et al. Impact of Genes Highly Correlated with MMSET Myeloma on the Survival of Non-MMSET Myeloma Patients. *Clin. Cancer Res.*, 22(16):4039–4044, Aug 2016.

[348] H. Qu, H. Sun, and X. Wang. Neogenin-1 Promotes Cell Proliferation, Motility, and Adhesion by Up-Regulation of Zinc Finger E-Box Binding Homeobox 1 Via Activating the Rac1/PI3K/AKT Pathway in Gastric Cancer Cells. *Cell. Physiol. Biochem.*, 48(4):1457–1467, 2018.

[349] G. Malcherek, L. Mayr, P. Roda-Navarro, D. Rhodes, N. Miller, and J. Trowsdale. The B7 homolog butyrophilin BTN2A1 is a novel ligand for DC-SIGN. *J. Immunol.*, 179(6):3804–3811, Sep 2007.

[350] M. L. Moss and D. Minond. Recent Advances in ADAM17 Research: A Promising Target for Cancer and Inflammation. *Mediators Inflamm.*, 2017:9673537, 2017.

[351] Susan O'Brien, Farhad Ravandi, Todd Riehl, William Wierda, Xuelin Huang, et al. Valganciclovir prevents cytomegalovirus reactivation in patients receiving alemtuzumab-based therapy. *Blood*, 111(4):1816–1819, 2008.

[352] C. Datler and S. Grimm. Reconstitution of CKMT1 expression fails to rescue cells from mitochondrial membrane potential dissipation: implications for controlling RNAi experiments. *Biochim. Biophys. Acta*, 1833(12):2844–2855, Dec 2013.

[353] Y. Wang, F. Wang, R. Wang, P. Zhao, and Q. Xia. 2A self-cleaving peptide-based multi-gene expression system in the silkworm Bombyx mori. *Sci Rep*, 5:16273, Nov 2015.

[354] R. M. Lyu, P. M. Germano, J. K. Choi, S. V. Le, and J. R. Pisegna. Identification of an essential amino acid motif within the C terminus of the pituitary adenylate cyclase-activating polypeptide type I receptor that is critical for signal transduction but not for receptor internalization. *J. Biol. Chem.*, 275(46):36134–36142, Nov 2000.

[355] H. Moriya. Quantitative nature of overexpression experiments. *Mol. Biol. Cell*, 26(22):3932–3939, Nov 2015.